AFRL-ML-TY-TR-2003-4512

Tracer Techniques for DNAPL Source Delineation and *In-Situ* Flushing Techniques for Enhanced Source Removal: Pilot Scale Demonstrations at the Dover National Test Site

M.C. Brooks, and M.D. Annable
Department of Environmental Engineering Sciences
P.O. Box 116450
University of Florida
Gainesville, Florida 32611-6450

P. Suresh C. Rao
School of Civil Engineering
Purdue University
West Lafayette, Indiana 47907-1284

Approved for Public Release; Distribution Unlimited

AIR FORCE RESEARCH LABORATORY
MATERIALS & MANUFACTURING DIRECTORATE
AIRBASE TECHNOLOGIES DIVISION
139 BARNES DRIVE, STE 2
TYNDALL AFB FL 32403-5323

Reproduced From
Best Available Copy

20030220 095

NOTICES

USING GOVERNMENT DRAWINGS, SPECIFICATIONS, OR OTHER DATA INCLUDED IN THIS DOCUMENT FOR ANY PURPOSE OTHER THAN GOVERNMENT PROCUREMENT DOES NOT IN ANY WAY OBLIGATE THE US GOVERNMENT. THE FACT THAT THE GOVERNMENT FORMULATED OR SUPPLIED THE DRAWINGS, SPECIFICATIONS, OR OTHER DATA DOES NOT LICENSE THE HOLDER OR ANY OTHER PERSON OR CORPORATION; OR CONVEY ANY RIGHTS OR PERMISSION TO MANUFACTURE, USE, OR SELL ANY PATENTED INVENTION THAT MAY RELATE TO THEM.

THIS REPORT IS RELEASABLE TO THE NATIONAL TECHNICAL INFORMATION SERVICE
5285 PORT ROYAL RD.
SPRINGFIELD VA 22 161
TELEPHONE 703 487 4650; 703 4874639 (TDD for the hearing-impaired)
E-MAIL orders@ntis.fedworld.gov
WWW http://www.ntis.gov/index.html

AT NTIS, IT WILL BE AVAILABLE TO THE GENERAL PUBLIC, INCLUDING FOREIGN NATIONS.

THIS TECHNICAL REPORT HAS BEEN REVIEWED AND IS APPROVED FOR PUBLICATION.

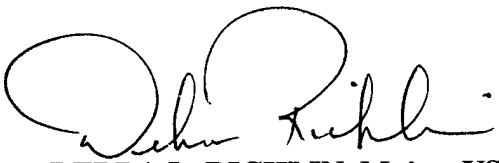

DEBRA L. RICHLIN, Major, USAF
Program Manager

GLEN T. SHEN, Ph.D.
Chief, Weapons Systems Logistics Branch

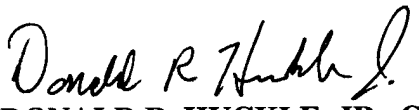

DONALD R. HUCKLE, JR., Colonel, USAF
Chief, Air Expeditionary Forces Technologies Division

Do not return copies of this report unless contractual obligations or notice on a specific document requires its return.

REPORT DOCUMENTATION PAGE

Form Approved
OMB No. 0704-0188

Public reporting burden for this collection of information is estimated to average 1 hour per response, including the time for reviewing instructions, searching existing data sources, gathering and maintaining the data needed, and completing and reviewing the collection of information. Send comments regarding this burden estimate or any other aspect of this collection of information, including suggestions for reducing this burden, to Washington Headquarters Services, Directorate for Information Operations and Reports, 1215 Jefferson Davis Highway, Suite 1204, Arlington, VA 22202-4302, and to the Office of Management and Budget, Paperwork Reduction Project (0704-0188), Washington, DC 20503.

1. AGENCY USE ONLY *(Leave blank)*	2. REPORT DATE	3. REPORT TYPE AND DATES COVERED
	15 September 2001	Final Report Jun 1998 – Sept 2001

4. TITLE AND SUBTITLE
Tracer Techniques for DNAPL Source Delineation and In-Situ Flushing Techniques for Enhanced Source Removal: Pilot Scale Demonstration at the Dover National Test site

5. FUNDING NUMBERS
Contract #:FO8637-97-C-6018
JON: 4223W404 PE:
PR:
TA:
WU:

6. AUTHOR(S) Brooks, Michael C.; Annable, Michael D.; Rao, Suresh C.

7. PERFORMING ORGANIZATION NAME(S) AND ADDRESS(ES)
Department of Environmental Engineering Sciences
P.O. Box 116450
University of Florida
Gainesville, Florida 32611-6450

School of Civil Engineering
Purdue University
West Lafayette, Indiana 47907-1284

8. PERFORMING ORGANIZATION REPORT NUMBER
NA

9. SPONSORING/MONITORING AGENCY NAME(S) AND ADDRESS(ES) (Program Mgr Name & Ph #)
Air Force Research Laboratory
Airbase Technologies Division (AFRL/MLQL)
139 Barnes Drive, Suite 2
Tyndall AFB, Florida 32403-5323

10. SPONSORING/MONITORING AGENCY REPORT NUMBER
AFRL-ML-TY-TR-2003-4512

11. SUPPLEMENTARY NOTES

Availability of this report is specified on the verso of front cover.

12a. DISTRIBUTION/AVAILABILITY STATEMENT
DISTRIBUTION UNLIMITED

12b. DISTRIBUTION CODE
(Leave this block blank)

13. ABSTRACT:
The objective of this study was to evaluate the performance of innovative tracer techniques for dense nonaqueous phase liquid (DNAPL) characterization and in-situ cosolvent and surfactant flushing for DNAPL removal in an isolated test cell (3.0m x 4.5m x 12.3m) located at the Dover National Test Site, Dover AFB, DE. As part of a larger project to assess the performance of several in-situ flushing technologies for DNAPL source removal, it involved controlled releases of up to 100L of perchloroethylene (PCE) into test cells for each remedial technology. Subsequent to PCE release, two partitioning tracer tests were conducted: one before and another after the remedial test. The University of Florida (UF) conducted the first remedial demonstration, cosolvent flushing, and the second remedial demonstration, surfactant flushing, was conducted jointly by UF and the University of Oklahoma (UO). The focus of this report is the four partitioning tracer tests and the cosolvent flushing demonstration.

14. SUBJECT TERMS: DNAPL, DNAPL Source Delineation, Enhanced Source Removal, Groundwater Cleanup

15. NUMBER OF PAGES
261

16. PRICE CODE

17. SECURITY CLASSIFICATION OF REPORT	18. SECURITY CLASSIFICATION OF THIS PAGE	19. SECURITY CLASSIFICATION OF ABSTRACT	20. LIMITATION OF ABSTRACT
Unclassified	Unclassified	Unclassified	SAR

NSN 7540-01-280-5500

Standard Form 298 (Rev. 2-89)
Prescribed by ANSI Std. 239-18

AQ403-04-0951

EXECUTIVE SUMMARY

The objective of this study was to evaluate the performance of innovative tracer techniques for dense nonaqueous phase liquid (DNAPL) characterization and in-situ cosolvent and surfactant flushing for DNAPL removal in an isolated test cell (3.0m x 4.5 m x 12.3 m) located at the Dover National Test Site. As part of a larger project to assess the performance of several in-situ flushing technologies for DNAPL source removal, it involved controlled releases of up to 100 L of perchloroethylene (PCE) into test cells for each remedial technology. Subsequent to PCE release, two partitioning tracer tests were conducted: one before and another after the remedial test. The first remedial demonstration, cosolvent flushing, was conducted by the University of Florida (UF), and the second remedial demonstration, surfactant flushing, was conducted jointly by UF and the University of Oklahoma (OU). The focus of this report is the four partitioning tracer tests and the cosolvent flushing demonstration.

In situ cosolvent flushing is an innovative technique where cosolvents, such as alcohols, are flushed through source zones containing nonaqueous phase liquids (NAPLs). Cosolvents increase the quantity of contaminants transported in the flushing fluid by increasing the solubility, desorption, and mass transfer rate of the NAPL components or by free-phase mobilization through reduction in the NAPL-water interfacial tension. For this demonstration, an ethanol solution, ranging from 95% to 60% volumetric fraction, was used to flush the cell. Based on the phase behavior of the water-ethanol-PCE system, the main remedial mechanism was enhanced dissolution. By mass balance, it was estimated that 83 L of PCE were present in the test cell at the start of the test. Over a 40-day period, 64% of the PCE was removed by flushing with the alcohol solution. The maximum PCE concentration in the flushing effluent ranged from approximately 1,500 to 3,500 mg/L. High removal efficiencies at the end of the demonstration indicated that more PCE could have been removed had it been possible to continue the demonstration. Results from pre- and post-flushing partitioning tracer tests overestimated the treatment performance, however, both tests missed significant amounts of PCE. Inaccessibility of the tracers to PCE may also mean that some PCE was inaccessible to the alcohol solution, which may explain why more PCE was not removed. The flux-averaged aqueous PCE concentrations were reduced by a factor of 3 to 4 in the extraction wells that showed the highest PCE removal. The ethanol solution extracted from the test cell was recycled using activated carbon and air stripping treatment. Both treatment processes were successful in removing PCE for recycling purposes, while having minimal impact on the ethanol content in the treated fluids.

Preliminary results from the surfactant flushing demonstration indicate that about 70% (49 of 70 L) of the initial PCE volume was removed over a 43-day period. When comparing this result to that of the cosolvent flushing demonstration (53 of 83 L), it should be recognized that the test conditions were not identical. The PCE distribution in the two tests may have been different, and the pumping pattern used in the two tests was different.

Two general observations can be made based on the results from the first three partitioning tracer tests: (1) the PCE volume predicted varied within each test depending on the partitioning tracer, and (2) the predicted PCE volume was less than expected, even when using the data for partitioning tracers with the largest partitioning coefficients (18% to 80% of the expected volume). In contrast, the last partitioning tracer test displayed relatively little prediction variation, and its predicted PCE volume was larger than the expected PCE volume

(143% for the tracer with the largest partitioning coefficient). However, the similarity in predicted PCE volumes between Test 3 and Test 4 (pre- and post surfactant flushing), at least for the tracers with the highest partitioning coefficients, does not agree with the preliminary results of PCE volume removed during the surfactant flood, and calls into question the reliability of the test results. An increase in background sorption of tracers due to the presence of residual surfactant sorbed to the aquifer matrix was the likely reason for larger retardation. Finally, uncertainties introduced in accounting for tracer degradation were significant in the first partitioning tracer test. The estimates of PCE volumes ignore background tracer retardation, and would be even less if corrections were included.

ACKNOWLEDGEMENTS

This project was funded by the United States (US) Department of Defense Strategic Environmental Research and Development Program (SERDP), which is a collaborative effort involving the US Environmental Protection Agency (EPA), US Department of Energy, and US Department of Defense. This document has not been subjected to peer review within the funding agency, and the conclusions stated here do not necessarily reflect the official views of the agency nor does this document constitute an official endorsement by the agency. The authors thank all those who helped with the sampling and analysis including Sten Berglund, Jaehyun Cho, Clayton Clark II, Lane Evans, Kirk Hatfield, Andrew James, James Jawitz, Heonki Kim, Irene Poyer, Claire Shukla, Gloria Sillan, William R. Wise, and Meifong Zhou from the University of Florida; Gavin James from the University of Oklahoma; Mark Hogan and Rob Young from Mantech Environmental Research Services Corporation; Mark Hasegawa and Jarod Norris from SURBEC; Tim McHale, Dover National Test Site Program Manager, Air Force Research Laboratory; Carl G. Enfield, Bart Faulkner, John Hoggatt, Tony Lee, Susan Mravik, and A. Lynn Wood from the U. S. Environmental Protection Agency; and Major Paul Devane from Armstrong Laboratories, Tyndall AFB.

CONTRIBUTING AUTHORS

Michael D. Annable, University of Florida
Michael C. Brooks, University of Florida
Jaehyun Cho, University of Florida
Carl G. Enfield, U.S. Environmental Protection Agency
Wendy D. Graham, University of Florida
Kirk Hatfield, University of Florida
Andrew I. James, University of Florida
James W. Jawitz, University of Florida
P. Suresh C. Rao, Purdue University
Michael Van Valkenburg, University of Florida
William R. Wise, University of Florida
A. Lynn Wood, U.S. Environmental Protection Agency

TABLE OF CONTENTS

LIST OF TABLES

LIST OF FIGURES

1. INTRODUCTION

1.1. Project overview

The objective of the study was to evaluate the feasibility and effectiveness of in-situ flushing techniques for DNAPL source-zone remediation, as well as partitioning interwell tracer tests for characterizing DNAPL volume and distribution. The United States Environmental Protection Agency (EPA) National Risk Management Research Laboratory sponsored a project to assess the performance of remedial technologies for DNAPL source removal. In this project, researchers at EPA and five universities agreed to perform a series of DNAPL remedial demonstrations at the Dover National Test Site (DNTS). The DNTS is located on the Dover Air Force Base (AFB) in Dover, Delaware, and includes facilities for field-scale remedial experimentation (Thomas, 1996). In these demonstrations, EPA researchers created the DNAPL source zone within the test cells by releasing up to 100 L of PCE under controlled conditions. Release of perchloroethylene (PCE) into the cells was approved by the Delaware Department of Natural Resources and Conservation (Noll et al., 1998). Information on the volume and distribution of the PCE released was not revealed to the university researchers until the completion of their remedial demonstrations. Each remedial demonstration included two partitioning tracer tests: one before and another after the remedial test.

The first remedial demonstration, conducted by the University of Florida (UF), was enhanced dissolution by in-situ alcohol flushing. The second demonstration, conducted jointly by UF and the University of Oklahoma (OU), was enhanced dissolution by surfactant flushing. In the second demonstration, UF served as the lead investigative team for both partitioning-tracer tests, with OU providing support. For the surfactant flushing demonstration, OU served as the lead investigative team with UF providing support. Results from the surfactant flushing demonstration included herein are limited to those necessary for the discussion of the associated partitioning tracer tests, and for a preliminary comparison to results from the alcohol flushing demonstration. Table 1-1 summarizes the activities conducted in the cell, from the beginning of the project through to the end of the post-surfactant partitioning tracer test.

The remainder of this section provides information on the test cell construction, instrumentation, and geology. Section 2 summarizes laboratory and other work conducted in support of the field demonstrations. Sections 3 and 4 present the results from the partitioning tracer tests and cosolvent flood, respectively. Performance evaluations are discussed in Section 5, and a summary with recommendations are given in Section 6.

1.2. Site background

The demonstrations were conducted in an isolated test cell, constructed using Waterloo sheet piling with interlocking joints driven into the clay confining unit (Starr et al., 1992), and surrounded by a second enclosure of sheet piling forming a secondary containment barrier. The cell was instrumented with 12 wells, 18 release points, and 18 multi-level sampler (MLS) locations (Figure 1-1). Each well was screened from 6.1 meters to 13.3 m below ground surface

Table 1-1. Activities conducted in the cell.

Activity		Date
Hydraulic Test		September 5 - 8, 1997
Background tracer test		May 28 - June 4, 1998
First Controlled PCE Release		June 10 – 12, 1998
Conservative Interwell Tracer Test		June 19 – 26, 1998
Pre-Cosolvent Flood Tracer Test	(Test 1)	July 1 - 12, 1998
Ethanol Flushing Test		February 2 - March 12, 1999
Post-Cosolvent Flood Tracer Test	(Test 2)	May 7 - 19, 1999
Vertical Circulation Tracer Test		December 14 - 15, 1999
Second Controlled PCE Release		March 13, 2000
Pre-Surfactant Flood Tracer Test	(Test 3)	June 13 – 30, 2000
Surfactant Flushing Test		August 2 - September 15, 2000
Post-Surfactant Flood Tracer Test	(Test 4)	October 9 –26, 2000

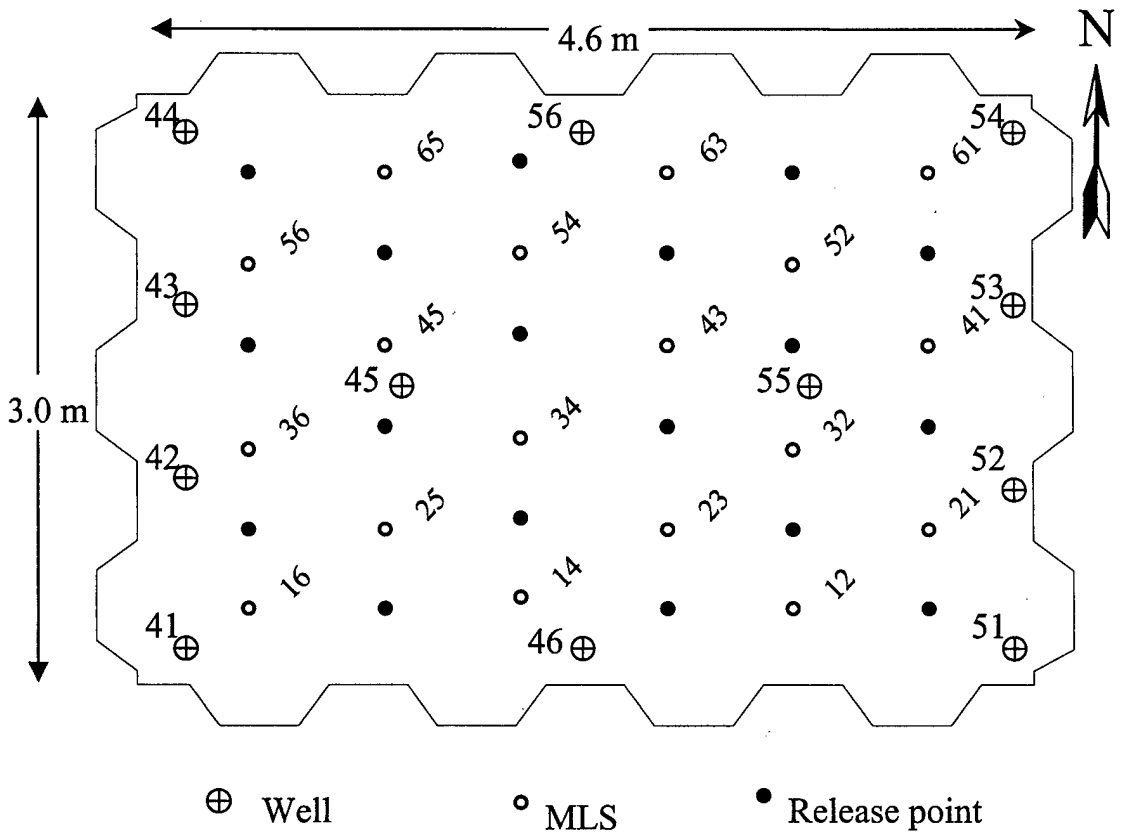

Figure 1-1. Cell instrumentation layout (plan view).

(bgs). Release points terminated at 10.7 meters below grade with a sampling port located just above each release point at approximately 9.9 meters. Each MLS location had 5 vertical sampling points spaced 0.3 meters apart, distributed on a tetrahedral grid over the bottom 1.5 meters of the cell.

The site geology consisted of the Columbia Formation, characterized by silty, poorly sorted sands, underlain by the Calvert Formation, the upper portion of which was characterized by silty clay with thin layers of silt and fine sand (Noll et al., 1998). This layer formed the

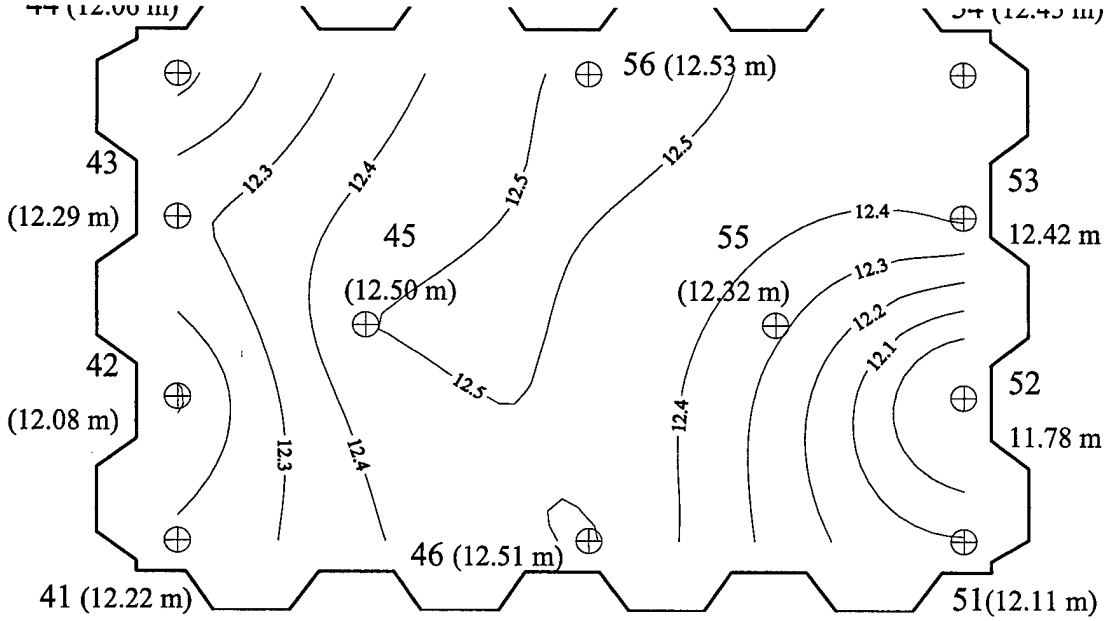

⊕ Well

confining unit into which the sheet pile was driven. Boring logs from the wells installed in the cell generally indicated alternating layers of silty sand, poorly sorted sand, and well sorted sand over the logging interval from approximately 10.1 to 12.5 m below grade. The presence of iron oxides was also noted in several logs. The depth to clay measured at each well location is shown in Figure 1-2. The clay is generally lower in the middle of the cell (wells 46, 45, and 56), and in the northeast corner (well 53 and 54), which suggests the potential exists for DNAPL pooling and subsequent hydrodynamic constraints in these areas. Based on the hydraulic gradient measured under steady flow during hydraulic testing, the estimated hydraulic conductivity averaged over the cell was approximately 2.5 m/day.

Figure 1-2. Depth to clay from grade measured at each well, and the estimated clay-surface contours based on that data (Plan view).

2. SUPPORTING INVESTIGATIONS

Various activities were conducted in support the field-scale demonstrations. Laboratory work was conducted to estimate tracer partitioning coefficients, tracer background retardations, impacts of residual flushing agents on partitioning tracer performance, and impacts of pumping pattern on partitioning tracer performance. Modeling work was also completed to help select the best pumping pattern to use during the partitioning tracer tests. In support of the cosolvent flood, work was conducted to estimate the solubility of PCE in the cosolvent solutions, and mobilization of PCE during cosolvent flushing. In addition, work was completed to quantify the uncertainty of the field demonstrations based on measurement uncertainty.

2.1. Determination of Partitioning Coefficients

Methods. The partitioning tracers used in the field tests are listed in the order of increasing hydrophobicity in Table 2-1. To estimate the tracer partitioning coefficients, batch experiments were conducted at UF using tetrachloroethylene (PCE) purchased from Arcos Organics (99% pure). Volumetric NAPL:water ratios of 1:10, 1:20, and 1:100 were prepared in 40-mL vials with different tracer solutions. The tracer solutions were produced by serial dilution of a stock tracer solution, the concentration of which was similar in magnitude to the tracer injection concentrations used in the field. Each tracer solution was mixed with the PCE at a specified volume ratio, rotated overnight, and then allowed to settle for approximately two hours before analysis. The equilibrated aqueous samples were analyzed for alcohol tracers using a gas chromatograph with a flame ionization detector (GC/FID). In order to minimize co-tracer effects (Dai, 1997; Wise et al., 1999), batch experiments were conducted using two suites of tracers: suite 1 consisted of *n*-heptanol and 2-ethyl-1-hexanol, and suite 2 consisted of *n*-hexanol; 2,4-dimethyl-3-pentanol; 2-octanol; and 3,5,5-trimethyl-1-hexanol. These were used to represent the tracer suites used in the field experiments. Two tracers used in the first field experiment, 3-heptanol and *n*-octanol, were not

Table 2-1. NAPL-water partitioning coefficients.

Tracer	K_{NW}	R^2
n-hexanol	8	0.992
3-heptanol	25	0.995
2,4-dimethly-3-pentanol	30	0.993
n-heptanol	32	0.997
2-octanol	110	0.990
2-ethyl-1-hexanol	120	0.983
n-octanol	170	>0.98
3,5,5-trimethyl-1-hexanol	230	0.992

included in these batch experiments. Separate batch experiments were conducted using 3-heptanol; 2-octanol; and 2,6-dimethyl-2-heptanol at NAPL volume ratios of 1:5, 1:10, and 1:20.

Results. Estimates of tracer partitioning coefficients, based on linear regression (with zero intercepts) of results from the batch experimental results, are presented in Table 2-1 along with the coefficient of determination (r^2) from the linear regression. The equilibrium concentration of the partitioning tracers in the PCE as a function of their aqueous phase concentration is shown in Figure 2-1. All tracers show deviation from linear partition at higher concentrations. This non-linear behavior was observed by Dai (1997), and has been discussed by Wise et al. (1999) and Wise (1999). To prevent complications due to non-linear partitioning behavior, tracer tests should be designed such that the concentration of the injected tracer are within the linear range of the partitioning data. Injecting tracers at concentrations sufficiently low to ensure linear partitioning, however, is not always practical due to the need to accurately quantify the tracer concentrations in the tails of the breakthrough curves. Using a linear analysis of partitioning when the partitioning process is nonlinear, as observed here, results in a systematic overestimate of NAPL saturation (Wise, 1999). This conclusion is based on the nature of the partitioning process (i.e., upward concavity as shown in Figure 2-1, and Wise et al., 1999), and on the assumption that the "linear" partitioning coefficient is derived from the low-concentration region of the isotherm, where a linear fit to the data is justified (see Figure 2-1, and Wise 1999).

2.2. Background Tracer Sorption

Methods. A column experiment was conducted to investigate the extent of alcohol tracer sorption onto the soil matrix. The column, approximately 2.5 cm in diameter and 5 cm long, was packed with soil from core samples taken from the test cell. A tracer suite consisting of methanol; *n*-hexanol; 2,4-dimethyl-3-pentanol; 2-octanol; and 2,6-dimethyl-2-heptanol was flushed through a column for approximately 5.5 pore volumes.

Results. Estimates of background retardation of tracers are summarized in Table 2-2, and ranged from 1.003 for *n*-hexanol to 1.017 for 2,6-dimethyl-2-heptanol. These values are generally low, and indicate that sorption of the alcohol tracers onto the soil from the cell should not pose a significant problem relative to the target retardation of 1.2, as recommended by Jin et al. (1997) for reliable NAPL-volume predicitons. Using partitioning coefficients of 8 and 218 for *n*-hexanol and 2,6-dimethyl-2-heptanol, respectively, the estimated (false) PCE saturation

Table 2-2. Summary of background retardation values resulting from alohol tracer sorption onto the soil matirx.

Tracer	Background Retardation	Equivalent PCE Saturation
n-Hexanol	1.003	0.0004
2,4-Dimethyl-3-pentanol	1.003	0.0001
2-Octanol	1.016	0.0001
2,6-dimethyl-2-heptanol	1.017	0.0001

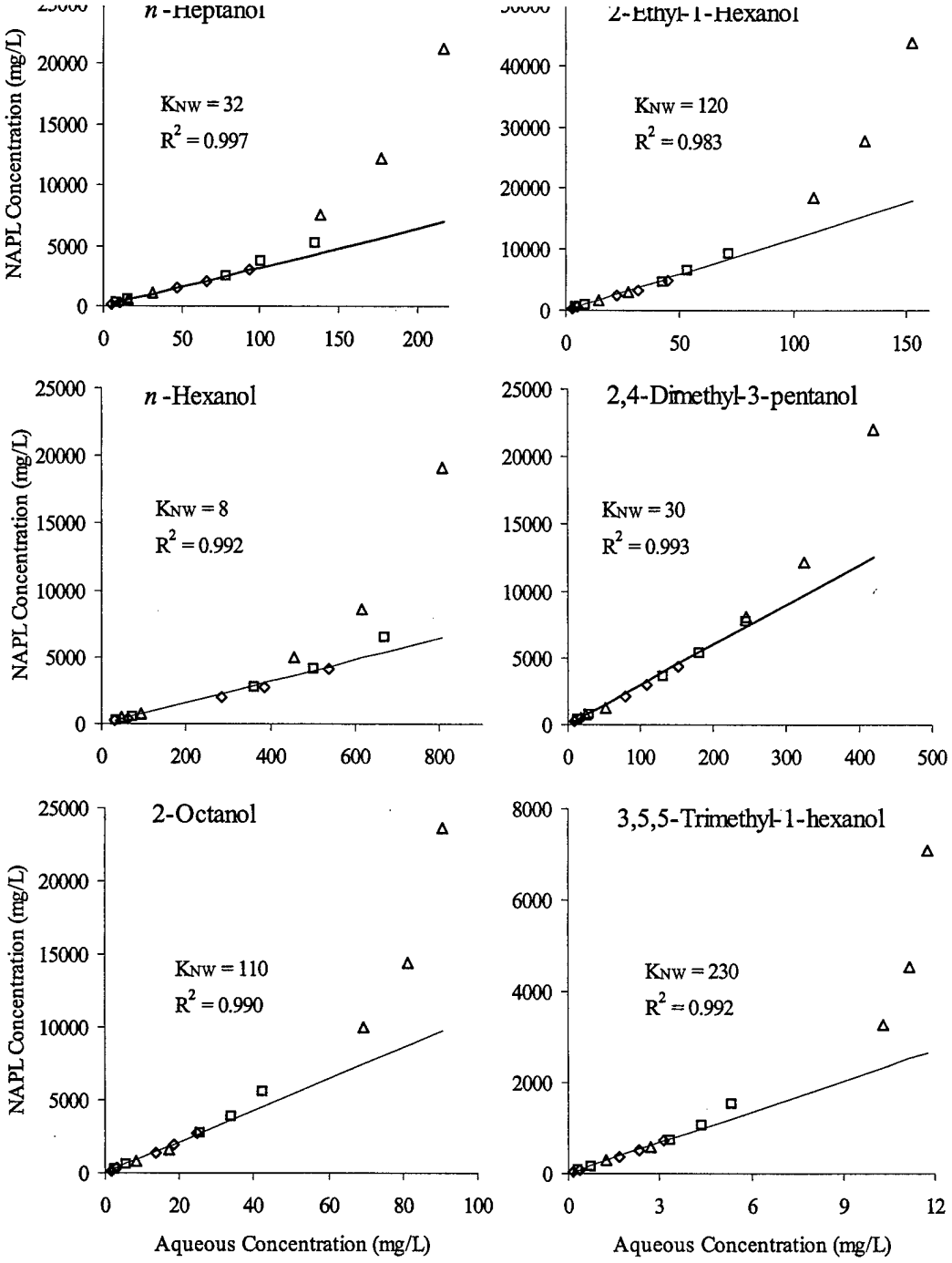

associated with these retardation values are 0.0004 and 0.0001.

Figure 2-1. NAPL-water partitioning batch experiments. Slope of line represents tracer partitioning coefficient (K_{NW}). The NAPL:water ratios used in the batch experiments were 1:10 (diamonds), 1:20 (squares), and 1:100 (triangles).

2.3. Partitioning Tracers and Residual Flushing Agents

Methods. Batch experiments and column displacement experiments were conducted to investigate the impact of residual cosolvent and surfactant flushing solutions on NAPL volume predictions using partitioning tracers (See Cho et al., manuscript in preparation, Appendix A). The experiments were conducted using three cosolvent solutions (ethanol, *tert*-butanol, and

isopropanol) and three surfactant solutions [DowFax 8390 (alkyl diphenyl oxide disulfonates), Brij 97 (polyoxylethylene(10)oleyl ether), and AMA 80 (dihexyl sulfosuccinate)]. These surfactants were identified as having optimal solubilization profiles for PCE (Sabatini, OU, personal communication). The tracer suite used in the experiments consisted of one nonpartitioning tracer (methanol) and three partitioing tracers (*n*-hexanol, 2-methyl-3-hexanol, and 2,4-dimethyl-3-pentanol). Perchloroethylene was used as the DNAPL in all experiments. Batch and column experiments were conducted to measure the tracer partitioning coefficients in various cosolvent fractions (between 0 and 10%) and surfactant fractions (0 to 0.5%).

Results. Batch experiments indicated that partitioning coefficient values were a function of the cosolvent type and concentration. The tracer partitioning coefficients linearly decreased with increases in ethanol cosolvent, and linearly increased for increases in *tert*-butanol cosolvent fractions, but did not change with increases in isopropanol. Results from the column experiments with residual ethanol cosolvent were consistent with the batch test results. Partitioning tracers underestimated the PCE saturation by 1 to 10% as the cosolvent fraction was increased due to reductions in partitioning tracer retardation. The impact of residual cosolvent was found to decrease as the PCE saturation increased.

Batch equilibrium tests with residual surfactants (* 0.5 %) showed that as the fraction of surfactants increased, the partitioning coefficients linearly decreased for DowFax 8390, and slightly increased for Brij 97, but remained unchanged for AMA 80. Results from column tests through clean sand media with residual DowFax 8390 were consistent with the batch test results. Column results with residual surfactants without NAPL showed false indications of NAPL; AMA 80, Brij97, DowFax 8390 gave false NAPL saturations of 0.24, 4.3, 23 %, respectively (see Figure 2-2). Since AMA 80 produced the least interference with the partitioning tracers in the laboratory experiments, it was selected for use in the field surfactant flushing demonstration.

2.4. Cosolvent Fraction, PCE Solubility, and Interfacial Tension

Methods. Laboratory experiments were conducted to investigate the relationship between cosolvent fraction and PCE solubility, and cosolvent fraction and equilibrium interfacial tension (Van Valkenburg, 1999). Ethanol and isopropyl alcohol were used as the cosolvents. Various cosolvent fractions were mixed with PCE at a 1:1 ratio in 40 mL vials, and allowed to equilibrate on a mechanical rotator for 48 hours, and subsequently settle for 24 hours. Aqeous samples were then collected from the vials and analyzed for PCE using a GC/FID, and for interfacial tension using a Du Nuoy ring tensiometer.

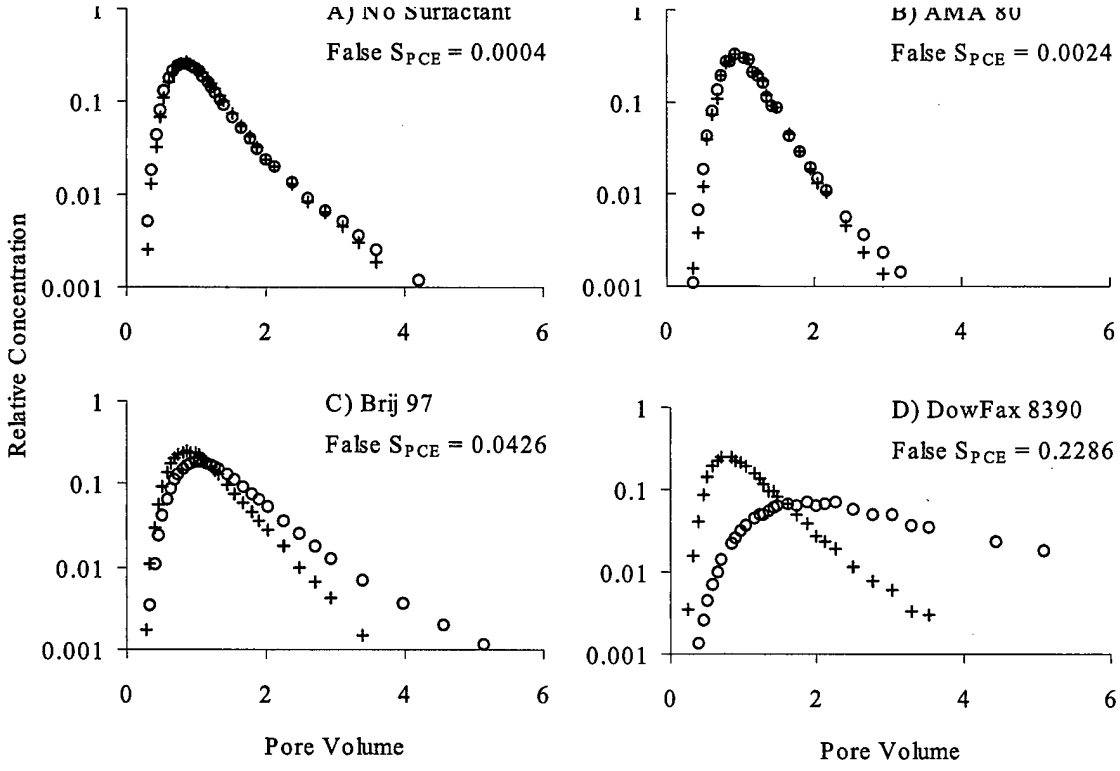

Figure 2-2. Results from column experiments with A) no surfactant, B) AMA 80, C) Brij 97, and D) DowFax 8390 residual surfactant solution and no NAPL. Shown are BTCs for the nonpartitioning tracer (methanol, plus symbols) and partitioning tracer (hexanol, circles). Adapted from Cho et al. (2001, Appendix A).

Results. Loglinear relationships were found to more accurately predict PCE solubilities at higher cosolvent fractions (> 50%), while deviations from the log-linear model were observed at

smaller (<50%) cosolvent volume fractions (Figure 2-3). The cosolvency power for the log-

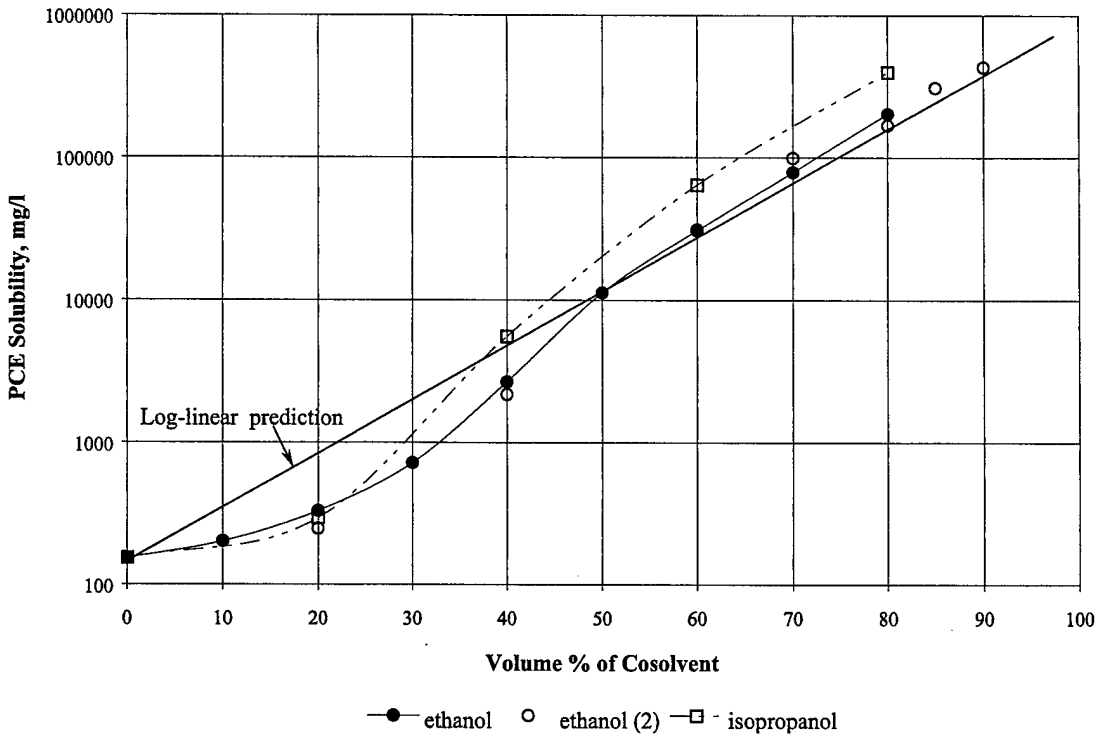

linear model of PCE solubility in an ethanol-water solution was estimated as 3.73. A log-linear model was developed to describe the relationship between interfacial tension and cosolvent fraction (Figure 2-4). It was determined that the PCE solubility could be used to accurately predict interfacial tension for cosolvent fractions of interest to NAPL remediation.

2.5. PCE Mobilization During Cosolvent Flushing

Methods. Two-dimensional flow chamber (61-cm width, 39.4-cm tall, and 1.4-cm thick) studies were conducted to determine qualitative and quantitative performance of cosolvents targeted at pooled PCE residing above a finer capillary barrier (Van Valkenburg and Annable, 2001, submitted to *Journal of Contaminant Hydrology*, See Appendix A). Three types of studies

Figure 2-3. PCE solubility as a funciton of cosolvent fraction (Van Valkenburg, 1999; Figure 2-2).

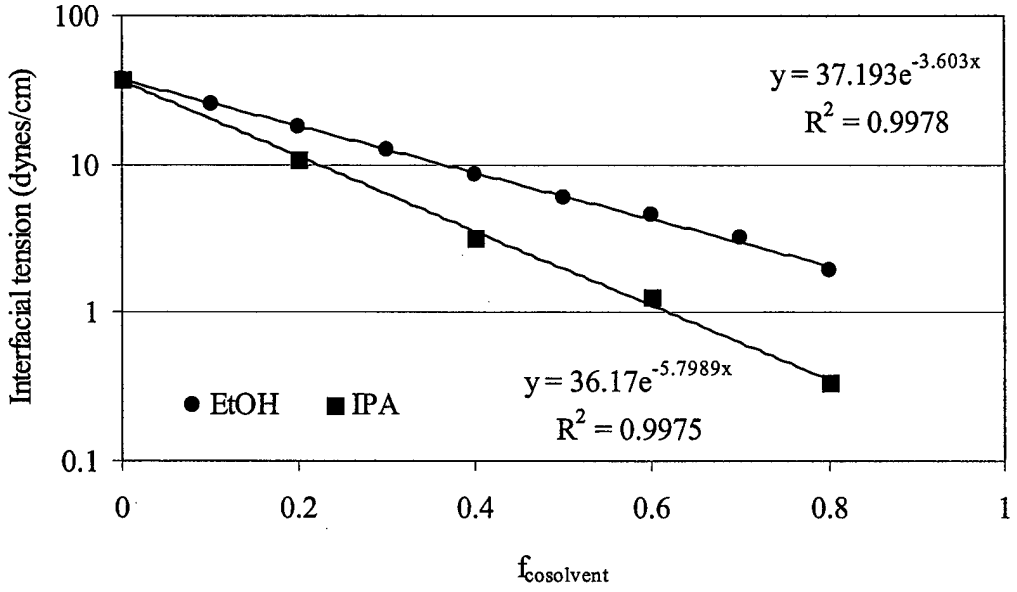

Figure 2-4. Interfacial tension as a funciton of cosolvent fraction (adapted from Van Valkenburg, 1999; Figure 2-7).

were conducted: 1) step inputs of reagent alcohol (90.4 volume % ethanol, 4.6 volume % methanol, and 5.0 volume % isopropanol), which produced essentially no PCE swelling, 2) gradient input of reagent alcohol, and 3) step inputs of tertiary butyl alcohol (a PCE swelling alcohol). The chamber was packed with 20/30 Ottawa sand, and included a capillary barrier consisting of a 1-cm thick sand lens. The capillary barrier consisted of 100-140, 60-70, 40-50, and 30-40 sieved sand. The PCE was colored with Oil-red-O dye, and was injected into the sand media approximately 1 cm above the capillary barrier using a syringe with a 16 gauge long stainless steel needle. Between 2.7 to 3.5 ml of PCE were injected and remained in the media.

Results. Downward mobilization of DNAPL, up gradient along an overriding cosolvent front, was observed. This produced significant pooling above the capillary barrier that in some cases led to entry into the capillary barrier. Entry pressure calculations provided excellent predictions of DNAPL breakthrough into the capillary barrier. A gradient injection of cosolvent did not appear to provide any benefit because of the rapid decline in interfacial tension compared to the rate of DNAPL solubilization. Use of the swelling alcohol (tertiary butyl alcohol) resulted in DNAPL swelling and reduced entry into the capillary barrier. However, entrapment of swelled PCE could potentially lead to longer remediation times. Based on these results, it was decided to inject the cosolvent solution during the field demonstration using a step change from water, rather than injection using a concentration gradient.

2.6. Moment and Partitioning-Tracer Uncertainty Analysis

Methods. General stochastic methods were investigated whereby the uncertainty in volume and concentration measurements were used to estimate the uncertainty of the zeroth and normalized first moments. These methods were based on the assumption that moments are calculated from the breakthrough curves by numerical integration using the trapezoidal rule.

The uncertainty associated with the NAPL volume estimates using partitioning tracers was then quantified by propagating uncertainty in moments to NAPL volume estimates (Brooks, 2000).

Results. The relative uncertainty in the moment was found to be less than that for relative volume and concentration measurements. The normalized first moment was impacted less than the zeroth moment. Moment uncertainties were more sensitive to concentration uncertainties as opposed to volume uncertainties. Propagation of moment uncertainty through the partitioning tracer theory quantitatively indicate how the uncertainty in NAPL volume grows as the retardation factor decreases. These errors have been found to be relatively small; less than 10% for retardation factors greater than approximately 1.2. These results are in agreement with those presented by Dwarakanath et al. (1999) and Jin et al. (2000).

2.7. Partitioning Tracers and Nonuniform Flow Fields

Methods. James et al. (2000, see Appendix A) developed a method to predict the NAPL-saturation spatial distribution using partitioning tracer data collected from MLSs. The method used a Gauss-Newton procedure to estimate the spatial distribution of the log NAPL/water volumetric ratio (Y) that minimized the weighted sum of the deviation of modeling-predicted temporal moments from their measured values, and the deviation of Y from prior estimates. The moment sensitivities and the estimation error covariance calculated in the method can be used to evaluate the information obtained from various pumping schemes for a given NAPL distribution. Three pumping configurations (line drive, double five spot, and inverted double five spot) and two NAPL spatial distributions (random, spatially-correlated NAPL field and block of NAPL) were investigated.

Results. The model simulations indicated that the double five spot and the inverted double five spot produce temporal moments that have a higher sensitivity to NAPL/water volumetric ratios and more accurate NAPL-saturation spatial distribution estimates than the line-drive pattern. The improved estimation of the five-spot pattern over the line-drive pattern is a function of the NAPL distribution, and therefore cannot be generalized to all cases. It was recommended that the developed method be used prior to partitioning tracers test to investigate several pumping configurations to determine the water velocity distributions, the sensitivities of tracer moments to NAPL distribution, and a preliminary estimate of the estimate of the reduction in NAPL estimation error for each configuration. The configurations investigated were based on the Dover field site. Based on the preferable performance of the five-spot pattern over the line-drive pattern, the five spot pattern was employed in for the subsequent field tracer tests.

3. PARTITIONING TRACER TESTS

A total of six tracer tests were conducted in the cell between May, 1998 and October, 2000 (Table 1-1). One tracer test was conducted prior to the first release of PCE into the cell to assess background sorption of tracers (hereafter referred to as the background tracer test). Three tracer tests were conducted between the first and second PCE release, and two were conducted after the second release. The first tracer test after the initial release was conducted to investigate non-reactive transport characteristics in a line drive flow pattern using bromide as a nonpartitioning tracer. EPA researchers conducted this test and the results were not used in the design or interpretation of the partitioning tracer tests, and as such are not discussed here. The remaining four tracer tests were conducted to characterize the PCE in the cell before and after the cosolvent flood (referred to as Test 1 and Test 2, respectively), and before and after the surfactant flood (referred to as Test 3 and Test 4, respectively). Brooks et al. (2001, Appendix A) present the results and a discussion of these tests, and this section is an abbreviated version of that work.

Each of these tests followed the same general experimental protocol: pulse injection of a tracer suite followed by water injection for a specified period, collection of well effluent samples over the test duration, laboratory analysis of the samples, and moment analysis of the resulting breakthrough curves (BTCs). Tracers used in the tests are summarized in Table 3-1. Samples were analyzed for alcohol tracers by gas chromatography with a flame ionization detector, and for inorganic tracers using liquid chromatography with an ultraviolet detector. Selected effluent samples near the end of the test where also analyzed for alcohol tracers using a head-space sampling method to better quantify the tracer concentrations in the tails of the BTCs. Breakthrough curves were exponentially extrapolated to minimize truncation errors (Annable et al., 1998), zeroth and first-normalized moments were estimated using trapezoidal approximations, and the nonpartitioning and partitioning tracer moments were then used to estimate DNAPL saturations and volumes using the methods outlined by Jin et al. (1995).

Table 3-1. Tracers used in the partitioning tracer tests. The partitioning coefficients (KNW) are for PCE-water partitioning.

Tracer		Used in Tests
Conservative		
Bromide		BG, 4
Iodide		1[a], 2[a], 3
Methanol		BG, 1[a], 2[a], 3, 4
tert-Butyl alcohol	(TBA)	1[b], 3, 4
Isobutyl alcohol	(IBA)	1[c], 2[d]
Isopropyl alcohol	(IPA)	1[d]
Partitioning		
n-Hexanol		1[a], 2[a], 3, 4
2,4-Dimethyl-3-pentanol	(DMP)	BG, 1[a], 2[a], 3, 4
3-Heptanol		1c
n-Heptanol		1[d], 2[d]
2-Octanol		1[a], 2[a], 3, 4
2-Ethyl-1-Hexanol	(2E1H)	2[d]
n-Octanol		BG, 1[b]
3,5,5-Trimethyl-1-Hexonal	(TMH)	2[a], 3, 4

[a]Common lower-zone tracer; [b]Well 45 unique, lower-zone tracer; [c]Well 55 unique, lower-zone tracer; [d]Common upper-zone tracer.

Table 3-2 summarizes the length, tracer pulse duration, total extraction rate, and saturated thickness from each test.

3.1 Background Tracer Test

Table 3-2. Summary of conditions for partitioning tracer tests.

Test	Duration (Days)	Tracer Pulse Duration (Days)	Flow Rate (L/min)	Saturated Thickness (m)
BG	7.0	0.29	3.9	4.6
1	11.6	0.33	6.6	3.7
2	12.0	0.36	6.8	3.6
3	17.2	0.48	3.8	3.9
4	17.0	0.42	3.7	3.5

Methods. A double five-spot pumping pattern, which consisted of six injection wells (41, 44, 46, 51, 54, and 56) along the perimeter of the cell and two extraction wells (45 and 55) in the center of the cell (Figure 1-1), was used to inject and extract fluids during the test. The extraction flow rate from the two center wells (45 and 55) were approximately 2.0 L/min and 1.9 L/min, respectively.

Results. Results from the background sorption tracer test are summarized in Table 3-3. For both wells, the percent recovery decreased in the order of bromide, DMP, methanol, and *n*-octanol. The tail of the BTC for *n*-octanol declined significantly relative to the other tracers in both wells, suggesting tracer degradation may have occurred. The effective porosity in the cell was estimated at approximately 0.17 based on moment analysis of the methanol nonpartitioning tracer. Bromide retardation can result from anion exchange with iron oxides (Brooks et al., 1998), which may explain the apparent bromide retardation of 1.35 to 1.26 relative to methanol in this test. Due to the potential retardation of both bromide and iodide by this mechanism, their use as a non-partitioning tracer was disregarded. Measured retardation factors for DMP of 1.12 and 1.14 represent an equivalent background PCE saturation of 0.004 and 0.005, which are approximately an order of magnitude greater than those estimated from the laboratory experiments (see Section 2.2). The equivalent PCE volume, based on the methanol swept volume, is 52 L. However, for complications discussed later in this section, corrections for background sorption based on these results were not deemed applicable to later tracer tests.

Table 3-3. Summary of results from the background sorption tracer test.

Tracer	Mass Recovery	Swept Volume (L)		Retardation[1]	
		EW 45	EW 55	EW 45	EW 55
Methanol	100%	6390	5310		
Bromide	115%	8780	6720	1.35	1.26
DMP	108%	7300	5950	1.14	1.12
n-Octanol	92%	4400	4420	0.69	0.83

[1]Retardation relative to methanol.

3.2 Partitioning Tracer Tests

Methods. Prior to conducting each partitioning tracer test, each well was checked for free-phase PCE. Before Test 1, free phase PCE was detected in well 56 only using an electronic

interface probe, and a peristaltic pump was subsequently used to remove approximately three liters of PCE from the well. In Test 3, a bailer attached to threaded PVC pipe sections was used to surge the bailer at the bottom of the well. By this method, free-phase PCE was removed from wells 41 (0.14 L), 46 (1.7 L), 51 (1.2 L), and 53 (0.3 L). The volumes of PCE removed from wells 46 and 51 suggested a large fraction of the PCE was located in the southeast portion of the cell. No free-phase PCE was detected in any wells prior to Tests 2 (based on the electronic-interface probe) and 4 (based on the bailer method).

A double inverted five-spot pattern was used in the first two partitioning tracer tests, which consisted of six extraction wells (41, 44, 46, 51, 54, and 56) located around the perimeter of the test cell and two injection wells (45 and 55) located in the center. In an effort to increase the measured partitioning tracer retardation at the extraction wells, the flow domain was segregated into upper and lower zones. In the injection wells, inflatable packers were used to segregate fluid into the upper and lower portions of the wells. The average saturated thickness of the flow domain was 3.7 m, so the center of the packers were placed at 1.8 m above the clay dividing the flow domains approximately in half. The average flow rate injected into the upper zone and lower zones was 3.7 L/min and 3.1 L/min, respectively. This approach was intended to deliver a suite of tracers into the lower zone in order to focus tracer flow though the suspected location of the DNAPL- contaminated zone. This would then produce higher retardations for the lower-zone tracers compared to a single tracer suite employed without upper-zone/lower-zone vertical separation. In the upper zone, very low retardation was expected. In an effort to provide further spatial resolution of the PCE distribution, unique tracer pairs (Table 3-1) were injected into the lower zone through each injection well. The unique nonpartitioning and partitioning tracers allowed the flow domain to be segregated into eight zones based on the extraction wells BTCs.

The injection/extraction pattern used in Tests 3 and 4 was changed to create a vertical circulating pattern around wells 41, 44, 45, 46, 51, 54, 55, and 56 (Figure 1-1). Each vertical circulation well (VCW) included an inflatable packer (approximately 1.4 m long) installed to isolate a 0.3 m section of well screen above the clay interface. Fluid was pumped through the packer and into the cell over this screen interval between 11.9 and 12.2 m bgs. Due to excessive pressure in the injection tubing in wells 44, 51, and 55, the packers were raised during the test by approximately 0.3 m, so the injection interval in these wells was approximately from 11.6 to 12.2 m bgs. Air bladder extraction pumps were installed such that the pump intakes were approximately 0.2 m above the top of the packers.

Results. A complete listing of moments and swept volumes for nonpartitioning tracers; and moments, retardations, saturations, and PCE volumes for partitioning tracers for each well can be found on the CD in Appendix B. A summary of results from the four partitioning tracer tests are given in Tables 3-4 and 3-5. These tables list the percent mass recovery for all tracers used in each test, swept volume estimates from the nonpartitioning tracers, and PCE volume estimates from the partitioning tracers.

Table 3-4. Summary of results from Test 1 (pre-cosolvent flood) and Test 2 (post-cosolvent flood).

	Test 1			Test 2		
Tracer	Mass Recovery (%)	Swept Volume (L)	PCE Volume (L)	Mass Recovery (%)	Swept Volume (L)	PCE Volume (L)

Upper Zone						
Isopropyl Alcohol[a]	86%	10,800	-	*na*	*na*	-
Isobutyl Alcohol[b]	*na*	*na*	*na*	91%	10,400	-
n-Heptanol	72%	-	0[c]	88%	-	5
2-Ethyl-1-Hexanol[b]	*na*	-	*na*	91%	-	1
Common Lower Zone						
Methanol	97%	3,800	-	89%	4,600	-
n-Hexanol	95%	-	71	90%	-	45
2,4-Dimethyl-3-pentanol	100%	-	33	91%	-	12
2-Octanol	104%	-	22	92%	-	6
3,5,5-Trimethyl-1-Hexonal[b]	*na*	-	*na*	97%	-	4
Unique Lower Zone						
tert-Butyl Alcohol[a, d]	100%	3,200	-	*na*	*na*	*na*
n-Octanol[a, d]	130%	-	16	*na*	*na*	*na*
Isobutyl Alcohol[b, e]	93%	2,500	-	*na*	*na*	*na*
3-Heptanol[b, e]	96%	-	27	*na*	*na*	*na*

[a]Test 1 only; [b]Test 2 only; [c]Retardation of *n*-heptanol relative to isopropyl alcohol was less than one; [d]Applied to injection well 45 only; [e]Applied to injection well 55 only.

Table 3-5. Summary of results from Test 3 (pre-surfactant flood) and Test 4 (post-surfactant flood).

Tracer	Test 3			Test 4		
	Mass Recovery (%)	Swept Volume (L)	PCE Volume (L)	Mass Recovery (%)	Swept Volume (L)	PCE Volume (L)
Methanol	103%	13,100	-	90%	11,800	-
tert-Butyl Alcohol	96%	12,200	-	91%	12,200	-
n-Hexanol	111%	-	191	80%	-	20
2,4-Dimethyl-3-pentanol	101%	-	78	88%	-	31
2-Octanol	106%	-	50	86%	-	30
3,5,5-Trimethyl-1-Hexonal	121%	-	34	90%	-	31

Figure 3-1 summarizes the range in retardation factors measured for each partitioning tracer. As expected, the retardation factors increased with the value of the measured partitioning coefficients. Retardation of *n*-hexanol was general below the suggested minimum acceptable value of 1.2. Jin (1995) showed that, as retardation coefficients decrease below 1.2, the error in the saturation estimate increased. Figure 3-2 summarizes swept volume and PCE volume estimates for each well for Test 1 through Test 4. While the total amount of PCE varied within each test as a function of the partitioning tracer, the proportion of PCE predicted for each well was similar for each partitioning tracer.

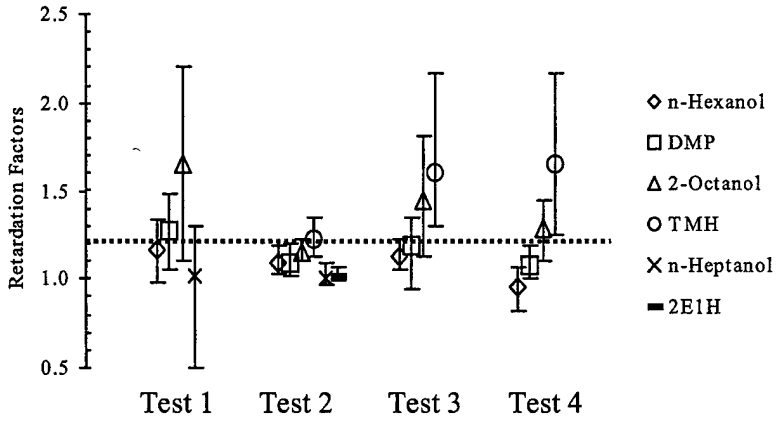

Figure 3-1. Summary of retardation factors from the four partitioning tracer tests. The symbols indicates mean values, and the extent of the bars represents the minimum and maximum values.

First Partitioning Tracer Test (Pre-cosolvent flood). Extraction well 51 had the largest tracer retardation factors. The BTCs for well 51 are shown on a semi-log graph in Figure 3-3, and indicate that the retardation was primarily in the tailing portion of the BTC. This indicated that the NAPL was non-uniformly distributed since a uniform distribution would produce a simple offset of the nonpartitioning and partitioning tracer BTCs (Jawitz et al., 1998). The total volume of DNAPL estimated in the lower-swept zone varied for each partitioning tracer, and ranged from 19 L based on 2-octanol to 61 L based on *n*-hexanol (Table 3-3).

Degradation Corrections. Both the upper-zone nonpartitioning tracer (IPA) and partitioning tracer (n-heptanol) showed poor recovery, and moment analysis of their BTCs produced retardation factors less than one for all wells. This is likely due to tracer degradation since straight–chain alcohols tend to degrade more rapidly in the environment based on the authors' experience in other partitioning tracer field trials. These tracers were not in the original suite of tracers designed for this test but were substituted for pentaflourobenzoic acid and 2,6-dimethyl-4-heptanol when regulatory approval for these tracers was denied just prior to the start of the tracer test. To provide an estimate of the volume of PCE in the upper swept zone, some correction for tracer degradation was required. The simplest approach was to assume a first-order degradation model and estimate the degradation rate constant necessary to recover the injected tracer mass. Each concentration measurement in the BTC is adjusted using:

$$C_{adj} = \frac{C}{e^{-kt}}$$

A) Test 1, Lower zone

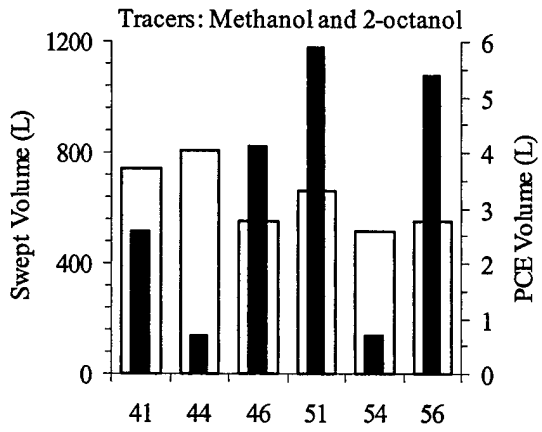

B) Test 2, Lower zone

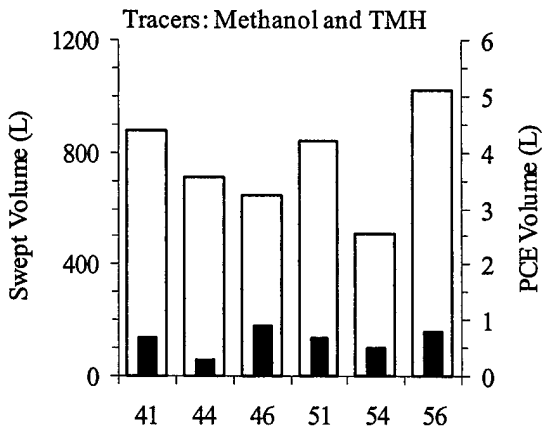

C) Test 1, Upper zone

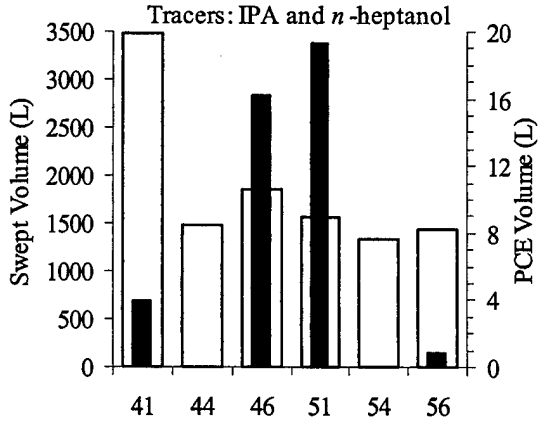

D) Test 2, Upper zone

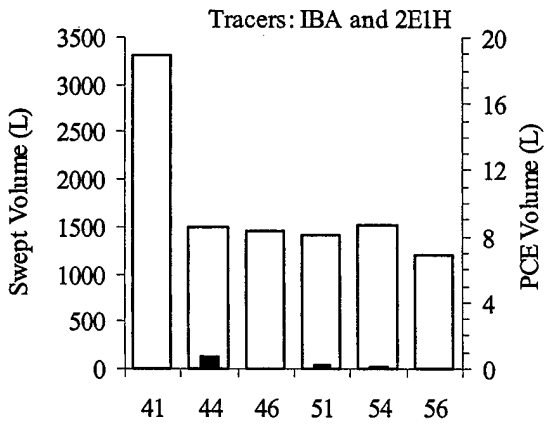

E) Test 3

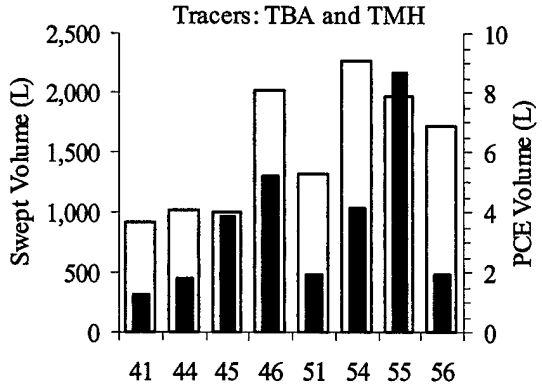

F) Test 4

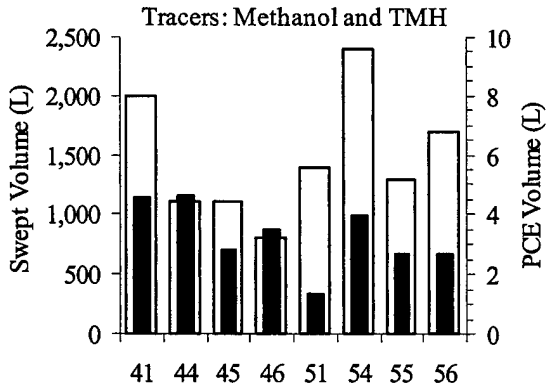

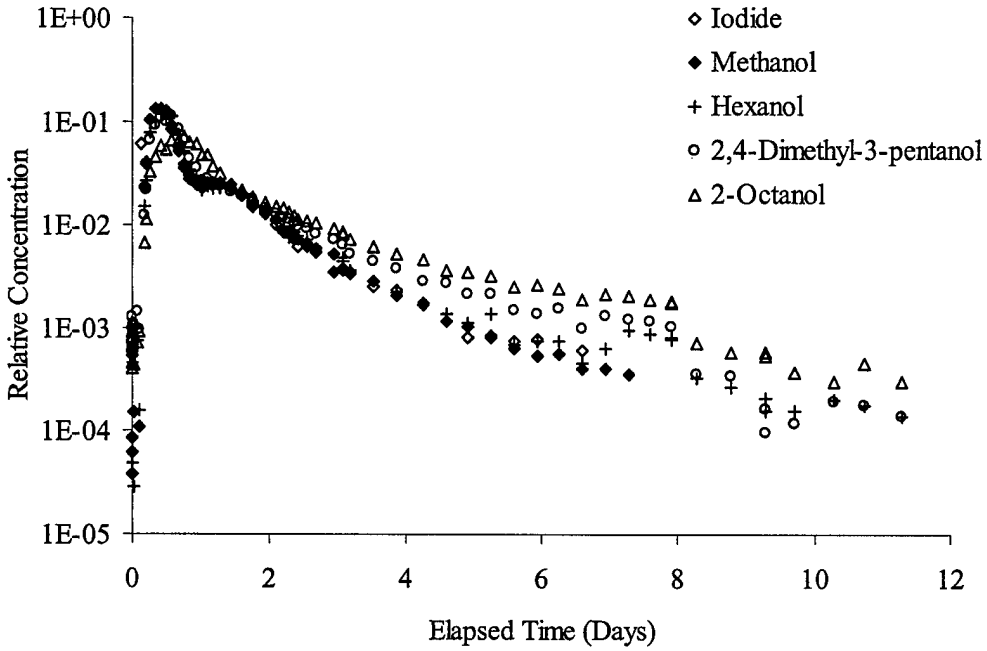

Figure 3-2. Swept volume (white bar) and PCE volume (black bar) estimates per well for A) Test 1, lower zone; B) Test 2, lower zone; C) Test 1, upper zone; D) Test 2, upper zone; E) Test 3; and F) Test 4.

Figure 3-3. Tracer breakthrough curves at well 51 for the common lower zone tracers.

where C is the measured concentration, C_{adj} is the estimated concentration with no degradation, k is the decay coefficient, and t is the time that the sample was collected after the mean of the tracer pulse injection. In recalculating the zeroth moment of each tracer, the degradation coefficient was adjusted to achieve 100% mass recovery. This approach required two critical assumptions: (1) the tracer degradation is assumed to follow first-order kinetics, and (2) a single k value represents the entire test cell. The approach used here ignores the width of the tracer pulse (i.e., Dirac input assumed), but this approximation should have minimal impact on the adjusted moments.

The degradation corrected BTCs for well 51 are shown in Figure 3-4 and the upper-zone tracer moments for all wells are included on the CD in Appendix B. The retardation in two of the extraction wells (44 and 54) remained less than one, and the saturations were assumed zero for summing the NAPL present in the cell. The total volume of PCE estimated using the degradation corrected BTCs was 47 L. This represents a significant volume of PCE relative to the volume of PCE estimated in the lower zone (19 to 61 L). The degradation correction therefore takes on significance in data interpretation for estimating PCE saturation. This also indicates that a substantial fraction of the PCE present in the test cell was in the upper-swept

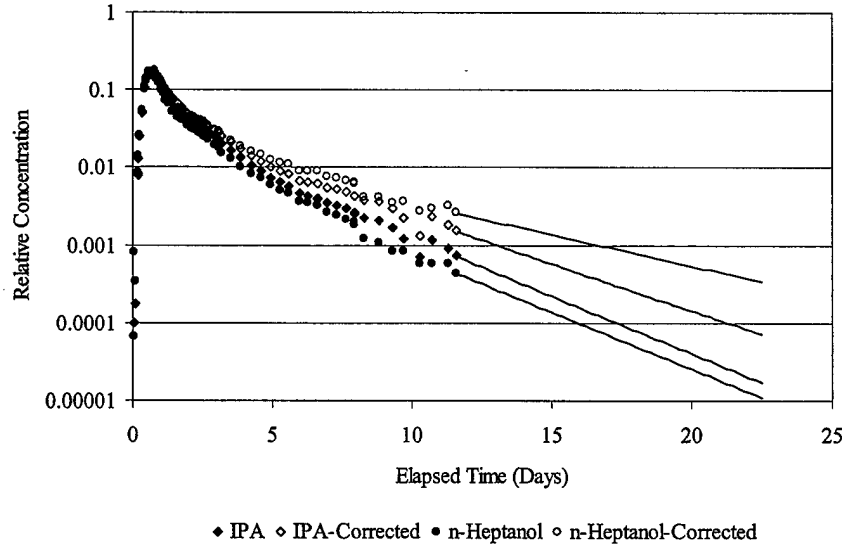

zone. This may indicate that PCE was located higher in the test cell than anticipated based on the release locations, or, the upper-zone tracers traveled into the lower zone further than expected.

Figure 3-4. Upper zone tracer breakthrough curves at EW 51 before and after correction for tracer degradation. The solid line represents the extrapolated portion of the BTCs.

Of the 108 potential multilevel sampling locations, approximately 35 yielded breakthrough responses adequate for moment analysis to determine partitioning tracer retardation. Approximately 60 samplers failed to due faulty valves and system leaks. These problems were later corrected such at that all-108 samplers worked for the post-flushing partitioning tracer test. The multilevel sampler data was used to estimate the spatial distribution of PCE using an inverse modeling approach described by James et al., (1997), and the results are shown in Figure (3-5).

Second Partitioning Tracer Test (Post-cosolvent flood). Tracer mass recoveries ranged from 89% to 97%, and degradation corrections were not considered necessary. The total swept zone, based on nonpartitioning tracers methanol in the lower zone and IBA in the upper zone, was approximately 15,000 L, or 9% smaller than the total swept zone estimated in Test 1 using methanol in the lower zone and IPA (corrected for degradation) in the upper zone. A total of 5.0 L was estimated based on partitioning tracers 2E1H in the upper zone and TMH in the lower-zone (Table 3-4). Three of the six retardation factors using 2E1H were less than 1, and the remaining retardation factors were less than 1.2, which indicates a high degree of uncertainty associated with these results.

Third Partitioning Tracer Test (Pre-surfactant flood). Residual ethanol from the cosolvent flood produced some analytical interference in the methanol laboratory analysis. Consequently, TBA was used as the nonpartitioning tracer in the subsequent analysis. The volume of PCE based on partitioning tracers *n*-hexanol, DMP, 2-octanol, and THM was 191 L, 78 L, 41 L, and 28 L, respectively. Selected tracer BTCs are shown for well 51 in Figure 3-6. As noted for the first tracer test, retardation of the partitioning tracer relative to the nonpartitioning tracer was primarily in the tailing portion of the BTC, indicating a non-uniform NAPL distribution (Jawitz et al., 1998, see Appendix A). A disadvantage to vertical circulation

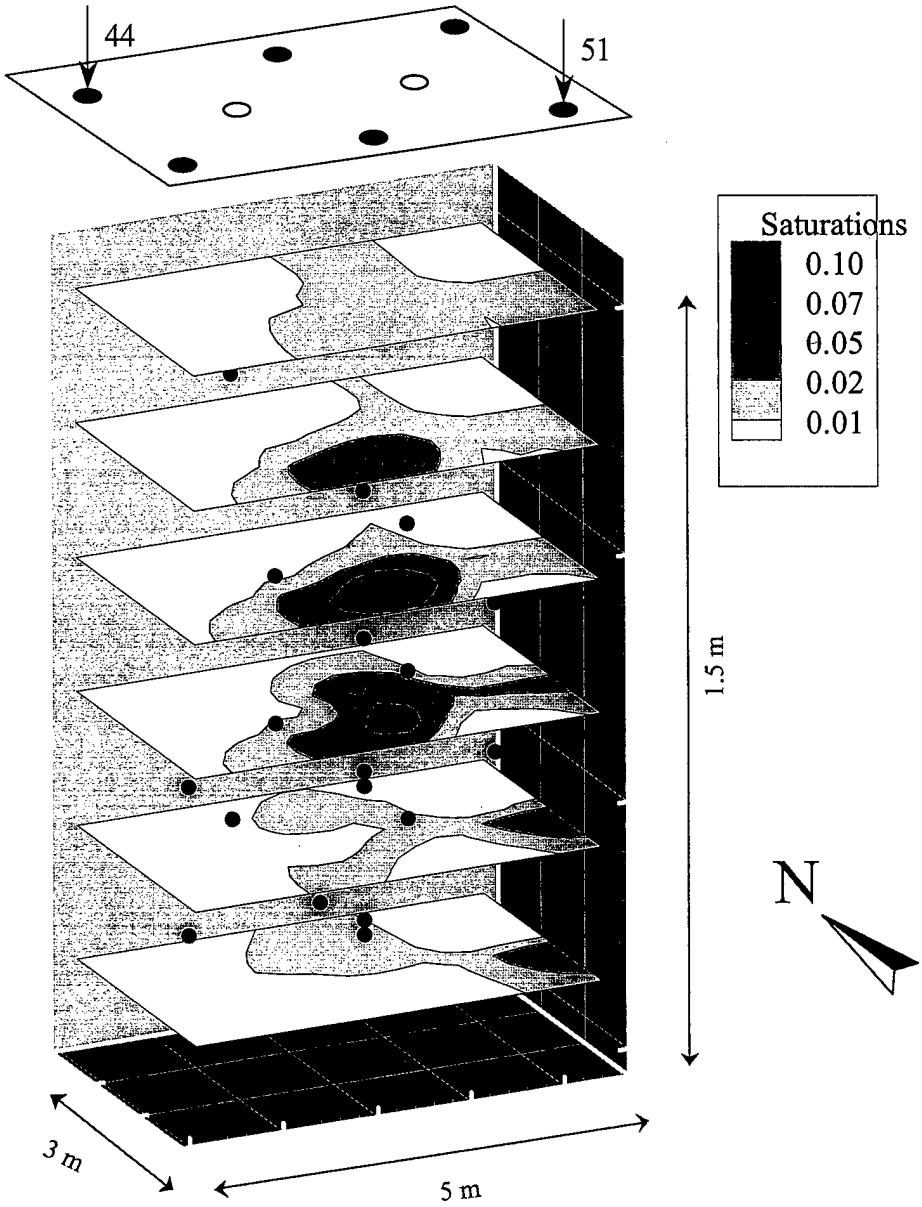

wells is the potential for the tracer to short circuit the formation and flow directly from the injection to extraction portions of the well. The bimodal nature of the BTC from well 51 (Figure

Figure 3-5. Prediction of PCE saturation based on an inverse modeling approach (James et al., 1997) using the MLS data collected from the first partitioning tracer test.

3-6), which was also observed in well 44, is evidence that some short-circuiting occurred in these wells during this test.

Forth Partitioning Tracer Test (Post-surfactant flood). In contrast to the last tracer test where methanol analytical interference was suspected, components use in the surfactant flushing

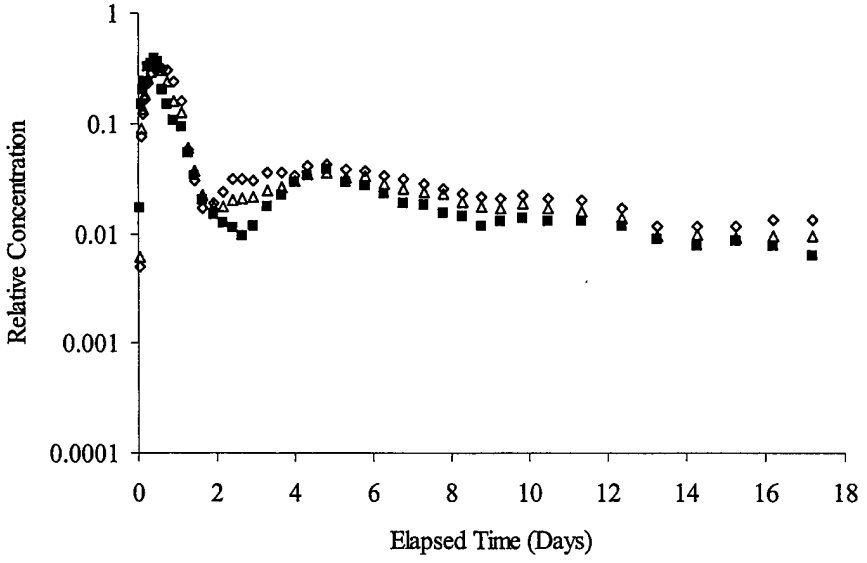

solution interfered with TBA laboratory analysis and methanol was therefore used as the non-reactive tracer. The volume of PCE based on partitioning tracers DMP, 2-octanol, and THM was

Figure 3-6. Breakthrough curves measured during Test 3 at well 51 for *tert*-butyl alcohol (closed squares), 2-octanol (open diamonds), and 3,5,5-trimethyl-1-hexonal (open triangles).

31 L, 27 L, and 26 L, respectively. Partitioning tracer *n*-hexanol indicated 20 L of PCE, but this results was considered suspect given this tracer low mass recovery and the very low retardation factors associated with this tracer. The variability in predicted PCE volumes is much less than the variability from the previous tests. Furthermore, considering the tracer with the highest partitioning coefficient (TMH), there is little difference between the pre- and post-flushing results. On first inspection, this would indicate that little PCE was removed during the surfactant flood. This conclusion, however, is not supported by preliminary results from the surfactant flood. An alternative explanation could be the interference of partitioning tracer behavior by resident surfactants remaining in the cell. Laboratory results using n-hexanol suggest that tracer sorption resulting from surfactant interference could lead to retardation that represents 28 L of PCE, based on 0.24% false saturation (see Section 2.3) times a swept volume of 11,800 L (using methanol, see Table 3-5).

3.3 Discussion

3.3.1. Prediction Uncertainty

How well should the partitioning tracer methodology predict the PCE volume, in the absence of all complicating factors? Recent analyses suggest that for conservatively large errors in fundamental measurements, and for retardation factors of 1.2 or greater, the error in estimated PCE saturations and volumes are on the order of 10% or less, neglecting uncertainties associated with BTC extrapolation (Dwarakanath et al., 1999; Jin et al., 2000; Brooks, 2000). The regulatory permit restricted the PCE release volume to less than 100 L, which resulted in cell-

average PCE residual saturations of 0.005 and 0.0009 for Test 1 and Test 2, respectively, and 0.002 for Test 3 and 4. Thus, only tracers with large K_{nw} are expected to yield retardation factors larger than 1.2 recommended by Jin et al. (1995, 1997). However, non-uniform DNAPL distribution is manifested as extensive tailing in tracer BTCs, even for cases when the retardation factor is greater than or equal to 1.2. As such, moment analysis and PCE volume estimates are complicated by reliance on BTC data extrapolation beyond the region of analytical reliability of measured low tracer concentrations. Thus, all of our tests were performed near the lower limits of the tracer technique's design capabilities. Extrapolation of the BTC using an assumed model (typically an exponential function) is typically employed to minimize truncation errors (Pope et al., 1994; Annable et al., 1998). The extent to which the extrapolation calculations changed the PCE volume predictions in this work can be seen from results provided in Appendix B, and Figure 8 in Brooks et al. (2001, Appendix A). Other extrapolating functions or analysis procedures may prove better suited for accurately predicting the PCE volume.

An assessment of performance between the four tests should also be made with the recognition that, in general, the prediction uncertainty increased for each subsequent tracer test conducted in the cell. This results from factors which are not an inherent part of the partitioning-tracer methodology, but rather, from factors introduced due to the nature of the test setting and the structure of the project. There was also the added complexity of tracer degradation for the upper-zone tracers in Test 1, and the complicating potential for residual cosolvent flushing solution to impact partitioning tracer behavior for Tests 2, 3, and 4.

Other sources of uncertainty include nonlinear tracer partitioning and background tracer sorption. As discussed in Section 2.1, nonlinear tracer partitioning behavior would result in a systematic over prediction of PCE saturation. Results from the background tracer test yielded an equivalent background PCE volume of 52 L based on DMP results. This value represents a significant volume of PCE relative to the maximum release volume of 100 L, and more importantly, it represents a significant volume of PCE relative to the PCE volume estimates obtained in the later tracer tests. Due to potential changes in sorption characteristics after remedial flushing, corrections based on results from the background tracer test were considered inappropriate for tests other than Test 1. Moreover, corrections were only considered appropriate for PCE volume estimates based on DMP, due to potential changes in sorption characteristics for each tracer. Tracers with larger partitioning coefficients may in fact have greater background sorption due to their larger hydrophobicity. Finally, application of background sorption corrections was hindered by changes in the injection/extraction pattern and saturated thickness in the background tracer test and Test 1. Had it been possible to apply corrections for background tracer retardation, the estimated PCE volume would have been systematically smaller.

3.3.2. Hydrodynamic Accessibility

The discrepancy between predicted and expected PCE volumes could be the result of DNAPL migration to locations in the cell which were hydraulically isolated from the tracer flow fields, such as topographic low spots on the clay confining layer or "pools" formed in other locations. The elevation of the clay confining unit varied by approximately 0.6 m across the cell based on the boring log information. Free-phase PCE was collected from well 56 prior to Test 1 and the maximum depth to clay was estimated from the boring log for this well (Figure 1-2). It is possible therefore, that some PCE pooled in the low spot around this well, or other locations

that were lower than detected during coring. Jin et al. (1997) investigated errors in partitioning tracer predictions if pooled DNAPL were present using modeling simulations. The relative error between tracer predicted PCE volumes and expected PCE volumes based on those modeling scenarios are comparable to the relative errors reported herein. Likewise, relative errors reported herein are similar to those reported from laboratory experiments conducted to investigate the impact of preferential flow and physical nonequilibrium on partitioning tracer predictions (Nelson et al., 1999).

Limitations in hydrodynamic accessibility could also have occurred as a result of potential PCE injection into, or migration to layers of low conductivity within the flow field. Limitations in hydrodynamic accessibility could subsequently result as the tracers by-passed these low-conductivity regions. Hydrodynamic accessibility can be evaluated as a function of the pumping pattern for the pre-remedial demonstrations by a comparison of the swept volumes (determined from first normalized moments for the non-reactive tracers). These moments yield swept volume estimates of 16,600 L (Table 3 and 4, methanol for lower zone and IPA, corrected, for upper zone) for Test 1 and 12,200 L for Test 3 (Table 5). Based on the average water elevation over the duration of the test, an effective porosity estimate of 0.29 (0.26 if uncorrected IPA results are used) is obtained for Test 1, and 0.20 to 0.22 is obtained for Test 3 using TBA and methanol, respectively. Therefore, the double five-spot pumping pattern appears to have sampled a larger portion of the cell pore space. This could be explained using the conclusion reached from Chen and Knox (1997) that vertical circulation wells with unequal injection and extraction rates could produce dead zones not swept by the tracers. Since the total injection rate and extraction rate were approximately equal, the entire pore space should have been swept. However, on a more local scale, differences between injection and extraction rates may have contributed to more stagnant zones in the cell compared to the double five-spot pattern. Another disadvantage to vertical circulation wells lies in the potential for the tracer to short circuit the formation and flow directly from the injection to extraction portions of the well. The bimodal nature of the BTC from well 51 (Figure 3-5), which was also observed in well 44, is evidence that some short-circuiting occurred in these wells during Test 3.

3.3.3. Prediction Variability within a Single Test

As indicated by the results summarized in Tables 3-4 and 3-5, the tracers with smaller partitioning coefficients predicted more PCE than tracers with larger partitioning coefficients. It is unclear why this trend was observed, but one possible explanation is rate-limited mass transfer processes. Tracers with larger partitioning coefficients have larger affinities for the NAPL, and may therefore experience more rate-limited desorption than tracers with smaller partitioning coefficients (Heyse et al., 2001). Theoretical analysis (Valocchi, 1985) suggests that the first normalized moment of tracer BTCs, hence the estimated retardation factor, is not expected to be influenced by non-equilibrium sorption/partitioning. Extensive tailing of the BTCs resulting from non-equilibrium processes does increase the higher moments, reflecting increased spreading and tailing. In practice, therefore, underestimation of the first-normalized moment from measured tracer BTCs is likely due to problems of data truncation and errors associated with data extrapolation.

4. COSOLVENT FLUSHING

4.1 Field Methods

4.1.1 System Description

A double five-spot pattern, which consisted of six injection wells along the cell perimeter and two extraction wells in the center (Figure 1-1), was used to inject and extract fluids from the cell during ethanol flushing. This pattern was used because of the flexibility it afforded to target the ethanol to specific regions in the cell. The water level in the cell during the test was maintained at approximately 8.2 m below grade to provide sufficient hydraulic head for MLS operation, and to comply with regulatory requirements for an inward gradient relative to the regional groundwater level. The DNAPL, however, was estimated to be between 10.7 m and 12.2 m below grade based on the depth of the release points and the clay interface. Inflatable packers were therefore placed in each injection and extraction well to focus the ethanol solution to the lower portion of the cell, and to minimize ethanol dilution by separating the flow through the cell into upper and lower zones. Water was injected above the packers into the upper zone and ethanol solution was injected below the packers into the lower zone. Water was injected into the upper zone as a means to minimize upward migration of the ethanol solution injected into the lower zone. The packers were initially positioned to target the ethanol solution to the bottom 0.6 m of the cell in order to dissolve PCE near the clay, and created an alcohol layer to dissolve any PCE mobilized from the higher zones during later phases of the test. The packers were then gradually raised to the full flood-zone height, which corresponded to the bottom of the release points, 10.7 m below grade.

Falta (1998) presented a general discussion of cosolvent flooding performance based on NAPL-water-cosolvent phase behavior. Lunn and Kueper (1997), Hayden et al. (1999), and VanValkenburg (1999) presented phase-behavior information for water-ethanol-PCE systems. The ternary mixture of water-ethanol-PCE is a type II(-) phase system, which implies that two phases (aqueous and NAPL) are formed, with the ternary phase diagram tie lines having negative slopes. This behavior indicates that the ethanol preferentially partitions into water rather than PCE. The main remedial mechanism for type II(-) ternary systems is enhanced dissolution (Brandes and Farley, 1993).

The test began by injecting new 95% ethanol, 5% water solution (hereafter referred to as new ethanol solution) into the lower zone. Lower-zone cosolvent recycling started after the effluent ethanol content was high enough (approximately 70%) to make recycling feasible (6.9 days). The lower-zone fluid was recycled by pumping it through either two or three activated carbon drums in series, or during the latter part of the demonstration, a low profile air stripper and activated carbon drums. [See Hayden et al. (2001, Appendix A) for a detailed discussion on the use of activated carbon to treat effluent, cosolvent solutions.] The recycled ethanol solution was augmented with new ethanol solution as needed to maintain the ethanol content in the influent around 70%. An ethanol content of 70% was chosen to maintain a large PCE dissolution capacity in the solution, yet facilitate cosolvent recycling by minimizing the need to augment treated effluent with the new ethanol solution. Water was injected into the upper zone at the start of the test, and upper-zone recycling started after a sufficient volume of upper zone effluent had been stored (1.0 day). The upper-zone fluid was recycled by pumping it through two activated carbon drums in series.

The total volume of fluid (new ethanol, recycled ethanol, and water) injected into the lower zone was approximately 112,000 L. Recycled ethanol accounted for 47% of the fluid

injected into the lower zone. The total volume of water (containing a small percentage of ethanol) injected into the upper zone was 15,000 L. Recycling accounted for 77% of the fluid injected into the upper zone. The total amount of fluid injected into the lower zone was approximately eight times greater than that injected into the upper zone. Estimates of the number of pore volumes flushed through the upper and lower zones separately are not possible because the location of the separation between the two zones in the cell was not known. However, using the combined upper- and lower-zone extraction volumes, an average water table position of 4 m above the clay, and an effective porosity of 0.20, approximately 10 pore volumes were flushed through the cell.

4.1.2 Performance Monitoring

Samples were collected from the extraction wells and MLSs over the entire test duration (38.8 days). Samples were collected from the injection wells during recycling treatment to monitor the amount of PCE and ethanol that was re-injected into the cell. Influent and effluent samples were collected from each carbon drum and from the air stripper during recycling operations to monitor treatment performance. Samples were refrigerated on-site, and then shipped overnight in coolers to the University of Florida for storage until ethanol and PCE analysis were conducted. Samples were analyzed for ethanol by GC/FID. Samples were analyzed for PCE by a similar GC/FID method, as well as liquid chromatography using a packed column, UV detection, and a methanol (70%) and high performance liquid chromatography grade water (30%) mixture as the mobile phase. If free phase PCE was observed in sample vials in the laboratory, an acetone extract was used to dissolve the free phase PCE, and the sample was then analyzed by the GC/FID method.

Selected samples were analyzed in the field using a field GC to provide real-time information for operational decisions. Density measurements were also completed in the field using specific-gravity hydrometers. Injection and extraction flow rates, and water levels in the cell were monitored throughout the demonstration to maintain a steady flow field to the extent possible. Adjustments to influent flow rates were made in accordance with these data to minimize water-level fluctuations in the cell. Additional details about the procedures used in the ethanol flush can be found in Brooks (2000), and Brooks et al., (2001, Appendix A).

4.2. Results

PCE concentrations and the ethanol percentages from extraction well samples are plotted in Figure 4-1. The ethanol content in the lower zone increased over the first 5 days as the new

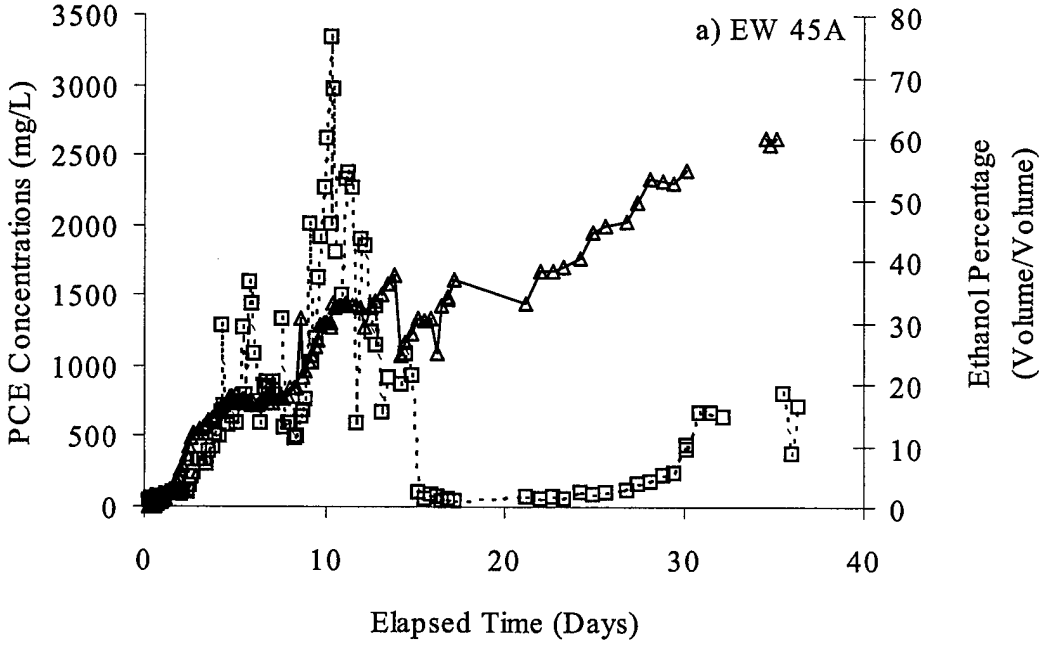
a) EW 45A
PCE Concentrations (mg/L)
Ethanol Percentage (Volume/Volume)
Elapsed Time (Days)
0
500
1000
1500
2000
2500
3000
3500
0
10
20
30
40
0
10
20
30
40
50
60
70
80

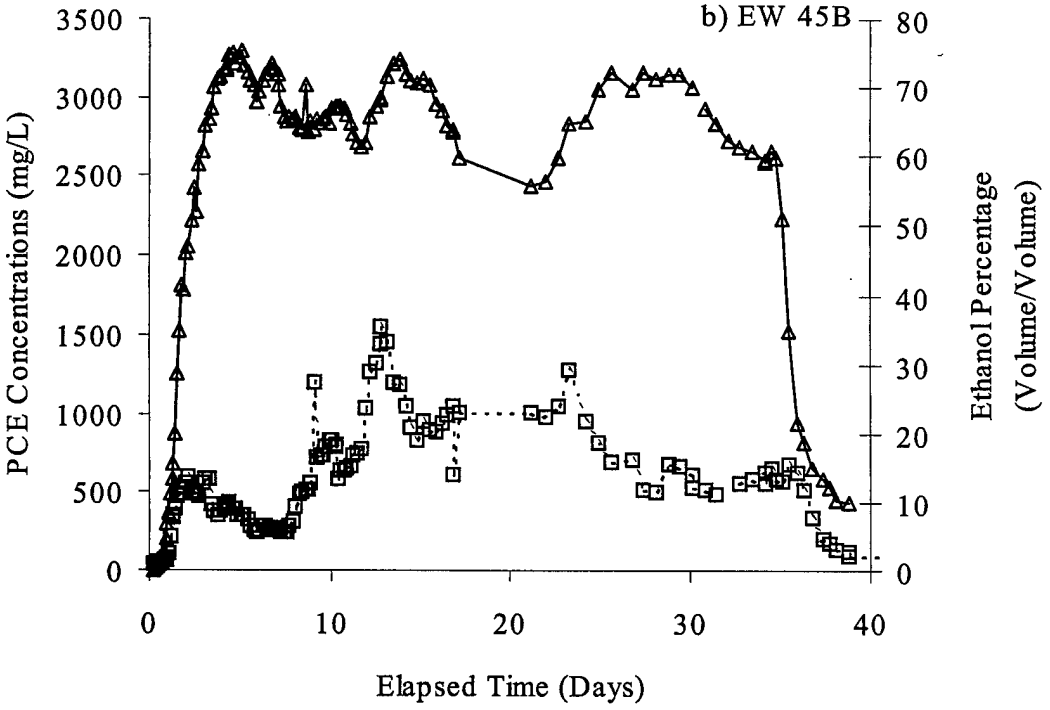
b) EW 45B
PCE Concentrations (mg/L)
Ethanol Percentage (Volume/Volume)
Elapsed Time (Days)
0
500
1000
1500
2000
2500
3000
3500
0
10
20
30
40
0
10
20
30
40
50
60
70
80

Figure 4-1. PCE concentrations (squares) and ethanol percentages (triangles) from a) upper zone extraction well 45A, and b) lower zone extraction well 45B.

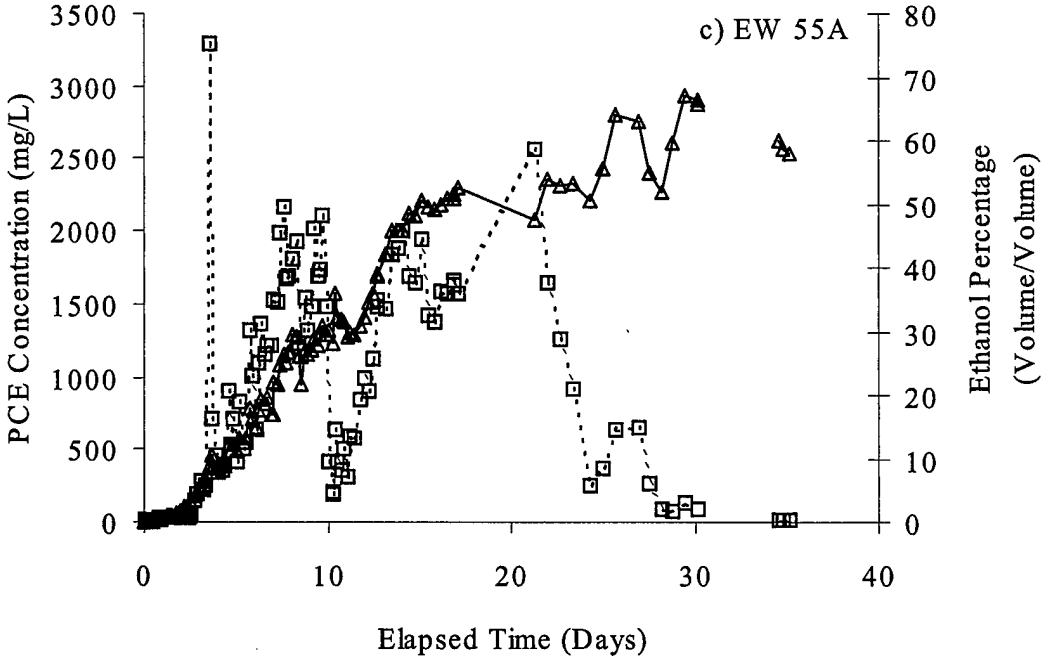
c) EW 55A
PCE Concentration (mg/L)
Ethanol Percentage (Volume/Volume)
Elapsed Time (Days)
0
500
1000
1500
2000
2500
3000
3500
0
10
20
30
40
50
60
70
80
0
10
20
30
40

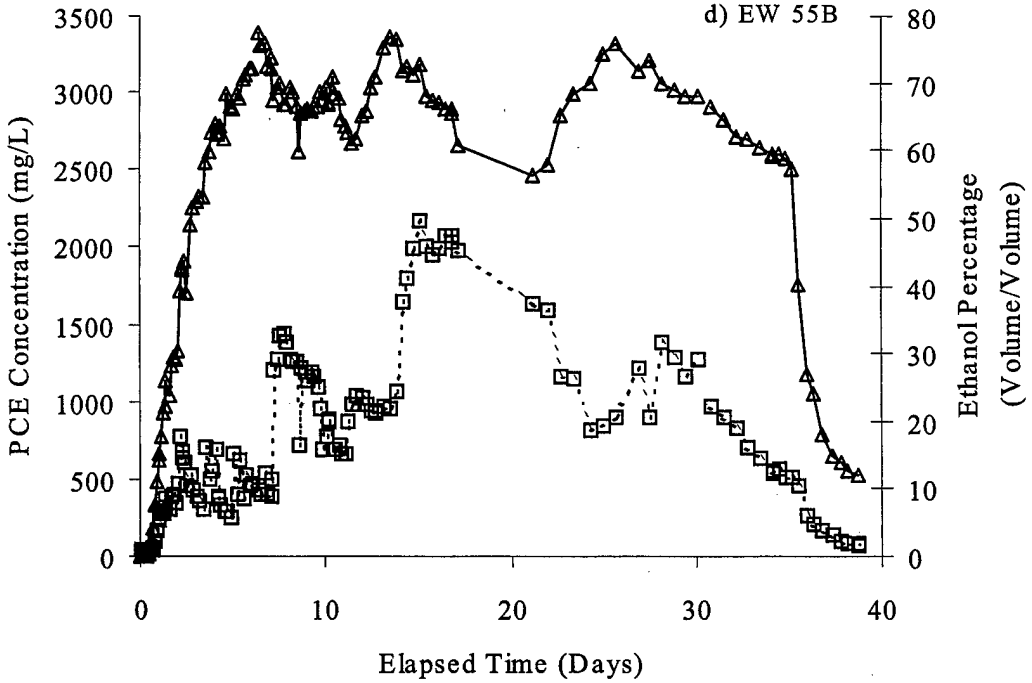
d) EW 55B
PCE Concentration (mg/L)
Ethanol Percentage (Volume/Volume)
Elapsed Time (Days)
0
500
1000
1500
2000
2500
3000
3500
0
10
20
30
40
50
60
70
80
0
10
20
30
40

Figure 4-1 continued. PCE concentrations (squares) and ethanol percentages (triangles) from c) upper zone extraction well 55A, and d) lower zone extraction well 55B.

95% ethanol solution displaced the resident water in the test cell. Changes in the ethanol content after approximately 5 days resulted from changes in flushing operations (i.e., ethanol recycling, ethanol augmentation, and changes in packer positions). Injection well 51 was converted to an extraction well for a 4-day period late in the test to help target the cosolvent solution to a nearby area of high concentration. Ethanol content and PCE concentrations from well 51 during this period are not shown in Figure 4-1. The ethanol content in the effluent from this well varied between 58 to 65%, and the PCE concentration varied from 1300 to 2300 mg/L.

The ratio of aqueous PCE concentration to PCE solubility limit for extraction wells 45 and 55 were investigated as a function of time (See Brooks et al., 2001, Figure 5-3, Appendix A). Separators were installed in the extraction well effluent lines to remove any free-phase PCE from the effluent. Over the course of the entire test, only 0.35 ± 0.01 L of free-phase PCE was collected from the upper-zone separators, and no free-phase PCE was collected from the lower-zone separators. The relatively small volume of free-phase PCE collected from the separators was supported by the fact that free-phase PCE was not observed when extraction well effluent samples were collected. The formation of an emulsion is the most likely explanation for the discrepancy between free-phase PCE volumes observed during the test, and those estimated from the laboratory samples. It is suspected that the emulsion formed in the extraction wells, rather than in the aquifer, due to mixing which diluted the ethanol content in the well, resulting in free-phase PCE formation and subsequent emulsification.

Free phase PCE was observed in only 16 of more than 5000 MLS samples collected, and only at selected depths in MLS locations 12 and 14. The majority of these observations occurred within the first day after the start of alcohol flushing. The PCE ranged from small drops, approximately 1 mm or smaller in diameter, to slugs no greater than 20 mL in volume. Concentrations of PCE in excess of estimated PCE solubility limits occurred in 56 samples (out of approximately 1500 samples analyzed) at selected depths in MLS locations 12, 14, 21, 25, 32, 41, 43, and 63. However, only at MLS locations 12, 14, 25, 41, and 63 were concentrations observed significantly higher than the solubility limit (>1.5 times the solubility limit). The difference in the number of observations of free-phase PCE during sample collection, and the number of samples with PCE concentrations greater than PCE solubility limits is also attributed to the formation of an emulsion as pore fluids converged and mixed in the samplers. The majority of these samples occurred within the first 5 days after the start of alcohol flushing. Furthermore, free-phase PCE was not detected in the well sumps using the interface probe when they were investigated prior to the start of the post-flushing partitioning tracer test. Based on this evidence, it is considered that limited mobilization occurred during alcohol flushing.

The PCE concentrations in the lower-zone extraction well effluent were well below the PCE solubility limits after approximately 3 days (See Brooks et al., 2001, Figure 5-3, Appendix A). The low PCE concentrations relative to PCE solubility could have resulted from mixing at the extraction wells, or from mass-transfer limitations. During the demonstration, the longest flow interrupt occurred from 17.5 to 20.9 days, when the system was intentionally turned off to investigate mass-transfer limitations. In general, evidence of mass-transfer limitations are manifested by increases in effluent contaminant concentrations after the flow interrupt (Brusseau

et al., 1997). No evidence of mass-transfer limitation is apparent from the breakthrough curves shown in Figure 4-1. Localized mass-transfer limitations may have occurred, but were not observed as elevated PCE concentrations in the extraction well effluent. Therefore, effluent PCE concentrations were most likely observed to be less than the PCE solubility limit due to mixing at the extraction wells.

4.2.1. PCE Recovery

Approximately 52.6 ± 0.7 L of PCE were removed from the test cell, based on the zeroth moment of the PCE breakthrough curves measured at the extraction wells. The error estimate for the amount of PCE extracted was based on the propagation of errors in volume and concentration measurements through the zeroth moment calculations. Errors in volume measurements (±25 L) were based on one half of the smallest division of the tank volume scale, and errors in concentration were conservatively assumed to be ±15% of the measured concentration. Using an average PCE concentration (2096 ± 51 mg/L) based on all MLS samples analyzed, the total volume of fluid removed by the MLSs during the test (916 ± 42 L), and the volume of free-phase PCE removed through the MLSs (0.08 ± 0.04 L), the total amount of PCE removed by the MLSs was estimated at 1.3 ± 0.1 L. Thus, the total amount of PCE removed from the test cell by the extraction wells and the MLSs was 53.9 ± 0.7 L, while that injected during alcohol recycling was estimated at 0.5 ± 0.04 L. Therefore, the net amount of PCE removed from the cell was estimated to be 53.4 ± 0.7 L.

All extracted fluids were stored in three tanks at the end of the demonstration. Samples were collected from each tank and were analyzed for PCE and ethanol. A second estimate of the PCE removed from the test cell was obtained by adding the amount of PCE in the storage tanks to the amount of PCE removed by activated carbon and air stripping treatment. Based on the tank volumes and PCE concentrations, the mass of PCE in the tanks at the end of the demonstration was 19 ± 3 L. Based on influent and effluent treatment samples, the volume of PCE removed by activated carbon was 16.6 ± 0.9 L, and the amount removed by air stripping was 11.1 ± 0.8 L. The preceding errors are based on assumed errors of 15% for the treatment volumes and 15% for the influent and effluent concentrations. This tank-based approach yielded an estimate of 47 ± 3 L of PCE, which is 11% less than the 53 L estimated from the extraction well and MLS samples. The tank-based estimate could be less because the tank samples were collected from valves located on the bottom of the tanks, and density-driven vertical segregation of fluids may have occurred. This would result in a non-uniform distribution of PCE within the tank, as more PCE would tend to dissolve in the higher ethanol fraction fluid accumulated at the top of the tank due to its lower density. Due to such potential bias in the tank-based estimate, the previous estimate of 53 L is considered more robust.

4.2.2. Ethanol Recovery

A total of 41,700 L of 95% ethanol solution was delivered to the test cell. Through recycling operations, the total amount of ethanol injected into the test cell over the course of the test was 69,400 L. A total of 62,500 L of ethanol, or 90% of that injected, was recovered from

the test cell during alcohol flushing and water flooding, and an additional 3,800 L were removed during the post-cosolvent flood partitioning tracer test, yielding a total ethanol recovery of 96%. Samples collected during the pre-surfactant flood partitioning tracer test were also analyzed for ethanol, and from those results, only an additional 390 L more ethanol were removed.

4.3 Recycling Treatment

To our knowledge, this is the first cosolvent-flushing demonstration in which an alcohol cosolvent effluent was treated and re-injected. Activated carbon drums were used to treat the effluent alcohol solution for the first two-thirds of the demonstration. Hayden et al. (2001, Appendix A) discuss the use of activated carbon to treat effluent, cosolvent solutions. Influent and effluent aqueous PCE concentrations from each drum were monitored and drums were removed from service once the effluent PCE concentration equaled the influent PCE concentration. Approximately 3 to 6 L of PCE was adsorbed in each drum before PCE breakthrough occurred. For the final third of the demonstration, a series combination of air stripping and activated carbon was used to evaluate cosolvent recycling by air stripping. The average air-stripping treatment efficiency was 91%. Ethanol content was not significantly affected by either the activated-carbon or air-stripping treatment processes. The ethanol content in the effluent samples after the treatment processes was reduced by an average of approximately 1% relative to the influent ethanol content. Cosolvent recycling was a significant factor in this demonstration, as evident by the fact that the volume of alcohol solution delivered to the test cell, and consequently, the volume of PCE removed from the test cell, were approximately doubled by recycling.

5. PERFORMANCE EVALUATION

5.1 Comparison to Release Information

Release Details. The release of PCE into the cell was designed to produce a DNAPL distribution within the target flow zone between 10.7 and 12.3 m bgs. Researchers from EPA conducted the release by pumping selected volumes of PCE down the release tubes to a depth of 10.7 m, at a typical flow rate of 0.57 L/min for the first release, and a higher, typical rate of 0.90 L/min for the second release. The intent of the release method was to encourage lateral and vertical spreading of PCE in the formation while minimizing pooling of the DNAPL on the clay-confining unit, and therefore minimize the potential for downward migration of PCE through natural fractures in the clay or openings produced during sheet pile installation. Results from controlled releases in 2-dimensional physical models and numerical simulations suggested that DNAPL would initially spread laterally along the water table and migrate downward as the DNAPL head increased or the water table elevation was lowered. Thus, the water table elevation in the test cell was manipulated to facilitate first horizontal and then vertical spreading of the DNAPL. The water table elevation was positioned at approximately 0.3 m below the release tubes prior to PCE injection. Water was extracted from the cell during and immediately after the DNAPL release and continued until the transient water table elevation was approximately 0.3 m

above the clay interface. Tap water was then injected into the cell to raise the water table to an elevation above the PCE injection level. The total volume of PCE injected during the first

A) First PCE Release

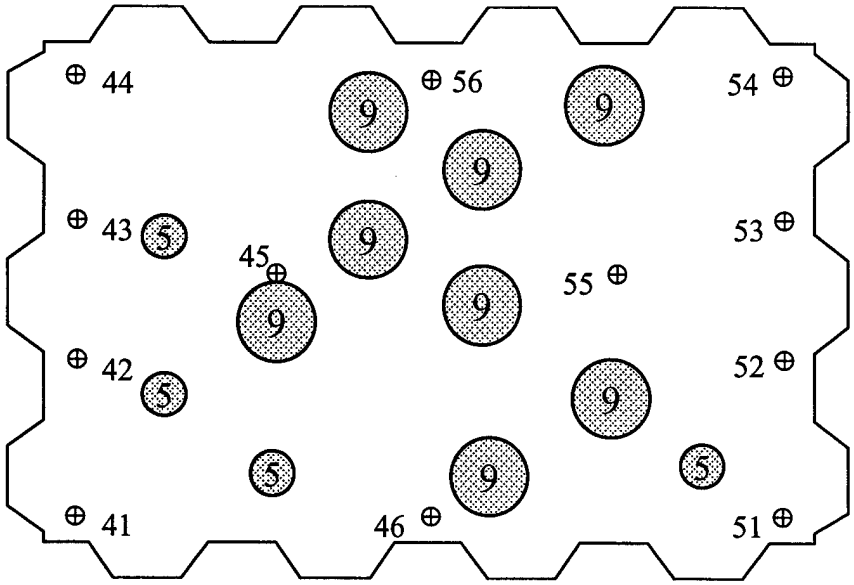

release was 91.7 L, and the total volume of PCE injected during the second release was 49.4 L. The spatial injection patterns for the first and second releases are shown in Figure 5-1.

B) Second PCE Release

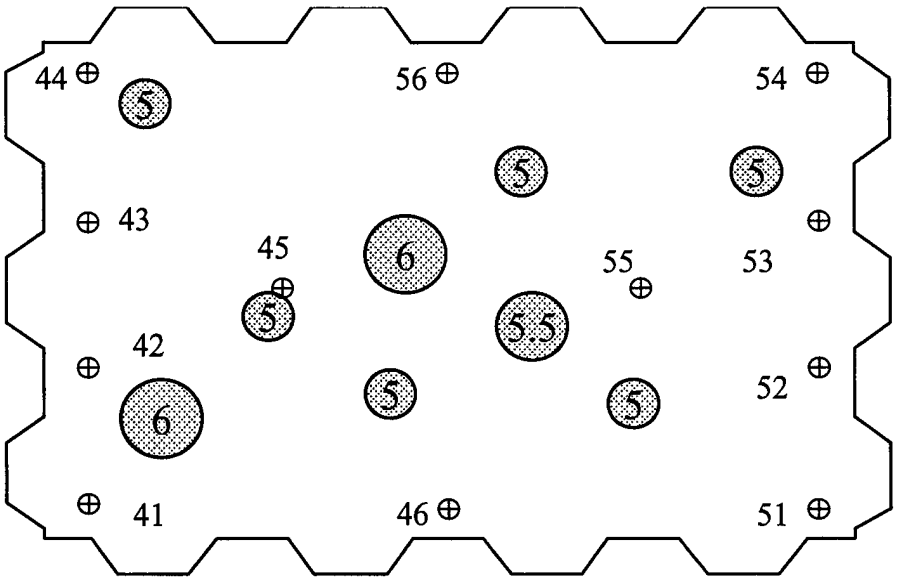

Figure 5-1. PCE injection locations and volumes for A) the first and B) second controlled release. The PCE release volume per location is indicated in liters by the number within the circles. (Plan view).

5.1.1 Partitioning Tracer Tests

Comparison of First Release to Tracer tests 1 and 2. The line-drive conservative tracer test conducted by EPA (Table 5-1) removed 3 L of PCE through dissolution by flushing approximately 5 pore volumes of water through the cell, and another 3 L of PCE were removed as free product from well 56 prior to the start of tracer Test 1. Therefore, 86 L of PCE were in the cell at the start of tracer Test 1. Using only the lower-zone tracer results of 2-octanol, since this tracer displayed the largest retardation factors and therefore presumably yields the most reliable volume estimates, 22 L were predicted, or 26% of the expected volume. Using lower-zone 2-octanol results and degradation-corrected, upper-zone *n*-heptanol results, 69 L or 80% of

Table 5-1. Volume (L) of PCE injected and extracted from the cell.

Item	Added	Removed	Volume in Place
First Controlled DNAPL released	91.7		91.7
Amount at the start of Line-Drive Test			91.7
Removed by dissolution during Line-Drive Test		3.1	
Free-phase removed from EW 56 prior to Test 1		2.8	
Amount at the start of Test 1			85.8
Removed by dissolution during Test 1		2.6	
DNAPL removed by MLSs prior to flush		0.2	
Amount at the start of ethanol flood			83.0
Total removed though EWs		52.6	

Total removed through MLSs		1.2	
DNAPL removed through MLSs		0.08	
Total PCE injected through recycling	0.5		
Net PCE extracted		53.9	
Amount at the start of Test 2			29.6
Removed by dissolution during Test 2		1.14	
Amount left from first demonstration			28.5
Removed by Vertical Circulation Test		0.35	
Second Controlled DNAPL released	49.4		
Free-phase removed prior to Test 3		3.3	
Amount at the start of Test 3			74.3
Removed by dissolution during Test 3		4.0	
DNAPL removed by MLSs prior to flush		0.2	
Amount at the start of surfactant flood			70.1
Net PCE extracted by surfactant flood		48.9	
Amount at the start of the fourth Test 4			21.2
Removed by dissolution during Test 4		0.73	
Remaining at the completion of 2nd Demo.			20.4

the expected volume was predicted. These comparisons neglect degradation of PCE as well as the dissolved PCE mass. Approximately 2 L (assuming equilibrium dissolution) or less of PCE may have been resident in solution when the tracer test was initiated and would not be part of the tracer estimate. Accounting for the mass of PCE removed by tracer Test 1 and the cosolvent flood (Brooks, 2000), 30 L of PCE were estimated in the cell at the start of tracer Test 2. The estimate of the PCE in the cell, based on the upper- and lower-zone tracers with the largest partitioning coefficients was 5 L, or 17% of the expected value. A spatial comparison between the PCE release pattern and the predicted spatial pattern in given by Brooks et al. (2001, Appendix A).

It is apparent that both tracer tests underestimated the volume of PCE present in the test cell, based on the results of tracers with the largest partitioning coefficients. In terms of PCE volume, the first two tracer tests underestimated the amount of PCE released into the cell by about 17 L to 25 L. This might suggest that 17 L to 25 L of PCE were not hydraulically accessible to the tracers. This NAPL could have been pooled on the clay or located in isolated corners or regions of the test cell. The fact that the cosolvent flood failed to remove approximately 30 L of NAPL may also support this conclusion (see Section 5.1.2). The fact that the pre-flushing tracer test has high uncertainties caused by degradation of the upper zone tracers must be recognized when reaching this conclusion.

Comparison of Second Release to Tracer Tests 3 and 4. The comparison of results from the third tracer test to the second release information must be made recognizing that the level of uncertainty of this comparison is higher than the first comparison due to the activities conducted in the cell prior to the second PCE release (i.e., first PCE release and cosolvent flood). If the basis for evaluating the tracer predictions is the total PCE estimated in the cell at the start of the third tracer test, then the expected PCE volume is 74 L (28.5 L remaining from the cosolvent demonstration, plus 49.4 L injected during the second release, minus 3.7 L removed between the release and the start of Test 3 as either free-phase or dissolved PCE). Based on the tracer with retardation factors consistently larger than 1.2 (TMH), the predicted PCE volume is 33 L (Table

3-5), or approximately 45% of the expected volume. Based on the mass of PCE removed during tracer Test 3, and preliminary results from the surfactant flood, the amount of PCE in the cell at the start of tracer Test 4 was 21 L. Based on the TMH results from Test 4, the predicted PCE volume was 30 L, or 143% of the expected volume.

5.1.2 Cosolvent and Surfactant Flushing

The volume of PCE in the test cell at the start of the alcohol flushing test was 83.1 L (Table 5-1). The performance of the alcohol-flushing test was judged using this value. The flushing demonstration removed 53.4 L of PCE, which is 64% of the 83.1 L of PCE estimated in the test cell at the start of the test. Therefore, approximately 29.7 L of PCE remained in the cell at the end of the demonstration. Figure 5-2 presents the aqueous PCE concentrations from field analysis of MLS samples collected 32.3 days after the start of the test. Based on this figure, areas of high concentrations are evident near MLS locations 25 and 12, which supports the conclusion that a significant volume of PCE was left in the test cell.

By comparison, the volume of PCE estimated in the cell at the start of the surfactant flushing test was 70.1 L of PCE (Table 5-1). The surfactant flushing demonstration removed 48.9 L

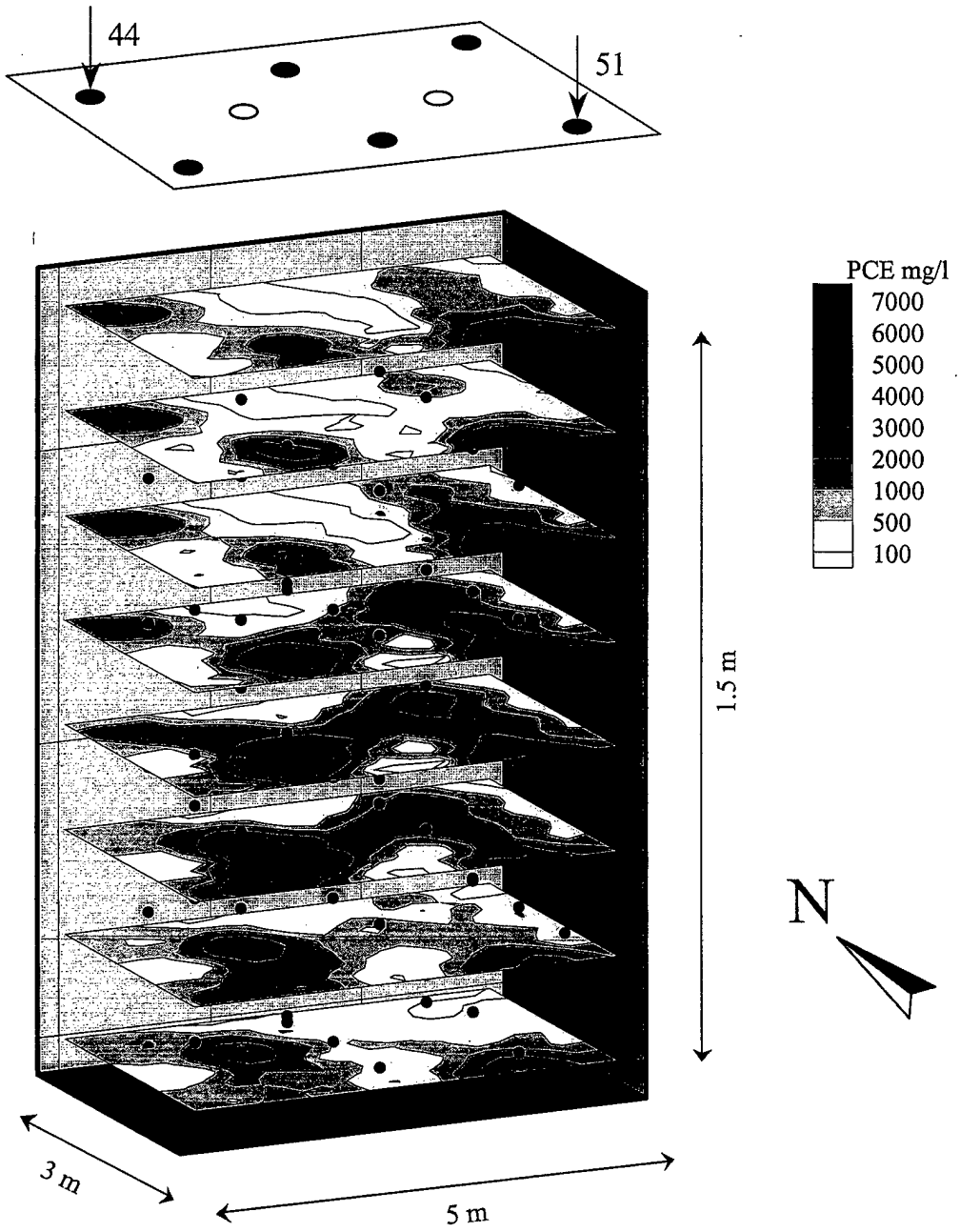
44
51
PCE mg/l
7000
6000
5000
4000
3000
2000
1000
500
100
1.5 m
N
3 m
5 m

Figure 5-2. Aqueous PCE distribution based on MLS samples from the end of the ethanol flushing demonstration.

(based on preliminary data), which is 70% of the 70.1 L of PCE estimated in the cell at the start of the surfactant flood. By this comparison, it is apparent that the surfactant demonstration preformed better than the cosolvent demonstration. However, the main remedial mechanism for both cosolvent and surfactant floods is dissolution. Under the conditions used in the two demonstrations, the PCE solubility in the cosolvent solution was on the order of 80,000 to 100,000 mg/L (see Figure 2-3), and the PCE solubility in the surfactant solution was on the order of 40,000 mg/L. Under equal conditions, the cosolvent solution would be expected to remove more mass. However, the contaminant distributions and the pumping patterns were different between the two tests, both of which must be appropriately considered when comparing results between the cosolvent and surfactant floods.

5.2. Efficiency and Effectiveness

The contaminant volume removed divided by the volume of flushing fluid has been used to describe the efficiency of in-situ flushing remediation systems (Jawitz et al., 1997; Sillan et al., 1998b). Efficiency is defined here as the cumulative volume of DNAPL removed per cumulative volume of applied remedial fluid. If the volume of remedial fluid is limited to the ethanol delivered to the test cell, then the cell-averaged removal efficiency was $1x10^{-3}$ liters of PCE per liter of ethanol (53 L PCE/ 41,700L ethanol). If the volume of remedial fluid includes the total amount of ethanol and water injected from the start of the demonstration to the start of the final water flood, then the removal efficiency was $6x10^{-4}$ liters of PCE per liter of injected fluid (53 L PCE/ 94,500 L ethanol and water). An estimate of pump-and-treat performance in the test cell can be made based on the amount of PCE removed during Test 1 (the pre-flushing partitioning tracer test). A removal efficiency of $2x10^{-5}$ is obtained by the ratio of PCE removed to the volume of water flushed through the cell. Therefore, the removal efficiency for alcohol flushing was 30 times better than the pump-and-treat efficiency. Table 5-2 compares the removal efficiencies from this study to those of other field-scale, source-zone remedial demonstrations. Removal efficiencies from this study were comparable to the other DNAPL remedial demonstration conducted in Jacksonville, Florida, but were less than those calculated for the studies conducted at Hill AFB. This may be explained by the fact that the contaminant at Hill AFB was a more homogeneously distributed light NAPL (LNAPL), and would therefore allow for more efficient contact with the flushing solution.

Removal efficiencies, calculated as cumulative PCE volume removed per cumulative extracted volume, are shown for each well in Figure 5-3 as a function of time. Once the extraction well packers were raised to their maximum height at 13.9 days, the removal efficiencies in extraction wells 45A, 45B, and 55A remained constant at approximately $4x10^{-4}$ to $5x10^{-4}$, while the removal efficiency in 55B remained constant at approximately $6x10^{-4}$ to $7x10^{-4}$. This indicates that PCE mass removal was fairly constant during the demonstration. This further suggests that continued flushing should have increased removal effectiveness, but this was prevented because of personnel limitations, project schedule, and budget considerations. Based on the constant removal efficiencies indicated in Figure 5-3, it is estimated that a significant

portion of the remaining PCE could have been removed if the demonstration had been continued. Neglecting decreases in performance resulting from diminishing NAPL content, it is estimated that the majority of the remaining PCE (30 L) would have been removed if the system had been operated for another 3 weeks. However, this prediction is inconsistent with the fact that both pre- and post-flushing partitioning tracer tests underestimated the volume of DNAPL by approximately 17 to 25 L. Assuming that between 17 to 25 L of PCE was inaccessible to both the partitioning tracers and to the ethanol-flushing solution, the removal efficiency may have substantially decreased due to contact limitations before the majority of the remaining DNAPL was removed. Temporary extraction well 51B had the highest removal efficiency of approximately $1x10^{-3}$, which may suggest an advantage to changing the flow field during flushing when hot spots are identified.

Table 5-2. Comparison of removal efficiencies from several source-zone remedial demonstrations.

Demonstration	Location	NAPL Type	Removal Efficiency[1]	Removal Efficiency[2]	Reference
Enhanced Dissolution by ethanol flushing	DNTS, Delaware	DNAPL (PCE)	0.002 to 0.0007	0.001 to 0.0006	
Enhanced Dissolution by ethanol flushing	Jacksonville, Florida	DNAPL (PCE)	0.001	0.001	Sillan et al., 1999
Enhanced Dissolution by ethanol flushing	Hill AFB, Utah	LNAPL (multi-component)	0.005		Rao et al., 1997; Sillan et al., 1997
Enhanced Dissolution by surfactant flushing	Hill AFB, Utah	LNAPL (multi-component)	0.005		Jawitz et al., 1998
Mobilization and enhanced dissolution by cosolvent flushing	Hill AFB, Utah	LNAPL (multi-component)	0.01		Falta et al., 1999
Enhanced Dissolution by Cyclodextrin flushing	Hill AFB, Utah	LNAPL (multi-component)	0.007		McCray and Brusseau, 1998
Dissolution by water (pump-and-treat)	DNTS, Delaware	DNAPL (PCE)		0.00002	
Dissolution by water (pump-and-treat)	Hill AFB, Utah	LNAPL (multi-component)		0.0002 to 0.000001	Rao et al., 1997; Sillan et al., 1997

[1]Removal efficiency based on partitioning tracer results; [2]Removal efficiency based on mass in flushing effluent.

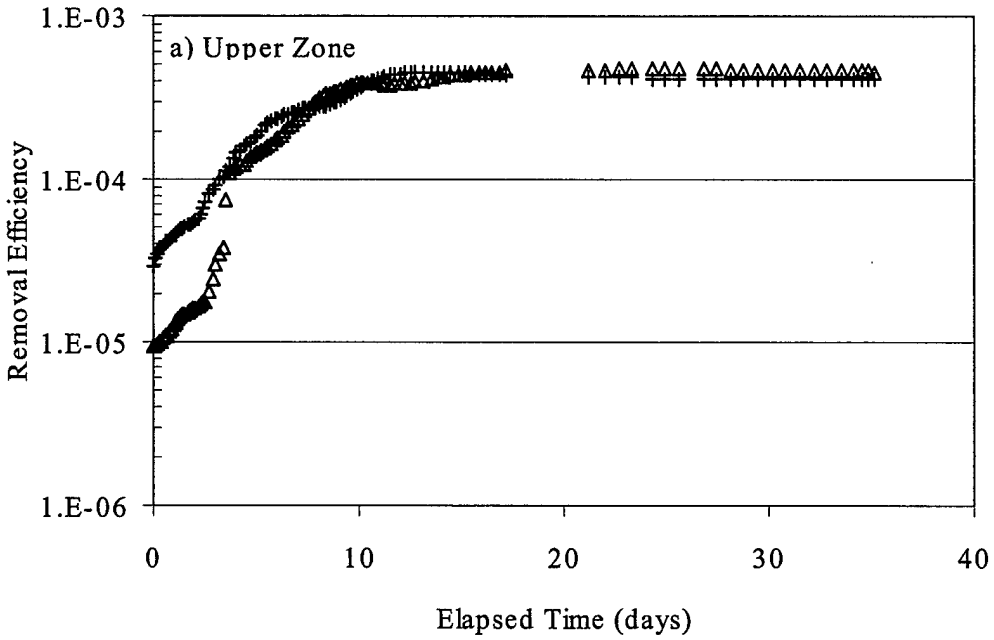
a) Upper Zone
Removal Efficiency
1.E-03
1.E-04
1.E-05
1.E-06
0
10
20
30
40
Elapsed Time (days)

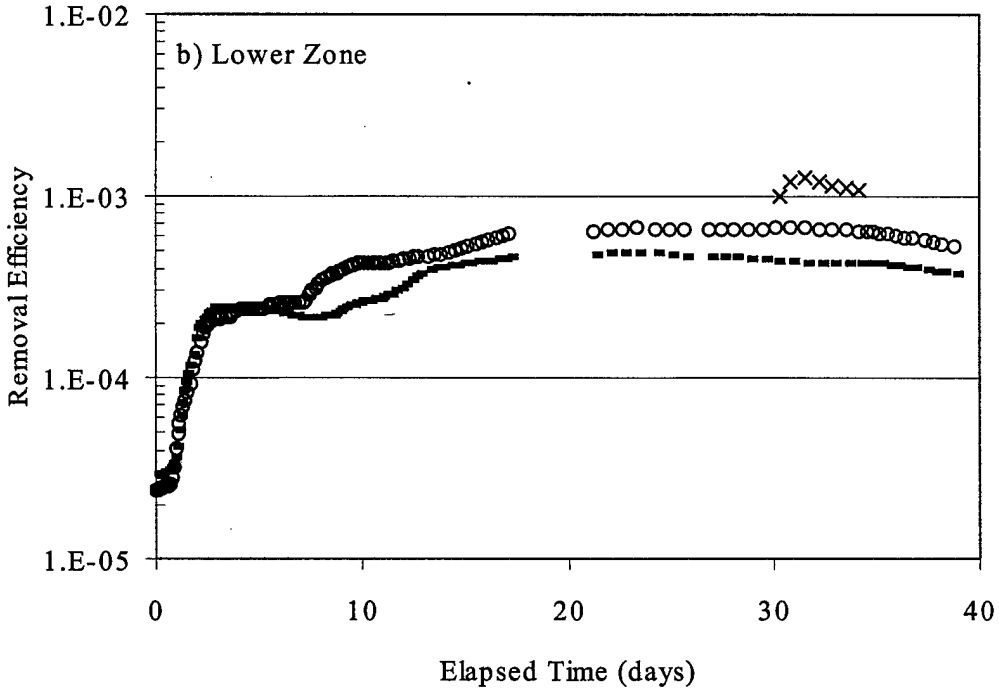
b) Lower Zone
Removal Efficiency
1.E-02
1.E-03
1.E-04
1.E-05
0
10
20
30
40
Elapsed Time (days)

Figure 5-3. Removal efficiency for a) upper zone: 45A (plus symbols) and 55A (triangles); and b) lower zone: 45B (minus symbol), 55B (circles), and 51B (x).

Jawitz et al. (1997) defined removal effectiveness as the fraction of cumulative volume removed within a swept zone. The overall average reduction in PCE volume from the lower zone in the test cell was 82%, based on the pre- and post-flushing partitioning tracer tests (This estimate increases to 93% if the upper zone tracer results are included). This remedial performance estimate is higher than the performance estimate (64%) based on the comparison of

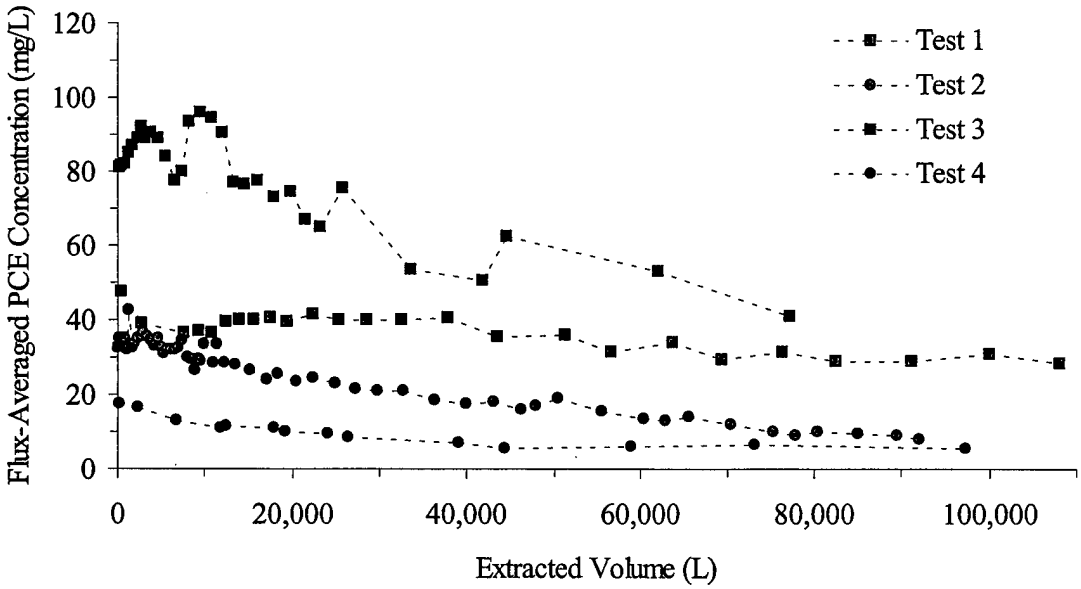

released and extracted PCE volumes. It is concluded that both partitioning tracer tests underestimated the PCE volume in the test cell, and the underestimate of PCE volume in the post-flushing partitioning tracer test is the principle reason for the overestimate of remedial performance. Factors which limited contact between the tracers and PCE may also have limited contact between the alcohol solution and the PCE, which may explain the low PCE recovery (64%) for the alcohol flood.

5.3. Aqueous PCE Concentrations

Fluxed-averaged PCE concentrations, calculated on a cell-wide basis, are shown in Figure 5-4 for Tests 1 through 4. It is readily apparent from this figure that the PCE concentration in the effluent from Test 3 (pre-surfactant flood) was higher than the effluent PCE concentration from Test 1 (pre-cosolvent flood). The largest difference between the two lies in the beginning of the tests, however, the line-drive tracer test (not shown) was conducted prior to Test 1, and the discrepancy between Test 1 and Test 3 may be explained, at least in part, by this fact.

Figure 5-4. Flux-averaged PCE concentrations based on the total cell effluent from the partitioning tracer tests.

The flux-averaged aqueous PCE concentrations from extraction well samples collected at the end of the pre-flushing partitioning tracer test ranged from 8 mg/L (EW 44) to 47 mg/L (EW 51). Subsequent to flushing, reductions in aqueous concentrations were observed in all extraction wells. The flux-averaged aqueous PCE concentrations from extraction well samples collected at the end of the post-flushing partitioning tracer test ranged from 6 mg/L (EW 44) to 19 mg/L (EW 41). The aqueous PCE concentrations changed the least in extraction wells 41, 44, and 54 (percent reductions of 37%, 25%, and 23%, respectively). These three wells also had the lowest PCE removal effectiveness based on the partitioning tracer test results. Larger decreases in aqueous PCE concentration were observed in extraction wells 46, 51, and 56 (percent reductions of 79%, 77%, and 72%, respectively), which correspond to the wells with the higher values of removal effectiveness. The apparent correlation between removal effectiveness and flux-averaged aqueous concentrations (Figure 5-5) supports the use of removal effectiveness as a measure of remedial performance. More importantly, these data suggest that partial reductions in DNAPL mass can result in decreased flux-averaged aqueous PCE concentrations, at least under forced-gradient conditions. A similar analysis using TMH results from the pre- and post-surfactant flushing tracer tests is prevented by the suspected interference in partitioning behavior by residual surfactant solution.

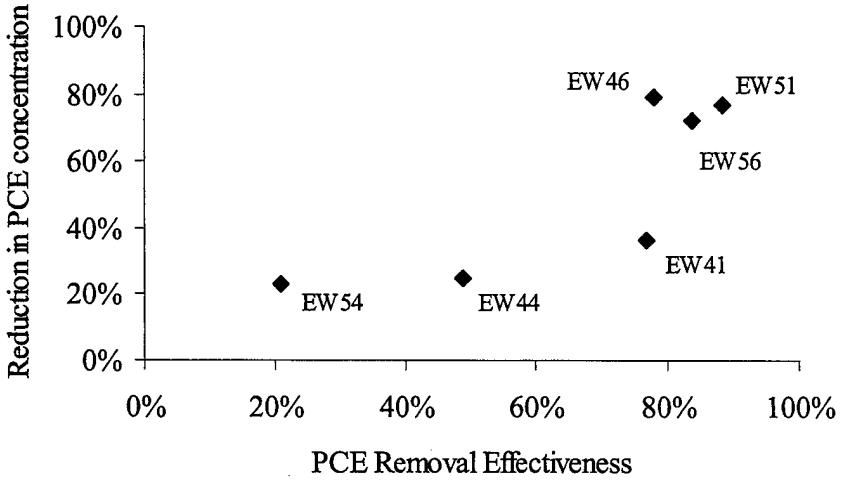

Figure 5-5. DNAPL removal effectiveness versus reduction in PCE concentrations, based on tracers with the largest partitioning coefficients.

6. INTERPRETIVE SUMMARY

Characterization of source zones is the first step for designing and implementing remediation strategies that are cost-effective in risk reduction at sites contaminated with DNAPLs. Also, decisions related to long-term stewardship for managing the dissolved plume and the impacts of source remediation also depend on best information available from site characterization efforts. Hydrogeologic heterogeneity and highly variable distribution of

DNAPLs pose two major challenges in attempts at site characterization and source remediation at most sites. During the last decade, innovative technologies have been introduced and field-tested for source zone characterization and remediation. Partitioning tracers technique has received a great deal of attention for quantifying DNAPL volume and distributions within the source zone. While the scientific basis for the tracer technique is sound and method is inherently robust, claims of success need to be tempered by three major constraints: (1) the exact volume of the DNAPL present at the sites is never known with certainty, and at best can be guessed based on site history and records of use and disposal; (2) alternative, traditional techniques (e.g., soil coring) used to verify the results of the tracer tests are themselves prone to significant uncertainty, unless large number of samples are taken at a prohibitive cost; and (3) errors, uncertainties and artifacts introduced by the manner in which the tracer tests are conducted and the data are processed/interpreted may lead to significant underestimation or overestimation of the DNAPL volume present within the test zone. Inability to estimate the initial DNAPL volume and distribution also constrains an unbiased assessment of the field-scale performance of aggressive, in-situ techniques for extraction (e.g., flushing) or destruction (e.g., oxidation) of DNAPLs from source zones.

In recognition of these difficulties, the US EPA sponsored a SERDP-funded series of field tests at the DNTS to evaluate tracer techniques and in-situ flushing techniques. The project goals were to address three major questions: (1) how well do the tracer tests perform in characterizing the DNAPL source zone? (2) what is the effectiveness and efficiency of in-situ flushing technologies perform in extracting the DNAPL? and (3) where is the unextracted DNAPL and what are its impacts on resident- and flux-averaged concentrations of the DNAPL in groundwater. The experimental strategy adopted by the US EPA was to design field tests in isolated test cells in which a single-component DNAPL was released to create a source zone. These tests were conduct as a series of "double blind" tests in which (1) the US EPA scientists released a known volume of PCE at specific locations at a specific rate, but did not know the resulting spatial distribution of the PCE; and (2) the university researchers who conducted the tracer and flushing studies were unaware of the volume of PCE or the release strategies used by US EPA. Only at the end of the tracer and flushing tests did EPA reveal the information to the university researchers, and then the performance of the characterization and remediation techniques was assessed using the release information. Each university team conducted two tracer tests (pre- and post-remediation) and one flushing test. The in-situ flushing techniques for enhanced extraction of PCE evaluated were: (1) alcohol flooding for either solubilization or mobilization; (2) surfactant flushing; (3) air sparging; and (4) cyclodextrin flushing. Since the initial volume of PCE present in the test cell was known for each of these flushing demonstrations, the absolute and relative performance of these source extraction techniques can be evaluated.

The University of Florida (UF) team conducted four tracer tests, two subsequent to a PCE release, and two after in-situ flushing. The team also conducted the in-situ flushing with ethanol for enhanced solubilization of PCE, and supported the University of Oklahoma team in conducting the surfactant-flushing test. This report summarizes only the results from the four tracer tests and the alcohol-flushing test; others will report the findings from the subsequent tracer and flushing tests.

The regulatory permit issued for the tests restricted the total volume of the PCE released by EPA in to the test cell to be less than 100 liters. The resulting average PCE residual saturation was about 0.01. Such a low residual saturation, and the resulting tracer retardation, presented a

challenging task in designing the tests and in interpreting the data for DNAPL quantification while operating at the lower limits of reliability of the technique. Various experimental strategies (e.g., pumping patterns, vertical segregation of wells, multiple tracers) were attempted to overcome this fundamental constraints, and were met with varying degree of success. However, in the first three tracer tests conducted by the University of Florida team, the PCE volume known to be present in the test cell was underestimated by 80% to 17% based on tracers with the largest partitioning coefficients. Results from the last partitioning tracer test predicted PCE more PCE than expected (143% for the tracer with the largest partitioning coefficient). However, the similarity in predicted PCE volumes between Test 3 and Test 4 (pre- and post-surfactant flushing), at least for the tracers with the highest partitioning coefficients, does not agree with the preliminary results of PCE volume removed during the surfactant flood, and calls into question the reliability of the test results. The volume of PCE not detected suing the tracer tests was assumed to be located in regions that have significant limitation of hydrodynamic access. Given that these tests were conducted in confined cells, this performance was not expected, especially since it has been reported by several investigators that laboratory tracer tests performed in large flow chambers performed better. The UF tracer tests at DNTS also revealed several unanticipated complications, ranging from tracer losses via degradation to increased background adsorption of tracers due to sorption of the surfactant on the aquifer matrix. Careful attention should be paid to recognizing and eliminating such artifacts in tracer test data analysis and interpretation.

In-situ ethanol flushing, using a double five-spot well pattern, resulted in enhanced PCE solubilization without apparent mobilization. During the ethanol flood, pore-water concentrations of PCE measured using a network of multi-level samplers exceeded 50,000 mg/L in several instances, while the flux-averaged PCE concentrations in the extracted fluids reached a maximum of 3,400 mg/L. The ethanol flood was terminated after 39 days, and resulted in the extraction of about 53 liters. This represents an average extraction effectiveness of 64% (i.e., 53 L extracted of the initial 83 L). As in the tracer tests, it is surmised that the PCE not extracted might be located in zones with limited hydrodynamic accessibility during the ethanol flood. However, high PCE concentrations in extracted fluids just prior to termination of alcohol injection do suggest that more PCE could have been extracted if the flushing had been continued. The efficiency of PCE extraction by the ethanol flood was estimated to be approximately 10^{-3}. This low efficiency was achieved in spite of the facts that the extracted fluids were treated and re-injected. The efficiency for the Dover test was about an order of magnitude less than that for another alcohol flushing field test conducted by the UF team at the Sages dry cleaner site in Florida. The lower efficiency is attributed to greater hydrogeologic heterogeneity at the DNTS site compared to more homogeneous formation at the Sages site.

Preliminary data from more recently completed flushing tests conducted by other university teams at the DNTS indicate that PCE extraction effectiveness was about the same as that achieved in our alcohol-flushing test. However, a comparison of the relative performance of different flushing tests must take in to account the fact that (1) the mechanism governing enhanced PCE extraction is different in each test, (2) the pumping strategies and the resulting flow patterns are different, and (3) the initial spatial distribution of PCE was different even though the total volume was essentially similar. In spite of these differences, these results lend further support to our suggestion that about 30% of the released PCE might be located in inaccessible regions within the test cell. Indirect evidence for the spatial distribution of the PCE remaining in the cell is provided by the data for dissolved PCE concentrations measured using

the network of multi-level samplers. Aqueous PCE concentrations, however, do not tell us much about the volume of PCE that might be present at these MLS sampling locations; they only indicate the presence of DNAPL within the zone of sampling at each location. Direct evidence to confirm this hypothesis can only be provided by soil coring at the end of the tests at DNTS, an activity planned by US EPA.

Another performance metric used to evaluate the in-situ alcohol flushing was the reduction in flux-averaged PCE concentrations in extracted fluids from six wells. The double, five-spot pumping strategy used during the tracer tests and the ethanol flood allowed the estimation of PCE removal effectiveness within six swept zones in the test cell. The data suggest that for wells that had higher effectiveness (i.e., greater fraction of initial PCE was removed) also had larger decreases in flu-averaged PCE concentration as a result of the alcohol flushing. In fact, the non-linear relationship ($y = \alpha x^{\beta}$; $\beta < 1$) between the removal effectiveness (x) and flux-concentration (y) was consistent with predictions based on recent modeling of source-zone remediation (see Rao et al., 2001; Enfield et al., 2001) and at variance with conclusions reached by others (Sales and McWhorter, 2000). We conclude that DNAPL mass removal from source zones might provide some direct, short-term benefits (e.g., flux reduction), but whether the magnitude of such contaminant flux reductions is sufficient to reduce risks and/or alter the dissolved plume behavior or whether such mass removal is cost-effective have yet to be determined. Such issues are the topics of current technical debates and regulatory policy concerns.

The test results do prompt several important practical questions. What was the impact of the DNAPL scenario on the resulting spatial distribution of the DNAPL? How would the initial PCE spatial distribution have been altered if PCE was released in the *vadose zone* and allowed to enter and distribute within the saturated zone? Which strategies would be more successful in extracting the PCE left within the test cell, and not extracted by different flushing agents tested to date? Can other remediation strategies (e.g., oxidation, thermal, electrokinetic) remove or destroy the PCE left behind? What reductions in risk had been achieved by the removal of about 60 to 70% of the PCE? Answering these questions is a task left to further studies at DNTS or other sites.

7. REFERENCES

Annable, M.D., Rao, P.S.C., Graham, W.D., Hatfield, K., Wood, A.L., 1995. Use of partitioning tracers for measuring residual NAPL distribution in a contaminated aquifer: Preliminary results from a field-scale test. 2nd Tracer Workshop, Austin, TX, pp. 77-85.

Annable, M.D., Rao, P.S.C., Hatfield, K.H., Graham, W.D., Wood, A.L., Enfield, C.G., 1998. Partitioning tracers for measuring residual NAPL: Field-scale test results. *Journal of Environmental Engineering*. 124 (6), 498-503.

Brandes, D., and K. Farley, 1993. Importance of phase behavior on the removal of residual DNAPLs from porous media by alcohol flooding. *Water Environment Research 65*, 869-878.

Broholm, K., S. Feenstra, and J. A. Cherry, 1999. Solvent release into a sandy aquifer. 1. Overview of source distribution and dissolution. *Environmental Science Technology*, 33(5), 681-690.

Brooks, M.C., 2000. Characterization and remediation of a controlled DNAPL release: field study and uncertainty analysis. Ph.D. Dissertation, University of Florida, Gainesville, Florida, 147 pp.

Brooks, M.C., Annable, M.D., Rao, P.S.C., Hatfield, K., Jawitz, J.W., Wise, W.R., Wood, A.L., C.G. Enfield, 2000. Field-scale cosolvent flushing of DNAPL from a controlled release. In review, *Water Resources Research.*

Brooks, M.C., Annable, M.D., Rao, P.S.C., Hatfield, K., Jawitz, J.W., Wise, W.R., Wood, A.L., C.G. Enfield, 2001. Controlled Release, Blind Tests of DNAPL Characterization using Partitioning Tracers. In review, *Journal of Contaminant Hydrology.*

Brooks, S.C., Taylor, D.L., Jardine, P.M., 1998. Thermodynamics of bromide exchange on ferrihydrite: Implications for bromide transport. *Soil Science Society of America Journal,* 62(5), 1275-1279.

Brusseau, M.L., Nelson, N.T., Cain, R.B., 1999. The partitioning tracer method for in-situ detection and quantification of immiscible liquids in the subsurface. In *Innovative Subsurface Remediation, Field Testing of Physical, Chemical, and Characterization Technologies*, ACS Symposium Series 725, edited by M.L. Brusseau, D.A. Sabatini, J.S. Gierke, and M.D. Annable, American Chemical Society, Washington, D.C., 208-225.

Brusseau, M. L., Q. Hu, and R. Srivastava, 1997. Using flow interruption to identify factors causing nonideal contaminant transport. *Journal of Contaminant Hydrology*, 24(3-4), 205-219.

Cain, R.B., Johnson, G.R., McCray, J.E., Blanford, W.J., Brusseau, M.L., 2000. Partitioning tracer tests for evaluating remediation performance. *Ground Water*, 38(5), 752-761.

Cooke, C.E., Jr., 1971. Method for determining residual oil saturation. U.S. Patent 3,590,923., U.S. Patent Office, Washington, D.C.

Dean, H.A., 1971. Method for determining fluid saturation in reservoirs. U.S. Patent 3,623,842, U.S. Patent Office, Washington, D.C.

Dwarakanath, V., Deeds, N., Pope, G.A., 1999. Analysis of partitioning interwell tracer tests. *Environmental Science and Technology,* 33(21), 3829-3836.

Falta, R.W., Lee, C.M., Brame, S.E., Roeder, E., Coates, J.T., Wright, C., Wood, A.L., Enfield, C.G., 1999. Field test of high molecular weight alcohol flushing for subsurface nonaqueous phase liquid remediation. *Water Resources Research*, 35(7), 2095-2108.

Falta, R. W., 1998. Using phase diagrams to predict the performance of cosolvent floods for NAPL Remediation. *Ground Water Monitoring and Remediation*, 18(3), 94-102.

Hayden, N. J., Brooks, M.C., Annable, M.D., Zhou, H., 2001. Activated carbon for the removal of tetrachloroethylene (PCE) from alcohol solutions, Accepted by *Journal of Environmental Engineering.*

Hayden, N. J., J. Diebold, and G. Noyes, 1999. Phase behavior of chlorinated solvent + water + alcohol mixtures with application to alcohol flushing. *Journal of Chemical and Engineering Data*, 44(5), 1085-1090.

Hayden, N.J., Linnemeyer, H.C., 1999. Investigation of partitioning tracers for determining coal tar saturation in soils. In *Innovative Subsurface Remediation, Field Testing of Physical, Chemical, and Characterization Technologies*, ACS Symposium Series 725, edited by Brusseau, M.L., Sabatini, D.A., Gierke, J.S., Annable, M.D., American Chemical Society, Washington, D.C., 208-225.

Heyse, E., Augustijn, D.C.M., Rao, P.S.C., Delfino, J.J., 2001. Nonaqueous phase liquid dissolution and soil organic matter sorption in porous media: Review of system similarities. *CRC Critical Reviews in Environmental Control* (In Review; submitted March 2001).

Imhoff, P. T., S. N. Gleyzer, J. F. Mcbride, L. A. Vancho, I. Okuda, and C. T. Miller, 1995. Cosolvent-enhanced remediation of residual dense nonaqueous phase liquids: experimental investigations. *Environmental Science and Technology*, 29(8), 1966-1976.

James, A.I., Graham, W.D., Hatfield, K., Rao, P.S.C., Annable, M.D., 1997. Optimal estimation of residual NAPL saturations using partitioning tracer concentration data. *Water Resources Research*, Vol. 33, No. 12, pp. 2621-2636.

Jawitz, J.W., Sillan, R.K., Annable, M.D., Rao, P.S.C., Warner, K., 2000. In-situ alcohol flushing of a DNAPL source zone at a dry cleaner site. *Environmental Science and Technology*, 34(17), 3722-3729.

Jawitz, J.W., Annable, M.D., Rao, P.S.C., Rhue, R.D., 1998a. Field implementation of a winsor type I surfactant/alcohol mixture for in situ solubilization of a complex LNAPL as a single-phase microemulsion. *Environmental Science and Technology*, 32(4), 523-530.

Jawitz, J.W., Annable, M.D., Rao, P.S.C., 1998b. Characterizing the spatial distribution of non-aqueous phase contaminants using partitioning tracers and the method of moments. International Conference and Special Seminars on Groundwater Quality: Remediation and Protection, IAHS, Tubingen, Germany, 422-425.

Jawitz, J. W., R. K. Sillan, M. D. Annable, and P. S. C. Rao, 1997. Methods for Determining NAPL Source Zone Remediation Efficiency of In-Situ Flushing Technologies, *In Situ Remediation of the Geoenvironment*, Proceedings of the Conference, Minneapolis, Minnesota, Geotechnical Special Publication No. 71, 271-283.

Jin, M., Delshad, M., Dwarakanath, V., McKinney, D.C., Pope, G.A., Sepehrnoori, K., Tilburg, C., Jackson, R.E., 1995. Partitioning tracer test for detection, estimation, and remediation performance assessment of subsurface nonaqueous phase liquids. *Water Resources Research*, 31(5): 1201-1211.

Jin, M., Delshad, M., Dwarakanath, V., McKinney, D.C., Pope, G.A., Sepehrnoori, K., Tilburg, C.E., 1995. Partitioning tracer test for detection, estimation, and remediation performance assessment of subsurface nonaqueous phase liquids. *Water Resources Research*, 31(5), 1201-1211.

Jin, M., Butler, G.W., Jackson, R.E., Mariner, P.E., Pickens, J.F., Pope, G.A., Brown, C.L., McKinney, D.C., 1997. Sensitivity models and design protocols for partitioning tracer tests in alluvial aquifers. *Ground Water*, 35(6): 964-972.

Kueper, B. H., D. Redman, R. C. Starr, S. Reitsma, and M. Mah, 1993. A field experiment to study the behavior of tetrachloroethylene below the water table: spatial distribution of residual and pooled DNAPL. *Ground Water*, 31(5), 756-766.

Lee, C.M., Meyers, S.L., Wright, C.L., Jr., Coates, J.T., Haskell, P.A., Falta, R.W., Jr., 1998. NAPL compositional changes influence partitioning coefficients. *Environmental Science and Technology*, 32(22), 3574-3578.

Lowe, D. F., C. L. Oubre, and C. H. Ward, editors, 1999. *Surfactants and Cosolvents for NAPL Remediation, A Technology Practices Manual.* Lewis Publishers, Boca Raton, 412 pgs.

Lunn, S. R. D., and B. H. Kueper, 1997. Removal of pooled dense, nonaqueous phase liquid from saturated porous media using upward gradient alcohol floods. *Water Resources Research*, 33(10), 2207-2219.

MacKay, D. M., and J. A. Cherry, 1989. Groundwater contamination: Pump-and-treat remediation. *Environmental Sciences and Technology*, 23(6), 630-636.

McCray, J.E., and Brusseau, M.L., 1998. Cyclodextrin-enhanced flushing of multiple-component immiscible organic liquid contamination at the field scale: Mass removal effectiveness. *Environmental Science & Technology*, 32(9), 1285-1293.

Nelson, N.T., Oostrom, M., Wietsma, T.W., Brusseau, M.L., 1999. Partitioning tracer method for the in situ measurement of DNAPL saturation: Influence of heterogeneity and sampling method. *Environmental Science & Technology*, 33(22), 4046-4053.

Nelson, N.T., Brusseau, M.L., 1996. Field study of the partitioning tracer method for detection of dense nonaqueous phase liquid in a trichloroethene-contaminated aquifer. *Environmental Science & Technology*, 30(9): 2859-2863.

Noll, M.R., Farrington, S.P., McHale, T.J., 1998. *Permit Application for United States Air Force Groundwater Remediation Field Laboratory, Cosolvent Solubilization Technology Demonstration.* Submitted to the Delaware Department of Natural Resources and Environmental Control, May.

Pope, G.A., Jackson, R.E., 1999a. Characterization of organic contaminants and assessment of remediation performance in subsurface formations. U.S. Patent 6,003,365, U.S. Patent Office, Washington, D.C.

Pope, G.A., Jackson, R.E., 1999b. Characterization of organic contaminants and assessment of remediation performance in subsurface formations. U.S. Patent 5,905,036, U.S. Patent Office, Washington, D.C.

Rao, P.S.C., Annable, M.D., Kim, H., 2000. NAPL source zone characterization and remediation technology performance assessment: Recent developments and applications of tracer techniques, *Journal of Contaminant Hydrology.* 45 (1-2), 63-78.

Rao, P.S.C., Annable, M.D., Sillan, R.K., Dai, D., Hatfield, K.H., Graham, W.D., Wood, A.L., Enfield, C.G., 1997. Field-scale evaluation of in-situ cosolvent flushing for enhanced aquifer remediation. *Water Resources Research*, 33 (12), 2673-2686.

Saripalli, K.P., M. D. Annable, and P.S.C. Rao, 1997. Estimation of Nonaqueous Phase Liquid-Water Interfacial Areas in Porous Media following Mobilization by Chemical Flooding. Environmental Science and Technology, Vol. 31, No. 12, pp. 3384-3388.

Starr, R.C., Cherry, J.A., Vales, E.S., 1992. A new steel sheet piling with sealed joints for groundwater pollution control. 45th Canadian Geotechnical Conference, Toronto, Ontario.

Sillan, R. K., M. D. Annable, P. S. C. Rao, D. Dai, K. Hatfield, W. D. Graham, A. L. Wood, and C. G. Enfield, 1998a. Evaluation of in situ cosolvent flushing dynamics using a network of spatially distributed multilevel samplers. *Water Resources Research*, 34(9), 2191-2202.

Sillan, R. K., J. W. Jawitz, M. D. Annable, and P. S. C. Rao, 1998b. Influence of hydrodynamic and contaminant spatial variability on in situ flushing effectiveness and efficiency. *Groundwater Quality: Remediation and Protection*, Proceedings of the GQ'98 Conference, Tübingen, Germany, IAHS Publication no. 250, 407-414.

Tang, J.S., 1995. Partitioning tracers and in-situ fluid-saturation measurements. *SPE Formation Evaluation*, 10 (1), 33-39.

Thomas, A., 1996. GRFL: An opportunity in groundwater remediation research. *The Civil Engineer,* 4 (2), 34-35.

Valocchi, A., 1985. Validity of the local equilibrium assumption for modeling sorbing solute transport through homogeneous soils. *Water Resources Research*, 21 (6), 808-820.

Van Valkenburg, M. E., 1999. *Solubilization and Mobilization of Perchloroethylene by Cosolvents in Porous Media.* Ph.D. Dissertation, 159 pp., Department of Environmental Engineering Sciences, University of Florida, Gainesville.

Willson, C.S., Pau, O., Pedit, J.A., Miller, C.T., 2000. Mass transfer rate limitation effects on partitioning tracer tests. *Journal of Contaminant Hydrology*, 45 (1-2), 79-97.

Wise, W.R., 1999. NAPL characterization via partitioning tracer tests: quantifying effects of partitioning nonlinearities. *Journal of Contaminant Hydrology*, 36 (1-2), 167-183.

Wise, W.R., Dai, D., Fitzpatrick, E.A., Evans, L.W., Rao, P.S.C., Annable, M.D., 1999. Non-aqueous phase liquid characterization via partitioning tracer tests: A modified Langmuir relation to describe partitioning nonlinearities. *Journal of Contaminant Hydrology*, 36 (1-2), 153-165.

APPENDIX A: MANUSCRIPTS

Brooks et al., 2001. Field-scale cosolvent flushing of DNAPL from a controlled release – Submitted.

Brooks et al., 2001. Controlled release, blind tests of DNAPL characterization by partitioning tracers - Draft.

Brooks et al., 2001. General methods for estimating uncertainty in trapezoidal rule-based moments - Draft.

Cho et al., Estimating NAPL saturation using partitioning tracers: Influence of residual cosolvents – Draft.

Cho et al., Influence of residual surfactant on partitioning tracers. – Draft.

Hayden et al., 2000. Activated carbon for the removal of tetrachloroethylene (PCE) from alcohol solutions – Accepted, JEE.

James et al., 2000. Estimation of spatially variable residual nonaqueous phase liquid saturations in nonuniform flow fields using partitioning tracers – Published.

Jawitz et al., 1998. Characterizing the spatial distribution of non-aqueous phase contaminant using partitioning tracers and the method of moments. Groundwater Quality: Remediation and Protection, Edited by M. Herbert and K. Kovar, IAHS Publication no. 250, 1998, pp. 422-425.

Van Valkenburg and Annable, 2001. Mobilization and entry of DNAPL pools into finer sand media by cosolvents: two-dimensional chamber studies – Submitted.

APPENDIX B: DATA CD

Field-Scale Cosolvent Flushing of DNAPL from a Controlled Release

Michael C. Brooks[1], Michael D. Annable[1], P. Suresh C. Rao[2], Kirk Hatfield[1], James W. Jawitz[3], William R. Wise[1], A. Lynn Wood[4], and Carl G. Enfield[5]

[1]Inter-Disciplinary Program in Hydrologic Sciences
University of Florida,
Gainesville, FL 32611-6450

[2]School of Civil Engineering
Purdue University
West Lafayette, IN 47907-1284

[3]Department of Civil and Materials Engineering
University of Illinois at Chicago
Chicago, Illinois 60607

[4]National Risk Management Research Laboratory
U. S. Environmental Protection Agency
Ada, OK 74820

[5]National Risk Management Research Laboratory
U. S. Environmental Protection Agency
Cincinnati, OH 45268

Submitted for Publication in
Water Resources Research
February 18, 2000

Revised and Resubmitted
February 19, 2001

Abstract

A DNAPL source zone was established within an isolated cell through a controlled release of perchloroethylene (PCE). The cell was flushed with an ethanol-water solution for approximately 40 days to enhance dissolution of the PCE. The amount of PCE removed during the alcohol flushing demonstration was 53 L, which represents a 64% flushing effectiveness, defined as the fractional mass of PCE removed. This estimate of effectiveness is based on the knowledge of the actual PCE volume introduced into the cell, and is not hampered by uncertainty in characterization techniques. The ethanol solution extracted from the cell was recycled using activated carbon and air stripping treatment. High removal efficiencies at the end of the demonstration indicated that more PCE could have been removed had the demonstration continued.

1 Introduction

Conventional remediation methods, such as pump-and-treat, can take many decades to remove dense nonaqueous phase liquids (DNAPLs) (Mackay and Cherry, 1989). Among enhanced source-zone removal techniques that can expedite site remediation, in-situ cosolvent flushing involves the addition of miscible organic solvents to water to increase the solubility or mobility of the NAPL (Imhoff et al., 1995; Rao et al., 1997; Lowe et al., 1999). Low molecular weight alcohols have principally been used as cosolvents for enhanced source zone remediation (Lowe et al., 1999). The remedial performance assessments of recent in-situ alcohol-flushing demonstrations were determined by comparing results from pre- and post-flushing contaminant characterization techniques (e.g., soil cores, partitioning interwell tracer tests (PITTs), and groundwater samples), and from comparing the amount of contaminant removed during in-situ flushing to the amount estimated by pre-flushing characterization techniques (Rao et al., 1997; Sillan et al., 1998a; Falta et al., 1999; Jawitz et al., 2000). The accuracy of such assessments was

hindered by uncertainties in the characterization methods used to estimate the amount and distribution of the NAPL in the source zone. A controlled release experiment, in which a known volume of NAPL is carefully released into an isolated cell, provides a unique opportunity to better evaluate aggressive remediation techniques. Several controlled-release experiments have been conducted in the unconfined, sand aquifer at Canadian Forces Base Borden, Ontario, but the purpose of these investigations was characterization of NAPL distribution, not remediation (for example, see Kueper et al., 1993; Broholm et al., 1999).

The present field-scale test was conducted at the Dover National Test Site (DNTS), located at Dover Air Force Base (AFB) in Dover, Delaware. The DNTS is a field-scale laboratory, designed as a national test site for evaluating remediation technologies (Thomas, 1996). This demonstration was the first in a series of tests designed to compare the performance of several DNAPL remediation technologies, with each demonstration following a similar test protocol. Researchers from the U. S. Environmental Protection Agency (EPA) begin each demonstration by releasing a known volume of PCE into an isolated cell. However, the amount, locations, and method of release are not revealed to the researchers responsible for conducting the characterization and remediation components of their test protocol. After a release, a PITT is completed to characterize the volume and distribution of PCE, followed by the remedial demonstration. Finally, a post-demonstration PITT is conducted to evaluate the remedial performance. Since multiple remedial technologies were planned for each cell, DNAPL characterization using soil cores was not feasible. The purpose of this paper is to present the results of the first remediation demonstration, enhanced dissolution by ethanol flushing, completed in the spring of 1999.

2 Site Characterization

2.1 Site Description

The demonstration permit application (Noll et al., 1998) provided detailed information on the site geology and the cell installation and instrumentation. The following summary provides information relevant to this study. The site geology consists of the Columbia Formation, characterized by silty, poorly sorted sands. This is underlain by the Calvert Formation, the upper portion of which is characterized by silty clay with thin layers of silt and fine sand. This layer forms the aquitard for the surficial aquifer. Noll et al. (1998) reported that the average hydraulic conductivity of the surficial aquifer ranges from 2.4 m/day to 10.4 m/day based on pump tests. Boring logs from the wells installed in the cell generally indicated alternating layers of silty sand, poorly sorted sand, and well sorted sand; and an average depth to clay of approximately 12 m below grade. The grade elevation varied by 0.2 m across the cell, consequently all references to grade are based on an average grade elevation. The minimum observed clay depth was 11.8 m below grade in well 52, and the maximum observed clay depth was 12.5 m below grade in well 56 (Figure 1).

The 3-m by 5-m by 12-m cell was constructed by driving Waterloo sheet piling with interlocking joints through the surficial aquifer into the confining unit. The cell was instrumented with 12 wells, 18 release points, and 18 multi-level sampling (MLS) locations (Figure 1). Each well was screened from 6.1 m to 12.5 m below grade. A 0.3 m section of casing was installed below each screen and served as a sump for collecting DNAPL in the event it entered the wells. Each release point terminated at 10.7 m below grade, underneath a sampler installed above it at approximately 9.9 m. Each MLS location had 5 vertical sampling points spaced 0.3 m apart, distributed over the bottom 1.5 m of the cell on a tetrahedral grid.

Measurements of porosity and hydraulic conductivity in the cell were based on results from hydraulic and tracer tests conducted prior to the DNAPL release. Hydraulic conductivity ranged from 2.4 m/day to 3.0 m/day based on the hydraulic gradient measured under steady flow during the hydraulic test. The effective porosity in the cell was estimated at approximately 0.20 based on moment analysis of the data from the nonreactive tracer test conducted prior to DNAPL release. This represents a swept volume of approximately 14,000 L.

2.2 PCE Emplacement

Between June 10 and 12, 1998, EPA personnel released a total of 91.7 ± 0.5 L [see Brooks (2000) for a discussion of uncertainty estimates] of PCE at several locations within the cell (Figure 1). EPA researchers conducted the release by pumping the PCE down the release points at an approximate flow rate of 0.6 L/min. To reduce the likelihood of PCE pooling on the clay-confining unit, the water table was lowered below the release elevations (11.0 m below grade) prior to PCE injection. Immediately following the release, the water table was lowered further to facilitate vertical spreading of the DNAPL between the release points and the clay-confining unit. When the water table reached approximately 11.9 m below grade, groundwater extraction was terminated and water injection was initiated to raise the water table back to the pre-release elevation (8.5 m below grade).

Approximately 150,000 L of water were flushed through the cell as a result of several tracer tests conducted between PCE emplacement and the start of the ethanol flood. Based on moment analysis of PCE breakthrough curves from these tracer tests, a total of 5.6 ± 0.1 L of PCE were removed by dissolution (this represents an average aqueous PCE concentration of approximately 60 mg/L). Prior to the start of the ethanol flushing test, an additional 2.8 ± 0.2 L of free-phase PCE were removed from the sump in well 56 (the only well in which free-phase PCE was detected), and

0.2 ± 0.05 L of free-phase PCE were removed from the MLSs. Therefore, the estimated volume of PCE in the cell at the start of the ethanol flushing test was 83.1 ± 0.6 L. The performance of the ethanol-flushing test was judged using this value.

3 Methods

3.1 System Description

A double five-spot pattern, which consisted of six injection wells along the cell perimeter and two extraction wells in the center (Figure 1), was used to inject and extract fluids from the cell during ethanol flushing. This pattern was used because of the flexibility it afforded to target the ethanol to specific regions in the cell. The water level in the cell during the test was maintained at approximately 8.2 m below grade to provide sufficient hydraulic head for MLS operation, and to comply with regulatory requirements for an inward gradient relative to the regional groundwater level. The DNAPL, however, was estimated to be between 10.7 m and 12.2 m below grade based on the depth of the release points and the clay interface. Inflatable packers were therefore placed in each injection and extraction well to focus the ethanol solution to the lower portion of the cell, and to minimize ethanol dilution by separating the flow through the cell into upper and lower zones. Water was injected above the packers into the upper zone and ethanol solution was injected below the packers into the lower zone. Water was injected into the upper zone as a means to minimize upward migration of the ethanol solution injected into the lower zone. The packers were initially positioned to target the ethanol solution to the bottom 0.6 m of the cell in order to dissolve PCE near the clay, and to dissolve any PCE mobilized from the higher zones during the test. The packers were then gradually raised to the full flood-zone height, which corresponded to the bottom of the release points, 10.7 m below grade.

Falta (1998) presented a general discussion of cosolvent flooding performance based on NAPL-water-cosolvent phase behavior. Lunn and Kueper (1997), Hayden et al. (1999), and VanValkenburg (1999) presented phase-behavior information for PCE-water-ethanol systems. The ternary mixture of water-ethanol-PCE is a type II(-) phase system, which implies that two phases (aqueous and NAPL) are formed, with the ternary phase diagram tie lines having negative slopes. This behavior indicates that the ethanol preferentially partitions into water rather than PCE. The main remedial mechanism for type II(-) ternary systems is enhanced dissolution (Brandes and Farley, 1993).

The test began by injecting new 95% ethanol, 5% water solution (hereafter referred to as new ethanol solution) into the lower zone. Lower-zone cosolvent recycling started after the effluent ethanol content was high enough (approximately 70%) to make recycling feasible (6.9 days). The lower-zone fluid was recycled by pumping it through either two or three activated carbon drums in series, or during the latter part of the demonstration, a low profile air stripper and activated carbon drums. The recycled ethanol solution was augmented with new ethanol solution as needed to maintain the ethanol content in the influent around 70%. An ethanol content of 70% was chosen to maintain a large PCE dissolution capacity in the solution, yet facilitate cosolvent recycling by minimizing the need to augment treated effluent with the new ethanol solution. Water was injected into the upper zone at the start of the test, and upper-zone recycling started after a sufficient volume of upper zone effluent had been stored (1.0 day). The upper-zone fluid was recycled by pumping it through two activated carbon drums in series.

The total volume of fluid (new ethanol, recycled ethanol, and water) injected into the lower zone was approximately 112,000 L. Recycled ethanol accounted for 47% of the fluid injected into the lower zone. The total volume of water (containing a small percentage of ethanol)

injected into the upper zone was 15,000 L. Recycling accounted for 77% of the fluid injected into the upper zone. To our knowledge, this is the first cosolvent-flushing demonstration in which the effluent was treated and re-injected. Cosolvent recycling was a significant factor in this demonstration, as evident by the fact that the volume of ethanol solution delivered to the cell, and consequently, the volume of PCE removed from the cell, were approximately doubled by recycling. Approximately 3 to 6 L of PCE were adsorbed in each drum before PCE breakthrough occurred. The average air-stripping treatment efficiency was 91%. Ethanol content was not significantly affected by either the activated-carbon or air-stripping treatment processes. The ethanol content in the effluent samples after the treatment processes was reduced by an average of approximately 1% relative to the influent ethanol content.

The total amount of fluid injected into the lower zone was approximately eight times greater than that injected into the upper zone. Estimates of the number of pore volumes flushed through the upper and lower zones separately are not possible because the location of the separation between the two zones in the cell was not known. However, using the combined upper- and lower-zone extraction volumes, an average water table position of 4 m above the clay, and an effective porosity of 0.20, approximately 10 pore volumes were flushed through the cell.

3.2 Performance Monitoring

Samples were collected from the extraction wells and MLSs over the entire test duration (38.8 days). Samples were collected from the injection wells during recycling treatment to monitor the amount of PCE and ethanol that was re-injected into the cell. Influent and effluent samples were collected from each carbon drum and from the air stripper during recycling operations to monitor treatment performance. Samples were refrigerated on-site, and then shipped overnight in coolers to the University of Florida for storage until ethanol and PCE analysis were conducted.

Samples were analyzed for ethanol by gas chromatography (GC) using a capillary column and a flame ionization detector (FID). Samples were analyzed for PCE by a similar GC/FID method, as well as liquid chromatography using a packed column, UV detection, and a methanol (70%) and high performance liquid chromatography grade water (30%) mixture as the mobile phase. If free phase PCE was observed in sample vials in the laboratory, an acetone extract was used to dissolve the free phase PCE, and the sample was then analyzed by the GC/FID method.

Selected samples were analyzed in the field using a field GC to provide real-time information for operational decisions. Density measurements were also completed in the field using specific-gravity hydrometers. Injection and extraction flow rates, and water levels in the cell were monitored throughout the demonstration to maintain a steady flow field to the extent possible. Adjustments to influent flow rates were made in accordance with these data to minimize water-level fluctuations in the cell. Additional details about the procedures used in the ethanol flush can be found in Brooks (2000).

4 Results and Discussion

4.1 PCE Recovery

PCE concentrations and the ethanol percentages from extraction well samples are plotted in Figure 2. The ethanol content in the lower zone increased over the first 5 days as the new 95% ethanol solution displaced the resident water in the cell. Changes in the ethanol content after approximately 5 days resulted from changes in flushing operations (i.e., ethanol recycling, ethanol augmentation, and changes in packer positions). Between 27.7 to 34.7 days, injection into wells 41, 51, and 54 was stopped, injection into wells 41, 46, and 56 was increased, and well 51 was converted to an extraction well (between 30.2 to 34.2 days only) in order to target the ethanol solution to locations within the cell with high PCE concentrations. Ethanol content and PCE

concentrations from well 51 during the period it was converted to an extraction well (30.2 to 34.2 days) are not shown in Figure 2. The ethanol content in the effluent from this well varied between 58 to 65%, and the PCE concentration varied from 1,300 to 2,300 mg/L.

The ratio of aqueous PCE concentration to PCE solubility limit for extraction wells 45 and 55 are plotted in Figure 3 as a function of time. The PCE solubility limit, which is a function of the ethanol content, was based on PCE solubility limits reported by Van Valkenburg (1999). The ratio of the PCE concentration in solution to the PCE solubility limits for well 51 (not shown in Figure 3) ranged from 0.04 to 0.08. PCE concentrations above PCE solubility limits, which suggests free-phase PCE, are evident for a short duration (approximately 1 to 2 days) in the lower-zone effluent, and for a longer period (approximately 2-13 days) in the upper-zone effluent. Free-phase PCE represented by a ratio greater than unity is 0.04 ± 0.004 L for the lower zone, and 3.2 ± 0.1 L for the upper zone. Gravity separators were installed in the extraction well effluent lines to remove any free-phase PCE from the effluent. Over the course of the entire test, only 0.35 ± 0.01 L of free-phase PCE were collected from the upper-zone separators, and no free-phase PCE was collected from the lower-zone separators. Free-phase PCE was not observed when extraction well effluent samples were collected. The formation of an emulsion is the most likely explanation for the discrepancy between free-phase PCE volumes observed during the test, and those estimated from the laboratory samples. It is suspected that the emulsion formed in the extraction wells, rather than in the aquifer, due to mixing which diluted the ethanol content in the well, resulting in free-phase PCE precipitation and subsequent emulsion formation.

Free-phase PCE was observed in only 16 of more than 5,000 MLS samples collected, and only at selected depths in MLS locations 12 and 14. The majority of these observations occurred within the first day after the start of ethanol flushing. PCE concentrations in excess of estimated

PCE solubility limits occurred in 56 samples (out of approximately 1,500 samples analyzed) at selected depths in MLS locations 12, 14, 21, 25, 32, 41, 43, and 63. The difference in the number of observations of free-phase PCE during sample collection, and the number of samples with PCE concentrations greater than PCE solubility limits is also attributed to the formation of an emulsion. The majority of these samples occurred within the first 5 days after the start of ethanol flushing. Furthermore, free-phase PCE was not detected in the well sumps using the interface probe when they were investigated after the ethanol flushing test was concluded. Based on this evidence, it is our opinion that DNAPL mobilization occurred only at a few locations during ethanol flushing.

The PCE concentrations in the lower-zone extraction well effluent were approximately one to two orders of magnitude below the PCE solubility limits after approximately 3 days (Figure 3). This could have resulted from mixing at the extraction wells, or from mass-transfer limitations. During the demonstration, the longest flow interrupt occurred from 17.5 to 20.9 days, when the system was intentionally turned off to investigate mass-transfer limitations. No evidence of mass-transfer limitation, as manifested by increases in effluent contaminant concentrations (Brusseau et al., 1997), is apparent from the breakthrough curves shown in Figure 2. Localized mass-transfer limitations may have occurred, but were not observed as elevated PCE concentrations in the extraction well effluent. Therefore, effluent PCE concentrations were most likely observed to be much less than the PCE solubility limit due to mixing at the extraction wells.

Approximately 52.6 ± 0.7 L of PCE were removed from the cell, based on the zeroth moment of the PCE breakthrough curves measured at the extraction wells. The error estimate for the amount of PCE extracted was based on the propagation of errors in volume and concentration measurements through the zeroth moment calculations (Brooks, 2000). Using an average PCE concentration (2096 ± 51 mg/L) based on all MLS samples analyzed, the total volume of fluid

removed by the MLSs during the test (916 ± 42 L), and the volume of free-phase PCE removed through the MLSs (0.08 ± 0.04 L), the total amount of PCE removed by the MLSs was estimated at 1.3 ± 0.1 L. Thus, the total amount of PCE removed from the cell by the extraction wells and the MLSs was 53.9 ± 0.7 L, while that injected during ethanol recycling was estimated at 0.5 ± 0.04 L. Therefore, the net amount of PCE removed from the cell was 53.4 ± 0.7 L, which is 64% of the 83.1 ± 0.6 L of PCE estimated in the cell at the start of the test.

4.2 Treatment Efficiency

The contaminant volume removed divided by the volume of flushing fluid has been used to describe the efficiency of in-situ flushing remediation systems (Jawitz et al., 1997; Sillan et al., 1998b). We define efficiency as the cumulative volume of DNAPL removed per cumulative volume of applied remedial fluid. Using the ethanol delivered to the cell as the basis, the cell-averaged removal efficiency was $1x10^{-3}$ liters of PCE per liter of ethanol (53 L PCE/ 41,700L ethanol). On the basis of the total amount of ethanol and water injected from the start of the demonstration to the start of the final water flood, the removal efficiency was $6x10^{-4}$ liters of PCE per liter of injected fluid (53 L PCE/ 94,500 L ethanol and water). An estimate of pump-and-treat performance in the cell can be made based on the amount of PCE removed by dissolution into water during pre-flushing tests . A removal efficiency of $2x10^{-5}$ is based on the ratio of PCE removed to the volume of water flushed through the cell. The removal efficiencies for ethanol flushing were one to two orders of magnitude greater than the pump-and-treat efficiency.

Removal efficiencies, calculated as cumulative PCE volume removed per cumulative extracted volume, are shown for each well in Figure 4 as a function of time. Once the extraction well packers were raised to their maximum height at 13.9 days, the removal efficiencies in extraction wells 45A, 45B, and 55A remained constant at approximately $4x10^{-4}$ to $5x10^{-4}$, while the

removal efficiency in 55B remained constant at approximately $6x10^{-4}$ to $7x10^{-4}$. This indicates that PCE mass removal was fairly constant during the demonstration, and suggests that continued flushing should have increased removal effectiveness. This was prevented, however, by the fact that financial and human resources available for the project were exhausted after approximately 39 days of ethanol flushing (an additional two weeks beyond the original schedule). Neglecting decreases in performance resulting from diminishing NAPL content (i.e., constant removal efficiencies), it is estimated that the majority of the remaining PCE would have been removed if the system had been operated for another 21 days. Temporary extraction well 51B had the highest removal efficiency of approximately $1x10^{-3}$, which may suggest an advantage to changing the flow field during flushing when hot spots are identified.

Results from this demonstration support the use of cosolvent flushing in full scale applications, as evident by the fact that removal efficiencies were one to two order of magnitude greater than those estimated for pump and treat technology under similar conditions. This study demonstrated that further improvements in DNAPL extraction efficiency may be achieved by: (1) changing pumping patterns during flushing to target alcohol to "hot zones"; as was demonstrated for well 51; and (2) treating the extracted fluids to remove significant contaminant mass and then re-injecting the alcohol. Regulatory constraints on re-injection of treated fluids is an issue, but more efficient and cost-effective treatment technologies may allow this as a more feasible option. On the other hand, the results also indicate that complete DNAPL removal may still represent a significant technological challenge, as evident by the fact that only 64% of the DNAPL in the cell at the start of the test was removed.

Acknowledgments

The authors gratefully acknowledge the help of Sten Berglund, Jaehyun Cho, Clayton Clark, Lane Evans, Andrew James, Heonki Kim, Irene Poyer, Claire Shukla, Gloria Sillan, and Meifong Zhou from the University of Florida; Tim McHale, Mark Hogan, and Rob Young from Mantech Environmental Research Services Corporation; Bart Faulkner, John Hoggatt, and Susan Mravik from the U. S. Environmental Protection Agency; and Major Paul Devane from Armstrong Laboratories, Tyndall AFB. This project was funded by the U. S. Department of Defense Strategic Environmental Research and Development Program (SERDP), which is a collaborative effort involving the U. S. EPA, U. S. DOE, and U. S. DOD. This document has not been subjected to peer review within the funding agency, and the conclusions stated here do not necessarily reflect the official views of the agency nor does this document constitute an official endorsement by the agency.

The Dover National Test Site is one of four National Environmental Technology Site (NETTS) locations established and managed by SERDP. The demonstration complied with prescribed NETTS protocols and guidelines for quality assurance, health and safety, technical completeness, and regulatory compliance. The support of the NETTS facilities and test location manager and staff are gratefully acknowledged. For further information on NETTS locations or SERDP, contact Cathy Vogel or Matt Chambers at 703-478-5186 or visit the SERDP web site at www.serdp.gov.

References

Broholm, K., S. Feenstra, and J. A. Cherry, Solvent release into a sandy aquifer. 1. Overview of source distribution and dissolution, *Environmental Science Technology*, 33(5), 681-690, 1999.

Brandes, D., and K. Farley, Importance of phase behavior on the removal of residual DNAPLs from porous media by alcohol flooding, *Water Environment Research 65*, 869-878, 1993.

Brooks, M. C., *Characterization and Remediation of DNAPL Resulting from a Controlled Release*, Ph.D. Dissertation, 147 pgs, Department of Environmental Engineering Sciences, University of Florida, Gainesville, Florida, December, 2000.

Brusseau, M. L., Q. Hu, and R. Srivastava, Using flow interruption to identify factors causing nonideal contaminant transport, *Journal of Contaminant Hydrology*, 24(3-4), 205-219, 1997.

Falta, R. W., C. M. Lee, S. E. Brame, E. Roeder, J. T. Coates, C. Wright, A. L. Wood, and C. G. Enfield, Field test of high molecular weight alcohol flushing for subsurface nonaqueous phase liquid remediation, *Water Resources Research*, 35(7), 2095-2108, 1999.

Falta, R. W., Using phase diagrams to predict the performance of cosolvent floods for NAPL Remediation, *Ground Water Monitoring and Remediation*, 18(3), 94-102, 1998.

Hayden, N. J., J. Diebold, and G. Noyes, Phase behavior of chlorinated solvent + water + alcohol mixtures with application to alcohol flushing, *Journal of Chemical and Engineering Data*, 44(5), 1085-1090, 1999.

Imhoff, P. T., S. N. Gleyzer, J. F. Mcbride, L. A. Vancho, I. Okuda, and C. T. Miller, Cosolvent-enhanced remediation of residual dense nonaqueous phase liquids: experimental investigations, *Environmental Science and Technology*, 29(8), 1966-1976, 1995.

Jawitz, J. W., R. K. Sillan, M. D. Annable, and P. S. C. Rao, Methods for Determining NAPL Source Zone Remediation Efficiency of In-Situ Flushing Technologies, *In Situ Remediation of the Geoenvironment*, Proceedings of the Conference, Minneapolis, Minnesota, Geotechnical Special Publication No. 71, 271-283, 1997.

Jawitz, J. W., R. K. Sillan, M. D. Annable, P. S. C. Rao, and K. Warner, In-situ Alcohol Flushing of a DNAPL Source Zone at a Dry Cleaner Site, *Environmental Science and Technology*, 34(17), 3722-3729, 2000.

Kueper, B. H., D. Redman, R. C. Starr, S. Reitsma, and M. Mah, A field experiment to study the behavior of tetrachloroethylene below the water table: spatial distribution of residual and pooled DNAPL, *Ground Water*, 31(5), 756-766, 1993.

Lowe, D. F., C. L. Oubre, and C. H. Ward, editors, *Surfactants and Cosolvents for NAPL Remediation, A Technology Practices Manual*, Lewis Publishers, Boca Raton, 412 pgs., 1999.

Lunn, S. R. D., and B. H. Kueper, Removal of pooled dense, nonaqueous phase liquid from saturated porous media using upward gradient alcohol floods, *Water Resources Research*, 33(10), 2207-2219, 1997.

MacKay, D. M., and J. A. Cherry, Groundwater contamination: Pump-and-treat remediation, *Environmental Sciences and Technology*, 23(6), 630-636, 1989.

Noll, M. R., S. P. Farrington, and T. J. McHale, *Permit Application for United States Air Force Groundwater Remediation Field Laboratory, Cosolvent Solubilization Technology Demonstration*, submitted to the Delaware Department of Natural Resources and Environmental Control, May, 1998.

Rao, P. C. S., M. D. Annable, R. K. Sillan, D. Dai, K. Hatfield, and W. D. Graham, Field-scale evaluation of in situ cosolvent flushing for enhanced aquifer remediation, *Water Resources Research*, 33(12), 2673-2686, 1997.

Sillan, R. K., M. D. Annable, P. S. C. Rao, D. Dai, K. Hatfield, W. D. Graham, A. L. Wood, and C. G. Enfield, Evaluation of in situ cosolvent flushing dynamics using a network of spatially distributed multilevel samplers, *Water Resources Research*, 34(9), 2191-2202, 1998a.

Sillan, R. K., J. W. Jawitz, M. D. Annable, and P. S. C. Rao, Influence of hydrodynamic and contaminant spatial variability on in situ flushing effectiveness and efficiency, *Groundwater Quality: Remediation and Protection*, Proceedings of the GQ'98 Conference, Tübingen, Germany, IAHS Publication no. 250, 407-414, 1998b.

Thomas, A., GRFL: An opportunity in groundwater remediation research, *The Civil Engineer*, 4(2), 34-35, 1996.

Van Valkenburg, M. E., *Solubilization and Mobilization of Perchloroethylene by Cosolvents in Porous Media*, Ph.D. Dissertation, 159 pp., Department of Environmental Engineering Sciences, University of Florida, Gainesville, 1999.

List of Figures

Figure 1 Test cell instrumentation layout and PCE injection locations and volumes (Plan view). The PCE release volume per location is indicated in liters by the number within the circles.

Figure 2 PCE concentrations and ethanol percentages from a) upper zone extraction well 45A, b) lower zone extraction well EW 45B, c) upper zone extraction well EW 55A, and d) lower zone extraction well EW 55B.

Figure 3 Ratio of PCE concentration to PCE solubility limit. The PCE solubility limits are a function of ethanol content, and were based on values reported by Van Valkenburg (1999).

Figure 4 Removal efficiency as a function of elapsed time. Removal efficiencies are calculated as the cumulative PCE volume removed per cumulative extracted volume.

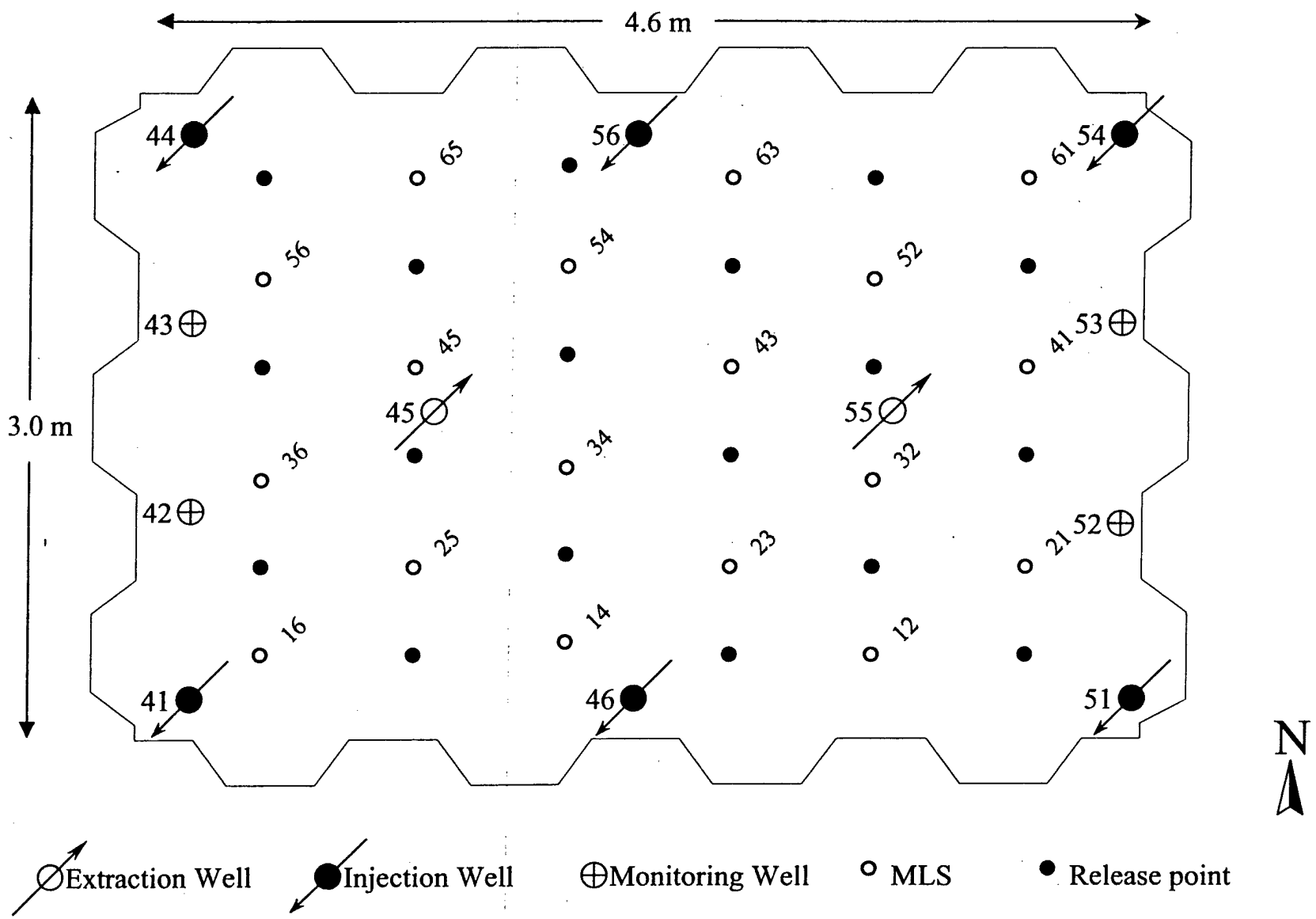

Figure 1 Test cell instrumentation layout. (Plan view.)

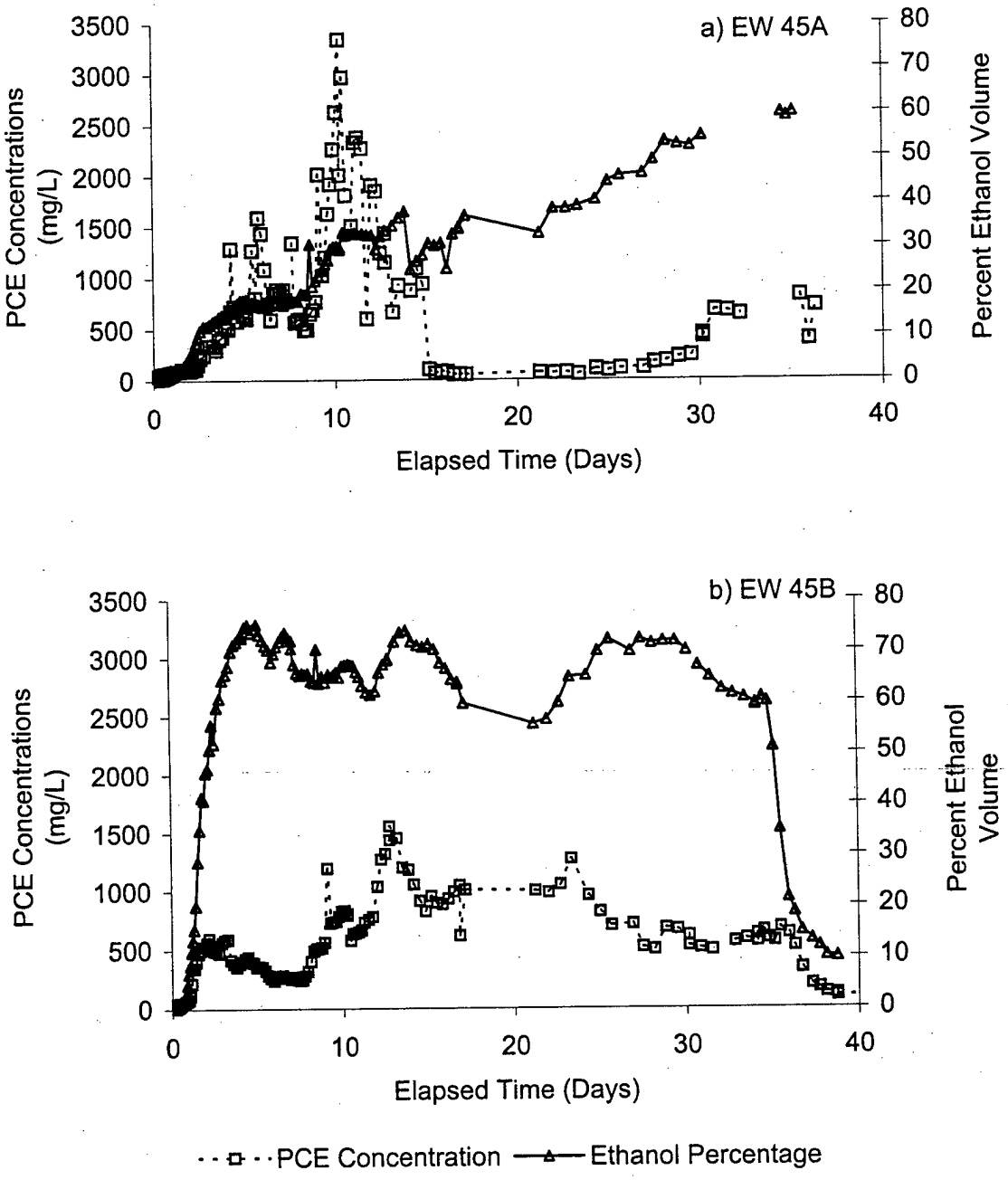

Figure 2 PCE concentrations and ethanol percentages from a) upper zone extraction well EW 45A, and b) lower zone extraction well EW 45B.

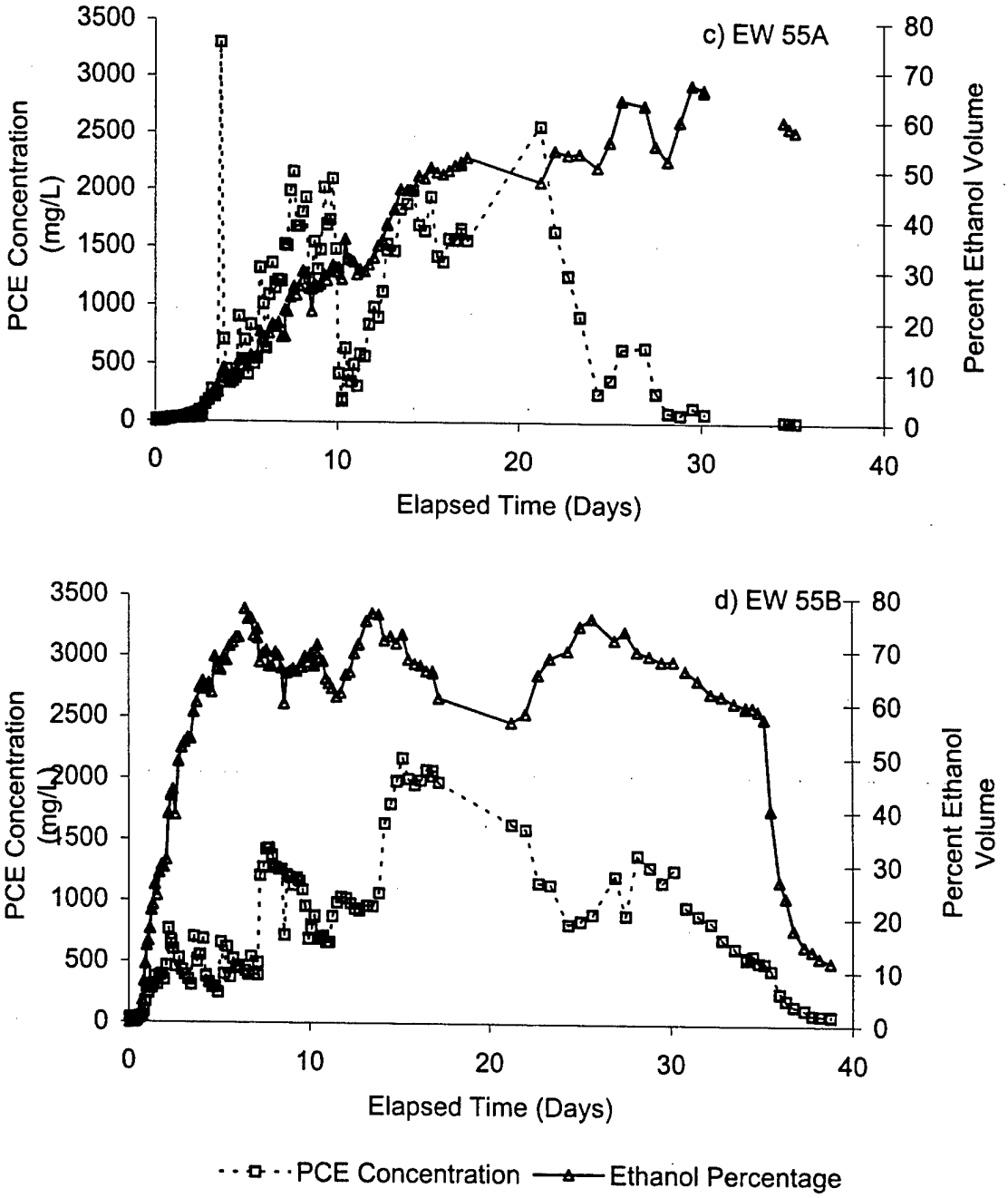

Figure 2 continued PCE concentrations and ethanol percentages from c) upper zone extraction well EW 55A, and d) lower zone extraction well EW 55B

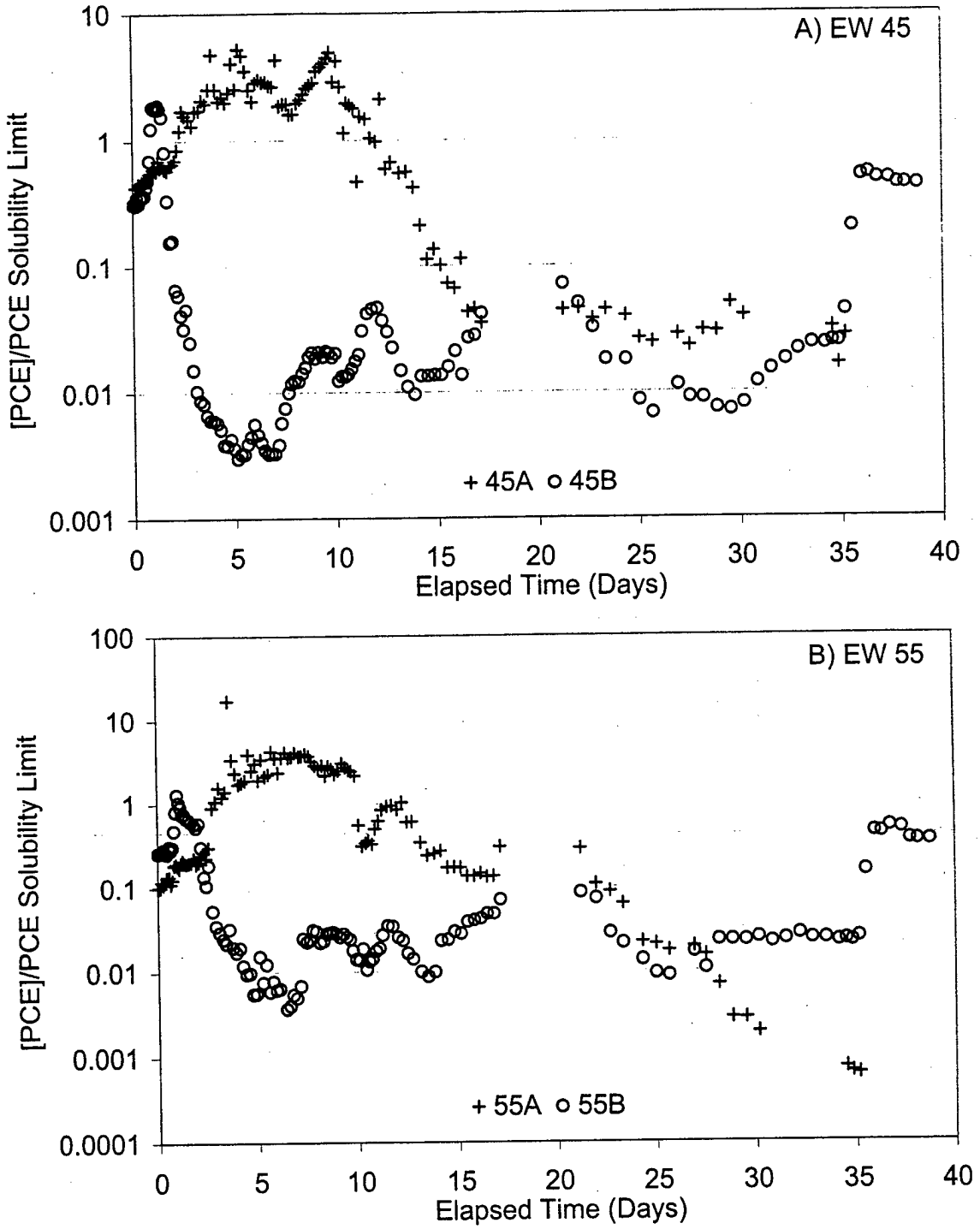

Figure 3 Ratio of PCE concentration to PCE solubility limit. The PCE solubility limits are a function of ethanol content, and were based on values reported by VanValkenburg (1999).

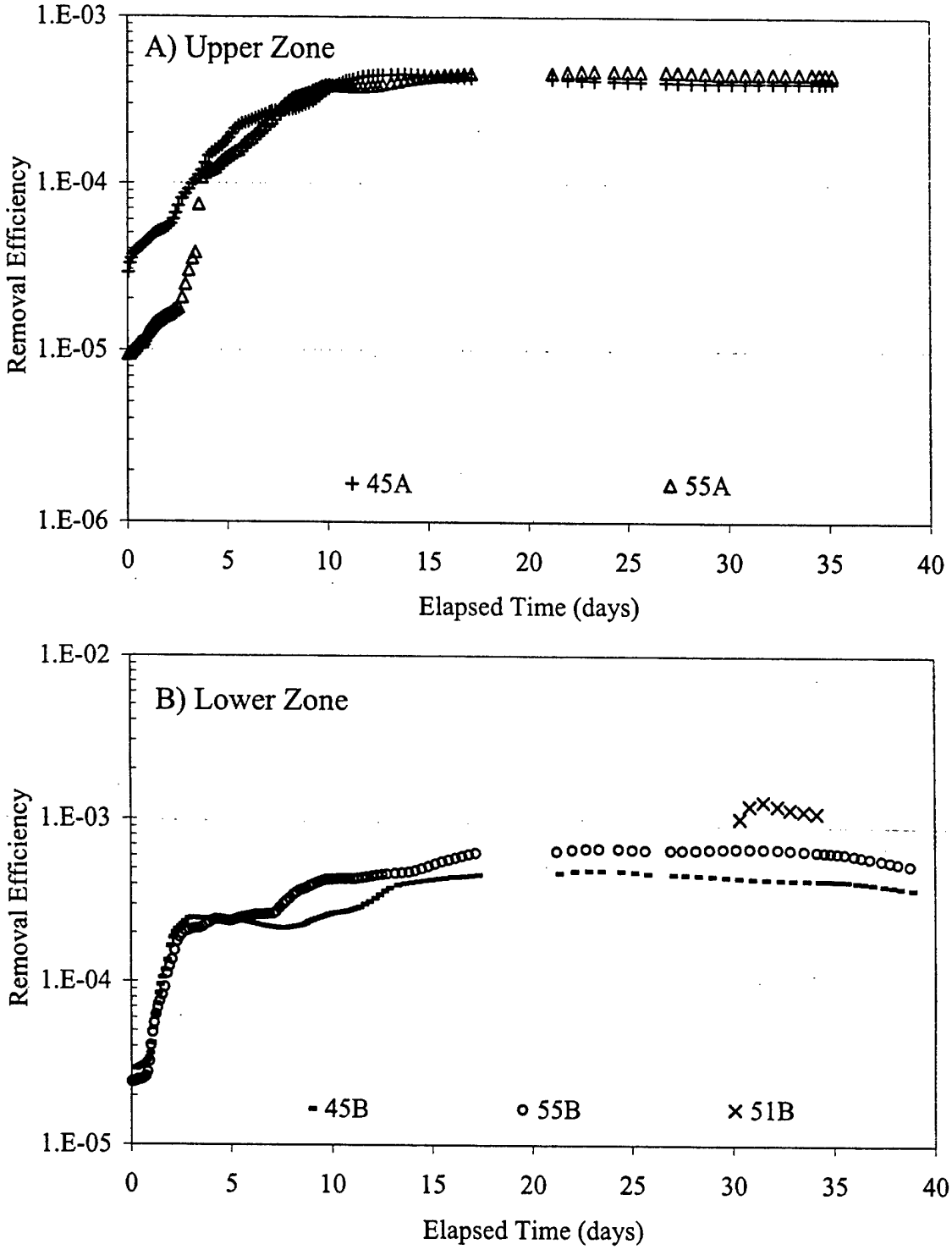

Figure 4 Removal efficiency as a function of elapsed time. Removal efficiencies are calculated as the cumulative PCE volume removed per cumulative extracted volume.

Controlled Release, Blind Tests of DNAPL Characterization using Partitioning Tracers

Michael C. Brooks[1], Michael D. Annable[1*], P. Suresh C. Rao[2], Kirk Hatfield[1], James W. Jawitz[1], William R. Wise[1], A. Lynn Wood[3], and Carl G. Enfield[4]

[1]Inter-Disciplinary Program in Hydrologic Sciences
University of Florida,
Gainesville, FL 32611-6450

[2]School of Civil Engineering
Purdue University
West Lafayette, IN 47907-1284

[3]National Risk Management Research Laboratory
U. S. Environmental Protection Agency
Ada, OK 74820

[4]National Risk Management Research Laboratory
U. S. Environmental Protection Agency
Cincinnati, OH 45268

*Corresponding author

Submitted for Publication in
Journal of Contaminant Hydrology
August 2, 2001

Abstract

The partitioning tracer technique for dense nonaqueous phase liquid (DNAPL) characterization was evaluated in an isolated test cell, in which controlled releases of perchloroethylene (PCE) had occurred. Four partitioning tracer tests were conducted, two using an inverted, double five-spot pumping pattern, and two using vertical circulation wells. Two of the four tests were conducted prior to remedial activities, and two were conducted after. Each test was conducted as a "blind test" where researchers conducting the partitioning tracer tests had no knowledge of the volume, method of release, nor resulting spatial distribution of DNAPL. Multiple partitioning tracers were used in each test, and the DNAPL volume estimates varied significantly within each test based on the different partitioning tracers. The tracers with large partitioning coefficients generally predicted a smaller volume of PCE than that expected based on the actual release volume. However, these predictions were made for low DNAPL saturations (average saturation was approximately 0.003), under conditions near the limits of the method's application. Furthermore, there were several factors that may have hindered prediction accuracy, including tracer degradation and remedial fluid interference.

Keywords: tracer test; partitioning tracer; DNAPL; perchloroethylene; groundwater; site characterization

1. Introduction

To characterize the volume and distribution of subsurface nonaqueous phase liquid (NAPL) contaminants using partitioning tracers, two or more tracers are injected at one or more locations in the source zone, and are displaced through the aquifer under a forced gradient. The selected tracers should have different partitioning coefficients (K_{NW}), thus resulting in differential retardation. The mean arrival time of the tracers, monitored at either multilevel samplers or extraction wells, depends on K_{NW} and the NAPL saturation (S_N) present along the flow paths. The use of partitioning tracers to characterize NAPL was developed within the petroleum industry early in the 1970's (Cooke, 1971; Dean, 1971). Tang (1995) reviewed petroleum industry applications of partitioning tracers and reported that over 200 tests had been conducted since 1971. Jin et al. (1995) described the application of partitioning tracer theory to source-zone NAPL characterization. Jin et al. (1997) presented design protocols for tracer tests, and patents for this application were issued in 1999 (Pope and Jackson, 1999a and 1999b).

The use of partitioning tracers for characterizing NAPL volume and distribution in the source zone has increased in recent years. Much of this use has been in conjunction with in-situ flushing efforts (Rao et al., 1997, Jawitz et al., 1998a; Falta et al., 1999; Jawitz et al., 2000). The first application to a NAPL-contaminated aquifer took place at Hill Air Force Base (AFB) in 1994 (Annable et al., 1995, 1998). Nelson and Brusseau (1996), Hayden and Linnemeyer (1999), Cain et al. (2000), and Jawitz et al. (2000) have reported other tests. According to Dwarakanath et al. (1999), over 40 field demonstrations of NAPL-contaminant characterization using partitioning tracers had been completed at that time, and to the authors' knowledge, approximately 10 more have been conducted since then.

The performance assessments of recent field-scale partitioning tracer tests were based on the comparison of results to other traditional contaminant characterization techniques, such as soil cores and groundwater samples (Rao et al., 1997; Annable et al., 1998; Jawitz et al., 1998a/b; Falta et al., 1999). While favorable agreement was obtained between the different characterization methods, the reliability of such assessments, and conclusions about partitioning tracer test accuracy are hindered by uncertainties in the other characterization methods. Furthermore, a number of factors have been identified which may influence the accuracy of NAPL characterization by partitioning tracers, including nonlinear partitioning behavior (Wise et al., 1999; Wise, 1999), nonequilibrium partitioning (Dwarakanath et al., 1999; Willson et al., 2000), background tracer retardation (Jin et al., 1997), poor sweep efficiency (Jin et al., 1997; Nelson et al., 1999), variable NAPL composition (Dwarakanath et al., 1999), tracer degradation (Annable et al., 1998; Brusseau et al., 1999), and heterogeneous NAPL distributions (Nelson et al., 1999; Rao et al., 2000). In addition, partitioning tracer tests conducted after remedial treatment may be influenced by potential flushing solutions (Lee et al., 1998; Rao et al., 2000). Reviews of partitioning tracer methods by Rao et al. (2000) and Brusseau et al. (1999) concluded that more field-scale evidence was necessary to better establish the reliability of NAPL characterization using partitioning tracers. A controlled release experiment, in which a known volume of NAPL is released into an isolated test cell, provides a unique opportunity to better evaluate partitioning tracer test performance and reliability.

The United States Environmental Protection Agency (EPA) National Risk Management Research Laboratory sponsored a project to assess the performance of remedial technologies for DNAPL source removal. In this project, researchers at EPA and five universities agreed to perform a series of DNAPL remedial demonstrations at the Dover National Test Site (DNTS).

The DNTS is located at Dover AFB in Dover, Delaware, and includes facilities for field-scale remedial experimentation (Thomas, 1996). In these demonstrations, EPA researchers released up to 100 L of PCE into isolated cells, following protocols approved by the Delaware Department of Natural Resources and Conservation (Noll et al., 1998). Information on the volume and distribution of the PCE released was, however, withheld from the university research groups until the completion of their tracer tests and remedial demonstrations. Subsequent to each PCE release, two partitioning tracer tests were conducted: one before and another after the remedial test. University of Florida (UF) conducted the first two partitioning tracer tests subsequent to the first controlled PCE release and a subsequent cosolvent flushing demonstration. The University of Oklahoma and UF jointly conducted the next two partitioning tracer tests, associated with the second controlled PCE release and subsequent surfactant flushing demonstration. The results of the cosolvent flood are discussed elsewhere (Brooks et al., 2000; Brooks, 2000), while analysis of the samples and data from the surfactant flood is incomplete.

The results from the four partitioning tracer tests are presented here in a chronological order without reference to the known DNAPL release information. A comparison of the tracer test results to the PCE release information follows, and finally, uncertainties and limitations associated with the predictions are discussed.

2. Methods

2.1. Site Description

The tests were conducted in an isolated cell, constructed using Waterloo® sheet piling with interlocking joints (Starr et al., 1992) driven into the clay confining unit, and surrounded by

a second enclosure of sheet piling forming a secondary containment barrier. The cell was instrumented with 12 wells and 18 DNAPL release points (Figure 1). The cell also contained 18 multi-level sampler locations; however, results from samples collected from these devices are not discussed here. Each well was screened from approximately 6.1 m to 13.3 m below ground surface (bgs), and the release points terminated at 10.7 m bgs.

The site geology consisted of the Columbia Formation, characterized by silty, poorly sorted sands, underlain by the Calvert Formation, the upper portion of which was characterized by silty clay with thin layers of silt and fine sand (Noll et al., 1998). This layer formed the confining unit into which the sheet pile was driven. Boring logs from the wells installed in the cell generally indicated alternating layers of silty sand, poorly sorted sand, and well sorted sand over the logging interval from approximately 10.1 to 12.5 m bgs. Iron oxidation was also noted in several logs. The average depth to clay was approximately 12.3 m bgs, while the minimum and maximum clay depth was 11.8 m bgs in well 52 and 12.5 m bgs in well 56 (Figure 1), respectively. Based on the hydraulic gradient measured under steady flow during hydraulic testing, the estimated hydraulic conductivity averaged over the cell was approximately 2.5 m/day.

2.2. Tracer Tests

Six tracer tests were conducted in the cell between May 1998 and October 2000 (Table 1). One tracer test was conducted prior to the first release of PCE into the cell to assess background sorption of tracers (hereafter referred to as the background tracer test). Three tracer tests were conducted between the first and second PCE release, and two were conducted after the second PCE release. After the initial PCE release, EPA conducted the first tracer test to

investigate non-reactive tracer (bromide) transport characteristics in a line-drive flow pattern. These results were not used in the design or interpretation of the partitioning tracer tests and are not discussed here.

Of the remaining four tracer tests, two were conducted to characterize the PCE in the cell before and after the cosolvent flood (referred to as Test 1 and Test 2, respectively), and the other two before and after the surfactant flood (referred to as Test 3 and Test 4, respectively). Each of these four tests followed the same general protocol: pulse injection of a tracer suite followed by water injection for a specified period, collection of well effluent samples over the test duration, laboratory analysis of the samples, and moment analysis of the resulting tracer breakthrough curves (BTCs).

The tracers used in the tests are summarized in Table 2. Samples were analyzed for alcohol tracers using gas chromatography with a flame ionization detector, and for inorganic tracers using liquid chromatography with an ultraviolet detector. Selected effluent samples near the end of the test where also analyzed for alcohol tracers using a headspace sampling method to better quantify the low tracer concentrations in the tails of the BTCs. Breakthrough curves were exponentially extrapolated to minimize truncation errors (Pope et al., 1995; Annable et al., 1998), and the zeroth and first-normalized moments were estimated using trapezoidal approximations. The first, normalized moments were then used to estimate DNAPL saturations and volumes using the methods outlined by Jin et al. (1995). Tracer partitioning coefficients (Table 2) were estimated from batch laboratory experiments. Specific details for each tracer test are summarized in the following paragraphs.

2.2.1. Background Tracer Test

A double five-spot pumping pattern, which consisted of six injection wells (41, 44, 46, 51, 54, and 56) along the perimeter of the cell and two extraction wells (45 and 55) in the center of the cell (Figure 1), was used to inject and extract fluids during this test. The extraction flow rate of 3.9 L/min was distributed equally among the two center wells (45 and 55). The saturated zone thickness was 4.6 m. The percent recovery of tracers ranged from 115% for bromide to 92% for *n*-octanol. The tail of the BTC for *n*-octanol declined significantly relative to the other tracers in both wells, resulting in a retardation factor relative to methanol of less than one, and suggesting tracer degradation may have occurred. The effective porosity in the cell was estimated at approximately 0.17 based on moment analysis of the BTC for methanol, a non-partitioning tracer. Bromide retardation can result from anion exchange with iron oxides (Brooks et al., 1998), which may explain the apparent bromide retardation of 1.35 (well 45) to 1.26 (well 55) relative to methanol in this test. Due to the potential retardation of both bromide and iodide by this mechanism, their use as a non-partitioning tracer was disregarded. Measured retardation factors for DMP of 1.12 (well 55) and 1.14 (well 45) represent an equivalent background PCE volume (based on the combined methanol swept volume of 11,700 L) of 52 L. However, for complications discussed in Section 4, corrections for background sorption based on these results were not deemed applicable to later tracer tests.

2.2.2. First Partitioning Tracer Test (Pre-cosolvent flood)

Prior to conducting the first partitioning tracer test (pre-cosolvent flood), each well was checked for free-phase PCE using an interface probe. Well 56 had the only PCE present, and a peristaltic pump was used to remove approximately three liters of PCE from the well. The PCE

may have entered the well either by migration along a low-conductivity layer present in the target flow zone, or by migration on the clay confining unit.

A inverted, double five-spot pattern was employed for this test, which consisted of six extraction wells (41, 44, 46, 51, 54, and 56) located around the perimeter of the test cell and two injection wells (45 and 55) located in the center (Figure 1). The inverted, double five-spot pumping pattern was chosen over a line-drive pumping pattern based on modeling studies which indicated that the temporal moments were more sensitive to NAPL saturation using the former pumping pattern (James et al., 2000). Furthermore, the injection/extraction pattern was switched from the five-spot pattern in the background tracer test to an inverted five-spot pattern to improve estimation of the PCE spatial distribution using data from the extraction wells. The latter injection/extraction pattern divided the cell into six swept zones, compared to only two swept zones associated with the former. A total extraction rate of 6.6 L/min was distributed unequally among the six wells, and varied from 0.5 L/min (well 44) to 1.5 L/min (well 46). The thickness of the saturated zone was 3.7 m.

Since the DNAPL release points terminated at approximately 1.5 m above the clay-confining layer, it was expected that most of the PCE would be located in the bottom 1.5 m of the cell. Consequently, inflatable packers were placed in the injection wells to segregate injected fluid into upper and lower portions of the wells. The intent of this approach was to focus a suite of tracers to the suspected location of the DNAPL-contaminated zone. This would then produce higher retardation of partitioning tracers injected in the lower zone, compared to a single tracer suite employed without upper-zone/lower-zone vertical segregation. The average saturated thickness of the flow domain was 3.7 m, so the packers were centered at 1.8 m above the clay, dividing the flow domain into two approximately equal halves. The average flow rate injected

into the upper zone and lower zones was 3.7 L/min and 3.1 L/min, respectively. In an effort to provide further spatial resolution of the PCE distribution, unique tracer pairs (Table 2) were injected into the lower zone through each injection well. The unique non-partitioning and partitioning tracers allowed the flow domain to be segregated into eight zones based on the extraction wells BTCs.

2.2.3. Second Partitioning Tracer Test (Post-cosolvent flood)

The procedures for the second partitioning tracer test (post-cosolvent flood) were the same as the first partitioning tracer test, with the exception of modifications to the tracer suite (Table 2). Unique tracers were not used in the injection wells (45 and 55) to reduce the analytical workload. Isobutyl alcohol (IBA) was used in place of isopropyl alcohol (IPA), and 2-ethyl-1-hexanol (2E1H) was added to the upper-zone suite to avoid suspected degradation problems experienced in the first test. Since less DNAPL was expected, 3,5,5-trimethyl-1-hexanol (TMH) was added to the lower-zone suite because of its higher partitioning coefficient, which would produce more retardation, and therefore yield more reliable PCE volume estimates. No free-phase PCE was detected in the wells prior to tracer injection. The total extraction rate of 6.8 L/min was achieved by distributing extraction among the six wells, with extraction rates varying from 0.3 L/min (well 44) to 1.5 L/min (well 56). The saturated zone thickness for this test was 3.6 m.

2.2.4. Third Partitioning Tracer Test (Pre-surfactant flood)

Prior to the third partitioning tracer test (pre-surfactant flood, conducted after the second PCE release, Table 1), each well was checked for free-phase PCE using a bailer with a rigid push

rod. Free-phase PCE was removed from wells 41 (0.14 L), 46 (1.7 L), 51 (1.2 L), and 53 (0.3 L) (Figure 1). The volumes of PCE removed from wells 46 and 51 suggested a large fraction of the PCE was located in the southeast portion of the cell.

The injection/extraction pattern used in this test was changed to create a vertical circulating pattern around wells 41, 44, 45, 46, 51, 54, 55, and 56 (Figure 1). This pattern was used because of the potential advantage it offers by forcing flow normal to horizontal laminations associated with a heterogeneous formation, including the low-conductivity layers that may be by-passed in a horizontal flow field. Each vertical circulation well included an inflatable packer (approximately 1.4 m long) installed to isolate a 0.3 m section of well screen above the clay interface. Fluid was pumped through the packer and into the cell over this screen interval between 12.0 and 12.3 m bgs. Due to excessive pressure in the injection tubing in wells 44, 51, and 55, the packers were raised during the test by approximately 0.3 m, so the injection interval in these wells was approximately from 11.7 to 12.3 m bgs. Air bladder extraction pumps were installed such that the pump intakes were approximately 0.2 m above the top of the packers. The flow rates through each vertical circulation well varied from approximately 0.13 L/min (well 51) to 0.90 L/min (well 55), and averaged 0.48 L/min, yielding a total extraction rate of 3.8 L/min over a saturated zone thickness of 3.9 m.

2.2.5. Fourth Partitioning Tracer Test (Post-surfactant flood)

The fourth partitioning tracer test (post-surfactant flood) employed identical procedures to that used in the third tracer test. No free-phase PCE was detected in the wells prior to the test. The flow rates through each vertical circulation well varied from approximately 0.17 L/min (well

46) to 0.73 L/min (well 55), and averaged 0.46 L/min, with a total extraction rate of 3.7 L/min over a saturated thickness of 3.5 m.

3. Results

3.1. Tracer Tests

3.1.1. First Partitioning Tracer Test (Pre-cosolvent flood)

A summary of the results from the first partitioning tracer test (pre-cosolvent flood) is given in Table 3. Results for selected tracers (methanol and 2-octanol) for each extraction well are summarized in Figure 2. Extraction well 51 had the largest tracer retardation factors. Selected BTCs for well 51 are shown on a semi-log graph in Figure 3, and indicate that the retardation was primarily in the tailing portion of the BTC. This indicated that the NAPL was non-uniformly distributed since a uniform distribution would produce a simple offset of the nonpartitioning and partitioning tracer BTCs (Jawitz et al., 1998b). The total volume of DNAPL estimated in the lower-swept zone varied for each partitioning tracer, and ranged from 22 L based on 2-octanol to 71 L based on *n*-hexanol (Table 3).

Both the upper-zone nonpartitioning tracer (IPA) and partitioning tracer (*n*-heptanol) showed relatively poor recovery (86% and 72%, respectively), and moment analysis of their BTCs produced retardation factors less than one (Table 4). This is likely due to tracer degradation since straight–chain alcohols tend to degrade more rapidly in the environment based on the authors' experience in other partitioning tracer field trials. These tracers were not in the original suite of tracers designed for this test but were substituted for pentaflourobenzoic acid

and 2,6-dimethyl-4-heptanol when regulatory approval for these latter tracers was denied just prior to the start of the test. To provide an estimate of the volume of PCE in the upper swept zone, some correction for tracer degradation was required. The simplest approach was to assume a first-order degradation model and estimate the degradation rate constant necessary to recover the injected tracer mass. Each concentration measurement in the BTC was adjusted using:

$$C_{adj} = \frac{C}{e^{-kt}}$$

where C is the measured concentration, C_{adj} is the estimated concentration with no degradation, k is the decay coefficient, and t is the time that the sample was collected after the mean of the tracer pulse injection. In recalculating the zeroth moment of each tracer, the degradation coefficient was adjusted to achieve 100% mass recovery. This approach required two critical assumptions: (1) the tracer degradation is assumed to follow first-order kinetics, and (2) a single k value represents the entire test cell. The approach used here ignores the width of the tracer pulse (i.e., Dirac input assumed), but this approximation should have minimal impact on the adjusted moments.

The degradation-corrected, upper-zone BTCs for well 51 are shown in Figure 3B and the degradation-corrected, upper-zone tracer moments for all wells are listed in Table 4. The tracer retardation in two of the extraction wells (44 and 54) remained less than one, and the saturations were assumed zero for summing the NAPL present in the cell. The volume of PCE estimated using the degradation corrected BTCs was 47 L. This represents a significant volume of PCE relative to the volume of PCE estimated in the lower zone (22 to 71 L). The degradation correction therefore takes on importance. This also indicates that a substantial fraction of the PCE present in the test cell was in the upper-swept zone. This may indicate that PCE was

located higher in the test cell than anticipated based on the release locations, or that the upper-zone tracers traveled into the lower zone more than expected.

The estimated total swept volume for this test was 16,600 L, based on methanol results in the lower zone and degradation-corrected IPA results in the upper zone, and the estimated volume of PCE was 69 L, based on the degradation corrected n-heptanol results in the upper zone and 2-octanol in the lower zone (Tables 3 and 4). The lower-zone PCE volume estimate was based on 2-octanol results because retardation factors for 2-octanol (Figure 4) were most consistently within the recommended range of 1.2 to 4.0 (Jin et al., 1997). The results for each extraction well (EW) were used to estimate the spatial distribution of PCE within the test cell. The six EWs had six unique swept zones based on results from the methanol tracer in the lower zone and the IPA tracer in the upper zone. Results from the lower-zone unique tracers applied to the two injection wells were used to separate the lower-zone swept volume (based on methanol) associated with EWs 46 and 56 into two parts, thereby delineating eight separate swept zones within the lower portion of the test cell. The results of the unique tracer suites are presented in Table 3. The results of the spatial analysis, based on EWs, are presented in Figure 5. Note that much of the PCE was found in the southeast corner of the cell.

3.1.2. Second Partitioning Tracer Test (Post-cosolvent flood)

The results from the second partitioning tracer test (post-cosolvent flood) are summarized in Table 3, with individual extraction well results for selected tracers (methanol and TMH) presented in Figure 2. Tracer mass recoveries ranged from 88% to 97%, and as such, degradation corrections were not considered necessary. The total swept zone, based on nonpartitioning tracers (methanol in the lower zone and IBA in the upper zone), was

approximately 15,000 L, or approximately 10% smaller than the total swept zone estimated in Test 1. The estimated volume of PCE in the lower zone ranged from 45 L based on *n*-hexanol to 4 L based on TMH, and the PCE volume in the upper zone ranged from 5 L based on *n*-heptanol to 1 L based on 2E1H. A total of 5 L were estimated based on partitioning tracers 2E1H in the upper zone and TMH in the lower-zone (Table 3), selected because they generally had the largest retardation factors (Figure 4). All retardation factors for 2E1H were less than 1.2, which indicates a greater uncertainty in the PCE volume estimates compared to estimates based on retardation factors larger than 1.2 (Jin et al., 1997).

3.1.3. Third Partitioning Tracer Test (Pre-surfactant flood)

Results from the third partitioning tracer test (pre-surfactant flood) are summarized in Table 5; selected tracer (TBA and TMH) results for each extraction well are shown in Figure 2. Mass recoveries for the alcohol tracers ranged from 96% (TBA) to 121% (TMH). Residual ethanol from the cosolvent flood produced some analytical interference in the methanol laboratory analysis. Consequently, TBA was used as the non-partitioning tracer in the subsequent analysis. The swept volume estimate based on TBA was 12,200 L. The estimated volume of PCE ranged from 191 L based on *n*-hexanol to 33 L based on THM, with the estimated volume of PCE based on TMH (33 L) considered most reliable because this tracer's retardation factors were all greater than 1.2 (Figure 4). Selected tracer BTCs are shown for wells 51 and 55 in Figure 6. As noted for the first tracer test, retardation of the partitioning tracer relative to the non-partitioning tracer was primarily in the tailing portion of the BTC for well 51, indicating a non-uniform NAPL distribution. In contrast, there appears to be a clearer peak separation in well 55, which may result from the efficiency with which the vertical circulating

pattern intercepts PCE distributed in the swept zone. The spatial distribution of the PCE based on the vertical circulation wells is shown in Figure 7.

3.1.4. Fourth Partitioning Tracer Test (Post-surfactant flood)

Results from the last partitioning tracer test (post-surfactant flood) are summarized in Table 5, and selected tracer (methanol and TMH) results for each extraction well are shown in Figure 2. Mass recoveries ranged from 86% (2-octanol) to 91% (TBA), with the exception of *n*-hexanol with a mass recovery of 80%. All mass recoveries were less than those from Test 3. In contrast to the last tracer test where methanol analytical interference was suspected, components used in the surfactant flushing solution interfered with TBA laboratory analysis and methanol was therefore used as the non-reactive tracer. The swept volume estimates based on the extrapolated, normalized first moment of methanol was 11,800 L. The estimated volume of PCE ranged from 20 L based on *n*-hexanol to 31 L based on DMP. The predicted PCE volumes were much less variable than in the previous tests, and there is little difference between the pre- and post-flushing results for TMH, the tracer with the largest retardation factors. On first inspection, this would indicate that little PCE was removed during the surfactant flood. This conclusion, however, is not supported by preliminary results from the surfactant flood, which indicate that approximately 49 L were removed. An alternative explanation could be the interference of partitioning tracer behavior by resident surfactants remaining in the cell.

3.2. Controlled Release Conducted by EPA

3.2.1. Release Details

The release of PCE into the cell was designed to produce a DNAPL distribution within the target flow zone between 10.7 and 12.3 m bgs. Researchers from EPA conducted the release by pumping selected volumes of PCE down the release tubes (to a depth of 10.7 m) at a typical flow rate of 0.57 L/min for the first release, and a higher, typical rate of 0.90 L/min for the second release. The intent of the release method was to encourage lateral and vertical spreading of PCE in the formation while minimizing pooling of the DNAPL on the clay-confining unit, and therefore minimize the potential for downward migration of PCE through natural fractures in the clay or openings produced during sheet pile installation. Results from controlled releases in 2-dimensional physical models and numerical simulations suggested that DNAPL would initially spread laterally along the water table and migrate downward as the DNAPL head increased or the water table elevation was lowered. Thus, the water table elevation in the test cell was manipulated to facilitate first horizontal and then vertical spreading of the DNAPL. The water table elevation was positioned at approximately 0.3 m below the release tubes prior to PCE injection. Water was extracted from the cell during and immediately after the DNAPL release and continued until the transient water table elevation was approximately 0.3 m above the clay interface. Tap water was then injected into the cell to raise the water table to an elevation above the PCE injection level. The total volume of PCE injected during the first release was 91.7 L, and the total volume of PCE injected during the second release was 49.4 L. The spatial injection patterns for the first and second releases are shown in Figures 5 and 7, respectively.

3.2.2. Comparison of First Release to Tracer Tests 1 and 2

The line-drive conservative tracer test conducted by EPA (Table 1) removed 3 L of PCE through dissolution by flushing approximately 5 pore volumes of water through the cell, and another 3 L of PCE were removed as free product from well 56 prior to the start of tracer Test 1. Therefore, 86 L of PCE were in the cell at the start of tracer Test 1. A comparison of the predicted PCE volumes to the expected PCE volume is shown in Figure 8. Using only the lower-zone tracer results of 2-octanol, since this tracer displayed the largest retardation factors and therefore presumably yields the most reliable volume estimates, 22 L were predicted, or 26% of the expected volume. Using lower-zone 2-octanol results and degradation-corrected, upper-zone *n*-heptanol results, 69 L or 80% of the expected volume was predicted. These comparisons neglect degradation of PCE as well as the dissolved PCE mass. Approximately 2 L (assuming equilibrium dissolution) or less of PCE may have been resident in solution when the tracer test was initiated and would not be part of the tracer estimate. Accounting for the mass of PCE removed by tracer Test 1 and the cosolvent flood (Brooks, 2000), 30 L of PCE were estimated in the cell at the start of tracer Test 2. The estimate of the PCE in the cell, based on the upper- and lower-zone tracers with the largest partitioning coefficients was 5 L, or 17% of the expected value (Figure 8).

The spatial distribution of the release can be compared to the spatial resolutions based on the EW data from Test 1 (Figure 5). The comparison must be made recognizing that the DNAPL may have migrated to different regions of the test cell based on the geologic structure of the media in the test cell. The spatial pattern of the lower-zone and upper-zone PCE distribution based on the extraction wells generally agree with the release data in a qualitative comparison. Higher saturation zones are located in the lower swept zones of wells 46 and 56 where

significant mass was released, and little PCE was detected in the lower swept zone of wells 44 and 54. Migration of PCE into the region swept by well 51 may have occurred based on the comparison of the high PCE volumes detected in both the lower and upper zones relative to the release volume in that region.

It is apparent that both tracer tests underestimated the volume of PCE present in the test cell, based on the results of tracers with the largest partitioning coefficients. In terms of PCE volume, the first two tracer tests underestimated the amount of PCE released into the cell by about 17 L to 25 L. This might suggest that 17 L to 25 L of PCE were not hydraulically accessible to the tracers. This NAPL could have been pooled on the clay or located in isolated corners or regions of the test cell. The fact that the cosolvent flood failed to remove approximately 30 L of NAPL may also support this conclusion (Brooks et al., 2000; Brooks, 2000). The fact that the pre-flushing tracer test has high uncertainties caused by degradation of the upper zone tracers must be recognized when reaching this conclusion.

3.2.3. Comparison of Second Release to Tracer Tests 3 and 4

The comparison of results from the third tracer test to the second release information must be made recognizing that the level of uncertainty of this comparison is higher than the first comparison due to the activities conducted in the cell prior to the second PCE release (i.e., first PCE release and cosolvent flood). If the basis for evaluating the tracer predictions is the total PCE estimated in the cell at the start of the third tracer test, then the expected PCE volume is 74 L (28.5 L remaining from the cosolvent demonstration, plus 49.4 L injected during the second release, minus 3.7 L removed between the release and the start of Test 3 as either free-phase or dissolved PCE). Based on the tracer with retardation factors consistently larger than 1.2 (TMH),

the predicted PCE volume is 33 L (Table 5), or approximately 45% of the expected volume. Based on the mass of PCE removed during tracer Test 3, and preliminary results from the surfactant flood, the amount of PCE in the cell at the start of tracer Test 4 was 21 L. Based on the TMH results from Test 4, the predicted PCE volume was 30 L, or 143% of the expected volume.

4. Discussion

4.1. Prediction Uncertainty

How well should the partitioning tracer methodology predict the PCE volume, in the absence of all complicating factors? Recent analysis suggest that for conservatively large errors in fundamental measurements, and for retardation factors of 1.2 or greater, the error in estimated PCE saturations and volumes are on the order of 10% or less, neglecting uncertainties associated with BTC extrapolation. The inherent uncertainty associated with partitioning tracer methodology is relatively small, as shown in recent work by Dwarakanath et al. (1999) and Jin et al. (2000) on the errors in PCE saturation estimates based on partitioning tracer theory. The random errors associated with sample analysis and flow measurements can be propagated through the moment calculations in an effort to provide a measure of the error in the PCE volume estimates as well (Brooks, 2000).

The regulatory permit restricted the PCE release volume to less than 100 L, which resulted in cell-average PCE residual saturations of 0.005 and 0.0009 for Test 1 and Test 2, respectively, and 0.002 for Test 3 and 4. Thus, only tracers with large K_{nw} are expected to yield retardation factors larger than 1.2 recommended by Jin et al. (1995, 1997). However, non-uniform DNAPL distribution is manifested as extensive tailing in tracer BTCs, even for cases

when the retardation factor is greater than or equal to 1.2. As such, moment analysis and PCE volume estimates are complicated by reliance on BTC data extrapolation beyond the region of analytical reliability of measured low tracer concentrations. Thus, all of our tests were performed near the lower limits of the tracer technique's design capabilities. Extrapolation of the BTC using an assumed model (typically an exponential function) is typically employed to minimize truncation errors (Pope et al., 1994; Annable et al., 1998). Figure 8 indicates the extent to which the extrapolation calculations changed the PCE volume predictions in this work. Other extrapolating functions or analysis procedures may prove better suited for accurately predicting the PCE volume.

An assessment of performance between the four tests should also be made with the recognition that, in general, the prediction uncertainty increased for each subsequent tracer test conducted in the cell. This results from factors which are not an inherent part of the partitioning-tracer methodology, but rather, from factors introduced due to the nature of the test setting and the structure of the project. There was also the added complexity of tracer degradation for the upper-zone tracers in Test 1, and the complicating potential for residual cosolvent flushing solution to impact partitioning tracer behavior for Tests 2, 3, and 4.

Another source of uncertainty was background tracer sorption. Results from the background tracer test yielded an equivalent background PCE volume of 52 L based on DMP results. This value represents a significant volume of PCE relative to the maximum release volume of 100 L, and more importantly, it represents a significant volume of PCE relative to the PCE volume estimates obtained in the later tracer tests. Due to potential changes in sorption characteristics after remedial flushing, corrections based on results from the background tracer test were considered inappropriate for tests other than Test 1. Moreover, corrections were only

considered appropriate for PCE volume estimates based on DMP, due to potential changes in sorption characteristics for each tracer. Tracers with larger partitioning coefficients may in fact have greater background sorption due to their larger hydrophobicity. Finally, application of background sorption corrections was hindered by changes in the injection/extraction pattern and saturated thickness in the background tracer test and Test 1. Had it been possible to apply corrections for background tracer retardation, the estimated PCE volume would have been systematically smaller.

4.2. Hydrodynamic Accessibility

The discrepancy between predicted and expected PCE volumes could be the result of DNAPL migration to locations in the cell which were hydraulically isolated from the tracer flow fields, such as topographic low spots on the clay confining layer or "pools" formed in other locations. The elevation of the clay confining unit varied by approximately 0.6 m across the cell based on the boring log information. Free-phase PCE was collected from well 56 prior to Test 1 and the maximum depth to clay (12.5 m) was estimated from the boring log for this well. It is possible therefore, that some PCE pooled in the low spot around this well, or other locations that were lower than detected during coring. Jin et al. (1997) investigated errors in partitioning tracer predictions if pooled DNAPL were present using modeling simulations. The relative error between tracer predicted PCE volumes and expected PCE volumes based on those modeling scenarios are comparable to the relative errors reported herein. Likewise, relative errors reported herein are similar to those reported from laboratory experiments conducted to investigate the impact of preferential flow and physical nonequilibrium on partitioning tracer predictions (Nelson et al., 1999).

Limitations in hydrodynamic accessibility could also have occurred as a result of potential PCE injection into, or migration to layers of low conductivity within the flow field. Limitations in hydrodynamic accessibility could subsequently result as the tracers by-passed these low-conductivity regions. Hydrodynamic accessibility can be evaluated as a function of the pumping pattern for the pre-remedial demonstrations by a comparison of the swept volumes (determined from first normalized moments for the non-reactive tracers). These moments yield swept volume estimates of 16,600 L (Table 3 and 4, methanol for lower zone and IPA, corrected, for upper zone) for Test 1 and 12,200 L for Test 3 (Table 5). Based on the average water elevation over the duration of the test, an effective porosity estimate of 0.29 (0.26 if uncorrected IPA results are used) is obtained for Test 1, and 0.20 to 0.22 is obtained for Test 3 using TBA and methanol, respectively. Therefore, the double five-spot pumping pattern appears to have sampled a larger portion of the cell pore space. This could be explained using the conclusion reached from Chen and Knox (1997) that vertical circulation wells with unequal injection and extraction rates could produce dead zones not swept by the tracers. Since the total injection rate and extraction rate were approximately equal, the entire pore space should have been swept. However, on a more local scale, differences between injection and extraction rates may have contributed to more stagnant zones in the cell compared to the double five-spot pattern. Another disadvantage to vertical circulation wells lies in the potential for the tracer to short circuit the formation and flow directly from the injection to extraction portions of the well. The bimodal nature of the BTC from well 51 (Figure 6), which was also observed in well 44, is evidence that some short-circuiting occurred in these wells during Test 3.

4.3. Prediction Variability within a Single Test

As indicated by the results summarized in Tables 3 and 5, the tracers with smaller partitioning coefficients predicted more PCE than tracers with larger partitioning coefficients. It is unclear why this trend was observed, but one possible explanation is rate-limited mass transfer processes. Tracers with larger partitioning coefficients have larger affinities for the NAPL, and may therefore experience more rate-limited desorption than tracers with smaller partitioning coefficients (Heyse et al., 2001). Theoretical analysis (Valocchi, 1985) suggests that the first normalized moment of tracer BTCs, hence the estimated retardation factor, is not expected to be influenced by non-equilibrium sorption/partitioning. Extensive tailing of the BTCs resulting from non-equilibrium processes does increase the higher moments, reflecting increased spreading and tailing. In practice, therefore, underestimation of the first-normalized moment from measured tracer BTCs is likely due to problems of data truncation and errors associated with data extrapolation.

5. Summary and Conclusions

The primary objective of the partitioning tracer "blind" tests reported here was to evaluate the reliability with which DNAPL volume within a source zone can be estimated for the case where the total volume of DNAPL released into a hydraulically isolated test cell was exactly known. A total PCE release volume of less than 100 liters (regulatory permit limits) and the resulting average PCE residual saturation of about 0.01, as well as the expected heterogeneous PCE spatial distribution all contributed to a challenging task at the very outset. As a result, the tracer tests were being conducted possibly near the limits of the technology. These problems were expected to be even more vexing for the post-remediation tracer tests because the PCE volume would be smaller since PCE mass was removed by in-situ flushing, and

much of the remaining PCE is likely to be located in hydrodynamically inaccessible zones of the swept volume. Various design and experimental strategies (multiple tracers with a range of partitioning coefficients in all tests, vertical segregation in Tests 1 and 2, vertical pumping patterns in Tests 3 and 4) were attempted to overcome each of these limitations in conducting the tracer tests. However, interpretation of the data from each tracer test was confounded by additional complications.

In all tracer tests, the PCE volume was underestimated. This could be attributed to low average residual saturations of PCE, as discussed above. While selection of tracers with larger partition coefficient is warranted, increased mass-transfer constraints limited data interpretation. The reported estimates of PCE volumes ignore background tracer retardation, and would be even less if corrections were included. Two general observations can be made based on the results from the first three partitioning tracer tests: (1) the PCE volume predicted varied within each test depending on the partitioning tracer, and (2) the predicted PCE volume was less than expected, even when using the data for partitioning tracers with the largest partitioning coefficients (18% to 80% of the expected volume). In contrast, the last partitioning tracer test displayed relatively little prediction variation, and its predicted PCE volume was larger than the expected PCE volume (143% for the tracer with the largest partitioning coefficient). However, the similarity in predicted PCE volumes between Test 3 and Test 4 (pre- and post-surfactant flushing), at least for the tracers with the highest partitioning coefficients, does not agree with the preliminary results of PCE volume removed during the surfactant flood, and calls into question the reliability of the test results. An increase in background sorption of tracers due to the presence of residual surfactant sorbed to the aquifer matrix was the likely reason for larger retardation. Finally,

uncertainties introduced in accounting for tracer degradation were significant in the first partitioning tracer test.

A general conclusion that can be drawn from these experimental results is that tracer test data need to be critically evaluated for multiple confounding factors and artifacts. The hydrogeological and biogeochemical characteristics of the source zone, heterogeneous DNAPL distributions, tracer selection, injection/extraction schemes, and prior activities in the source zone all play a role in determining the outcome of the partitioning tracer tests. Interpreting the results from the partitioning tracer tests must be reviewed with these factors in mind.

The tracer tests, under the conditions of our studies, provided a reliable qualitative confirmation of the presence of DNAPL within the swept zone. But, the quantitative estimates of DNAPL volume were subject to large errors. However, in all four tests, results from the tracer suite did bracket the expected volume. The reliability of the tracer technique is likely to be better for the cases where the DNAPL volume is greater or the average DNAPL saturation is larger, but controlled experiments to confirm this have not been conducted.

Acknowledgments

The authors gratefully acknowledge the help of Sten Berglund, Jaehyun Cho, Clayton Clark, Lane Evans, Andrew James, Heonki Kim, Suzy Kuhn, Irene Poyer, Claire Shukla, Gloria Sillan, and Meifong Zhou from the University of Florida; Gavin James from the University of Oklahoma; Mark Hogan and Rob Young from Mantech Environmental Research Services Corporation; Mark Hasegawa and Jarod Norris from SURBEC; Tim McHale, Dover National Test Site Program Manager, Air Force Research Laboratory; Russel Cook, Bart Faulkner, John Hoggatt, Tony Lee, and Susan Mravik from the EPA; and Major Paul Devane from Armstrong

Laboratories, Tyndall AFB. This project was funded by the United States Department of Defense (DOD) Strategic Environmental Research and Development Program (SERDP), which is a collaborative effort involving the EPA, DOD, and the United States Department of Energy. This document has not been subjected to peer review within the funding agency, and the conclusions stated here do not necessarily reflect the official views of the agency nor does this document constitute an official endorsement by the agency.

The Dover National Test Site is one of four National Environmental Technology Site (NETTS) locations established and managed by SERDP. The demonstration complied with prescribed NETTS protocols and guidelines for quality assurance, health and safety, technical completeness, and regulatory compliance. The support of the NETTS facilities and test location manager and staff are gratefully acknowledged. For further information on NETTS locations or SERDP, contact Cathy Vogel or Matt Chambers at 703-478-5186 or visit the SERDP web site at www.serdp.gov.

References

Annable, M.D., Rao, P.S.C., Graham, W.D., Hatfield, K., Wood, A.L., 1995. Use of partitioning tracers for measuring residual NAPL distribution in a contaminated aquifer: Preliminary results from a field-scale test. *2nd Tracer Workshop*, Austin, Texas, pp. 77-85.

Annable, M.D., Rao, P.S.C., Hatfield, K.H., Graham, W.D., Wood, A.L., Enfield, C.G., 1998. Partitioning tracers for measuring residual NAPL: Field-scale test results. *Journal of Environmental Engineering*. 124 (6), 498-503.

Brooks, M.C., 2000. Characterization and remediation of a controlled DNAPL release: field study and uncertainty analysis. Ph.D. Dissertation, University of Florida, Gainesville, Florida, 147 pp.

Brooks, M.C., Annable, M.D., Rao, P.S.C., Hatfield, K., Jawitz, J.W., Wise, W.R., Wood, A.L., C.G. Enfield, 2000. Field-scale cosolvent flushing of DNAPL from a controlled release. Submitted to *Water Resources Research.*

Brooks, S.C., Taylor, D.L., Jardine, P.M., 1998. Thermodynamics of bromide exchange on ferrihydrite: Implications for bromide transport. *Soil Science Society of America Journal*, 62(5), 1275-1279.

Brusseau, M.L., Nelson, N.T., Cain, R.B., 1999. The partitioning tracer method for in-situ detection and quantification of immiscible liquids in the subsurface. In *Innovative Subsurface Remediation, Field Testing of Physical, Chemical, and Characterization Technologies*, ACS Symposium Series 725, edited by M.L. Brusseau, D.A. Sabatini, J.S. Gierke, and M.D. Annable, American Chemical Society, Washington, D.C., 208-225.

Cain, R.B., Johnson, G.R., McCray, J.E., Blanford, W.J., Brusseau, M.L., 2000. Partitioning tracer tests for evaluating remediation performance. *Ground Water*, 38(5), 752-761.

Cooke, C.E., Jr., 1971. Method for determining residual oil saturation. U.S. Patent 3,590,923., U.S. Patent Office, Washington, D.C.

Dean, H.A., 1971. Method for determining fluid saturation in reservoirs. U.S. Patent 3,623,842, U.S. Patent Office, Washington, D.C.

Dwarakanath, V., Deeds, N., Pope, G.A., 1999. Analysis of partitioning interwell tracer tests. *Environmental Science and Technology,* 33(21), 3829-3836.

Falta, R.W., Lee, C.M., Brame, S.E., Roeder, E., Coates, J.T., Wright, C., Wood, A.L., Enfield, C.G., 1999. Field test of high molecular weight alcohol flushing for subsurface nonaqueous phase liquid remediation. *Water Resources Research*, 35(7), 2095-2108.

Hayden, N.J., Linnemeyer, H.C., 1999. Investigation of partitioning tracers for determining coal tar saturation in soils. In *Innovative Subsurface Remediation, Field Testing of Physical, Chemical, and Characterization Technologies*, ACS Symposium Series 725, edited by Brusseau, M.L., Sabatini, D.A., Gierke, J.S., Annable, M.D., American Chemical Society, Washington, D.C., 208-225.

Heyse, E., Augustijn, D.C.M., Rao, P.S.C., Delfino, J.J., 2001. Nonaqueous phase liquid dissolution and soil organic matter sorption in porous media: Review of system similarities. *CRC Critical Reviews in Environmental Control* (In Review; submitted March 2001).

James, A.I., Graham, W.D., Hatfield, K., Rao, P.S.C., Annable, M.D., 2000. Estimation of spatially variable residual flow fields using partitioning tracer data. *Water Resources Research*, 36(4), 999-1012.

Jawitz, J.W., Annable, M.D., Rao, P.S.C., Rhue, R.D., 1998a. Field implementation of a winsor type I surfactant/alcohol mixture for in situ solubilization of a complex LNAPL as a single-phase microemulsion. *Environmental Science and Technology*, 32(4), 523-530.

Jawitz, J.W., Annable, M.D., Rao, P.S.C., 1998b. Characterizing the spatial distribution of non-aqueous phase contaminants using partitioning tracers and the method of moments. International Conference and Special Seminars on Groundwater Quality: Remediation and Protection, IAHS, Tubingen, Germany, 422-425.

Jawitz, J.W., Sillan, R.K., Annable, M.D., Rao, P.S.C., Warner, K., 2000. In-situ alcohol flushing of a DNAPL source zone at a dry cleaner site. *Environmental Science and Technology*, 34(17), 3722-3729.

Jin, M., Delshad, M., Dwarakanath, V., McKinney, D.C., Pope, G.A., Sepehrnoori, K., Tilburg, C., Jackson, R.E., 1995. Partitioning tracer test for detection, estimation, and remediation performance assessment of subsurface nonaqueous phase liquids. *Water Resources Research*, 31(5): 1201-1211.

Jin, M., Butler, G.W., Jackson, R.E., Mariner, P.E., Pickens, J.F., Pope, G.A., Brown, C.L., McKinney, D.C., 1997. Sensitivity models and design protocols for partitioning tracer tests in alluvial aquifers. *Ground Water*, 35(6): 964-972.

Jin, M., Jackson, R.E., Pope, G.A., 2000. The interpretation and error analysis of PITT data. In Treating dense nonaqueous-phase liquids (DNAPLs): Remediation of chlorinated and recalcitrant compounds, edited by Wickramanayake, G.B., Gavaskar, A.R., Gupta, N.,

Lee, C.M., Meyers, S.L., Wright, C.L., Jr., Coates, J.T., Haskell, P.A., Falta, R.W., Jr., 1998. NAPL compositional changes influence partitioning coefficients. *Environmental Science and Technology*, 32(22), 3574-3578.

Nelson, N.T., Brusseau, M.L., 1996. Field study of the partitioning tracer method for detection of dense nonaqueous phase liquid in a trichloroethene-contaminated aquifer. *Environmental Science & Technology*, 30(9): 2859-2863.

Nelson, N.T., Oostrom, M., Wietsma, T.W., Brusseau, M.L., 1999. Partitioning tracer method for the in situ measurement of DNAPL saturation: Influence of heterogeneity and sampling method. *Environmental Science & Technology*, 33(22), 4046-4053.

Noll, M.R., Farrington, S.P., McHale, T.J., 1998. *Permit Application for United States Air Force Groundwater Remediation Field Laboratory, Cosolvent Solubilization Technology Demonstration.* Submitted to the Delaware Department of Natural Resources and Environmental Control, May.

Pope, G.A., Jackson, R.E., 1999a. Characterization of organic contaminants and assessment of remediation performance in subsurface formations. U.S. Patent 6,003,365, U.S. Patent Office, Washington, D.C.

Pope, G.A., Jackson, R.E., 1999b. Characterization of organic contaminants and assessment of remediation performance in subsurface formations. U.S. Patent 5,905,036, U.S. Patent Office, Washington, D.C.

Pope, G.A., Jin, M., Dwarakanath, V., Rouse, B., Sepehrnoori, K., 1995. Partitioning tracer tests to characterize organic contaminants. *2nd Tracer Workshop*, Austin, Texas, pp. 65-75.

Rao, P.S.C., Annable, M.D., Sillan, R.K., Dai, D., Hatfield, K.H., Graham, W.D., Wood, A.L., Enfield, C.G., 1997. Field-scale evaluation of in-situ cosolvent flushing for enhanced aquifer remediation. *Water Resources Research*, 33 (12), 2673-2686.

Rao, P.S.C., Annable, M.D., Kim, H., 2000. NAPL source zone characterization and remediation technology performance assessment: Recent developments and applications of tracer techniques, *Journal of Contaminant Hydrology*. 45 (1-2), 63-78.

Starr, R.C., Cherry, J.A., Vales, E.S., 1992. A new steel sheet piling with sealed joints for groundwater pollution control. 45th Canadian Geotechnical Conference, Toronto, Ontario.

Tang, J.S., 1995. Partitioning tracers and in-situ fluid-saturation measurements. *SPE Formation Evaluation*, 10 (1), 33-39.

Thomas, A., 1996. GRFL: An opportunity in groundwater remediation research. *The Civil Engineer*, 4 (2), 34-35.

Valocchi, A., 1985. Validity of the local equilibrium assumption for modeling sorbing solute transport through homogeneous soils. *Water Resources Research*, 21 (6), 808-820.

Willson, C.S., Pau, O., Pedit, J.A., Miller, C.T., 2000. Mass transfer rate limitation effects on partitioning tracer tests. *Journal of Contaminant Hydrology*, 45 (1-2), 79-97.

Wise, W.R., 1999. NAPL characterization via partitioning tracer tests: quantifying effects of partitioning nonlinearities. *Journal of Contaminant Hydrology*, 36 (1-2), 167-183.

Wise, W.R., Dai, D., Fitzpatrick, E.A., Evans, L.W., Rao, P.S.C., Annable, M.D., 1999. Non-aqueous phase liquid characterization via partitioning tracer tests: A modified Langmuir relation to describe partitioning nonlinearities. *Journal of Contaminant Hydrology*, 36 (1-2), 153-165.

List of Tables

List of Figures

retardation factors, and the dashed line represents the recommended minimum retardation factor for use in partitioning tracer predictions (Jin et al., 1997). Retardation factors shown for *n*-heptanol in Test 1 are based on degradation-corrected results.

Figure 5. PCE distribution based on Test 1(pre-cosolvent flood) extraction well results. Upper-zone PCE volume (L) estimates are based on the corrected IBA and *n*-heptanol results, and the lower-zone PCE volume estimates are based on methanol, 2-octanol, and the four unique tracers. The PCE volume (L) injected per location during the first release is indicated by the number within the circles (Plan view).

Figure 6. Selected breakthrough curves from A) well 51 and B) well 55, Test 3 (pre-surfactant flood). Shown in each graph are *tert*-butyl alcohol (closed squares), 2-octanol (open diamonds), and 3,5,5-trimethyl-1-hexonal (open triangles).

Figure 7. PCE spatial distribution based on Test 3 (pre-surfactant flood) vertical circulation well results. The PCE volume (L) estimates are based on tracers TBA and TMH. The PCE volume (L) injected per location during the second release is indicated by the number within the circles. (Plan view).

Figure 8. Expected (striped region) and predicted (black, white, and dotted regions) PCE volumes for each test. For Test 1, the black, bottom region represents the volume predicted by the degradation-corrected, upper-zone tracers, and for Test 2, the black, bottom region represents the volume of PCE predicted by extrapolated, upper-zone IBA and 2E1H results. The dotted portion (top region) represents the increase in estimated PCE volume resulting from BTC extrapolation (lower-zone tracers only for Test 1 and Test 2).

Table 1. Activities conducted in the cell.

Activity	Date	Tracer Test Reference Number
Hydraulic Test	September 5 - 8, 1997	
Background Tracer Test	May 28 - June 4, 1998	Background
First Controlled PCE Release	June 10 - 12, 1998	
Conservative Tracer Test	June 19 - 26, 1998	
Pre-Cosolvent Flood Tracer Test	July 1 - 12, 1998	1
Ethanol Flushing Test	February 2 - March 12, 1999	
Post-Cosolvent Flood Tracer Test	May 7 - 19, 1999	2
Second Controlled PCE Release	March 13, 2000	
Pre-Surfactant Flood Tracer Test	June 13 - 29, 2000	3
Surfactant Flushing Test	August 2 - September 15, 2000	
Post-Surfactant Flood Tracer Test	October 9 - 26, 2000	4

Table 2. Tracers used in the partitioning tracer tests. The partitioning coefficients (K_{NW}) are for PCE-water partitioning.

Tracer	Abbreviation	K_{NW}	Used in Tests
Conservative			
Bromide		0	BG, 4
Iodide		0	1[a], 2[a], 3
Methanol		0	BG, 1[a], 2[a], 3, 4
tert-Butyl alcohol	TBA	0	1[b], 3, 4
Isobutyl alcohol	IBA	0	1[c], 2[d]
Isopropyl alcohol	IPA	0	1[d]
Partitioning			
n-Hexanol		8	1[a], 2[a], 3, 4
2,4-Dimethyl-3-pentanol	DMP	30	BG, 1[a], 2[a], 3, 4
3-Heptanol		25	1[c]
n-Heptanol		32	1[d], 2[d]
2-Octanol		110	1[a], 2[a], 3, 4
2-Ethyl-1-Hexanol	2E1H	230	2[d]
n-Octanol		170	BG, 1[b]
3,5,5-Trimethyl-1-Hexonal	TMH	230	2[a], 3, 4

[a]Common lower-zone tracer
[b]Well 45 unique, lower-zone tracer
[c]Well 55 unique, lower-zone tracer
[d]Common upper-zone tracer

Table 3. Summary of tracer results from Test 1 (pre-cosolvent flood) and Test 2 (post-cosolvent flood).

Tracer	Test 1			Test 2		
	Mass Recovery (%)	Swept Volume (L)	PCE Volume (L)	Mass Recovery (%)	Swept Volume (L)	PCE Volume (L)
Upper Zone						
Isopropyl Alcohol[a]	86%	10,800	-			
Isobutyl Alcohol[b]				91%	10,400	-
n-Heptanol	72%	-	0[e]	88%	-	5
2-Ethyl-1-Hexanol[b]				91%	-	1
Common Lower Zone						
Methanol	97%	3,800	-	89%	4,600	-
n-Hexanol	95%	-	71	90%	-	45
2,4-Dimethyl-3-pentanol	100%	-	33	91%	-	12
2-Octanol	104%	-	22	92%	-	6
3,5,5-Trimethyl-1-Hexonal[b]				97%	-	4
Unique Lower Zone						
tert-Butyl Alcohol[a,c]	100%	3,200	-			
n-Octanol[a,c]	130%	-	17			
Isobutyl Alcohol[a,d]	93%	2,500	-			
3-Heptanol[a,d]	96%	-	29			

[a]Test 1 only.
[b]Test 2 only.
[c]Well 45 unique lower zone tracer
[d]Well 55 unique lower zone tracer
[e]Retardaton of n-heptanol relative to isopropyl alcohol was less than one.

Table 4. Test 1 (pre-cosolvent flushing test) upper zone tracer results with degradation corrections.

	Isopropyl Alcohol				n-Heptanol					
Well	Mass Recovery (%)	Corrected Mass Recovery (%)	Corrected Arrival Time (days)	Corrected Swept Volume (L)	Mass Recovery	R	Corrected Mass Recovery	Corrected R	PCE Saturation	PCE Volume (L)
41	9%	12%	2.47	3800	5%	0.89	10%	1.10	0.0031	11.6
44	6%	7%	2.46	1700	3%	0.70	5%	0.50		
46	18%	20%	1.06	2300	17%	0.93	23%	1.19	0.0059	13.6
51	18%	21%	1.18	1800	16%	0.91	22%	1.30	0.0094	17.4
54	20%	22%	0.85	1500	17%	0.81	21%	0.90		
56	15%	17%	1.07	1700	14%	0.85	19%	1.08	0.0024	4.0
Total	87%	100%	-	12800	72%	-	100%	-	-	46.7

Table 5. Summary of tracer results from Test 3 (pre-surfactant flood) and Test 4 (post-surfactant flood).

Tracer	Test 3			Test 4		
	Mass Recovery (%)	Swept Volume (L)	PCE Volume (L)	Mass Recovery (%)	Swept Volume (L)	PCE Volume (L)
Methanol	103%	13,100	-	90%	11,800	-
tert-Butyl Alcohol	96%	12,200	-	91%	12,200	-
n-Hexanol	111%	-	191	80%	-	20
2,4-Dimethyl-3-pentanol	101%	-	78	88%	-	31
2-Octanol	106%	-	49	86%	-	29
3,5,5-Trimethyl-1-Hexonal	121%	-	33	90%	-	30

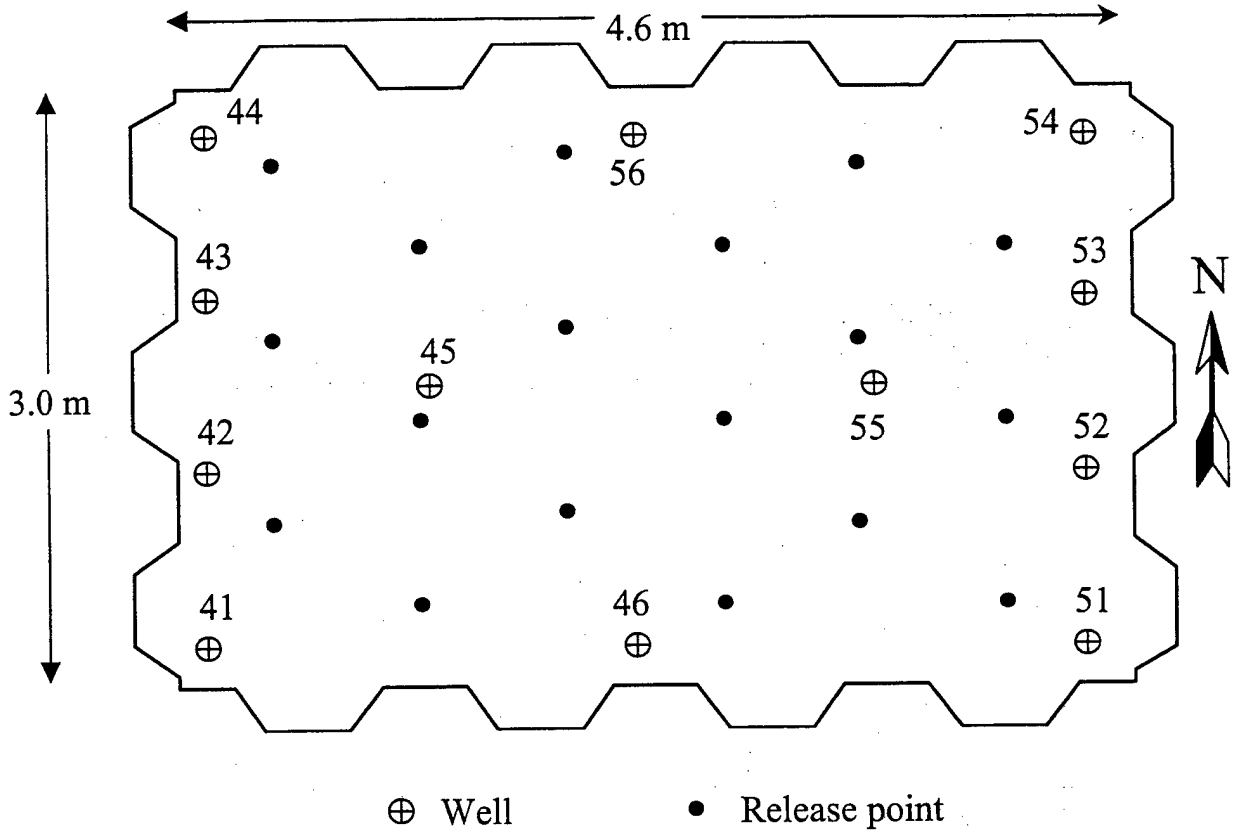

Figure 1 Test cell instrumentation layout. (Plan view.)

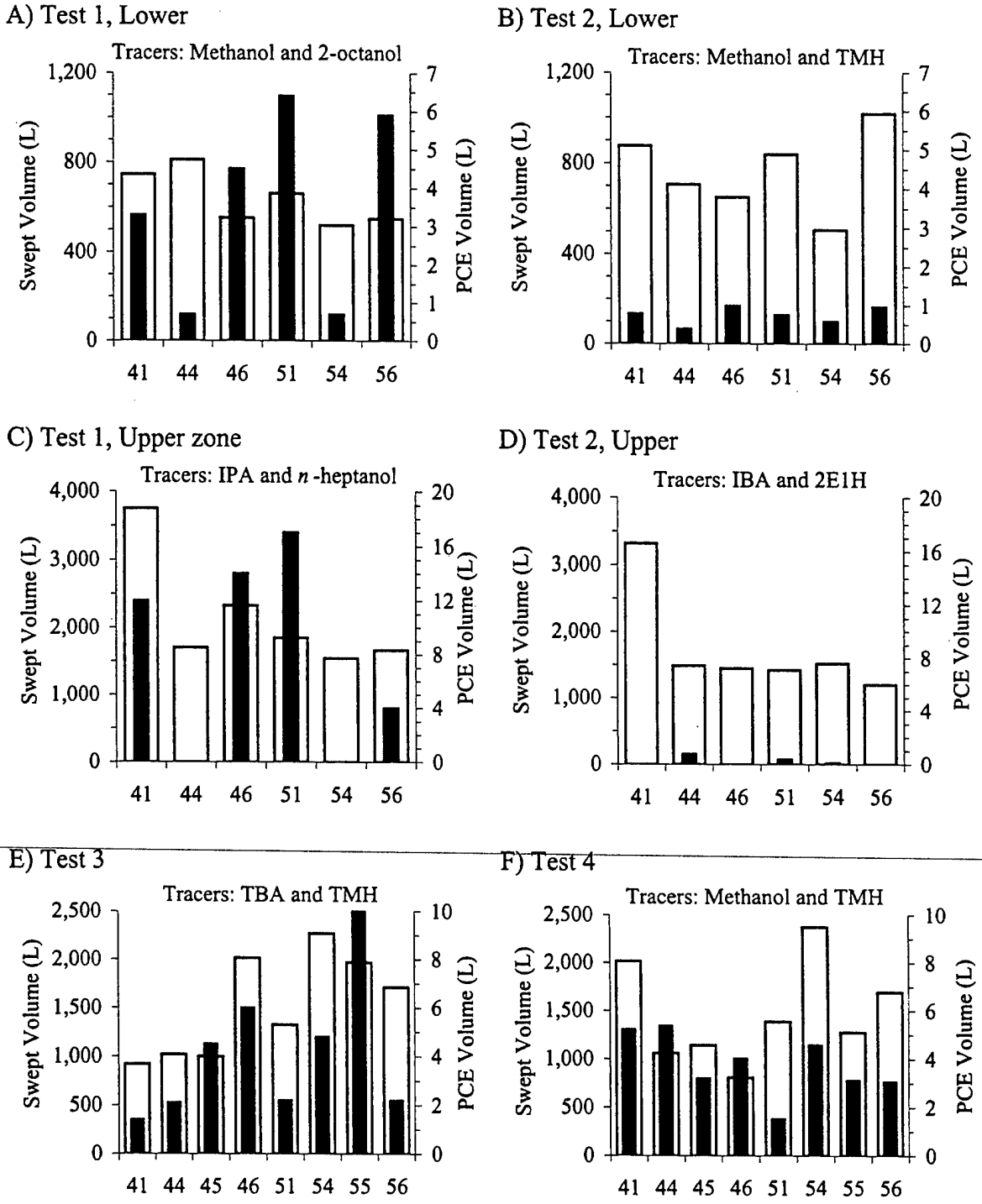

Figure 2. Swept volume (white bar) and PCE volume (black bar) estimates per well for A) Test 1, lower zone; B) Test 2, lower zone; C) Test 1, upper zone (based on degradation-corrected results); D) Test 2, upper zone; E) Test 3; and F) Test 4.

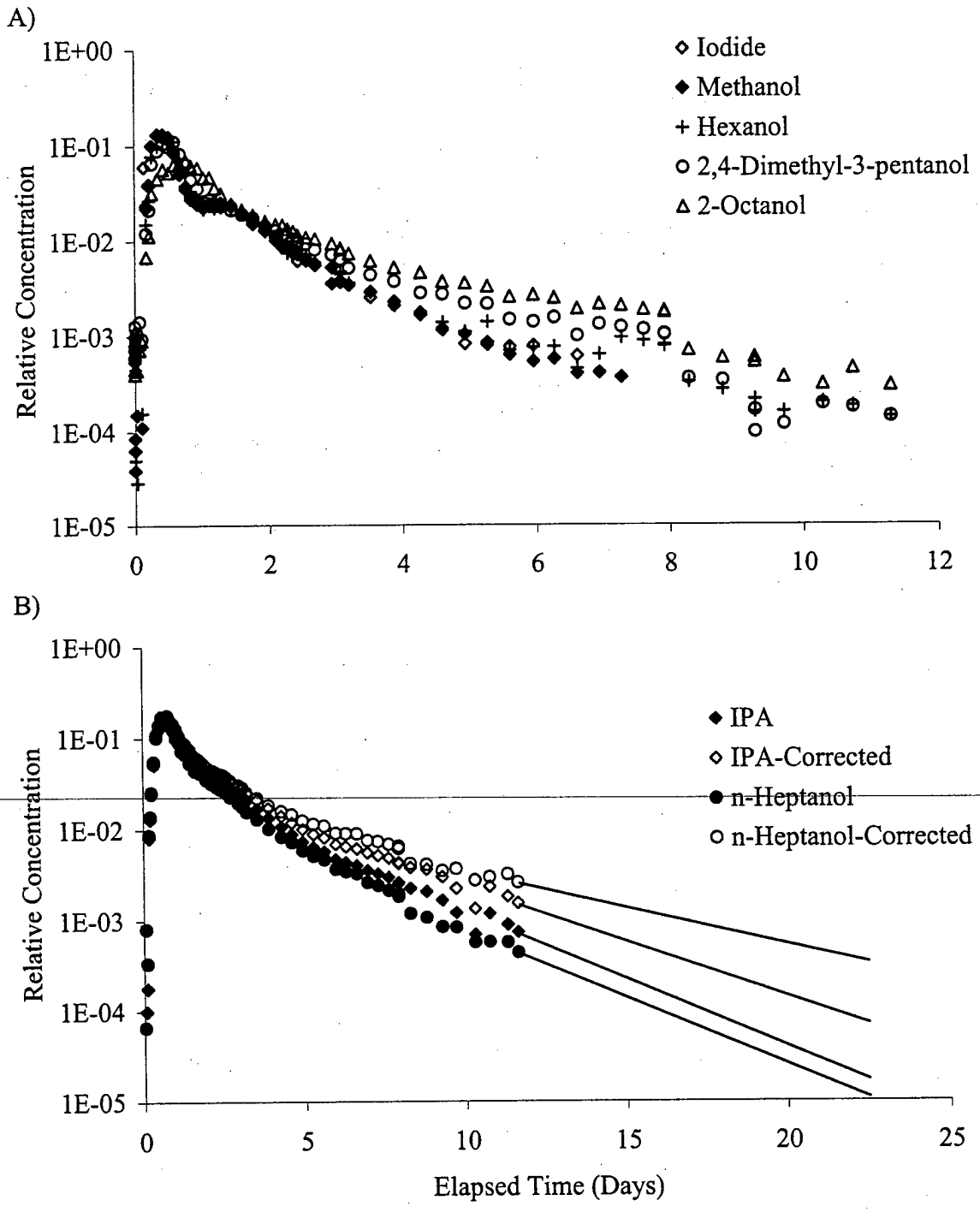

Figure 3. Tracer breakthrough curves at well 51 from Test 1 (pre-cosolvent flood). A) Common lower-zone tracers, and B) upper-zone tracers, before and after correction for tracer degradation. The solid lines represent the extrapolated portion of the BTCs.

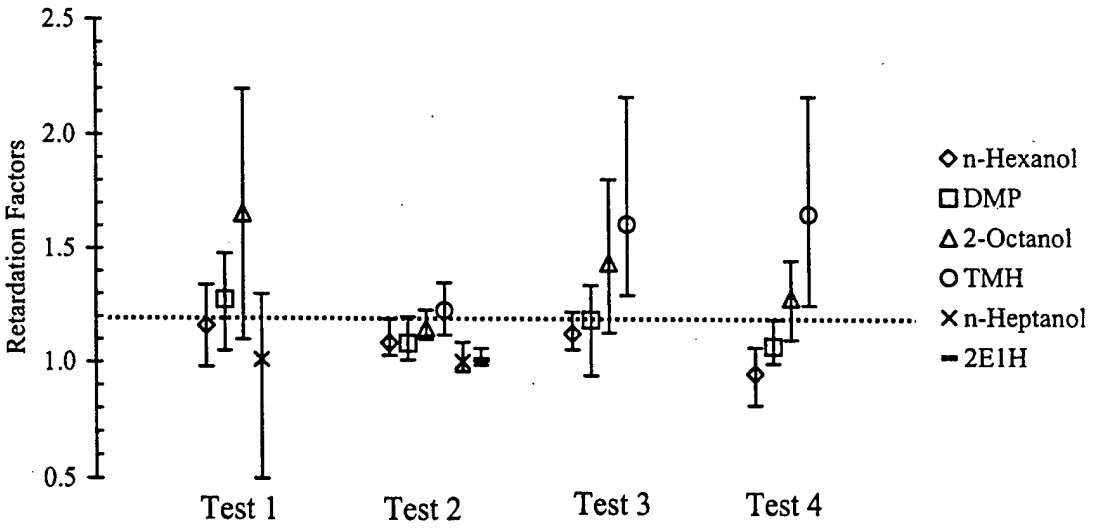

Figure 4. Summary of retardation factors measured in Test 1 through Test 4 (excluding

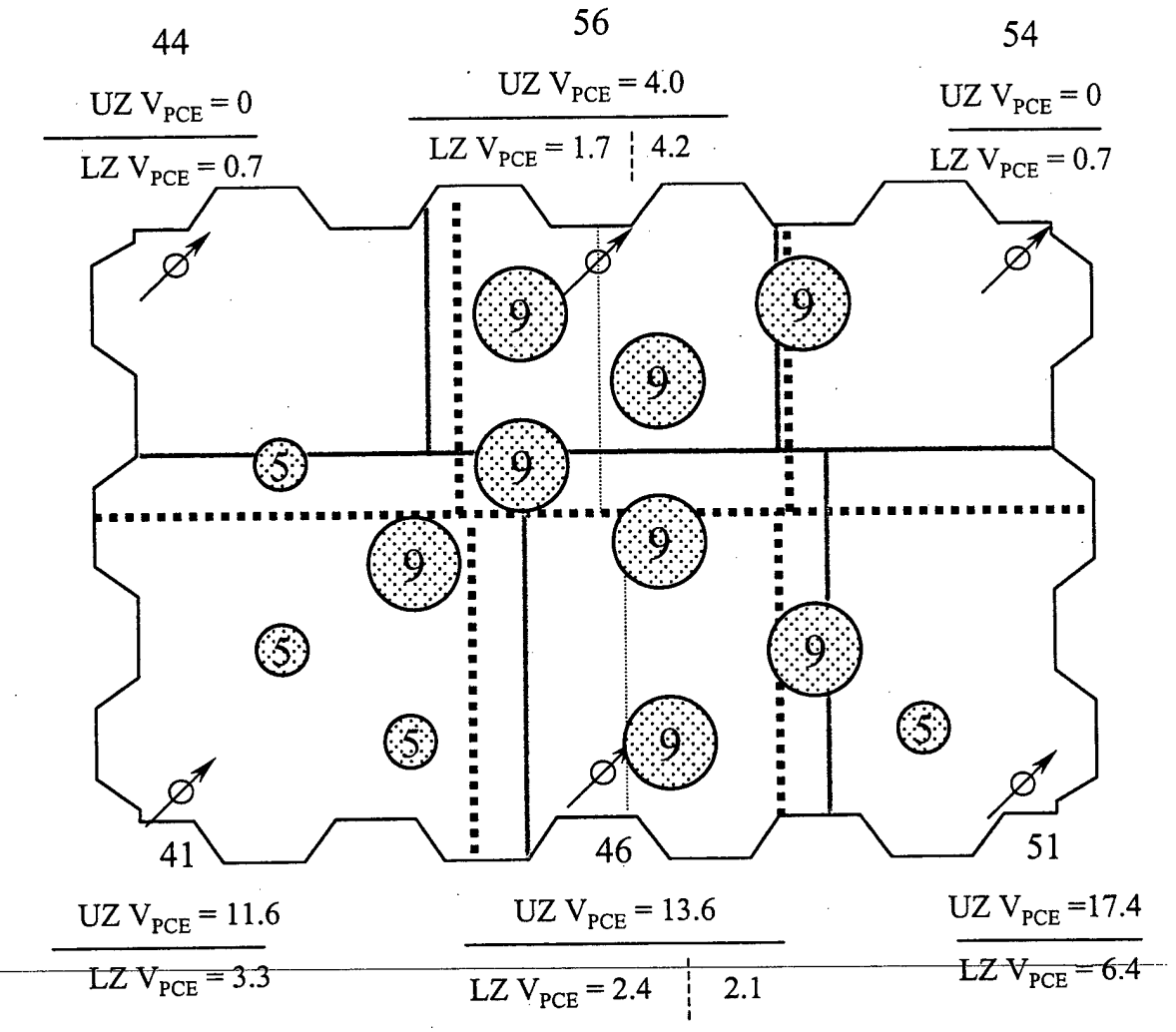

Figure 5. PCE distribution based on Test 1(pre-cosolvent flood) extraction well results. Upper-zone PCE volume (L) estimates are based on the corrected IBA and *n*-heptanol results, and the lower-zone estimates are based on methanol, 2-octanol, and the four unique tracers. The PCE volume (L) injected per location during the first release is indicated by the number within the circles (Plan view).

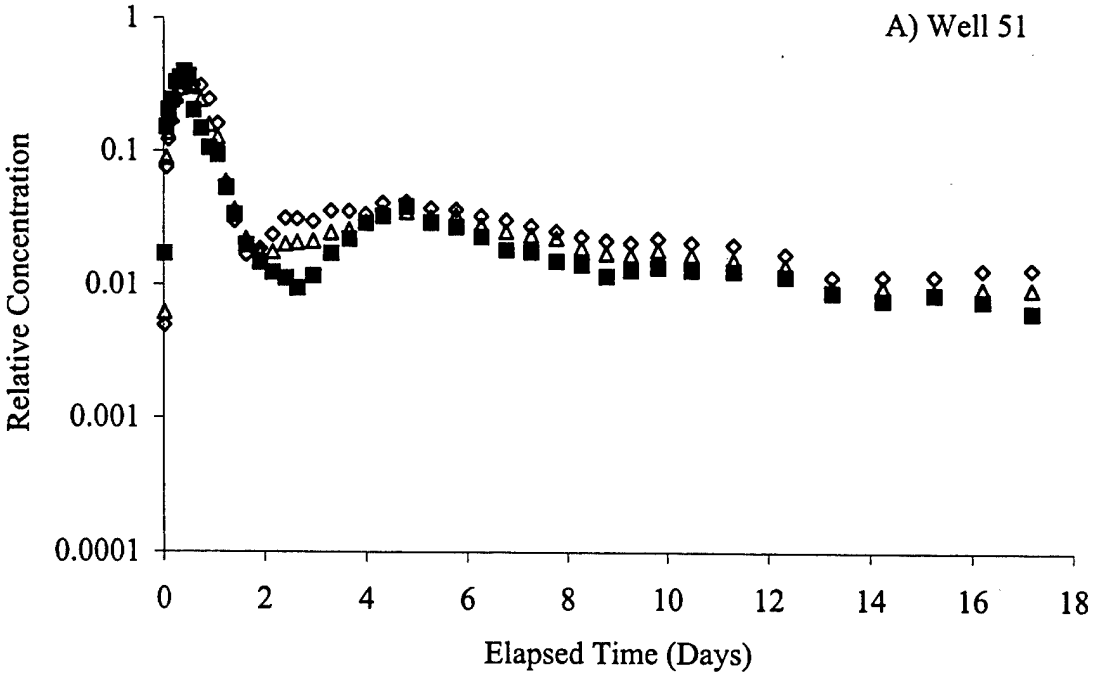

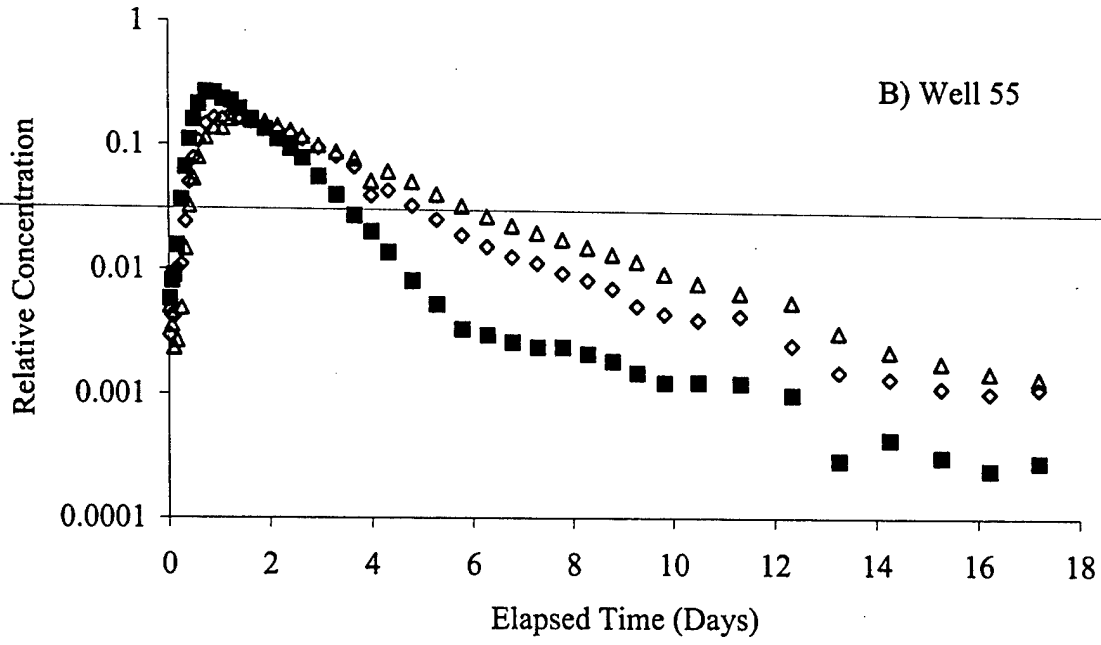

Figure 6 Selected breakthrough curves from A) well 51 and B) well 55, Test 3 (pre-surfactant flood). Shown in each graph are *tert*-butyl alcohol (closed squares), 2-octanol (open diamonds), and 3,5,5-trimethyl-1-hexonal (open triangles).

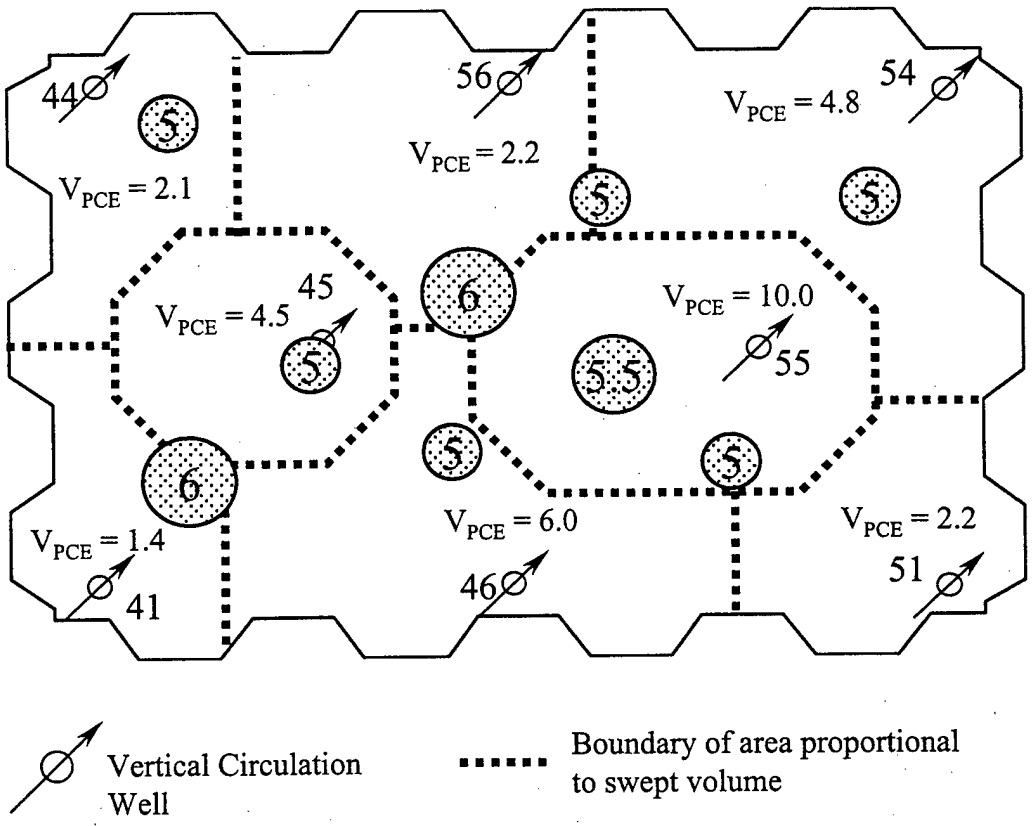

Figure 7. PCE spatial distribution based on Test 3 (pre-surfactant flood) vertical circulation well results. The PCE volume (L) estimates are based on tracers TBA and TMH. The PCE volume (L) injected per location during the second release is indicated by the number within the circles. (Plan view).

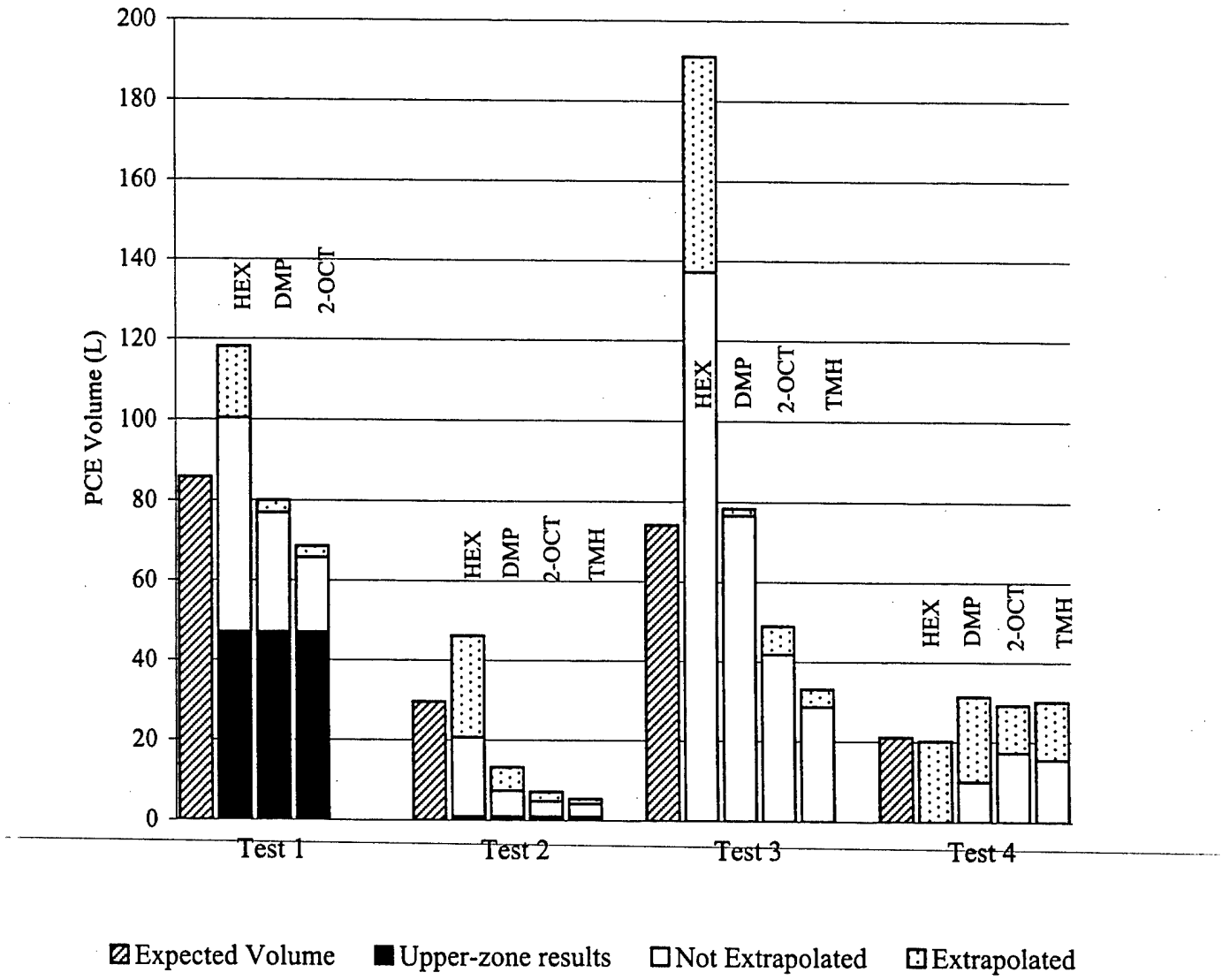

Figure 8. Expected (striped region) and predicted (black, white, and dotted regions) P

GENERAL METHODS FOR ESTIMATING UNCERTAINTY IN TRAPEZOIDAL RULE-BASED MOMENTS

Michael C. Brooks

Department of Environmental Engineering Sciences
University of Florida,
Gainesville, FL 32611-6450

Submitted for Publication in
Journal of Hydrology
August 1, 2001

Abstract

Introduction

There are many instances in hydrology and engineering where tracers are used to characterize system hydrodynamics. This typically involves measuring the system response to an injected tracer in the form of a breakthrough curve (BTC). Subsequent BTC analysis has varied, but has generally followed one of two methods: moment analysis or model analysis. Model analysis typically consists of a procedure whereby model parameters are determined such that the mathematical model prediction matches the tracer response (curve fitting), and hydrodynamic properties of the system are characterized by the model parameters. It has been reported that curve-fitting techniques produce more accurate results compared to the use of moments (Fahim and Wakao, 1982; Haas et al., 1997). The mathematical model must be based on the physical and chemical nature of the hydrodynamic system. The inability of mathematical models to accurately describe the physical and chemical nature of complex hydrodynamic systems is a disadvantage of this approach. In moment analysis, hydrodynamic properties of the system are investigated using moments calculated from the BTCs. For example, the zeroth moment of the BTC is a measure of the tracer mass recovered from the system, the first moment is a measure of the travel time through the system, and the second moment is a measure of the mixing in the system. Moments can be estimated from the BTCs either by direct numerical integration, or by fitting a curve to the BTC and then subsequent analysis is based on moments estimated from the mathematical curve (Jin et al., 2000, Haas et al., 1997, Helms, 1997). In the latter case, it is not necessary for the model to be an accurate representation of the physical system, all that is necessary is for the curve to accurately describe the shape of the breakthrough

curve. Helms (1997) showed that nonlinear regression methods were more reliable for estimating BTC moments than direct integration for imperfect BTCs. However, assuming an adequate number of data points are available to define a BTC, direct numerical integration of the BTC has been found to satisfactorily predict moments (Helms, 1997; Jin et al., 1995???). With this qualification, direct integration using the trapezoidal rule to estimate moments from BTCs is advantageous due to its simplicity.

Skopp (1984) stated that the accurate estimation of moments is prevented for two reasons. "First, the data obtained is invariably noisy; second, at some point the data must be truncated." Noisy data is the result of measurement error, and is inherent in any experimental procedure. The uncertainty associated with each measurement can be divided into what has traditionally been referred to as systematic and random errors. Systematic errors are generally defined as errors that affect the measurement in a consistent manner, and if identified can be corrected by applying an appropriate correction factor (Massey, p. 67, 1986). Systematic errors can be further classified as constant or proportional errors (Funk et al., 1995). Constant systematic errors have a magnitude that is independent of the measurement magnitude, while proportional systematic errors are scaled to the measurement magnitude. Random errors result from unidentifiable sources, and must be handled using stochastic methods. The accuracy of a measurement is therefore a function of both systematic and random errors, and the precision of multiple measurements is a function of random errors.

The uncertainty in an experimental result due to random measurement error can best be estimated by conducting statistical analysis on results from multiple trials of the same experiment. However, in many cases, it is not practical to conduct multiple trials of the same experiment, as in the case of large field-scale experiments. In such situations, it is necessary to

estimate experimental uncertainty by other means, such as error-propagation techniques. This basically consists of measuring or estimating uncertainty for fundamental variables, and then propagating the uncertainties through to the final experimental result. For moments based on direct numerical integration of the BTCs, fundamental variables consist of time or volume, and concentration. Eikens and Carr (1989) used error-propagation methods to estimate the uncertainty in statistical moments of chromatographic peaks. Their method was based on several simplifying assumptions, which limited application to temporal moments based on evenly spaced data and constant concentration uncertainty. Specifically, they presented formulas for the absolute zeroth, first normalized, and second normalized moments under the stated conditions.

This paper presents analytical and semi-analytical equations to estimate the uncertainty in moments resulting from systematic and random measurement errors. The method is based on the assumption that moments are estimated from experimentally measured BTCs by numerical integration using the trapezoidal rule. It is also assumed that a finite tracer pulse is used in the tracer test. However, the same methods could be used to develop uncertainty equations if tracer is introduced into the system by a step change in concentration. A synthetic data set is used to demonstrate uncertainty estimates with the equations. Uncertainly predictions resulting from random measurement errors are compared to results from a Monte Carlo analysis for validation. Finally, the equations are used to investigate general relationships between uncertainty in measurements and estimated moments.

THEORY

General Expressions

To establish the framework work for discussing systematic and random errors, the method used to calculate moments from experimental data by numerical integration using the Trapezoidal rule is outlined. An experimentally measured breakthrough curve can be represented by a series of volume and concentration measurements,

$V_1, \ldots V_{i-1}, V_i, V_{i+1}, \ldots V_n$, and $c_1^d, \ldots c_{i-1}^d, c_i^d, c_{i+1}^d, \ldots c_n^d$ (1)

where, V_i = i^{th} cumulative volume measurement [L^3], and c_i^d = i^{th} dimensioned concentration measurement [ML^{-3}]. Each dimensioned concentration, c_i^d, is converted to a dimensionless concentration, c_i, by dividing by the tracer injection concentration (c_0):

$$c_i = \frac{c_i^d}{c_0} \quad . \tag{2}$$

In general, the absolute k^{th} moment of the breakthrough curve, m_k [$L^{3(k+1)}$], is defined as:

$$m_k = \int_0^\infty c V^k dV \quad , \tag{3}$$

and can be approximated using the Trapezoidal rule:

$$m_k \cong \sum_{i=1}^{n-1} \Delta V_i \overline{V^k c_i} \quad , \tag{4a}$$

where, $\Delta V_i = (V_{i+1} - V_i)$ = change in cumulative volume over the i^{th} interval, and $\overline{V^k c_i} = (V_i^k c_i + V_{i+1}^k c_{i+1})/2$ = average product of cumulative volume raised to the k^{th} power and concentration over the i^{th} interval. Note that the numerical approximation methods used herein employ a forward difference scheme starting with i = 1. The absolute zeroth moment of the breakthrough curve, m_0 [L^3] is:

$$m_0 = \int_0^\infty c dV \cong \sum_{i=1}^{n-1} \overline{c}_i \Delta V_i \tag{4b}$$

where, $\overline{c}_i = (c_i + c_{i+1})/2$ = average concentration over the i^{th} interval, is a measure of the mass associated with the breakthrough curve, and is typically used to measure the tracer mass recovered, or to measure contaminant mass removed in groundwater remediation. The absolute first moment of the breakthrough curve, m_1 [L^6] can be approximated by:

$$m_1 = \int_0^\infty cVdV \cong \sum_{i=1}^{n-1} \Delta V_i \overline{Vc}_i \ , \qquad (4c)$$

where, $\overline{Vc_i} = (V_i c_i + V_{i+1} c_{i+1})/2$ = average product of cumulative volume and concentration over the i^{th} interval [L^3].

Haas (1996) discussed the difference between approximating moments using equation 4a and

$$m_k = \int_0^\infty cVdV \cong \sum_{i=1}^{n-1} \Delta V_i \overline{V}_i^k \overline{c}_i \ , \qquad (5)$$

where, $\overline{V}_i^k = (V_i^k + V_{i+1}^k)/2$ = average cumulative volume raised to the k^{th} power over the i^{th} interval [L^3]. He concluded that equation 4a produced a less biased estimate of the moments, and therefore should be used in preference to equation 5. As an illustration of this point, Figure 1 shows the percent difference between the first through the fourth absolute moments of the Normal probability density function estimated using equations 4a and 5, as a function of the number of intervals used in the Trapezoidal rule. The percent difference between the first absolute moment estimated using equations 4a and 5 is practically insignificant for 10 or more intervals. However, significant differences are observed for the higher moments. At least 80 intervals are needed to ensure the percent difference between the second through the fourth absolute moments using equations 4a and 5 is less than 1%. In addition, use of equation 4a allows for a more general expression of uncertainty in moments estimated from the Trapezoidal rule. Consequently, equation 4a is used in this work.

The pulse-corrected, normalized first moment, μ_1' [L^3] is defined as:

$$\mu_1' = \frac{m_1}{m_0} - \frac{V_p}{2}, \tag{5}$$

where V_p = tracer pulse volume [L^3]. The normalized first moment for nonreactive tracers is a measure of the volume swept by the tracer(s). This is generally referred to as the mean residence volume, or for groundwater tracer tests specifically, it is referred to as the swept pore volume.

Systematic Errors

The effect of systematic errors can be estimated in a deterministic manner by simply incorporating systematic errors into equations 1 through 5. This was done for both constant and proportional systematic errors in volume and concentration measurements, and those derivations and resulting formulas are presented in Appendix A.

Random Errors

The effects of random errors in volume and concentration measurements were estimated by applying propagation of error formulas to equations 1 through 5. The procedure is presented below for the k^{th} moment. Uncertainty formulas for the specific cases of the zeroth (k = 0) and first (k = 1) absolute moments are presented in Appendix B. Each measurement is assumed to have a zero-meaned, random error such that:

$$\alpha = \alpha^t + e_\alpha , \tag{7}$$

where, α = measured value, α^t = true value, and e_α = zero-meaned, random measurement error.

The expectation, or mean, μ_x, of a random variable x is defined as:

$$\mu_x = E[x] = \int_{-\infty}^{\infty} x p_x(x) dx , \tag{8a}$$

where, x = random variable, and $p_x(x)$ = probability density function of x. The variance of x, referred to as either var[x] or σ_x^2, is defined as:

$$\sigma_x^2 = \text{var}[x] = E[x^2] - \mu_x^2 \,. \qquad (8b)$$

Applying equations 8a and 8b to equation 7 results in:

$$E[\alpha] = \alpha' \text{ , and} \qquad (9a)$$

$$\text{var}[\alpha] = \text{var}[e_\alpha] \,, \qquad (9b)$$

respectively. Each dimensioned concentration is converted to a dimensionless concentration as shown in equation 2. Generally, the value of c_0 has less uncertainty than c_i^d because c_0 is a designed concentration produced at the start of tracer tests, and because multiple samples from the injection volume are generally collected and analyzed. Therefore, the error associated with c_0 is neglected, and the error associated with c_i is assumed equal to the error associated with c_i^d, scaled by c_0.

General Error Expression for the kth moment based on Trapezoidal rule approximation.

Referring to equation 4a, a general expression for the variance of the k^{th} moment can be developed by starting with the variance of ΔV_i , which can be expressed in terms of the variance in the i^{th} and $(i+1)^{th}$ cumulative volume measurements by:

$$\sigma^2_{\Delta V[i]} = \sigma^2_{V[i]} + \sigma^2_{V[i+1]} \,. \qquad (12)$$

Note that equation 12 reflects that the volume measurements are independent of one another. To avoid double subscripts, the notation V[i] is used to represent V_i . Formally, the expected value of a function, g(x,y), with two random variables (x and y) is:

$$E[g(x,y)] = \int_{-\infty}^{\infty}\int_{-\infty}^{\infty} g(x,y)\, p_{x,y}(x,y)\, dx\, dy \qquad (10a)$$

where $p_{x,y}(x,y)$ is the joint probability density function. If x and y are independent, then the expected value of the function is:

$$E[g(x,y)] = \int_{-\infty}^{\infty}\int_{-\infty}^{\infty} g(x,y)p_x(x)p_y(y)dxdy \qquad (10b)$$

where $p_x(x)$ and $p_y(y)$ are the density functions for random variables x and y, respectively. In order to estimate the variance of g(x,y), equation 10a or 10b would be used with

$$var[g(x,y)] = E\left[\{g(x,y)\}^2\right] - \{\mu_{g(x,y)}\}^2 . \qquad (11)$$

Assuming volume and concentration measurements are independent, equations 10b and 11 can be used to derive the formula for the variance of $V_i^k c_i$, which is:

$$\sigma^2\left(V_i^k c_i\right) = V_i^{2k}\sigma^2_{c[i]} + \sigma^2\left(V_i^k\right)c_i^2 + \sigma^2\left(V_{ki}^k\right)\sigma^2_{c[i]} \quad . \qquad (13)$$

The variance of $\overline{V^k c_i}$ in terms of the variance in the i^{th} and $(i+1)^{th}$ volume and dimensionless concentration is given by:

$$\sigma^2\left(\overline{V^k c_i}\right) = \frac{1}{4}\sigma^2\left(V_i^k c_i\right) + \frac{1}{4}\sigma^2\left(V_{i+1}^k c_{i+1}\right) . \qquad (14)$$

Note that equation 14 reflects that concentration measurements (for a given tracer) are independent from one another. The next step is to estimate the variance of $\overline{V^k c_i}\Delta V_i$. The terms $\overline{V^k c_i}$ and ΔV_i are not independent since both are a function of V_i and V_{i+1}. Consequently, the formal for the variance of the product $\overline{V^k c_i}\Delta V_i$ must account for the covariance, $\sigma(\overline{V^k c_i}, \Delta V_i)$, between the terms. Goodman (1960) presented a general formula for the product of correlated random variables. Under the assumption of bivariate normally distributed random variables, Bohrnstedt and Goldberger (1969) showed that the variance of the product of correlated random variables a and b is:

$$\sigma_{ab}^2 = \bar{a}^2\sigma_b^2 + \bar{b}^2\sigma_a^2 + [\sigma(a,b)]^2 + 2\bar{a}\bar{b}\,\sigma(a,b) + \sigma_a^2\sigma_b^2 \ . \qquad (26a)$$

Applying a = ΔV_i and b = $\overline{Vc_i}$ to equation B-26a yields:

$$\begin{aligned}&\sigma^2\left(\overline{V^k c_i}\Delta V_i\right) = \\ &\left(\overline{V^k c_i}\right)^2\sigma^2(\Delta V_i) + (\Delta V_i)^2\sigma^2\left(\overline{V^k c_i}\right) + \left[\sigma\left(\overline{V^k c_i}, \Delta V_i\right)\right]^2 \ , \\ &+ 2\overline{V^k c_i}\Delta V_i\sigma\left(\overline{V^k c_i}, \Delta V_i\right) + \sigma^2\left(\overline{V^k c_i}\right)\sigma^2(\Delta V_i)\end{aligned} \qquad (15)$$

Equation 15 is based on the assumption that $\overline{V^k c_i}$ and ΔV_i are bivariate normally distributed variables. As discussed by Bohrnstedt and Goldberger (1969), this assumption simplifies the general equation for the product of correlated random variables by eliminating terms raised to the third power and simplifying the evaluation of another. The assumption that $\overline{V^k c_i}$ and ΔV_i are bivariate normally distributed variables is made in order to use the simplified form of the product formula. The general definition of covariance is:

$$\sigma_{xy} = \mathrm{cov}[x,y] = E[(x-\mu_x)(y-\mu_y)] = E[xy] - \mu_x\mu_y \ . \qquad (16)$$

To evaluate the covariance between ΔV_i and $\overline{V^k c_i}$, each term is expressed using equation 7, and substituted into equation 16:

$$\mathrm{cov}\left[\Delta V_i, \overline{V^k c_i}\right] = E\left[(\Delta V_i^t + e_{\Delta V[i]})(\overline{V^k c_i}^t + e_{\kappa[i]})\right] - \Delta V_i^t\,\overline{V^k c_i}^t \ , \qquad (17a)$$

where $\kappa_i = \overline{V^k c_i}$. Simplying equation 17a yields:

$$\mathrm{cov}\left[\Delta V_i, \overline{V^k c_i}\right] = E\left[e_{\Delta V[i]} e_{\kappa[i]}\right] \ . \qquad (17b)$$

The value of k has to be defined to further simply equation 17b. The variance of the sum of $\overline{V^k c_i}\Delta V_i$ and $\overline{V^k c_{i+1}}\Delta V_{i+1}$ is given by:

$$\begin{aligned}&\mathrm{var}\left[\Delta V_i\overline{V^k c_i} + \Delta V_{i+1}\overline{V^k c_{i+1}}\right] = \\ &\mathrm{var}\left[\Delta V_i V^k c_i\right] + \mathrm{var}\left[\Delta V_{i+1} V^k c_{i+1}\right] + 2\,\mathrm{cov}\left[\Delta V_i V^k c_i, \Delta V_{i+1} V^k c_{i+1}\right]\end{aligned} \ . \qquad (18)$$

Note that $\overline{V^k c_i}\Delta V_i$ and $\overline{V^k c_{i+1}}\Delta V_{i+1}$ are not independent since they both use the $(i+1)^{th}$ measure of cumulative volume and concentration. Applying equation 16 to $\overline{V^k c_i}\Delta V_i$ and $\overline{V^k c_{i+1}}\Delta V_{i+1}$ yields:

$$\operatorname{cov}\left[\Delta V_i \overline{V^k c_i}, \Delta V_{i+1i} \overline{V^k c_{i+1}}\right] = E\left[\Delta V_i \overline{V^k c_i} \Delta V_{i+1} \overline{V^k c_{i+1}}\right] - \Delta V_i^t \overline{V^k c_i}^t \Delta V_{i+1}^t \overline{V^k c_{i+1}}^t , \qquad (19a)$$

To evaluate the first term on the right-hand side of equation 18a, each term is written in the form of equation 7:

$$E\left[\Delta V_i \overline{V^k c_i} \Delta V_{i+1} \overline{V^k c_{i+1}}\right] = E\left[\left(\Delta V_i^t + e_{\Delta V[i]}\right)\left(\overline{V^k c_i}^t + e_{\kappa[i]}\right)\left(\Delta V_{i+1}^t + e_{\Delta V[i+1]}\right)\left(\overline{V^k c_{i+1}}^t + e_{\kappa[i+1]}\right)\right] , \qquad (19b)$$

Expanding equation 19b, combining with equation 19a, and simplifying results in:

$$\begin{aligned}
\operatorname{cov}\left[\Delta V_i \overline{V^k c_i}, \Delta V_{i+1i} \overline{V^k c_{i+1}}\right] &= E\left[\Delta V_i^t \overline{V^k c_i}^t e_{\Delta V[i+1]} e_{\kappa[i+1]}\right] + \\
&E\left[\Delta V_i^t e_{\kappa[i]} \Delta V_{i+1} e_{\kappa[i+1]}\right] + E\left[\Delta V_i^t e_{\kappa[i]} e_{\Delta V[i+1]} \overline{V^k c_{i+1}}^t\right] + \\
&E\left[\Delta V_i^t e_{\kappa[i]} e_{\Delta V[i+1]} e_{\kappa[i+1]}\right] + E\left[e_{\Delta V[i]} \overline{V^k c_i}^t \Delta V_{i+1}^t e_{\kappa[i+1]}\right] + \\
&E\left[e_{\Delta V[i]} \overline{V^k c_i}^t e_{\Delta V[i+1]} \overline{V^k c_{i+1}}^t\right] + E\left[e_{\Delta V[i]} \overline{V^k c_i}^t e_{\Delta V[i+1]} e_{\kappa[i+1]}\right] + \\
&E\left[e_{\Delta V[i]} e_{\kappa[i]} \Delta V_{i+1} \overline{V^k c_{i+1}}^t\right] + E\left[e_{\Delta V[i]} e_{\kappa[i]} \Delta V_{i+1} e_{\kappa[i+1]}\right] + \\
&E\left[e_{\Delta V[i]} e_{\kappa[i]} e_{\Delta V[i+1]} \overline{V^k c_{i+1}}^t\right] + E\left[e_{\Delta V[i]} e_{\kappa[i]} e_{\Delta V[i+1]} e_{\kappa[i+1]}\right]
\end{aligned} \qquad (19c)$$

The value of k has to be defined in order to evaluate the eleven terms on the right-hand side of equation 19c. Finally, the variance of the absolute k^{th} moment using the trapezoidal rule is completed with:

$$\operatorname{var}[m_k] = \sum_{i=1}^{n-1} \operatorname{var}\left[\Delta V_i \overline{V^k c_i}\right] + 2\sum_{i=1}^{n-2} \operatorname{cov}\left[\Delta V_i \overline{V^k c_i}, \Delta V_{i+1} \overline{V^k c_{i+1}}\right] . \qquad (20)$$

Normalized Moment

To estimate the uncertainty associated with k^{th} normalized moment, it is necessary to estimate the uncertainty associated with the ratio of the k^{th} absolute moment to the zeroth moment. The uncertainty of a ratio of two numbers is typically estimated using a technique based on the Taylor series approximations, referred to as the Delta method, or the "error propagation formula" (Kendall and Stuart, pg. 246, 1977; Lynch and Walsh, Appendix A, 1998) Winzer (2000) discusses the accuracy of error propagation related to the ratio of two numbers using the Delta method, which in general can be expressed as:

$$\sigma_{b/a}^2 = \left(\frac{b}{a}\right)^2 \left(\frac{\sigma_a^2}{a^2} + \frac{\sigma_b^2}{b^2} - \frac{2\sigma_{a,b}}{ab}\right) \quad , \tag{21}$$

or, for the zeroth and absolute k^{th} moment:

$$\sigma_{\mu[k]}^2 = \left(\frac{m_k}{m_0}\right)^2 \left(\frac{\sigma_{m[0]}^2}{m_0^2} + \frac{\sigma_{m[k]}^2}{m_k^2} - \frac{2\sigma_{m[0]m[k]}}{m_0 m_k}\right) \tag{22}$$

Equations 21 and 22 are first order approximation because all terms in the Taylor series expansion with second and higher order derivatives are neglected (See Appendix C). The zeroth and k^{th} absolute moments are not independent since they are based on the same measurements of volume and concentration. Therefore, the covariance between the two is needed to apply equation 22. Due to the complexity of an analytical solution, a Delta method approximation to the covariance is used. For two random variables a and b, which are a function of random variables x_1 to x_n, the covariance between a and b is approximated by (see Appendix C):

$$\sigma(a,b) \cong \sum_{i=1}^{n}\sum_{j=1}^{n} \sigma(x_i, x_j)\left(\frac{\partial a}{\partial x_i}\right)\left(\frac{\partial b}{\partial x_j}\right) \tag{23}$$

For the covariance between the zeroth and k^{th} absolute moments, equation 22 becomes:

$$\sigma(m_0, m_k) \cong \sum_{i=1}^{2n}\sum_{j=1}^{2n} \sigma(x_i x_j)\left(\frac{\partial m_0}{\partial x_i}\right)\left(\frac{\partial m_k}{\partial x_j}\right) \qquad (24)$$

Since the zeroth and first absolute moments are calculated using the Trapezoidal Rule, the x variables in equation B-28a are the measured volume and concentration values:

$$\{x_1,...,x_i,...,x_n\} = \{V_1,...,V_i,...,V_n\}\text{, and} \qquad (24)$$

$$\{x_{n+1},...,x_{i+n},...,x_{2n}\} = \{c_1,...,c_i,...,c_n\}\ . \qquad (25)$$

Appendix C presents the specific case of the uncertainty of the first normalized moment. The uncertainty of the pulse corrected first normalized moment is:

$$\sigma^2_{\mu[1]'} = \sigma^2_{\mu[1]} + \sigma^2_{V[p]}, \qquad (26)$$

where $\sigma^2_{V[p]}$ is the variance of one half the tracer-pulse volume, which is estimated from the field techniques.

Special Case: Constant Flow rate

For the case where the flow rate is constant over the duration of the test, moments can be calculated on a temporal basis rather than a volumetric basis. From a practical standpoint, random errors in recording time can be neglected, and the equations for estimating moment uncertainty can be simplified. In this case, the uncertainty for the k^{th} temporal moment ($m_{k,t}$)can be written as:

$$\sigma^2_{m[k,t]} = \frac{1}{4}\Delta t_1^2 t_1^{2k}\sigma^2_{c[1]} + \sum_{i=1}^{n-2}\left[\frac{1}{4}\left(\Delta t_i^2 + \Delta t_{i+1}^2\right)t_{i+1}^{2k}\sigma^2_{c[i+1]}\right] + \frac{1}{4}\Delta t_n^2 t_n^{2k}\sigma^2_{c[n]}\ . \qquad (27a)$$

Under the further conditions of constant Δt, equation 27a becomes:

$$\sigma^2_{m[k,t]} = \frac{1}{4}\Delta t^2\left[t_1^{2k}\sigma^2_{c[1]} + 2\sum_{i=2}^{n-1}\left[t_i^{2k}\sigma^2_{c[i]}\right] + t_n^{2k}\sigma^2_{c[n]}\right], \qquad (27b)$$

and under final condition of constant σ_c, equation 27b reduces to:

$$\sigma^2_{m[k,t]} = \frac{1}{4}\Delta t^2 \sigma_c^2 \left[t_1^{2k} + 2\sum_{i=2}^{n-1}\left[t_i^{2k}\right] + t_n^{2k} \right] . \qquad (27c)$$

For the zeroth moment, equation 27c becomes:

$$\sigma^2_{m[0,t]} = \frac{1}{2}(n-1)\Delta t^2 \sigma_c^2 . \qquad (28)$$

(The equation for the zeroth-temporal moment reported by Eikens and Carr (1989) under the same conditions (constant Δt and σ_c) was $n\Delta t^2 \sigma_c{}^2$. The difference between their equation and that reported in equation (2-28) results from a difference in the formulation of the numerical approximation to the moment integral). The uncertainty in the flow rate is then used to estimate the uncertainty in the k^{th} volumetric moment:

$$\sigma^2\left(Qm_{k,t}\right) = Q^2\sigma^2_{m[k,t]} + \sigma^2_Q m^2_{k,t} + \sigma^2_Q \sigma^2_{m[k,t]} , \qquad (2\text{-}29)$$

where Q = the volumetric flow rate [L^3T^{-1}], and σ_Q^2 [L^6T^{-2}] is the variance of the flow rate. Equation (2-29) is based on the assumption of independence between measurement errors in the flow rate and temporal moments.

Validation and Analysis Using a Synthetic Data Set

A synthetic data set was generated to validate the method for estimating moment uncertainty and to investigate the impact of measurement uncertainty on moment calculations. The synthetic data set was generated using the solution to the one-dimensional advective-dispersive transport equation, subject to the initial condition of c(x,0) = 0 for x 0, and the boundary conditions of c(0,t) = c_0 for t 0, and c(, t) = 0 for t 0 (Lapidus and Amundson, 1952; Ogata and Banks, 1961). The nondimensional form of the solution, accounting for retardation, is

$$c(\tau, R, P_e) = \left(\frac{1}{2}\right)\left\{erfc\left[\sqrt{\frac{P_e}{4R\tau}}(R-\tau)\right] + \exp(P_e)erfc\left[\sqrt{\frac{P_e}{4R\tau}}(R+\tau)\right]\right\}, \quad (2\text{-}30)$$

where c is the dimensionless concentration (c^d/c_0), is the dimensionless pore volume (= vt/L, where v = pore velocity [LT^{-1}], t = time [T], and L = linear extent of the flow domain [L]), R = retardation factor (R = 1+(SK_{NW})/(1-S), where S = NAPL saturation and K_{NW} = NAPL partitioning coefficient), and P_e = Peclet number (P_e = vL/D, where D = dispersion coefficient [L^2T^{-1}]). Note that for the nonreactive tracer, R = 1. This solution is for a step input of tracer, and was used to generate a pulse-input solution by superposition, lagging one step-input solution by the tracer pulse-input length and subtracting it from another. The nondimensional pulse length (defined as $_p$ = vt_p/L, where t_p is the pulse duration [T]) was 0.1, and the Peclet number was 10. The nonreactive and reactive breakthrough curves represented the known, or true data set. The synthetic data set was chosen such that the zeroth moment of the tracers was 1, and the normalized first moment of the non-reactive tracer was 10. Unless noted otherwise, a total of 100 volume-concentration data points were used to represent the BTCs, and a retardation factor of 1.5 was used to generate the reactive breakthrough curve.

Results and Discussion

Systematic Errors

Constant systematic volume errors. The impact of constant systematic errors in volume measurements on the absolute zeroth moment and the normalized first moment are illustrated in Figure 2-2a. The volume error shown on the abscissa in Figure 2-2a is expressed as a fraction of the pore volume, as predicted by the non-reactive normalized first moment. Constant systematic errors in volume measurements have no impact on the zeroth moment

because this moment is based on a volume differential, and consequently the error is eliminated. However, higher-order moments, like the first-normalized moment (see Figure 2-2a), will be affected because of the volume dependency in the numerator of the moment calculation (see equation (2-4a) or (2-5)). As shown in Figure 2-2a, the normalized first moment is directly proportional to the constant systematic volume error.

Proportional systematic volume errors. The impact of proportional systematic errors in volume measurements on the absolute zeroth moment and normalized first moment are illustrated in Figure 2-2b. The error shown on the abscissa in Figure 2-2b is defined in the same manner above for the constant systematic volume error. Proportional systematic errors in volume measurements directly impact both the absolute zeroth moment and the normalized first moment. As shown in Figure 2-2b, the zeroth moment is directly proportional to the proportional systematic volume error. The normalized first moment is also directly proportional to the proportional systematic volume error, and the difference between the lines in Figure 2-2b is due to the correction of one-half the pulse volume. Errors in pulse volume were neglected in this analysis.

Constant systematic concentration errors. For this analysis, constant systematic errors are limited to magnitudes equal to or less than method detection limits, based on the assumption that larger values would be readily identified by typical quality assurance procedures used in the laboratory. Assuming typical values for alcohol tracers, i.e., injection concentrations on the order of 1000 mg/L and method detection limits on the order of 1 mg/L, dimensionless concentration errors could range from –0.001 to +0.001. The impacts of errors in this range on the absolute zeroth moment and normalized first moment are shown in Figure 2-3. It is noted that the effects of these types of errors will be more pronounced for smaller injection

concentrations, but they would also be easier to identify. For example, dimensionless errors ranging from –0.001 to +0.001 produce errors in the zeroth moment ranging from –7% to +7%. Mass recoveries ranging from 93% to 107% are not unrealistic, and do not necessarily indicate analytical problems. However, dimensionless concentration errors ranging from –0.01 to +0.01 (1 mgL^{-1} /100 mgL^{-1}) produce errors in the zeroth moment ranging from -70% to +70%. Mass recoveries less than 90% or greater than 110% should be used with caution, and certainly, mass recoveries as low as 30% or as large as 170% would clearly reflect a serious problem with the tracer data.

Proportional systematic concentration errors. As shown by equations (A-20a) through (A-20c) in Appendix A, the impact of proportional systematic errors in concentration measurements is eliminated by using dimensionless concentrations. Therefore, proportional systematic concentration errors do not impact moments.

Random Errors

Method validation. The variance of the zeroth and absolute first moments calculated by the analytical expressions were compared to variances estimated by the delta method. The zeroth-moment variance calculated by the two methods is the same since both expressions are exact. The first-absolute moment variance calculated by the two methods were similar, and the slight differences between the two were attributed to the delta-method approximation.

Monte Carlo analysis (see, for example, Gelhar, 1993) was used to verify normalized moment uncertainty estimates. Measurement uncertainty was assumed to be a normally distributed random variable with a zero mean. Concentration-measurement uncertainty was assigned using a coefficient of variation (CV), defined as the ratio of standard deviation to true measurement, between 0 and 0.15. Volume-measurement uncertainty was assigned by equating

volume standard deviation to a value less than or equal to one-half the interval between volume measurements (a constant interval was used). A unique measurement error was applied to each volume and concentration value in the synthetic data set. Moment calculations were then completed on the "measured" BTC. This process was repeated 10,000 times, and the averages and standard deviations of the moments were computed. Convergence of Monte Carlo results was tested by completing three identical simulations, each with 10,000 iterations; the CV for the moments differed by no more than 0.02%. Figure 2-4 shows BTCs for the synthetic non-reactive and reactive tracers, as well as "measured" BTCs generated from one Monte Carlo realization with the volume standard deviation and concentration CV defined as 0.15.

Table 2-1 compares the absolute zeroth and normalized first moment CVs using the semi-analytical equations to those estimated from the Monte Carlo simulation. Three cases are presented: the first with volume uncertainty (standard deviation) equal to 0.35 and no concentration uncertainty, the second with no volume uncertainty and concentration uncertainty equal to 0.15, and the third case with volume uncertainty equal to 0.35 and the concentration uncertainty equal to 0.15. The second-order covariance expression between the zeroth and absolute first moments (equation (2-24b)) provided much better agreement with the Monte Carlo results, and was therefore used in the semi-analytical method rather than the first-order covariance expression (equation (2-24a)). As shown in Table 2-1, the agreement between the two methods demonstrates that the semi-analytical method correctly accounts for the uncertainly in volume and concentration measurements.

Application. Based on the CV of the moments, concentration errors have a greater impact on the results than volume errors. This is illustrated in Figure 2-5, which shows the CV for the zeroth and normalized first moments as a function of volume and concentration errors.

Concentration errors are expressed as CV, and volume errors are expressed as the ratio of the volume measurement standard deviation to the swept volume. The robust nature of moment calculations is exemplified by the fact that relative uncertainty in moments is less than the relative uncertainty in volume and concentration measurements. In addition, measurement uncertainty has less impact on the first-normalized moment than the zeroth moment, which results from the fact that normalized moments are a function of the ratio of absolute moments.

It could be argued that the uncertainties in concentrations near the detection limit are higher than the uncertainties in concentrations near the largest concentration measurements on the BTC. To investigate the impact of variable concentration uncertainty, it was assumed that the concentration CV varied linearly between the CV of the maximum concentration (CV_{max}) and the CV of the detection-limit concentration (CV_{DL}). A detection limit of 0.001 (1 mg/L in 1,000 mg/L) was assumed for this analysis, and all concentrations equal to, or less than this value were assigned CV_{DL}. Figure 2-6 shows the CV for the zeroth and normalized first moments for $50\% < CV_{DL} < 200\%$, and for $CV_{max} = 5\%$, 10% and 15%. Volume errors were neglected in this analysis. The zeroth moment CV varies from 4 to 15%, and the normalized first moment CV varies from 2% to 7%. These results provide further support for the conclusion that the relative uncertainty in moments is less than the relative uncertainty in concentration measurements.

Conclusions

This chapter presented a generalized method for estimating the uncertainty of BTC moments calculated by numerical integration using the trapezoidal rule. The method can be applied to either temporal or volumetric moments, and in the latter case, explicitly accounts for errors in volume measurements. The complexity of the calculations for the zeroth moment is comparable to that associated with the typical propagation-of-errors formula. However, the

formulae for higher moments, as exemplified by the first-absolute moment formulae, are substantially more complex than the typical propagation of errors formula. The results have shown that the relative moment uncertainty is less than the relative volume and concentration measurement uncertainties, and that the normalized first moment is impacted less than the zeroth moment. Moment uncertainties are more sensitive to concentration uncertainties as opposed to volume uncertainties.

	S. A.	M. C.
Case A		
Mass	1.8	1.8
Swept Volume	0.9	0.9
Case B		
Mass	3.4	3.5
Swept Volume	1.1	1.0
Case C		
Mass	4.1	4.1
Swept Volume	1.4	1.4

Case A: volume error = 0.35 and concentration CV = 0; Case B: volume error = 0 and concentration CV = 0.15; and Case C: volume error = 0.35 and concentration CV = 0.15.

Absolute First Moment

The first absolute moment of the breakthrough curve, m_1 [L^6], can be approximated using the Trapezoidal rule as

$$m_1 \cong \sum_{i=1}^{n-1} \overline{Vc_i}\Delta V_i \quad . \tag{B-16}$$

The variance of ΔV_i is given by B-2 above. Assuming volume and concentration measurements are independent, the variance of the i^{th} product $V_i c_i$, is

$$\sigma^2(V_i\, c_i) = V_i^2\sigma^2_{c[i]} + \sigma^2(V_i)c_i^2 + \sigma^2(V_i)\sigma^2_{c[i]} \quad . \tag{B-17}$$

The variance of $\overline{Vc_i}$ in terms of the variance in the i^{th} and $(i+1)^{th}$ volume and dimensionless concentration product is given by

$$\sigma^2\left(\overline{Vc_i}\right) = \frac{1}{4}\sigma^2(V_i c_i) + \frac{1}{4}\sigma^2\left(V_{i+1}c_{i+1}\right) . \tag{B-18}$$

Note that equation (B-18) reflects that both volume and concentration measurements (for a given tracer) are independent from one another. The next step is to estimate the variance of $\overline{Vc_i}\Delta V_i$, which was done by applying equation (2-15) with k = 1:

$$\begin{aligned}&\sigma^2\left(\overline{Vc_i}\Delta V_i\right) = \\ &\left(\overline{Vc_i}\right)^2\sigma^2(\Delta V_i) + (\Delta V_i)^2\sigma^2\left(\overline{Vc_i}\right) + \left[\sigma\left(\overline{Vc_i}, \Delta V_i\right)\right]^2 \quad , \\ &+ 2\overline{Vc_i}\Delta V_i\sigma\left(\overline{Vc_i}, \Delta V_i\right) + \sigma^2\left(\overline{Vc_i}\right)\sigma^2(\Delta V_i)\end{aligned} \tag{B-19}$$

where $\sigma\left(\overline{Vc_i}, \Delta V_i\right)$ is the covariance between $\overline{Vc_i}$ and ΔV_i. Applying the general covariance definition (equation B-6) to $\overline{Vc_i}$ and ΔV_i yields

$$\mathrm{cov}\left[\Delta V_i, \overline{Vc_i}\right] = E\left[\Delta V_i\, \overline{Vc_i}\right] - \Delta V_i^t\, \overline{Vc_i}^t \quad . \tag{B-20a}$$

Expressing ΔV_i and $\overline{Vc_i}$ in terms of true values and zero-meaned errors, and substituting into equation (B-20a) gives

$$\mathrm{cov}\left[\Delta V_i, \overline{Vc_i}\right] = E\left[(\Delta V_i^t + e_{\Delta V[i]})(\overline{Vc_i}^t + e_{\kappa[i]})\right] - \Delta V_i^t \overline{Vc_i}^t \quad , \qquad \text{(B-20b)}$$

where $\kappa_i = \overline{Vc_i}$. Simplifying equation (B-20b) yields

$$\mathrm{cov}\left[\Delta V_i, \overline{Vc_i}\right] = E\left[e_{\Delta V[i]} e_{\kappa[i]}\right] \quad . \qquad \text{(B-20c)}$$

Equation (B-27c) can also be expressed as

$$\mathrm{cov}\left[\Delta V_i, \overline{Vc_i}\right] = E\left[(\Delta V_i - \Delta V_i^t)(\overline{Vc_i} - \overline{Vc_i}^t)\right] \quad , \qquad \text{(B-20d)}$$

or, expanding ΔV_i and $\bar{V}_i$ in terms of cumulative volume and concentration measurements,

$$\mathrm{cov}\left[\Delta V_i, \overline{Vc_i}\right] = E\left[\left\{(V_{i+1} - V_i) - \Delta V_i^t\right\}\left\{\frac{1}{2}(Vc_{i+1} + Vc_i) - \overline{Vc_i}^t\right\}\right], \qquad \text{(B-20e)}$$

and cumulative volume and concentration measurements in terms of true values and zero-meaned errors

$$\mathrm{cov}\left[\Delta V_i, \overline{Vc_i}\right] = E\left[\begin{array}{l}\left[\left(V_{i+1}^t + e_{V[i+1]} - V_i^t - e_{V[i]}\right) - \Delta V_i^t\right] * \\ \left\{\frac{1}{2}\left[\left(V_{i+1}^t + e_{V[i+1]}\right)\left(c_{i+1}^t + e_{c[i+1]}\right) + \left(V_i^t + e_{V[i]}\right)\left(c_{i+1}^t + e_{c[i+1]}\right)\right] - \overline{Vc_i}^t\right\}\end{array}\right], \qquad \text{(B-20f)}$$

or

$$\mathrm{cov}\left[\Delta V_i, \overline{Vc_i}\right] = E\left[\begin{array}{l}\left(e_{V[i+1]} - e_{V[i]}\right) * \\ \left\{\frac{1}{2}\left(V_{i+1}^t e_{c[i+1]} + e_{V[i+1]} c_{i+1}^t + e_{V[i+1]} e_{c[i+1]} + V_i^t e_{c[i]} + e_{V[i+1]} c_{i+1}^t + e_{V[i+1]} e_{c[i+1]}\right)\right\}\end{array}\right]. \qquad \text{(B-20g)}$$

Evaluating the product of the first and second terms on the right-hand side of equation (B-20g), and noting that the expected value of a zero-meaned random variable is zero, Equation (B-20g) is simplified to

$$\mathrm{cov}\left[\Delta V_i, \overline{Vc_i}\right] = \frac{1}{2}\left\{E\left[e_{V[i+1]}^2 c_{i+1}^t\right] - E\left[e_{V[i]}^2 c_i^t\right]\right\} \quad , \qquad \text{(B-20h)}$$

or

$$\mathrm{cov}\left[\Delta V_i, \overline{Vc_i}\right] = \frac{1}{2}\left(\sigma^2_{V[i+1]} c^t_{i+1} - \sigma^2_{V[i]} c^t_i\right). \tag{B-20i}$$

The variance of the sum of $\overline{Vc_i}\Delta V_i$ and $\overline{Vc_{i+1}}\Delta V_{i+1}$ is given by

$$\begin{aligned}&\mathrm{var}\left[\Delta V_i \overline{Vc_i} + \Delta V_{i+1} \overline{Vc}_{i\,i+1}\right] = \\ &\mathrm{var}\left[\Delta V_i \overline{Vc_i}\right] + \mathrm{var}\left[\Delta V_{i+1} \overline{Vc_{i+1}}\right] + 2\,\mathrm{cov}\left[\Delta V_i \overline{Vc_i}, \Delta V_{i+1} \overline{Vc_{i+1}}\right]\end{aligned}. \tag{B-21}$$

The products $\overline{Vc_i}\Delta V_i$ and $\overline{Vc_{i+1}}\Delta V_{i+1}$ are not independent since they both use the $(i+1)^{th}$ measure of cumulative volume and concentration. Applying equation (B-6) to $\overline{Vc_i}\Delta V_i$ and $\overline{Vc_{i+1}}\Delta V_{i+1}$ yields

$$\mathrm{cov}\left[\Delta V_i \overline{Vc_i}, \Delta V_{i+1i} \overline{Vc_{i+1}}\right] = E\left[\Delta V_i \overline{Vc_i} \Delta V_{i+1} \overline{Vc_{i+1}}\right] - \Delta V_i^t \overline{Vc_i}^t \Delta V_{i+1}^t \overline{Vc_{i+1}}^t, \tag{B-22a}$$

To evaluate the first term on the right-hand side of equation (B-22a), each term is written in terms of zero-meaned errors:

$$\begin{aligned}&E\left[\Delta V_i \overline{Vc_i} \Delta V_{i+1} \overline{Vc_{i+1}}\right] = \\ &E\left[\left(\Delta V_i^t + e_{\Delta V[i]}\right)\left(\overline{Vc_i}^t + e_{\kappa[i]}\right)\left(\Delta V_{i+1}^t + e_{\Delta V[i+1]}\right)\left(\overline{Vc_{i+1}}^t + e_{\kappa[i+1]}\right)\right]\end{aligned}, \tag{B-22b}$$

Evaluating the product on the right hand side of equation (B-22b), combining with equation (B-22a), and eliminating those terms containing the expectation of a zero-meaned value results in

$$\begin{aligned}&\mathrm{cov}\left[\Delta V_i \overline{Vc_i}, \Delta V_{i+1i} \overline{Vc_{i+1}}\right] = E\left[\Delta V_i^t \overline{Vc_i}^t e_{\Delta V[i+1]} e_{\kappa[i+1]}\right] + \\ &E\left[\Delta V_i^t e_{\kappa[i]} \Delta V_{i+1} e_{\kappa[i+1]}\right] + E\left[\Delta V_i^t e_{\kappa[i]} e_{\Delta V[i+1]} \overline{Vc_{i+1}}^t\right] + \\ &E\left[\Delta V_i^t e_{\kappa[i]} e_{\Delta V[i+1]} e_{\kappa[i+1]}\right] + E\left[e_{\Delta V[i]} \overline{Vc_i}^t \Delta V_{i+1}^t e_{\kappa[i+1]}\right] + \\ &E\left[e_{\Delta V[i]} \overline{Vc_i}^t e_{\Delta V[i+1]} \overline{Vc_{i+1}}^t\right] + E\left[e_{\Delta V[i]} \overline{Vc_i}^t e_{\Delta V[i+1]} e_{\kappa[i+1]}\right] + \\ &E\left[e_{\Delta V[i]} e_{\kappa[i]} \Delta V_{i+1} \overline{Vc_{i+1}}^t\right] + E\left[e_{\Delta V[i]} e_{\kappa[i]} \Delta V_{i+1} e_{\kappa[i+1]}\right] + \\ &E\left[e_{\Delta V[i]} e_{\kappa[i]} e_{\Delta V[i+1]} \overline{Vc_{i+1}}^t\right] + E\left[e_{\Delta V[i]} e_{\kappa[i]} e_{\Delta V[i+1]} e_{\kappa[i+1]}\right]\end{aligned} \tag{B-22c}$$

The terms in equation (B-22c) can be expressed as a function of the measured volume and concentration variances, as demonstrated above in equations (B-12) and (B-13) in evaluating the covariance between the i^{th} and $(i+1)^{th}$ products of differential volumes and average concentrations. The resulting expressions are

$$E\left[\Delta V_i^t \overline{Vc_i}^t e_{\Delta V[i+1]} e_{\kappa[i+1]}\right] = \frac{1}{2}\Delta V_i^t \overline{Vc_i}^t \left(c_{i+2}^t \sigma_{V[i+2]}^2 - c_{i+1}^t \sigma_{V[i+1]}^2\right) , \quad \text{(B-22d)}$$

$$E\left[\Delta V_i^t e_{\kappa[i]} \Delta V_{i+1} e_{\kappa[i+1]}\right] =$$
$$\frac{1}{4}\Delta V_i^t \Delta V_{i+1}^t \left[\left(V_{i+1}^t\right)^2 \sigma_{c[i+1]}^2 + \left(c_{i+1}^t\right)^2 \sigma_{V[i+1]}^2 + \sigma_{V[i+1]}^2 \sigma_{c[i+1]}^2\right] , \quad \text{(B-22e)}$$

$$E\left[\Delta V_i^t e_{\kappa[i]} e_{\Delta V[i+1]} \overline{Vc_{i+1}}^t\right] = -\frac{1}{2}\Delta V_i^t \overline{Vc_{i+1}}^t c_{i+1}^t \sigma_{V[i+1]}^2 , \quad \text{(B-22f)}$$

$$E\left[\Delta V_i^t e_{\kappa[i]} e_{\Delta V[i+1]} e_{\kappa[i+1]}\right] = -\frac{1}{2}\Delta V_i^t V_{i+1}^t \sigma_{V[i+1]}^2 \sigma_{c[i+1]}^2 , \quad \text{(B-22g)}$$

$$E\left[e_{\Delta V[i]} \overline{Vc_i}^t \Delta V_{i+1}^t e_{\kappa[i+1]}\right] = \frac{1}{2}\overline{Vc_i}^t \Delta V_{i+1}^t c_{i+1}^t \sigma_{V[i+1]}^2 , \quad \text{(B-22h)}$$

$$E\left[e_{\Delta V[i]} \overline{Vc_i}^t e_{\Delta V[i+1]} \overline{Vc_{i+1}}^t\right] = -\overline{Vc_i}^t \overline{Vc_{i+1}}^t \sigma_{V[i+1]}^2 , \quad \text{(B-22i)}$$

$$E\left[e_{\Delta V[i]} \overline{Vc_i}^t e_{\Delta V[i+1]} e_{\kappa[i+1]}\right] = -\frac{1}{2}\overline{Vc_i}^t c_{i+1}^t E\left[e_{V[i+1]}^3\right] , \quad \text{(B-22j)}$$

$$E\left[e_{\Delta V[i]} e_{\kappa[i]} \Delta V_{i+1}^t \overline{Vc_{i+1}}^t\right] = \frac{1}{2}\Delta V_{i+1}^t \overline{Vc_{i+1}}^t \left(c_{i+1}^t \sigma_{V[i+1]}^2 - c_i^t \sigma_{V[i]}^2\right) , \quad \text{(B-22k)}$$

$$E\left[e_{\Delta V[i]} e_{\kappa[i]} \Delta V_{i+1}^t e_{\kappa[i+1]}\right] = \frac{1}{2}\Delta V_{i+1}^t V_{i+1}^t \sigma_{V[i+1]}^2 \sigma_{c[i+1]}^2 , \quad \text{(B-22l)}$$

$$E\left[e_{\Delta V[i]} e_{\kappa[i]} e_{\Delta V[i+1]} \overline{Vc_i}^t\right] = -\frac{1}{2}\overline{Vc_{i+1}}^t c_{i+1}^t E\left[e_{V[i+1]}^3\right] , \text{ and} \quad \text{(B-22m)}$$

$$E\left[e_{\Delta V[i]} e_{\kappa[i]} e_{\Delta V[i+1]} e_{\kappa[i+1]}\right] = -\frac{3}{4}\sigma_{V[i+1]}^4 \sigma_{c[i+1]}^2 + \frac{1}{4}c_{i+1}^t c_{i+2}^t \sigma_{V[i+1]}^2 \sigma_{V[i+2]}^2$$
$$-\frac{1}{4}c_i^t c_{i+2}^t \sigma_{V[i]}^2 \sigma_{V[i+2]}^2 + \frac{1}{4}c_i^t c_{i+1}^t \sigma_{v[i]}^2 \sigma_{V[i+1]}^2 - \frac{1}{4}V_{i+1}^2 \sigma_{V[i+1]}^2 \sigma_{c[i+1]}^2 - \frac{3}{4}c_{i+1}^2 \sigma_{V[i+1]}^4 \quad \text{(B-22n)}$$

Assuming the measurement errors have symmetric probability distribution functions, the expectations listed in equations (B-22k) and (B-22m) are equal to zero. Therefore, the covariance between $\overline{Vc_i}\Delta V_i$ and $\overline{Vc_{i+1}}\Delta V_{i+1}$ can be expressed as

$$\begin{aligned}
&\mathrm{cov}\left[\Delta V_i \overline{Vc_i}, \Delta V_{i+1i} \overline{Vc_{i+1}}\right] = \frac{1}{2}\Delta V_i{}^t \overline{Vc_i}{}^t \left(c_{i+2}^t \sigma_{V[i+2]}^2 - c_{i+1}^t \sigma_{V[i+1]}^2\right) \\
&+\frac{1}{4}\Delta V_i{}^t \Delta V_{i+1}^t \left[\left(V_{i+1}^t\right)^2 \sigma_{c[i+1]}^2 + \left(c_{i+1}^t\right)^2 \sigma_{V[i+1]}^2 + \sigma_{V[i+1]}^2 \sigma_{c[i+1]}^2\right] \\
&-\Delta V_i{}^t \overline{Vc_{i+1}}{}^t c_{i+1}^t \sigma_{V[i+i]}^2 + -\frac{1}{4}\Delta V_i{}^t V_{i+1}^t \sigma_{V[i+1]}^2 \sigma_{c[i+1]}^2 + \frac{1}{2}\overline{Vc_i}{}^t \Delta V_{i+1}^t c_{i+1}^t \sigma_{V[i+1]}^2 \\
&-\overline{Vc_i}{}^t \overline{Vc_{i+1}}{}^t \sigma_{V[i+1]}^2 + \frac{1}{2}\Delta V_{i+1}^t \overline{Vc_{i+1}}{}^t \left(c_{i+1}^t \sigma_{V[i+1]}^2 - c_i^t \sigma_{V[i]}^2\right) \\
&+\frac{1}{2}\Delta V_{i+1}^t V_{i+1}^t \sigma_{V[i+1]}^2 \sigma_{c[i+1]}^2 - \frac{3}{4}\sigma_{V[i+1]}^4 \sigma_{c[i+1]}^2 + \frac{1}{4}c_{i+1}^t c_{i+2}^t \sigma_{V[i+1]}^2 \sigma_{V[i+2]}^2 \\
&-\frac{1}{4}c_i^t c_{i+2}^t \sigma_{V[i]}^2 \sigma_{V[i+2]}^2 + \frac{1}{4}c_i^t c_{i+1}^t \sigma_{v[i]}^2 \sigma_{V[i+1]}^2 - \frac{1}{4}V_{i+1}^2 \sigma_{V[i+1]}^2 \sigma_{c[i+1]}^2 - \frac{3}{4}c_{i+1}^2 \sigma_{V[i+1]}^4
\end{aligned} \quad \text{. (B-22l)}$$

Applying equation (B-29a) to all n-1 intervals, the variance of the absolute 1st moment using the trapezoidal rule becomes

$$\mathrm{var}[m_1] = \sum_{i=1}^{n-1} \mathrm{var}\left[\Delta V_i \overline{Vc_i}\right] + 2\sum_{i=1}^{n-2} \mathrm{cov}\left[\Delta V_i \overline{Vc_i}, \Delta V_{i+1} \overline{Vc_{i+1}}\right]. \quad \text{(B-23)}$$

Estimating NAPL Saturation Using Partitioning Tracers:

Influence of Residual Cosolvents

Jaehyun Cho[1], Michael D. Annable[1], and P. Suresh C. Rao[2]

September 9, 2001 Draft

Submitted for publication in

Environmental Science and Technology

Corresponding Author:

Michael D. Annable
Department of Environmental Engineering Sciences
University of Florida, P.O. Box 116450
Gainesville, FL 32611-6450
Phone : (352) 392-3294; Fax: (352) 392-3076
e-mail: manna@eng.ufl.edu

[1]Department of Environmental Engineering Sciences, University of Florida, P.O. Box 116450, Gainesville, FL 32611-6450
[2]School of Civil Engineering, Purdue University, West Lafayette, IN, 47907-1284

Abstract

Batch equilibrium and column miscible displacement tests were used to elucidate the influence of residual cosolvents on partitioning and transport of alcohol tracers through sandy soil columns containing trapped PCE. Batch equilibrium tests showed that as the volume fraction of cosolvent (f_c) (≤10%, vol.) increased, partitioning coefficients (K_{nc}) for the alcohol tracers linearly decreased for ethanol, linearly increased for tert-butanol, and did not exhibit an evident change for isopropanol. These observations are consistent with measured changes in solubility (S_c) of the alcohol tracers in the presence of the same cosolvents (≤10%, vol.). Column miscible displacement tests using ethanol as a residual cosolvent (≤10%, vol.) exhibited earlier partitioning tracer breakthrough which caused an under-estimation of NAPL saturation (S_n). The estimation error increased with higher initial residual cosolvent in the columns. The S_n under-estimates were not significant, but were 1 to 10% lower than the actual S_n (0.18). The estimated partitioning coefficients based on column tests (K_{col}), were consistently less than those based on batch tests. Column tests with low (0.5%) and high (15%) S_n revealed that the residual cosolvent effect was different depending on the amount of NAPL in the column. Using ethanol for a cosolvent (10%) and 2,4-dimethyl-3-pentanol as a partitioning tracer, the S_n values were under-estimated by about 17% and 5%, respectively, in the low and high NAPL saturation columns.

Introduction

The partitioning tracer technique has been used to characterize residual saturation and distribution of non-aqueous phase liquids (NAPLs) trapped in porous media (1-6). The technique is based on the differences in travel time of non-partitioning and partitioning tracers through a NAPL source zone (7). The tracer technique has been evaluated at both field (1-6) and laboratory (6-8) scales. The technique has been mainly employed at sites associated with aggressive in-situ remediation, such as cosolvent or surfactant flushing (9). After a cosolvent floood, which often includes a water flood, some residual cosolvent will likely remain in the swept zone following the effort to extract NAPL (1). The residual cosolvent can affect the partitioning and transport behavior of tracers used during a post-flushing tracer test.

In general, cosolvents present in the aqueous phase affect chemical characteristics, such as solubility and sorption (hence, activity). In completely water-miscible solvents, the solubility of hydrophobic organic chemicals (HOCs) increases in a log-linear manner (10-15), and sorption decreases log-linearly (16-22); as a result, the transport of HOC through soils is less retarded (22-24). However, the behavior of chemicals can vary depending on type and composition. For example, Coyle et al. (25) reported that the solubility of HOCs, such as PCB-47, PCB-153, and biphenyl, was depressed in the presence of partially miscible organic solvents (PMOS), such as methylene chloride and chloroform.

As a result, in the presence of a residual cosolvent, an estimate of NAPL saturation based on a partitioning tracer test can be in error. The NAPL saturation (S_n) can be under-estimated in the presence of cosolvents such as methanol, which cause solubility

enhancement of organic tracers. On the other hand, S_n can be over-estimated in the presence of other cosolvents such as methylene chloride, which cause solubility depression. Therefore, when a partitioning tracer test is conducted with a residual cosolvent present, it is important to consider the cosolvent effects. Relatively little data, however, are available on the effect of residual cosolvent on the partitioning tracer technique.

The objective of this study was to investigate the influence of residual cosolvent on the partitioning tracer technique for estimating S_n. We investigated partitioning and solubility behavior of alcohol tracers in the presence of residual cosolvents in batch equilibrium tests. The results were verified through miscible displacement tests in packed columns. We also examined how the magnitude of residual S_n modifies the impact of the cosolvent on the S_n estimates.

Theory

Addition of cosolvents generally increases aqueous solubility and decreases partitioning of HOCs; however, not every cosolvent increases the solubility of HOCs. Most completely water-miscible organic solvents, such as methanol, increase HOC solubility in a log-linear (10-15) fashion, since this type of cosolvent results in a decrease of the activity coefficient. However, some partially water-miscible organic solvents such as chloroform decrease HOC solubility in a log-linear fashion (25). One possible explanation is an increased activity of the PMOS in the HOC phase or solventing-out, in which dissolved PMOS can occupy a significant portion of the water molecular space, rendering them unavailable for HOC dissolution.

The log-linear cosolvent model is one of several theoretical approaches for predicting organic chemodynamics. While the log-linear model is applicable over a large

range of cosolvent volume fraction (f_c); at low f_c (0-0.3), a linear approximation may suffice (11, 17) and the relationship can be expressed:

$$S_c = S_w + a_c f_c \quad (1)$$

where S_c is the solubility in the presence of a cosolvent; S_w is the aqueous solubility, and a_c is the cosolvency factor; $a_c > 0$ for cosolvents such as methanol which enhance HOC solubility; $a_c < 0$ for cosolvents such as chloroform that depress solubility; $a_c \approx 0$ for cosolvents producing minimal change in solubility.

The solubility of HOCs is inversely related to its partitioning coefficient (22). Therefore, as the volume fraction of cosolvent increases, the partitioning and retardation of HOC decreases in a log-linear fashion (22). The following relationship was proposed by Rao et al. (22):

$$\log K_{nc} = \log K_{nw} - \alpha_c \sigma_c f_c \quad (2)$$

where the subscripts *n*, *w*, and *c* represent NAPL, water, and cosolvent respectively; K_{nc} is the partitioning coefficient measured in presence of a cosolvent; K_{nw} is the partitioning coefficient measured in water; α_c is an empirical constant which describes water-cosolvent interactions.

Materials and Methods

Materials. A suite of tracers was selected to examine solubility and partitioning behavior over a range of retardation factors. Methanol (Fisher, 98%) was used as a non-reactive tracer, while 4-methyl-2-pentanol (4M2P) (Acros, 99+%), n-hexanol (Acros, 98%), 2-methyl-3-hexanol (2M3H) (Acros, 98%), and 2,4-dimethyl-3-pentanol (2,4DMP) (Acros, 99+%) were used as partitioning tracers in both batch and column experiments. Ethanol (Spectrum Chemical, absolute 200 proof), Tertiary-butanol (TBA) (Aldrich, 99+%), and Isopropanol (IPA) (Fisher, Electronic use) were used as cosolvents. Tetrachloroethylene

(PCE) (Acros, 99%) was used as a NAPL for all batch and column experiments. The laboratory temperature during the experiments was 23 ± 3 °C. A 30-40 mesh silica sand (Ottawa) was used as porous medium in all miscible displacement experiments; alcohol tracers adsorption to this solid matrix was determined to be negligibly small.

Partitioning Experiments. To assess tracer partitioning in solutions with low cosolvent concentrations (≤ 10% by volume), batch equilibrium experiments were conducted. Isotherms for tracer partitioning into NAPL (PCE) were measured in aqueous/alcohol solutions using three cosolvents: ethanol, TBA, and IPA. The f_c used in batch equilibrium experiments were 0, 1, 3, 5, and 10%. Each cosolvent solution was transferred to 100 ml volumetric flasks, and four alcohol tracers were added with varying concentrations. Alcohol tracer mixtures prepared at each cosolvent fraction were added to an appropriate amount of PCE in 25 ml vials fitted with Teflon-lined screw caps. The vials were tumbled end-over-end on a laboratory-rotator (Glas-Col model RD 4512) for 24 hrs at room temperature. At the end of the equilibrium period, alcohol mixtures in supernatant solutions were analyzed by gas chromatography (Perkin Elmer GC, Autosystem XL).

Solubility Experiments. Tracer solubilities were measured using the cosolvent solutions referred to above. The prepared solutions (20 ml) were transferred into 25 ml vials fitted with Teflon-lined screw caps for each mixture. One alcohol tracer was added to each vial in an amount more than 3 times the maximum solubility in water. The vials were placed on a rotator for 24 hrs at room temperature. At the end of the equilibrium period, the vials were placed upside-down for at least 6 hrs to allow the remaining separate phase alcohol to rise and collect above the water. After equilibration was attained, a 5 ml aliquot of liquid was collected for analysis through the Teflon-lined septum using a glass gas-tight 5 ml syringe (Hamilton).

Miscible Displacement Experiments. A series of column tests was conducted with various fractions of a residual cosolvent (ethanol). The glass column used was 4.8 cm in diameter and 15 cm in length with Teflon end pieces (high performance liquid chromatography column from Kontes). Two layers of fine wire mesh and plastic screen were placed inside of the Teflon end pieces to allow for an even distribution of fluids and minimize column end effects.

Two different column packing methods were used for the miscible displacement experiments. In the first method, clean sand (30-40 mesh) was wet-packed in thin layers under continuous vibration. Each layer was stirred and tamped with a rod before adding new sand. The packed column was cleaned by passing 20 pore volumes of degased DI water and weighed. Then, NAPL was introduced at a low flow rate (0.5 ml/min) using a syringe pump. Some of the NAPL was subsequently displaced by injecting water. Different levels of S_n trapped in the pores were achieved by gradually increased flow rates (1, 3, 5, and 10 ml/min steps). In the second method, sand was pre-mixed with a small amount of PCE to create very low residual saturations (S_n = 0.0056). The pre-mixed sand was prepared by adding approximately 20% of the saturated water content (20 ml) and the required amount of PCE (2 ml). The sand mixture was shaken and stirred before and after adding PCE. The mixture was wet-packed as described above. The initial residual PCE saturations of columns packed by both methods were determined using partitioning tracer tests (7).

The packed columns were oriented vertically and connected to a high performance liquid chromatography (HPLC) pump (Perkin Elmer series LC 200 and Gilson model 320) through an inert valve which allowed switching among three reservoirs for the mobile phases. The first reservoir contained a mobile phase of solute-free PCE saturated water to

minimize the loss of residual PCE in the column, the second a PCE-saturated cosolvent solution, and the third an alcohol tracer solution. The residual cosolvent used in the column experiments was an ethanol/water binary mixture. The f_c's used in the column experiments were 0, 1, 3, 5, and 10% by volume.

The miscible displacement experiments were conducted with and without residual cosolvent present. The column was initially prepared by passing 20 pore volumes of degased-PCE-saturated water. Columns with residual cosolvent were created by flushing three pore volumes of a degased-PCE-saturated cosolvent solution. Effluent breakthrough curves (BTCs) were measured under steady water flow with a tracer pulse-input boundary condition. Replicate column tests for each residual cosolvent were conducted. R and S_n measured during each column test were used to estimate column-based partitioning coefficients.

Data analysis. All tracer partitioning equilibrium data obtained from batch tests with and without cosolvents were fit using a linear isotherm to obtain K_{nc} and K_{nw}. The Retardation factor (R) was calculated by moment analysis of effluent BTCs. The NAPL saturation was estimated using K_{nw} from batch tests, and the R_c value measured in the presence of cosolvent. The tails of BTCs were monitored until the injected relative tracer concentration was less than 10^{-2}. The measured data were log-linearly extrapolated up to 10^{-3}. For comparison with batch test results, K_{col} values were computed using R_c and the actual S_n values (i.e., S_n estimated using partitioning tracers in the absence of cosolvent) as follows:

$$K_{col} = \frac{(R_c - 1) \cdot (1 - S_n)}{S_n} \qquad (3)$$

Results and Discussion

Effect of Cosolvent on Solubility. The solubilities of three alcohol tracers were measured in the presence of low concentrations (0 to 10%) of cosolvents (ethanol, TBA, and IPA). The observed results (Figure 1) revealed three types of behavior depending on the cosolvent: enhancement of solubility (ethanol), reduction of solubility (TBA), and no observable change (IPA).

The solubility enhancement with ethanol is in good agreement with other studies (10-15). For instance, Yalkowsky (15) reported that in completely water-miscible solvents such as methanol, the solubility of HOCs increase log-linearly. However, our measurements showed a linear relationship which we believe was attributed to the low concentration of cosolvent used.

Solubility reduction, as observed with TBA, was also noted by others (25-26). Coyle et al. (25) reported that the solubility of HOCs was decreased in the presence of PMOS, such as methylene chloride, resulting from an activity increase of the PMOS in the HOC phase (25). Even though TBA is a CMOS such as methanol or ethanol, at low concentration the solubility behavior of the tracer alcohol in the TBA followed that of PMOS rather than the other CMOS. Additionally, our data showed that the solubility of the alcohol tracer in TBA solution decreased linearly until approximately 30% by volume TBA, at which point, solubility increased sharply with increasing concentration (> 30%) (unpublished data). The reason for the solubility reduction at low concentration is not clear, however, one possible explanation is an activity increase of TBA in the tracer-alcohol phase. Above 30%, however, the TBA began to partition into the alcohol, swelling it, and caused significant increases in solubility.

For the IPA-cosolvent system, the solubilities did not show any observable trend, with increasing volume fraction of IPA (Figure 1C). This contrasted with results reported in

the literature. Morris (12) reported that the solubility of naphthalene increased log-linearly with increasing the fraction of IPA. Pinal (11) and Valkenburg (27) also showed that IPA at high level (range 0-80%) is a strong cosolvent through experiments with TCE and PCE. However, our experiments were conducted at low concentrations (range 0-10%). Thus, we believe that the IPA-cosolvent has little affect on the solubility of the tracer-alcohol at low concentrations ($\leq$ 10%).

Effect of Cosolvent on Tracer Partitioning Isotherms. Partition coefficients, K_{nc}, were determined from the batch isotherm data shown in Figure 2. Based on the observed K_{nc} values, three types of partitioning behaviors were also found in accordance with the property of each cosolvent added in the aqueous phase.

In the presence of ethanol, the measured K_{nc} values decreased for all alcohol tracers used in this study, as the volume fraction of ethanol ($f_{c,EtOH}$) increased (Figure 2A). The K_{nc} and $f_{c,EtOH}$ values showed well correlated inverse-linear relationships with $r^2 \geq 0.95$. The K_{nc} values decreased approximately 15, 21, 18, and 18% compared to K_{nw} values measured in water, for 4M2P, n-hexanol, 2M3H, and 2,4DMP, respectively. Recall that the solubilities of the tracer-alcohols increased in the presence of $f_{c,EtOH}$ (Figure 1). The solubility increase is consistent with the decrease observed for partitioning since they are inversely related. These results indicate that residual ethanol-cosolvent can affect estimations of S_n using equation 3. The S_n has a functional relationship between K_{nw} and R. The R, which is a measure of partitioning tracer mobility, becomes smaller or larger according to a degree of partitioning of the tracer into NAPL. Reduced partitioning produces less retardation. In the presence of cosolvent such as ethanol, if the K_{nw} value determined in water is used, the S_n would be under-estimated.

In the presence of TBA, the K_{nc} values increased with increasing fraction TBA ($f_{c,TBA}$)(Figure 2B). The results showed a linear relationship between K_{nc} and $f_{c,TBA}$ (r^2 = 0.86-0.92). The K_{nc} values increased compared to K_{nw} approximately 35, 49, 24, and 16% for 4M2P, n-hexanol, 2M3H, and 2,4DMP, respectively. This partitioning increase has not been reported in the literature. However, the increase was expected based on the observed solubility reduction. The results may be due to a solventing-out effect as referred to by Coyle et al. (25). The dissolved TBA causes an increased partitioning of alcohol tracers by occupying water molecular space. In other words, an increase of a cosolvent such as TBA, unlike ethanol, results in a decreasing activity, producing increased partitioning. This result suggests that failing to consider the effect of such a cosolvent could result in overestimation of S_n.

In the presence of isopropanol as a cosolvent, the partitioning coefficients did not display an apparent trend (Figure 2C). This is consistent with the minimal affect on the solubilities of the tracer-alcohols (Figure 1).

Based on above observed results, at low concentration (≤ 10%) the relationships between K_{nc} and f_c can be divided into three types according to the properties of cosolvents used. The equation to describe the relationships is as follows:

$$K_{nc} = K_{nw} + b_c f_c \qquad (4)$$

$b_c < 0$ for ethanol
$b_c > 0$ for TBA
$b_c \approx 0$ for IPA

where, K_{nc} is the partitioning coefficient measured in presence of a cosolvent, K_{nw} is the partitioning coefficient measured in water, b_c is an empirical constant which describes water-cosolvent interactions with the subscript *c* designating cosolvent. The estimated b_c values along with a_c were shown in table 1.

Effect of Cosolvent on Tracer Retardation. Column miscible displacement tests were conducted to investigate the effect of residual cosolvent on tracer partitioning and transport behavior. The resident pore fluid used was a binary ethanol/water solution, with f_c ranging from 0 to 10%. The results are provided in Table 2. As expected, increasing f_c resulted in earlier breakthrough of the tracers. Therefore, using K_{nw} values measured in the absence of cosolvent, will produce lower S_n estimates.

The calculated S_n values at low f_c were 1 to 10% lower than the actual S_n, measured using tracer in the absence of ethanol (Table 2). While the error is fairly minor, we believe that its effect should not be neglected. We expect that the cosolvent effect will be larger depending on the magnitude of residual S_n, as discussed later.

Partitioning coefficients based on column tests (K_{col}) were calculated to compare to the batch-measured K_{nc}. The K_{col} values (Table 2) were computed using the R_c values measured with $f_{c,EtOH}$ and the actual S_n in Equation 3. Regressing K_{col} against $f_{c,EtOH}$ yielded high coefficients of determination with 0.99, 0.98, 0.90, and 0.97, respectively, for 4M2P, n-hexanol, 2M3H, and 2,4DMP. Figure 3 shows inverse-linear relations in good agreement with the batch results. The K_{col} values, however, were consistently higher than the K_{nc} values from batch tests. The slopes of the correlated curves for column results were lower than batch tests by factors of about 0.2, 0.6, 0.6, and 0.6, respectively, for 4M2P, n-hexanol, 2M3H, 2,4DMP.

The deviations between column and batch results are a result of two processess: cosolvent dilution and the difference in solute travel time. First, for deviation caused by cosolvent dilution, recall that the column miscible displacement tests were initiated with one pore volume of the residual ethanol cosolvent. The displaced ethanol solution was diluted with the injected alcohol tracer pulse and subsequent mobile phase, PCE saturated water,

which were cosolvent-free. This dilution can impact the partitioning process by reducing local ethanol concentration. Second, deviation is caused by solute travel time of the partitioning tracers compared to the displaced ethanol front, which is essentially non-partitioning. At the tracer front, interaction with the residual cosolvent is significant. However, as the experiment proceeds, the partitioning tracer transport through the column is retarded, while the residual ethanol is rapidly displaced. Because of this, the influence of the residual cosolvent is reduced. Therefore, in the presence of a resident cosolvent displaced by a cosolvent free solution, the calculated K_{col} values from column tests are higher than those from batch tests.

Impact of NAPL saturation on system behavior. As noted above, in the presence of residual cosolvent, the difference in travel times between the partitioning tracers and the cosolvent front can be a factor for estimating residual S_n using partitioning tracers. We hypothesize that the effect of a cosolvent will be different based on the amount of S_n present in the column during a post-flushing tracer test. To verify this, column experiments were performed with low and high NAPL (PCE) saturation in the presence of ethanol-cosolvent (10% by volume).

Effluent ethanol from the columns was monitored along with the partitioning tracers, n-hexanol and 2,4DMP. The BTCs are given in Figure 4 for the low and high NAPL saturations. The BTCs showed that the degree of mixing between residual ethanol and the injected tracers was different between the low and high saturation columns. The BTCs of methanol and ethanol-cosolvent, which are non-partitioning solutes, followed similar trajectory for both the low and high saturation, whereas those of n-hexanol and 2,4DMP were very different for both cases as expected.

For the low S_n in Figure 4A, the postal portion of ethanol-cosolvent BTC overlapped with the frontal over about 60% of the partitioning tracer BTCs (n-hexanol and 2,4DMP), indicating that over about 60% of the n-hexanol and 2,4DMP traveled in the presence of the ethanol-cosolvent through the column. On the other hand, for the high S_n in Figure 4B, the overlapped portion between ethanol and the partitioning tracer BTCs was minimal. This suggests that the affect of residual cosolvent should be more significant in the low S_n column than the high S_n. As seen in Table 3, the S_n estimated from the low saturation column in the presence of ethanol-cosolvent (10%) was about 17% less for 2,4DMP than the actual S_n estimated without ethanol-cosolvent. In the high PCE saturation column, the measured S_n in the presence of 10% ethanol was about 5% less for 2,4DMP than actual.

The K_{col} values were computed to evaluate the relative effect of residual ethanol-cosolvent for both low and high S_n cases. The K_{col} values (= 21.7 for 2,4DMP) estimated from the low S_n column was very close to the K_{nc} values (= 21.5) from the batch test measured in the presence of same 10% ethanol solution. However, the K_{col} value (24.8 for 2,4DMP) estimated from the high saturation column showed greater deviation from the K_{nc} value (21.5). This indicates that the magnitude of S_n may determine the degree of influence of resident cosolvent. Typically, post-flushing tracer tests have been conducted with less than one percent S_n in the field (1, 2). Low residual S_n can result in a greater cosolvent effect on S_n estimation using partitioning tracers. This stresses the importance of considering the effect of residual cosolvent when conducting post-flushing partitioning tracers.

Acknowledgements

This study was funded by the U. S. Department of Defense Strategic Environmental Research and Development Program (SERDP), which is a collaborative effort involving the

U. S. EPA, U. S. DOE, and U. S. DOD. This document has not been subjected to peer review within the funding agency, and the conclusions stated here do not necessarily reflect the official views of the agency nor does this document constitute an official endorsement by the agency. The author would like to thank William R. Wise, Michael Brooks, Irene Poyer, and Suzannah Kuhn who offered help in conducting experiments or provided useful comments for data analysis. This work was presented as a poster at the American Geotechnical Union Meetings, December 2000, San Francisco, CA.

Literature Cited

(1) Annable, M.D.; Rao, P.S.C.; Hatfield, K.; Graham, W.D.; Wood, A.L.; Enfield, C.G. J. Environ. Eng. **1998**, Vol.124, No.6.

(2) Annable, M.D.; Jawitz, J.W.; Rao, P.S.C.; Dai, D.P.; Kim, H.; Wood, A.L. Ground Water. **1998**, Vol.36, No.3.

(3) James, A.I.; Graham, W.D.; Hatfield, K.; Rao, P.S.C.; Annable, M.D. Water Resour. Res. **1997,** 33, 2621-2636.

(4) Annable, M.D.; Rao, P.S.C.; Haltfield, K.; Graham, W.D.; Wood, A.L. Water Resour.Res. **1995.**

(5) Dwarakanath, V.; Deeds, N.; Pope, G.A. Environ. Sci. Technol. **1999**, Vol. 33, 3829-3836

(6) Jin, M.; Butler, G.W.; Jackson, R.E.; Mariner, P.E.; Pickens, J.F.; Pope, G.A.; Brown, C.L.; Mckinney, D.C. Ground Water, **1997**, Vol. 35, 964-972

(7) Jin, M.; Delshad, M.; Dwarakanath, V.; McKinney, D.C.; Pope, G.A.; Sepehrnoori, K.; Tilburg, C.E. Water Resour. Res. **1995,** 31, 202-1211.

(8) Pope, G.A.; Jin,Minquan; Dwarakanath,Varadarajan; Rouse,Bruce; Sepehrnoori,Kamy. 2nd Tracer Workshop. Univ. of Texas at Austin, November 14&15, **1994.**

(9) Rao, P.S.C.; Annable, M.D.; Sillan, R.K.; Dai, D.; Hatfield, K.; Graham, W.D.; Wood, A.L.; Enfield, C.G. Water Resour. Res. **1997,** 33, 2673-2686.

(10) Li, A.; Anderson, A.W. Environ. Sci. Technol. **1994**, Vol.28, No.1.

(11) Pinal, R.; Rao, P.S.C.; Lee, L.S.; Cline, P.V. Environ. Sci. Technol. **1990,** 24, 639-647.

(12) Morris, K.R.; Abramowitz, R.; Pinal R.; Davis, P.; Yalkowaky, S.H. Chemosphere. **1988**, 17, 285-298.

(13) Rubino, J.T.; Yalkowsky, S.H. Pharm. Res. **1987,** 4, 220-230.

(14) Fu, J.K.; Luthy, R.G. J. Environ. Eng. **1986**, 112, 328-345.

(15) Yalkowsky, S.H.; Roseman, T.J. New York, **1986**.

(16) Bouchard, D.C. J. Contam. Hydrol. **1998**, *34*, 107-120.

(17) Hermann, S.E.; Powers, S.E. J. Contam. Hydrol. **1998**, *34*, 315-341.

(18) Kimble, K.D.; Chin, Yu-Ping; J. Contam. Hydrol.**1994**, *17*, 129-143.

(19) Brusseau, M.L.; Wood, A.L.; Rao, P.S.C. Environ. Sci. Technol. **1991**, 25, 903-910.

(20) Rao, P.S.C.; Lee, L.S.; Pinal, R. Environ. Sci. Technol. **1990**, 24, 647-654.

(21) Fu, J.K.; Luthy, R.G. J. Environ. Eng. **1986**, 112, 346-366.

(22) Rao, P.S.C.; Hornsby, A.G.; Kilcrease, D.P.; Nkedi-Kizza. J. Environ. Qual. **1985**, 14, 376-383.

(23) Bouchard, D.C. Chemosphere, **1998**, 36, 1883-1892.

(24) Wood, A.L.; Bouchard, D.C.; Brusseau, M.L.; Rao, P.S.C. Chemosphere, **1990**, 21, 575-587.

(25) Coyle, G.T.; Harmon, T.C.; Suffet, I.H. Environ. Sci. Technol. **1997**, 31, 384-389

(26) Groves, F.R., Jr. Environ. Sci. Tecchnol. **1988**, 22, 282-286.

(27) Van Valkenburg, M. E. Ph.D Dissertation. University of Florida, **1999**.

List of Figures

Figure 1. Relationship between tracer solubility (S_c) and cosolvent content (%, volume) for **(A) ethanol, (B) tert-butanol,** and **(C) isopropanol**

Figure 2. Relationship between tracer partition coefficient (K_{nc}) and cosolvent content (%, volume) for **(A) ethanol, (B) tert-butanol,** and **(C) isopropanol**

Figure 3. Comparison of the K_{nc} values measured from batch tests to the K_{col} estimated from column tests for 4-methyl-2-pentanol, n-hexanol, 2-methyl-3-hexanol, and 2,4-dimethyl-3-pentanol in the ethanol/water system; ◆ **Column test;** □ **Batch test**

Figure 4. Breakthrough curves of residual ethanol cosolvent and partitioning tracers (n-hexanol and 2,4-dimethyl-3-pentanol) to display a degree of mixing, explaining the effect of residual ethanol on the NAPL saturation estimation. Initial residual ethanol content in the columns is 10% (volume).

Table 1. Comparison of estimated a_c and b_c values from tracer solubility and partition experiments for four tracers

	Ethanol		TBA		IPA	
Tracers	**solubility[a]**	**partition[b]**	**solubility[a]**	**partition[b]**	**solubility[a]**	**partition[b]**
4M2P	nd	-0.06(0.93)	nd	+0.11(0.88)	nd	-0.01(0.00)
n-hexaol	+119(0.96)	-0.14(0.99)	-96(0.98)	+0.27(0.84)	+19(0.53)	-0.02(0.16)
2M3H	+119(0.99)	-0.43(0.99)	-83(0.96)	+0.47(0.86)	+34(0.41)	-0.13(0.61)
2,4DMP	+124(0.83)	-0.50(0.95)	-93(0.96)	+0.36(0.83)	+36(0.06)	-0.17(0.38)

[a] a_c values estimated by linear regression on solubility data for tracers-low cosolvents systems
[b] b_c values estimated by linear regression on partitioning coefficient data for tracers-low cosolvents systems

Table 2. Parameter values observed from miscible displacement experiments at low volume fractions of ethanol

Tracers	Ethanol, f_c	R_c	S_n	S_n%error[a]	K_{col}[b]	K_{nc}[c]
4-methyl-2-pentanol	0	1.84	0.188		3.60	3.60
	0.01	1.82	0.185	-1.54	3.53	3.50
	0.03	1.80	0.182	-3.14	3.46	3.37
	0.05	1.78	0.178	-5.44	3.36	3.23
	0.10	1.74	0.170	-9.41	3.19	3.07
n-hexanol	0	2.47	0.184		6.56	6.56
	0.01	2.47	0.183	-0.75	6.50	6.42
	0.03	2.45	0.181	-2.00	6.40	6.13
	0.05	2.41	0.176	-4.27	6.22	5.74
	0.10	2.36	0.172	-6.82	6.02	5.18
2-methyl-3-hexanol	0	6.28	0.189		22.7	22.7
	0.01	6.15	0.185	-1.98	22.1	22.3
	0.03	6.09	0.183	-3.03	21.8	21.1
	0.05	5.96	0.180	-5.03	21.3	20.4
	0.10	5.87	0.177	-6.47	20.9	18.5
2,4 dimethyl-3-pentanol	0	7.13	0.189		26.3	26.3
	0.01	7.10	0.189	-0.40	26.1	25.9
	0.03	7.02	0.187	-1.43	25.8	23.9
	0.05	6.86	0.183	-3.55	25.1	23.7
	0.10	6.71	0.179	-5.57	24.5	21.5

[a] calculated by ((S_n measured with each f_c) - (S_n with 0% f_c)) / (S_n with 0% f_c) H 100

[b] Partitioning coefficients estimated from column tests in the presence of ethanol-cosolvent

[c] Partitioning coefficients measured from batch tests in the presence of ethanol-cosolvent

Table 3. Comparison of parameter values observed from low and high NAPL (PCE) saturation column tests using 2,4-dimethyl-3-pentanol as a partitioning tracer

	Low saturation column		High saturation column	
Cosolvent (%)	**0% Ethanol**	**10% Ethanol**	**0% Ethanol**	**10% Ethanol**
Retardation factor (R_c)	1.15	1.12	5.78	5.51
Partitioning coefficient, K_{nc}	26.3[a]	21.7[b] (21.5)[a]	26.3[a]	24.8[b](21.5)[a]
PCE saturation, S_n[c]	0.0056	0.0046	0.154	0.147
S_n % error	-17.4		-4.90	

a K_{nc} values measured by batch tests with the 0% and 10% ethanol-cosolvent.
b K_{col} values estimated by column tests with residual 10% ethanol; calculated using Eq. (3).
c calculated using Eq. (3); using the R_c value obtained from each column test and the K_{nw} (26.25) from the batch test without cosolvent.

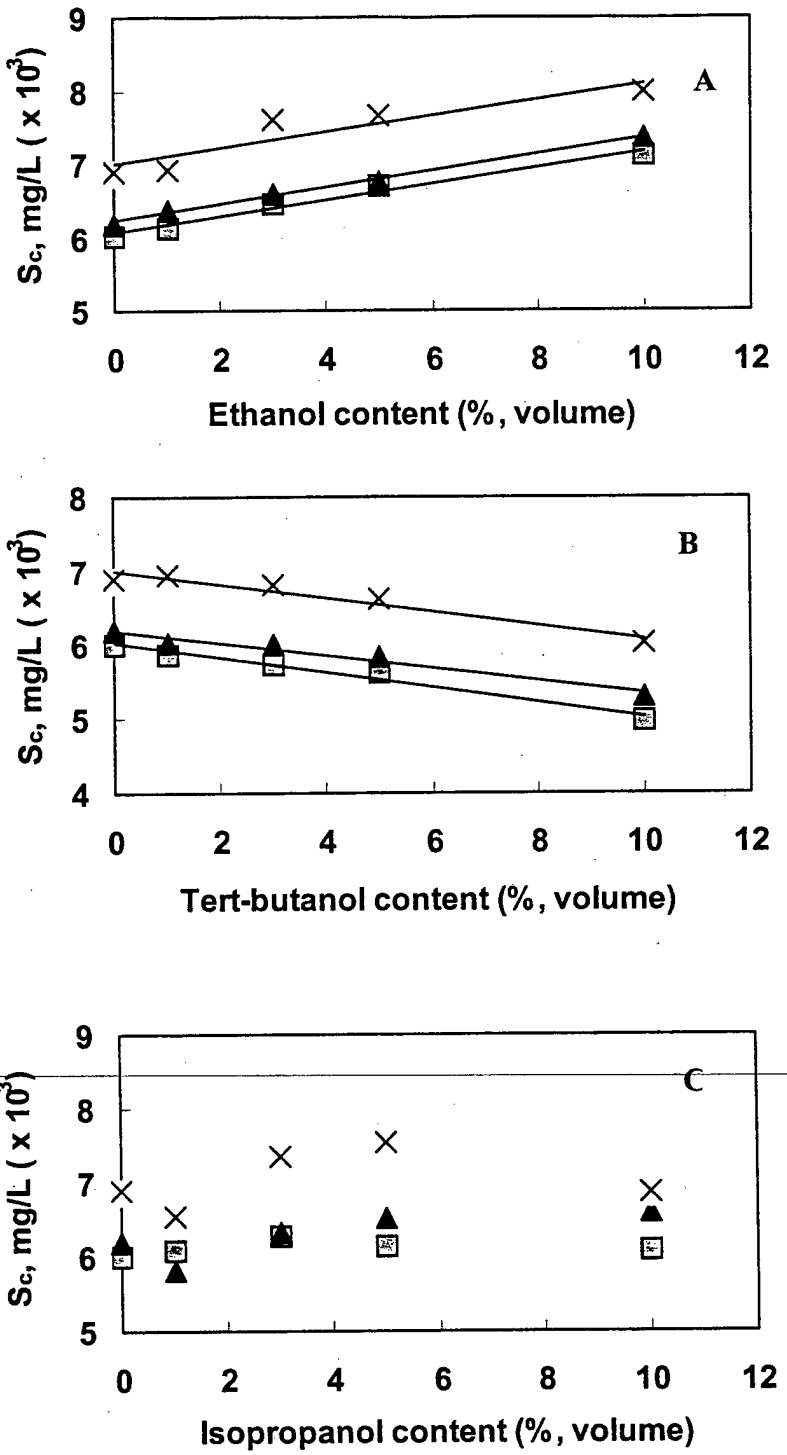
A
Sc, mg/L (x 10^3)
Ethanol content (%, volume)
B
Sc, mg/L (x 10^3)
Tert-butanol content (%, volume)
C
Sc, mg/L (x 10^3)
Isopropanol content (%, volume)
1-Hexanol
2-Methyl-3-Hexanol
2,4-Dimethyl-3-Pentanol

Figure 1

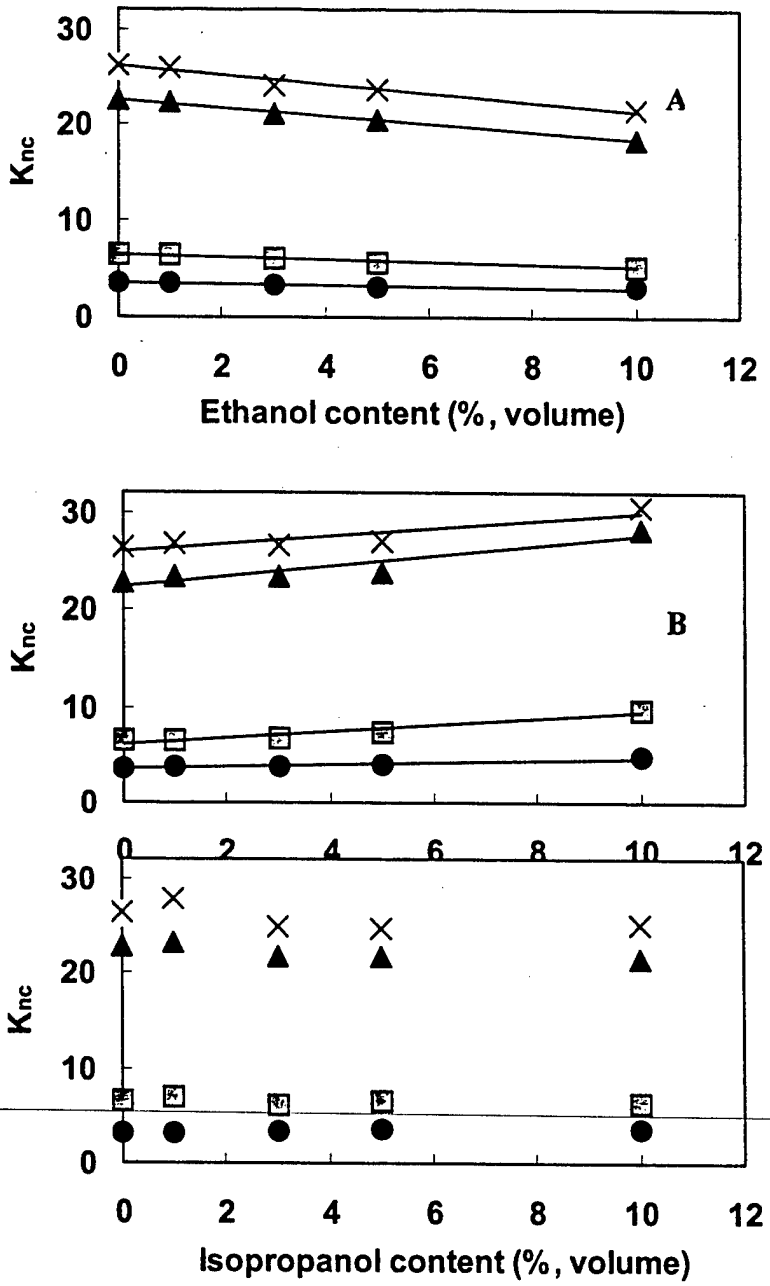
30
20
10
0
Knc
A
0
2
4
6
8
10
12
Ethanol content (%, volume)
B
Isopropanol content (%, volume)
4-methyl-2-pentanol
n-hexanol
2-methyl-3-hexanol
2,4-dimethyl-3-pentanol

Figure 2

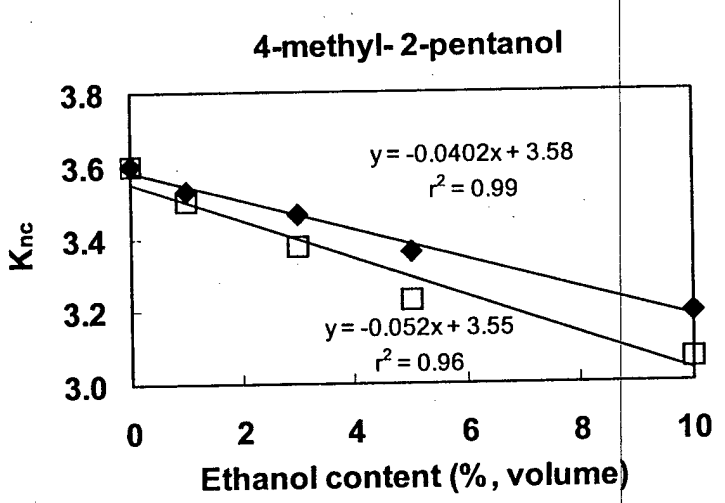
4-methyl- 2-pentanol
3.8
3.6
3.4
3.2
3.0
Knc
y = -0.0402x + 3.58
r2 = 0.99
y = -0.052x + 3.55
r2 = 0.96
0
2
4
6
8
10
Ethanol content (%, volume)

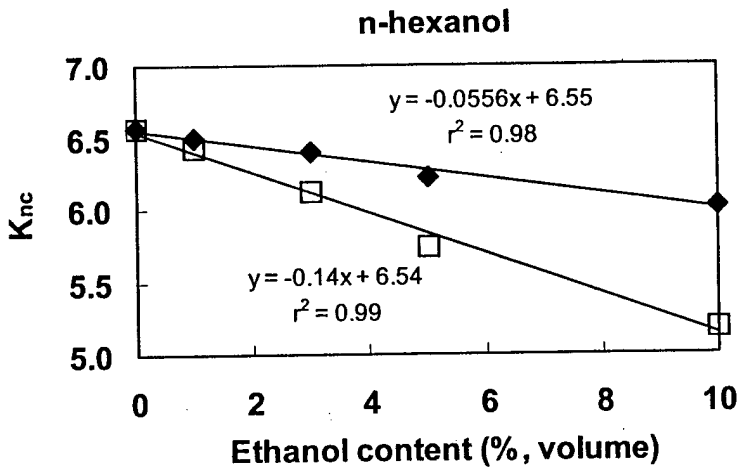
n-hexanol
7.0
6.5
6.0
5.5
5.0
Knc
y = -0.0556x + 6.55
r2 = 0.98
y = -0.14x + 6.54
r2 = 0.99
0
2
4
6
8
10
Ethanol content (%, volume)

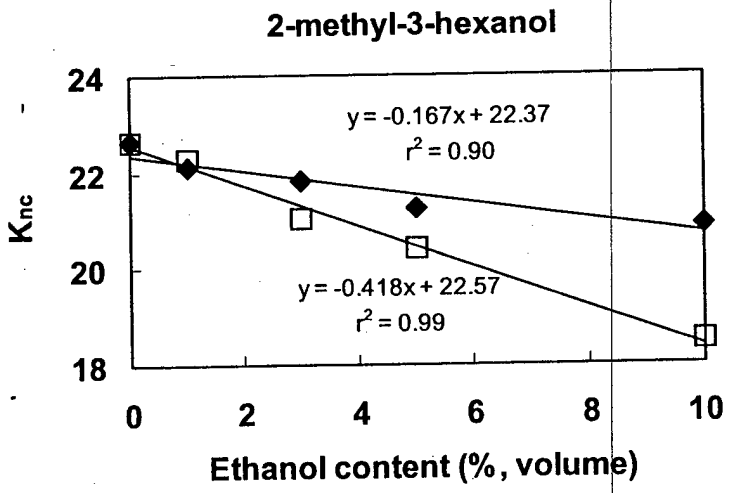
2-methyl-3-hexanol
24
22
20
18
Knc
y = -0.167x + 22.37
r2 = 0.90
y = -0.418x + 22.57
r2 = 0.99
0
2
4
6
8
10
Ethanol content (%, volume)

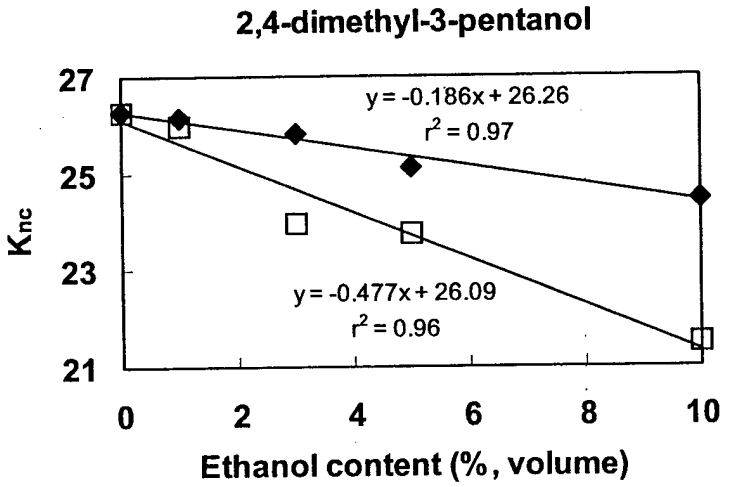
2,4-dimethyl-3-pentanol
27
25
23
21
Knc
y = -0.186x + 26.26
r2 = 0.97
y = -0.477x + 26.09
r2 = 0.96
0
2
4
6
8
10
Ethanol content (%, volume)

Figure 3

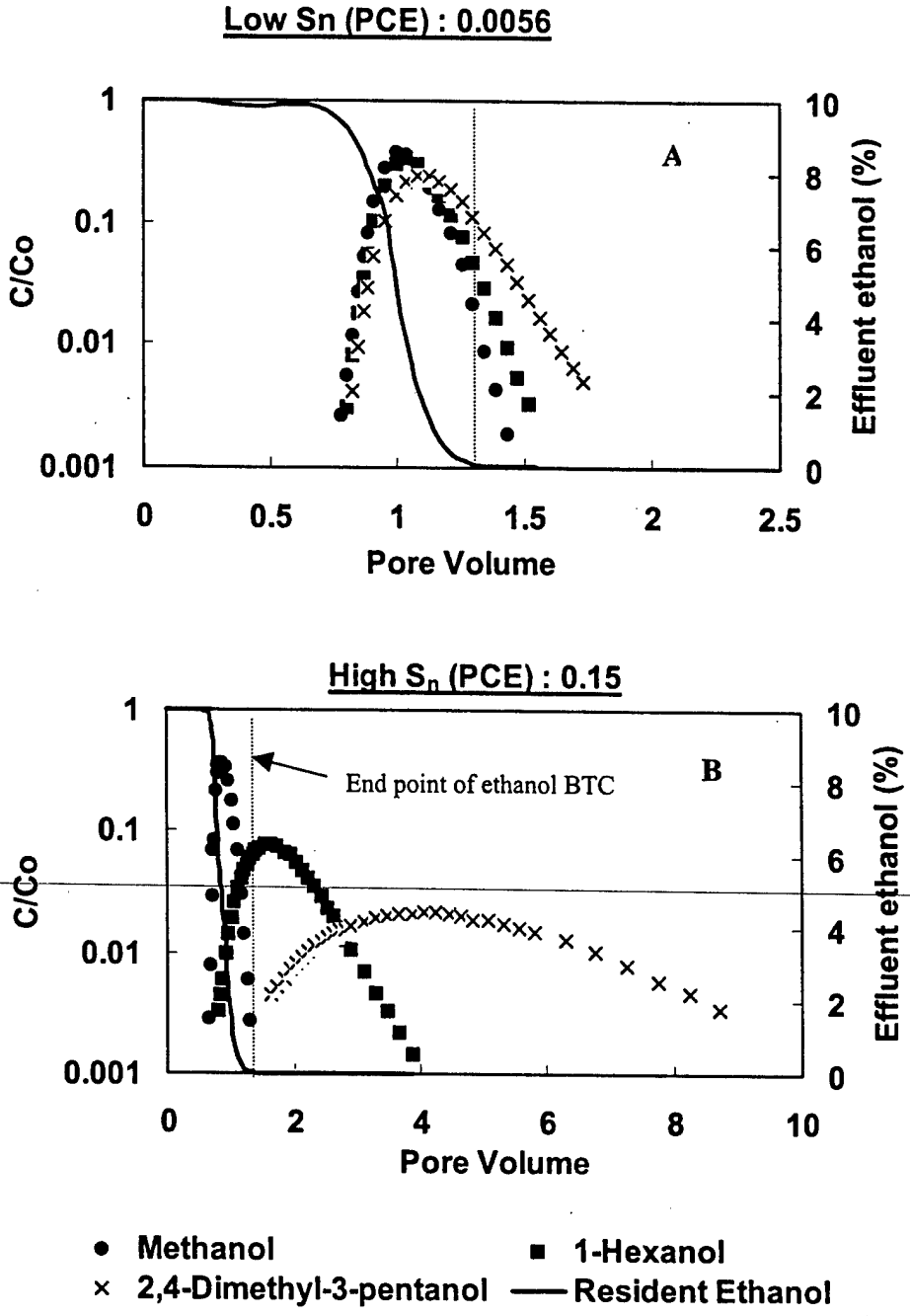
Low Sn (PCE) : 0.0056
A
C/Co
Effluent ethanol (%)
Pore Volume
High Sn (PCE) : 0.15
End point of ethanol BTC
B
C/Co
Effluent ethanol (%)
Pore Volume
Methanol
1-Hexanol
2,4-Dimethyl-3-pentanol
Resident Ethanol

Influence of Residual Surfactant on Partitioning Tracers

Jaehyun Cho[1], Michael D. Annable[1], and P. Suresh C. Rao[2]

September 16, 2001 Draft

Submitted for publication in

Journal of Contaminant Hydrology

Corresponding Author:

Michael D. Annable
Department of Environmental Engineering Sciences
University of Florida, P.O. Box 116450
Gainesville, FL 32611-6450
Phone: (352) 392-3294; Fax: (352) 392-3076
E-mail: manna@eng.ufl.edu

[1]Department of Environmental Engineering Sciences, University of Florida, P.O. Box 116450, Gainesville, FL 32611-6450
[2]School of Civil Engineering, Purdue University, West Lafayette, IN, 47907-1284

Abstract

Residual surfactants in aqueous and adsorbed phases were evaluated by estimating PCE saturation using partitioning tracers through batch equilibrium and column displacement tests. The batch equilibrium tests using residual surfactants ranging from 0.05 to 0.5 % by weight showed that as the concentrations of the surfactants increased, the partitioning coefficients linearly decreased for Diphenyl oxide disulfonates (DowFax 8390), increased for Polyoxyethylene (10) oleyl ether (Brij 97), and decreased slightly or exhibit no observable trend for Sodium dihexyl sulfosuccinate (AMA 80). Results from column tests using clean sand media with residual DowFax 8390 and PCE were consistent with those of batch tests. In the presence of DowFax 8390 (less than 0.5 % by weight), the PCE saturations were underestimated by up to about 20 %. Adsorbed surfactants on a clay-silt-sandy loamy soil with strongly positive charged oxides in the absence of PCE showed false indications of PCE saturation. Using no surfactant (background soil) gave a false PCE saturation of 0.0004 while soil contacted by AMA 80, Brij 97, and DowFax 8390 gave false PCE saturations of 0.0024, 0.043, and 0.229, respectively.

1. Introduction

Surfactants as micelle-forming surface active chemicals have been used as an enhanced flushing technology, principally in the oil industry or at organic liquid contaminated sites. The surfactants are classified, by the nature of their hydrophilic head groups as anionics, nonionics, and cationics. The anionic and nonionic surfactants have been good candidates as flushing agents since soil particles generally carry a negative charge. Their effectiveness at cleaning up contaminated sites has been demonstrated in previous studies (Abdul et al., 1990; Boving et al., 2000; Dwarakanath et al., 1999; Jawitz et al., 1998; Pennell et al., 1993; Rhue et al., 1999; Shiau et al., 1994). After remedial efforts and following a water flood, however, some amounts of the flushing agents are likely to remain adsorbed on the solid phase, or dissolved (as monomer or micelle) in the aqueous phase. The residual surfactants, which alter the partitioning properties of hydrophobic organic chemicals (HOCs) in the flushed zone, must be considered when the partitioning tracer technique (Pope et al., 1994; Jin et al., 1995; Annable et al., 1995) is used to characterize residual NAPL saturation.

The residual surfactant form will vary with concentration, chemical structure, soil property, and environmental aqueous conditions in soils (Abu-Zreig, 1999). In a NAPL/water system, initially the adsorbed surfactant tail groups are oriented parallel to the hydrophobic surface of the NAPL with a slightly tilted or L-shape and the hydrophilic head groups are oriented toward the aqueous phase (Rogen, 1989). As adsorption of the surfactant continues, the orientation of the adsorbed molecules is more perpendicular to the surface. At low aqueous surfactant concentration, the sorption coefficient of the surfactant onto NAPL increases dramatically, but decreases with increasing surfactant

concentration above the critical micelle concentration (CMC) (Zimmerman, 1999). The surfactant adsorption appears to level off near/above the CMC and this leveling off trend is attributed to the formation of micelles which limit the amount of surfactant adsorption onto the NAPL (Zimmerman, 1999; John et al., 2000).

In the soil/water system, while anionic surfactants repel from the negatively charged soil, nonionic surfactants generally adsorb onto the solid surface by hydrogen bonding. On the other hand, if the soil contains positively charged sites such as metal oxides (i.e., aluminum oxide), the anionic surfactants adsorb strongly onto the charged sites by ionic exchange or pairing (Holsen et al., 1991; Smith et al., 1991; Rouse et al., 1993; Sun and Jaffe, 1996). The adsorbed surfactants act as good hydrophobic media to allow partitioning of HOCs. Like the NAPL system, as the concentration of the surfactants exceeds the CMC, adsorption levels off and excess surfactants form micelles which have a hydrophobic interior where hydrophobic organic molecules can reside (Holsen et al., 1991; Ko et al., 1998a,b; Sun and Jaffe, 1996).

Residual surfactant from remedial activities can be a concern since partitioning tracers (Rao et al., 1997; Annable et al., 1998) have been employed at sites associated with chemical remediation. The partitioning behavior of tracers travelling through the porous media can be impacted by surfactants: 1) partitioning into the NAPL phase that results in an increase in the retardation of tracers, 2) forming micelles in the aqueous phase causing a decrease in the retardation of tracers, and 3) adsorption on the solid matrix that results in an increase in the retardation of tracers. As a result, the residual surfactants can give a false NAPL indication and be a limiting factor in the use of the partitioning tracer technique. This study investigates the influence of residual flushing

agent (surfactants) upon residual NAPL volume estimation using partitioning tracers. The objectives were to quantify the effect of residual surfactants on the partitioning and transport behavior of alcohol tracers through batch isotherm and column miscible tests. The effects of adsorbed surfactants on the solid matrix, including positively charged sites, were also investigated. Finally, the observed effects of residual surfactants were verified by a post-flushing tracer test following a surfactant flood.

2. Materials and Methods

2.1. Materials

Diphenyl oxide disulfonates (DowFax 8390) (Dow Chemical Co.), Sodium dihexyl sulfosuccinate (AMA-80-I) (Cytec Industries Inc.), and Polyoxyethylene (10) oleyl ether (Brij-97) (Uniqema Industries Inc.) were the surfactants used in this study. Their physical and chemical properties are given in Table 1. DowFax-8390 is a di-anionic surfactant with two negatively charged hydrophilic sulfonate heads and an alkyl chain. AMA-80-I is a mono-anionic surfactant in a mixture of isopropanol and water, and Brij-97 is a nonionic surfactant. Tetrachloroethylene (PCE) (Acros, 99 %) was used as a NAPL for all batch equilibrium and column experiments. A suite of tracers was selected to examine the effects of varying retardation factors. Methanol (Fisher, 98 %) was used as a non-partitioning tracer while 4-methyl-2-pentanol (4M2P) (Acros, 99+ %), n-hexanol (Acros, 98 %), and 2,4-dimethyl-3-pentanol (2,4DMP) (Acros, 99+ %) were used as partitioning tracers. All experiments were conducted at room temperature (23 ± 1 $^{\circ}$C). A clean silica sand (30-40 mesh, Ottawa) and a clay-silt-sandy loamy soil (Dover AFB site soil) including some metal oxides were used as porous media throughout the miscible

displacement experiments. The metal oxides in the soil were extracted by an acid digestion method for soil (U.S. EPA SW-846 3050B) and quantified by an inductive coupled plasma atomic emission spectrometry (Thermo Elemental Series Enviro 36).

2.2. Batch Isotherm Tests

A series of batch equilibrium experiments was conducted to evaluate the behavior of tracer partitioning in varying surfactant concentrations (≤ 0.5 % by weight). The partition isotherms were measured for three surfactant solutions (Brij 97, AMA 80, and DowFax 8390) with varying concentration (0.0, 0.05, 0.1, 0.3, and 0.5 %). Each surfactant solution was transferred to a 100 ml volumetric flask, and three alcohol tracers were added. The tracer mixtures of 21, 16, 14, and 12 ml prepared at each surfactant level were added to 3, 8, 10, and 12 ml of PCE, respectively, in 25 ml vials fitted with Teflon-lined screw caps. The vials were tumbled end-over-end on a laboratory-rotator (model RD 4512) for 24hrs at room temperature. At the end of the equilibrium period, the alcohol mixtures in the supernatant solutions were analyzed by Gas Chromatography (Perkin Elmer GC, Autosystem XL) with a flame-ionization detector.

2.3. Miscible Displacement Tests

Three series of miscible displacement tests were performed for this study. The first series of miscible displacement tests was conducted to evaluate the effects of residual surfactants in the aqueous phase. The column used was a glass column, 4.8 cm in diameter and 15 cm in length with Teflon end pieces (high performance liquid chromatography (HPLC) column from Kontes). Two layers of a fine wire mesh and a

plastic screen were placed inside of the Teflon end piece to minimize column end effects. The column was packed with pre-mixed sand containing PCE. The pre-mixed sand was prepared by adding 20 ml of water and 2 ml of PCE to 750 g ($\cong$ 300 cm^3) of sand and homogenizing. The columns used for the residual surfactant (DowFax 8390) tests were prepared for the miscible displacement experiments by flushing 3 pore volumes (PV) of DowFax solution through the column. The mobile phase and DowFax solution used PCE saturated water to minimize loss of residual PCE in the column. The partitioning tracer tests were conducted both with and without DowFax solution at varying concentrations (0.05, 0.1, 0.3, and 0.5 % by weight). The retardation factor and PCE saturation measured from each column test were used to estimate the partitioning coefficients.

The second series of miscible displacement tests was conducted for residual surfactants adsorbed on the solid matrix without NAPL. The column used was a glass column, 2.54 cm in diameter and 5 cm in length (HPLC column, Kontes) with Teflon end pieces and a fine wire mesh and a plastic screen. Clay-silt-sandy loamy soil (Dover AFB site soil) was wet-packed and cleaned by passing 20 PV of degased DI water. The clay-silt-sandy loamy soil contained some metal oxides (i.e., Fe^{+3} and Al^{+3}) which can exchange with a negative charged surfactant (i.e., DowFax 8390). Brij 97 (5 %), AMA 80 (5 %), and DowFax 8390 (5 %) solutions were used as surfactants. The column tests for adsorbed surfactants were prepared for the miscible displacement experiments by flushing 5 PV of each surfactant solution, and then 5 PV of water through the column. The partitioning tracer tests were conducted in the columns containing adsorbed surfactant and the results were used to determine a false indication of PCE.

The third series of miscible displacement tests was conducted to demonstrate the impact of the adsorbed surfactant through a flushing test. The column, media, and packing method used were the same as those of the second series. Column test 1 was conducted using a surfactant mixture (5 % DowFax 8390/ 3 % AMA 80/ 3 % NaCl / 3 % $CaCl_2$, wt.) as the flushing agent, but without PCE. The column was prepared by flushing 5 PV of the surfactant mixture, and then 5 PV of water through the column. The retardation factor from column test 1 was used to calculate a false indication of PCE.

Column test 2 was conducted with a residual PCE (S_{PCE} = 0.16). The PCE was introduced in the initially water saturated column using a syringe pump at 0.2 ml/min. Some of the PCE was displaced by injecting water to create a residual PCE saturation trapped in the pores. A pre-flushing partitioning tracer test was conducted to estimate the residual PCE volume trapped in the column. The trapped PCE in the column was flushed out with 20 PV of the same surfactant mixture as column 1 at 0.3 ml/min. The effluent PCE from the column was collected and analyzed to calculate the flushed and remaining PCE volume. Then, the column was flushed with 5 PV of degased DI water. Finally, a post-flushing tracer test was conducted to estimate the residual PCE volume. The estimated PCE volume was compared with that obtained from PCE mass balance ("initial PCE volume" minus "the recovered PCE volume" = "residual PCE").

3. Results and discussion

3.1. Effect of Surfactants on Batch Isotherms

In the presence of three surfactants (AMA 80, Brij 97, and DowFax 8390) ranging in concentration from 0 to 0.5 % by wt., alcohol tracer NAPL-water partitioning coefficients

(K_{ns}) were measured by batch isotherm experiments. The partitioning coefficients were determined by linear-least-square curve fitting. The K_{ns} values and regression coefficients, R^2, are shown in Table 2. The dependence of tracer partitioning coefficients on the surfactant type was observed for the range of concentrations used in this study. The partitioning of alcohol tracers into NAPL (PCE) decreased in the presence of anionic surfactants (AMA 80 and DowFax 8390), but increased in the presence of the nonionic surfactant (Brij 97) (Figure 1).

Unlike a NAPL/water system, the tracer partitioning behavior in a NAPL/surfactant system is a complex process involving the partitioning of the tracer into NAPL, sorbed surfactant, and surfactant micelles. At low concentrations below the CMC, the surfactant molecules adsorb to the NAPL-water interface or reside in aqueous phase as monomers. The alcohol tracers in the aqueous phase partition into the NAPL and the hydrophobic portion of the adsorbed surfactant. At high concentrations above the CMC, however, the surfactants generally form micelles with a hydrophobic inner core, allowing partitioning of alcohol tracers. In this system, partitioning of the alcohol tracers into NAPL with adsorbed surfactant competes with partitioning into surfactant micelles. Therefore, the micelles in the aqueous phase cause a decrease in NAPL partitioning of the alcohol tracers. The decrease of K_{ns} of HOCs resulting from micellar partitioning in a solid-water system has been reported (Sun et al., 1995, 1996; Ko et al., 1998 a, b). For the nonionic surfactant (Brij 97), however, the partitioning of the alcohol tracers increased with increasing surfactant concentration. This result requires an alternate explanation for the partitioning behavior of the alcohol tracers in the NAPL/surfactant system.

For anionic surfactants, the hydrophobic tail groups adsorb onto the hydrophobic NAPL, but are only slightly soluble in hydrocarbons (Rogen, 1989). The NAPL surface with the hydrophilic head groups oriented toward the aqueous phase may be less hydrophobic than the original NAPL (PCE). The lower hydrophobicity of the NAPL surface and the competition with micelles in the aqueous phase can cause a decrease in partitioning of the alcohol tracers into the NAPL phase. For Dowfax 8390 with twin hydrophilic heads, the partitioning coefficients (K_{ns}) decreased in a linear fashion with increasing DowFax concentration:

$$K_{ns} = K_{nw} - \alpha_s \cdot C_s \qquad (1)$$

where K_{nw} is the partitioning coefficient in water; C_s is the surfactant concentration (% by weight); α_s is an empirical constant; the subscripts, *n, w, s* denote NAPL, water, and surfactant. For AMA 80, however, the decrease was slight and some values were relatively uncertain at high concentrations. For Brij 97, the K_{ns} values increased and plateaued with increasing the surfactant concentration (≤ 0.5 % by weight). The increasing trend is of a Langmuir type:

$$K_{ns} = \frac{a \cdot b \cdot C_s}{1 + a \cdot C_s} + K_{nw} \qquad (2)$$

where *a* and *b* are empirical constants. Unlike anionic surfactants, for polyoxyethylenated (POE) nonionics such as Brij 97, the surfactant not only adsorbs onto the hydrocarbon, but is also soluble in the hydrocarbon (Rogen, 1989). The NAPL phase tends to become more hydrophobic because the surfactant is adsorbed onto and dissolved into the NAPL. Even though partitioning of alcohol tracers into the NAPL phase competes with that into

the micelles, the increase of the tracer partitioning due to higher hydrophobicity of the NAPL with the adsorbed nonionic surfactant may dominate the expected decrease of the partitioning due to the micelles. The other possible explanation for the observed behavior is a significant increase of interfacial area for the partitioning of alcohol tracers by formation of a macroemulsion, which is a stable suspension of particles. Alcohol tracers can partition into or be mixed with the macroemulsion phase (which is a single-phase mixture of surfactant, NAPL (PCE), and water), and then be separated from the aqueous phase. The separation means a decrease of the tracer partitioning in the aqueous phase while an increase into NAPL phase. The Brij 97 used in this study formed an opaque macroemusion phase with the NAPL (PCE)/alcohol tracers, and its stability also was longer (several days to several weeks) without any additives, resulting in an increase of the partitioning of the alcohol tracers. However, for the range of concentrations used in this study (0.05 to 0.5 % by weight), the DowFax 8390 did not form a macroemulsion, and the AMA 80 formed a slight macroemulsion while its lifetime was very short (a few minutes to a few hours). These observations suggest that the surfactant macroemusion formation and its lifetime may also contribute to an increase in the partitioning of alcohol tracers.

3.2. Effect of Residual Surfactants on Tracer Transport

A series of column tests were conducted to verify the observations from the batch equilibrium tests on partitioning and transport of alcohol tracers. The columns contained very low PCE saturation (S_{PCE} = 0.0125) trapped in a clean sandy medium, and DowFax 8390 ranging from 0 to 0.5 % wt. was used as a residual surfactant. The observed results

showed decreasing retardation with increasing residual surfactant concentration (Table 3). Here, we assume that adsorption of surfactant on the solid media (which causes an increase in tracer retardation) is negligible since the doubly negative charged DowFax is not attracted to the negative charged clean sand. A comparison of partitioning coefficients between batch and column tests provides a better understanding of the observed results. The partitioning coefficients from the column miscible test (K_{col}) can be estimated using equation (3):

$$K_{col} = \frac{(R_s - 1) \cdot (1 - S_{PCE})}{S_{PCE}} \qquad (3)$$

where R_s is a retardation factor obtained in the presence of residual surfactant, and S_{PCE} is an PCE saturation estimated from a tracer test without residual surfactant. The estimated K_{col} values from the column tests were compared with the K_{ns} from batch tests in Figure 2. Although showing slight deviation at high concentrations, the decreased partitioning behavior with increasing DowFax concentration is in good agreement with the K_{ns} from batch tests. Based on equation (3), the larger the partitioning coefficient, the smaller the NAPL saturation. Recall that in the presence of residual DowFax 8390, the K_{ns} was smaller than the K_{nw} in water. This means, as the larger partitioning coefficient (K_{nw}) is used with the smaller R_s measured in the presence of residual surfactant, the PCE saturations (S_{PCE}) would be under-estimated. The observed results showed that the S_{PCE} values were under-estimated from 4.3 to 21.7 % for n-hexanol and 0.2 to 24.7 % for 2,4DMP using varying residual concentrations (0.05 to 0.5 % by weight). Assuming about 10 % (≈ 0.4 to 0.8 % wt.) or lower residual for typical surfactant concentrations (≈

4 to 8 % wt.) (Dwarakanath et al., 1999) at post-flushing field sites, the observed results in this study show a potential for significant error in the presence of a residual surfactant.

3.3. Effect of Adsorbed Surfactants on the Solid Matrix

Alcohol tracer partitioning into adsorbed surfactant on a solid matrix was evaluated with a field site (Dover AFB) soil containing abundant metal oxides which have strongly positive charges. The main oxides in the soil consist of iron oxide (9800 mg/ kg soil) and aluminum oxide (4600 mg/ kg soil). Breakthrough curves (BTCs) of the tracers from the column tests with residual surfactants are shown in Figure 3. The retardation of the tracers showed a significant deviation dependent upon the structure of the surfactants used. The observed retardation factors (R_s) for n-hexanol are 1.003 for no surfactant (background soil), 1.016 for AMA 80, 1.303 for Brij 97, and 3.016 for DowFax 8390.

In general, anionic surfactants are oriented away from the negatively charged surface but if the soil contains positively charged oxides, the surfactants easily adsorb onto the surface with their negatively charged head groups by interactions such as ion exchange. The adsorption isotherm of ionic surfactants onto a charged site is typically S-shaped (Rogen et al., 1983; Holsen et al., 1991; and Ko et al., 1998a). The distribution coefficients (K_d) at low concentration increase with increasing surfactant concentration, and at high concentration (above the CMC) decrease since surfactant micelles in the aqueous phase begin to compete with the adsorbed surfactant (Sun et al., 1995; Ko et al., 1998a).

In this study water flooding (which typically has conducted before a post-flushing tracer test) (e.g., Rao et al., 1997) followed surfactant flooding. The subsequent water

flooding would remove partially or most of the adsorbed surfactants existing as monolayers or bilayers and most of the residual surfactants as micelles in the aqueous phase. The remaining surfactant is likely to be adsorbed phase (mainly a monolayer). The adsorbed surfactants with hydrophobic tail groups oriented toward the aqueous solution would act as a highly efficient hydrophobic medium into which alcohol tracer can partition (Holsen et al., 1991).

For AMA 80, while the R_s value (=1.016) is larger than the R_s (= 1.003) for background soil (no surfactant), the degree of retardation was not significant (Figure 3-A,B). This implies AMA 80 may be a good candidate for a surfactant remediation effort requiring a post-flushing tracer test. This may be due to less hydrophobicity of the short carbon chain (dihexyl groups) or the less residual amount due to weak adsorption binding which can be displaced easily by water.

However, for DowFax 8390, an extremely large R_s value (= 3.016) was observed (Figure 3D). This retardation seems to be attributed to its special chemical structure. The doubly charged sulfonate groups of DowFax 8390 adsorb strongly onto the positively charged oxides as compared to mono-anionics such as AMA 80. Therefore, the adsorbed hydrophilic moieties on the strong positive sites are likely to resist water flooding; that is, DowFax 8390 can not be displaced easily by the water flooding. This indicates that the adsorbed DowFax 8390 can cause a serious error on estimation of residual NAPL saturation during a post-flushing tracer test.

Adsorption behavior of a nonionic surfactant will be different from the above anionic surfactants. In general, nonionic surfactants such as Brij 97 adsorb onto surfaces with either hydrophilic or the hydrophobic group oriented toward the surface.

Polyoxyethlenated surfactants adsorb onto a silica surface through hydrogen bonding between SiOH groups on the surface and the oxygens of the oxyethylene groups (Rosen, 1989). This adsorption has been explained as the electrostatic interaction between the oxygens of the POE chain and the negatively charged soil surface by picking up protons from the water and acquiring positive charges.

These retardations resulting from the adsorbed surfactants cause a false PCE saturation (False S_{PCE}) by the post flushing tracer tests. The false S_{PCE} values can be calculated by equation (3) with K_{nw} (= 6.56) for n-hexanol and the observed R_s values. The false S_{PCE} values were 0.0004, 0.0024, 0.0426, and 0.2286 for no surfactant (background soil), for AMA 80, Brij 97, and DowFax 8390, respectively. Considering that typical post flushing tracer tests have been conducted with low NAPL saturation (approximately ranging 0.005 to 0.02)(Rao et. al., 1997), the impact of the residual surfactant on soil with the positively charged sites can be significant.

3.4. Demonstration through A Flushing Test

The effect of residual surfactant was demonstrated through partitioning tracer tests along with a surfactant flooding using columns packed with the same soil (Dover AFB site soil) as used previously. The surfactant mixture used as a flushing agent was 5 % DowFax 8390 / 3 % AMA 80 / 3% NaCl / 3 % $CaCl_2$. The solubility of PCE in this mixture was approximately 70000 mg/l. Partitioning tracer tests were conducted before and after the surfactant flooding test. BTCs for the pre- and post-flushing tracers are shown in Figure 4. The observed BTCs from the post-flushing tracer test with low S_{PCE} (0.0125 based on PCE mass balance) (Figure 5) showed a similar trend to those from the

pre-flushing tracer test with high S_{PCE} (0.16 by tracers). The estimated S_{PCE} values were 0.16 (1.27 ml PCE) and 0.16 (1.27 ml) for the pre flushing tracer test, and 0.13 (1.05 ml) and 0.15 (1.22 ml) for the post flushing tracer test after the surfactant flooding by 4M2P and n-hexanol, respectively. As calculated using only the results of these pre- and post-flushing tracer tests, the removal percentage of PCE by the surfactant flooding should be just about 10 %. Based on a mass balance between injected and extracted PCE (Table 4), however, the removal percentage of PCE was about 92% (1.17 ml / 1.27ml). This deviation between the S_{PCE} estimations based on the tracer tests and PCE mass balance is due to the residual (most adsorbed) flooding agent. The results from column 1 quantified the false S_{PCE} caused by the adsorbed surfactant mixture. This false S_{PCE} (= 0.12 and 0.14 for 4m2p and n-hexanol, respectively) can be subtracted from the estimated S_{PCE} (= 0.13 and 0.15 for 4m2p and n-hexanol, respectively) from the post-flushing tracer test, resulting in about $S_{PCE} \approx 0.01$ which approaches the S_{PCE} based on mass balance. As noted earlier, even though clean water followed the surfactant flood, some amount of surfactant would remain adsorbed to the solid matrix. In this case, the alcohol tracers partition into the adsorbed surfactant on the positively charged oxides as well as the PCE phase with adsorbed surfactant, causing a significant increase in tracer retardation.

4. Conclusions

The results from this study indicate that NAPL volume estimates using a post-flushing partitioning tracer test could be influenced by the residual surfactant flushing agent. The surfactants remain adsorbed on the solid phase (causing an increase in retardation of alcohol tracers) and dissolved (as monomers and micelles) in aqueous

phase (causing a decrease in retardation). In the PCE/surfactant system (≤ 0.5 % by weight), the partitioning coefficients of alcohol tracers into PCE decrease linearly with increasing concentration of anionic surfactants (AMA 80 and DowFax 8390), whereas they increase and then plateau with increasing concentration of nonionic surfactant (Brij 97). Results based on column tests with DowFax 8390 showed less retardation which was in good agreement with the lower partitioning coefficient. The lower retardation resulted in an under-estimation of PCE saturation up to 20 %. In a soil system that included abundant metal oxides which have strongly positive charges, surfactants were adsorbed weakly or strongly depending upon the structure of the surfactants used. The adsorbed surfactants with hydrophobic tail groups oriented toward aqueous solution would act as a hydrophobic medium into which alcohol tracer can partition. The resulting partitioning of the tracers into the hydrophobic medium causes a false S_{PCE} based on post-flushing partitioning tracer tests. The false S_{PCE} values were 0.0024, 0.0426, and 0.2286 for AMA 80, Brij 97, and DowFax 8390, respectively. Considering that post-flushing tracer tests have been typically conducted with low NAPL saturation, the adsorbed surfactants can cause significant over-estimation of NAPL saturation.

Acknowledgements

This study was funded by the U. S. Department of Defense Strategic Environmental Research and Development Program (SERDP), which is a collaborative effort involving the U. S. EPA, U. S. DOE, and U. S. DOD. This document has not been subjected to peer review within the funding agency, and the conclusions stated here do not necessarily reflect the official views of the agency nor does this document constitute an official

endorsement by the agency. This work was presented as a poster at the American Geotechnical Union Meetings, December 2000, San Francisco, CA.

References

Abdul, A.S.; Gibson, T.L.; Rai, D.N., 1990. Selection of surfactant for the removal of petroleum products from shallow sandy aquifers. Ground Water.28 (6), 920.

Abu-Zreig, M.; Rudra, R.P.; Dickinson, W.T.; Evans, L.J., 1999. Effect of surfactants on sorption of atrazine by soil. Journal of Contaminant Hydrology. 36, 249-263.

Annable, M.D.; Rao, P.S.C.; Haltfield, K.; Graham, W.D.; Wood, A.L., 1995. Use of partitioning tracers for measuring residual NAPL distribution in a contaminated aquifer: preliminary results from a field-scale test, Water Resources Research.

Annable, M.D.; Rao, P.S.C.; Hatfield, K.; Graham, W.D.; Wood, A.L.; Enfield, C.G., 1998. Partitioning tracers for measuring residual NAPL: field-scale test results, Journal of Environmental Engineering 124 (6).

Boving, T.B.; Brusseau, M.L., 2000. Solubilization and removal of residual trichloroethene from porous media: comparison of several solubilization agents. Journal of Contaminant Hydrology. 42, 51-67.

Dwarakanath, V.; Kostarelos, K.; Pope, G.A.; Shotts, D.; Wade, W.H., 1999. Anionic surfactant remediation of soil columns contaminated by nonaqueous phase liquids. Journal of Contaminant Hydrology 38, 465-488.

Holsen, T.M.; Taylor, E.R.; Seo, Y.; Anderson, P.R., 1991. Removal of sparingly soluble organic chemicals from aqueous solutions with surfactant-coated ferrihydrite. Environ. Sci. Technol. 25,1585-1589.

Jawitz, J.W.; Annable, M.D.; Rao, P.S.C.; Rhue, R.D., 1998. Field implementation of a Winsor Type I surfactant/alcohol mixture for in situ solubilization of a complex LNAPL as a single-phase macroemulsion. Environ.Sci. Technol. 32(4), 523-530.

Jin, Minquan; Delshad, Mojdeh; Dwarakanath, Varadarajan; McKinney, D.C.; Pope, G.A.; Sepehrnoori, Kamy; Tilburg, C.E., 1995. Partitioning tracer test for detection, estimation, and remediation performance assessment of subsurface nonaqueous phase liquids. Water Resourses Research 31(5), 1202-1211.

John, W.W.; Bao, G.; Johnson, W.P.; Stauffer, T.B., 2000. Sorption of nonionic surfactant oligomers to sediment and PCE DNAPL: effects on PCE distribution between water and sediment. Environ.Sci. Technol. 34, 672-679.

Ko, Seok-Oh; Schlautman, M.A.; Carraway, E.R., 1998a. Partitioning of hydrophobic organic compouns to sorbed surfactants. 1. experimental studies. Environ.Sci. Technol. 32, 2769-2775.

Ko, Seok-Oh; Schlautman, M.A.; Carraway, E.R., 1998b. Effects of solution chemistry on the partitioning of phenanthrene to Sorbed Surfactants. Environ.Sci.Technol. 32, 3542-3548.

Lowe, D.F.; Oubre, C.L.; Ward, C.H., 1999. Reuse of surfactants and cosolvents for NAPL remediation. Lewis publishers, New York.

Pennell, K.D.; Abriola, L.M.; Weber Jr., W.J., 1993. Surfactant-enhanced solubilization of residual dodecane in soil columns. 1. experimental investigation. Eviron.Sci. Technol. 27(12), 2332-2340.

Pope, G.A.; Jin,Minquan; Dwarakanath,Varadarajan; Rouse,Bruce; Sepehrnoori,Kamy., 1994. Partitioning tracer tests to characterize organic contaminants.2nd tracer workshop. Univ. of Texas at Austin.

Rao, P.S.C.; Annable, M.D.; Sillan, R.K.; Dai, D.; Hatfield, K.; Graham, W.D.; Wood, A.L.; Enfield, C.G., 1997. Field-scale evaluation of in situ cosolvent flushing for enhanced aquifer remediation. Water Resources Research. 33(12), 2673-2686.

Rogen, M.J., 1989. Surfactants and interfacial phenomena, second edition. John Wiley & Sons.

Rouse, J.D.; Sabatini, D.A.; Harwell J.H., 1993. Minimizing surfactant losses using twin-head anionic surfactants in subsurface remediation. Environ.Sci. Technol. 27, 2072-2078.

Rhue, R.D.; Rao, P.S.C.; Annable, M.D., 1999. Single-phase microemulsification of a complex light-nonaqueous-phase-liquid: laboratory evaluation of several mixtures of surfactant/alcohol solutions. Journal of Environmental Qual. 28(4), 1135-1144.

Shiau, B.J.; Sabatini, D.A.; Harwell, J.H., 1994. Solubilization and microemulsification of chlorinated solvents using direct food additive (edible) surfactants. Ground Water. Vol.32, No.4, pp561-569.

Smith, J.A. and Jeffe, P.R., 1991. Comparision of tetrachloromethane sorption to an alkylammonium-clay and alkyldiammonium-clay. Environ.Sci. Technol. 25, 2054-2058.

Sun, S.; Inskeep, W.P.;Boyd, S.A., 1995. Sorption of nonionic organic compounds in soil-water systems containing a micelle-forming surfactant. Environ.Sci. Technol. 29, 903-913.

Sun, S.; Jaffe, P.R., 1996. Sorption of phenanthrene from water onto alumina coated with dianionic surfactants. Environ.Sci.Technol. 30(10).

Zimmerman, J.B.; Kibbey, T.C.G.; Cowell, M.A.; Hayes, K.F., 1999. Partitioning of ethoxylated nonionic surfactants into nonaqueous-phase organic liquids: Influence on solubilization behavior. Environ.Sci. Technol. 33, 169-176.

Zou, M. and Rhue, R. Dean, 1999. Screening commercial surfactants suitable for remediating DNAPL source zones by miscible displacement techniques. Environ. Sci.Technol.

List of Figures

Table 1. Physical and chemical properties of surfactants used in the study.

Surfactants	Mono-anionic	Di-anionic	Non-ionic
Chemical name	Dihexyl Sulfosuccinate	Diphenyl Oxide Disulfonates	Polyoxyethylene (10) Oleyl Ether
Trade name	Aerosol MA 80-1	DowFAX 8390	Brij 97
Chemical Structure	$C_{16}H_{29}O_7NaS$	$C_{16}H_{33}\ C_{12}\ H_7O(SO_3Na)_2$	$C_{58}H_{116}O_{21}$
Mol wt.	388	642	1149
Water Solubility	Miscible	Miscible	Miscible
CMC (mM)	2.3[a]	3[b]	-
HLB	-	78.6[c]	12.4[d]

Notes : CMC is critical micelle concentration; mM is milliMolar.
[a] Lowe et al., 1999; [b] Rouse et al., 1993; [c]Dow Chemical Co.; [d] Zou and Rhue, 1999.

Table 2. Partitioning coefficients (K_{ns}) of alcohol tracers measured on various surfactant contents (% by weight).

Surfactants	contents (%, wt.)	4M2P	n-hexanol	2,4DMP
water	0	3.6(0.994)	6.56(0.999)	26.52(0.999)
AMA 80 I	0.05	3.48(0.998)	6.56(0.999)	25.69(0.999)
	0.1	3.40(0.998)	6.43(0.999)	25.43(0.999)
	0.3	3.30(0.997)	6.38(0.999)	25.32(0.999)
	0.5	3.08(0.999)	6.59(0.996)	25.54(0.999)
DowFax 8390	0.05	3.51(0.999)	6.45(0.999)	26.23(0.999)
	0.1	3.47(0.999)	6.19(0.999)	24.98(0.999)
	0.3	3.36(0.999)	5.76(0.999)	23.22(0.999)
	0.5	3.17(0.999)	5.19(0.999)	20.95(0.999)
Brij 97	0.05	3.49(0.999)	7.13(0.998)	26.07(0.999)
	0.1	3.68(0.996)	7.49(0.995)	26.94(0.999)
	0.3	3.90(0.989)	8.07(0.986)	27.31(0.999)
	0.5	4.01(0.982)	8.17(0.987)	26.96(0.999)

Table 3. Parameter values observed from column miscible experiments with PCE / DowFax 8390.

Tracers	Surfactant Content (%, wt.)	R_s	Estimated S_{PCE}	S_{PCE} % error	K_{col}
n-hexanol	0	1.111	0.0166		6.56[a]
	0.05	1.106	0.0159	-4.3	6.27[b]
	0	1.099	0.0149		6.56[a]
	0.1	1.086	0.0129	-12.9	5.70[b]
	0	1.055	0.0084		6.56[a]
	0.5	1.043	0.0066	-21.7	5.13[b]
2,4DMP	0	1.435	0.0163		26.25[a]
	0.05	1.434	0.0163	-0.2	26.14[b]
	0	1.378	0.0142		26.25[a]
	0.1	1.338	0.0127	-10.42	23.44[b]
	0	1.219	0.0083		26.25[a]
	0.5	1.167	0.0063	-24.71	19.96[b]

[a] Partitioning coefficients (K_{nw}) measured in water by the batch isotherm tests.
[b] Partitioning coefficients (K_{col}) values estimated by the column tests in the presence of residual surfactants.

Table 4. Results observed from pre- and post-flushing tracer tests and PCE mass balance from the flooding test with DowFax 8390 5%/ AMA 80 3%/NaCl 3%/ $CaCl_2$ 3%.

Column	Test Type	PV	4-methyl-2-pentanol		n-hexanol	
			R_s	S_{PCE}	R_s	S_{PCE}
Column 1	Tracer test for only adsorbed surfactant	8 ml	1.46	0.12	2.06	0.14
Column 2	Pre-flushing tracer test	8.1ml	1.68	0.16	2.27	0.16
Column 2	Post-flushing tracer test	8.1ml	1.55	0.13	2.17	0.15

	Trapped PCE before flooding		Removed PCE during flooding	Residual PCE after flooding	
	volume	S_{PCE}	volume	volume	S_{PCE}
Column 2	1.27ml	0.16	1.17ml	0.1ml	0.0125

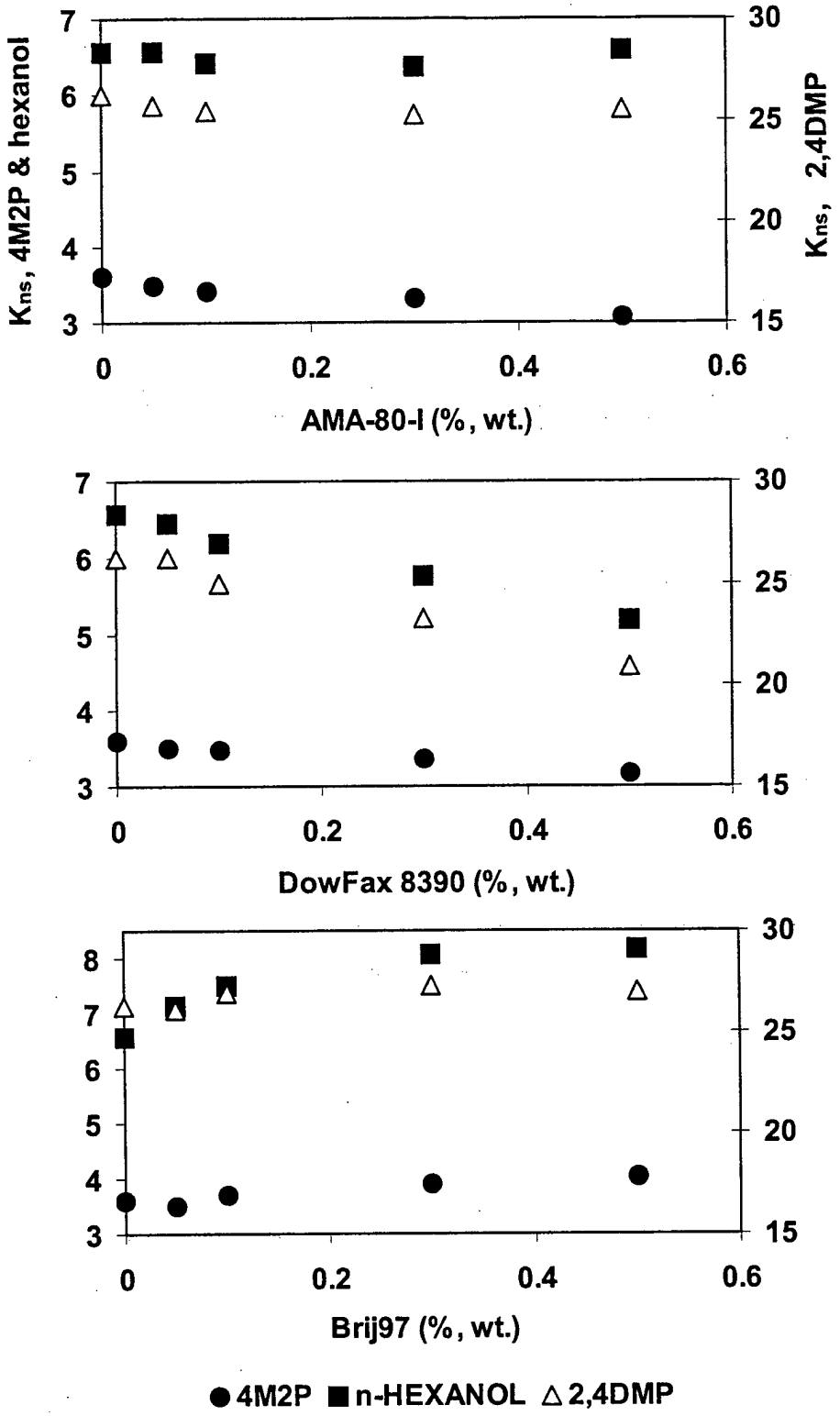
K_{ns}, 4M2P & hexanol
K_{ns}, 2,4DMP
AMA-80-I (%, wt.)
DowFax 8390 (%, wt.)
Brij97 (%, wt.)
● 4M2P ■ n-HEXANOL △ 2,4DMP

Figure 1

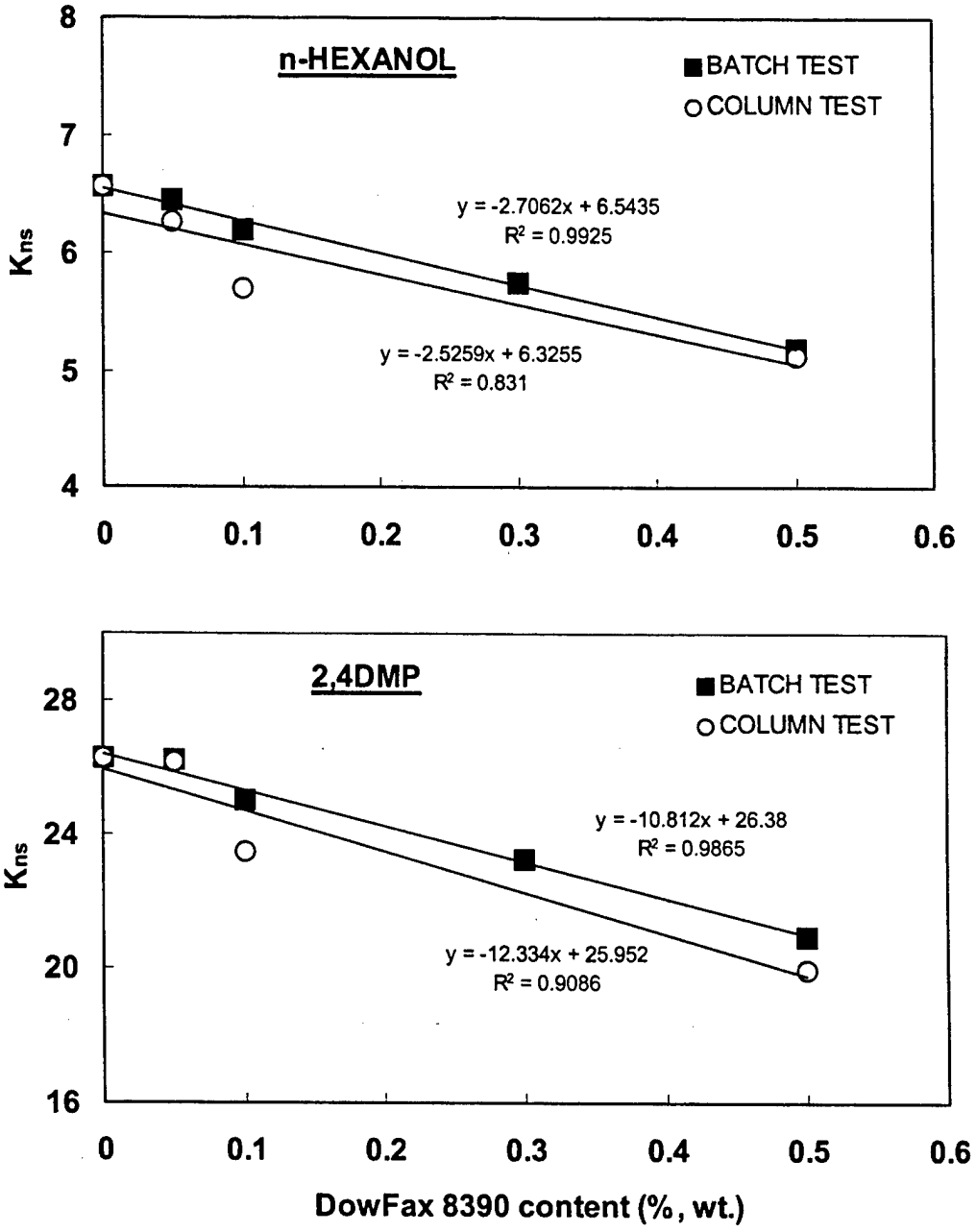
n-HEXANOL
BATCH TEST
COLUMN TEST
y = -2.7062x + 6.5435
R² = 0.9925
y = -2.5259x + 6.3255
R² = 0.831
Kns
8
7
6
5
4
0
0.1
0.2
0.3
0.4
0.5
0.6
2,4DMP
BATCH TEST
COLUMN TEST
y = -10.812x + 26.38
R² = 0.9865
y = -12.334x + 25.952
R² = 0.9086
Kns
28
24
20
16
0
0.1
0.2
0.3
0.4
0.5
0.6
DowFax 8390 content (%, wt.)

Figure 2

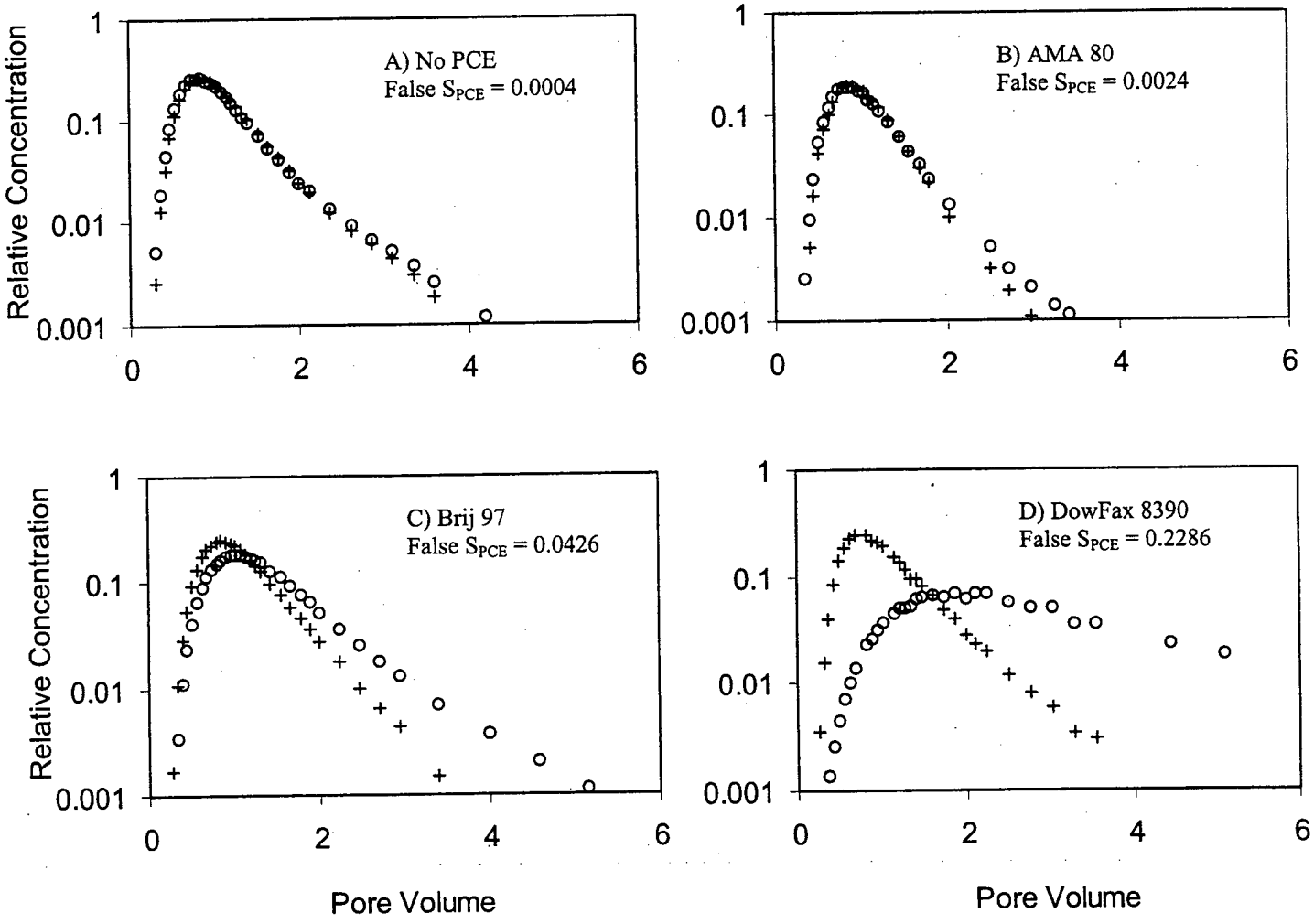
A) No PCE
False S_{PCE} = 0.0004
B) AMA 80
False S_{PCE} = 0.0024
C) Brij 97
False S_{PCE} = 0.0426
D) DowFax 8390
False S_{PCE} = 0.2286
Relative Concentration
Pore Volume
1
0.1
0.01
0.001
0
2
4
6

Figure 3

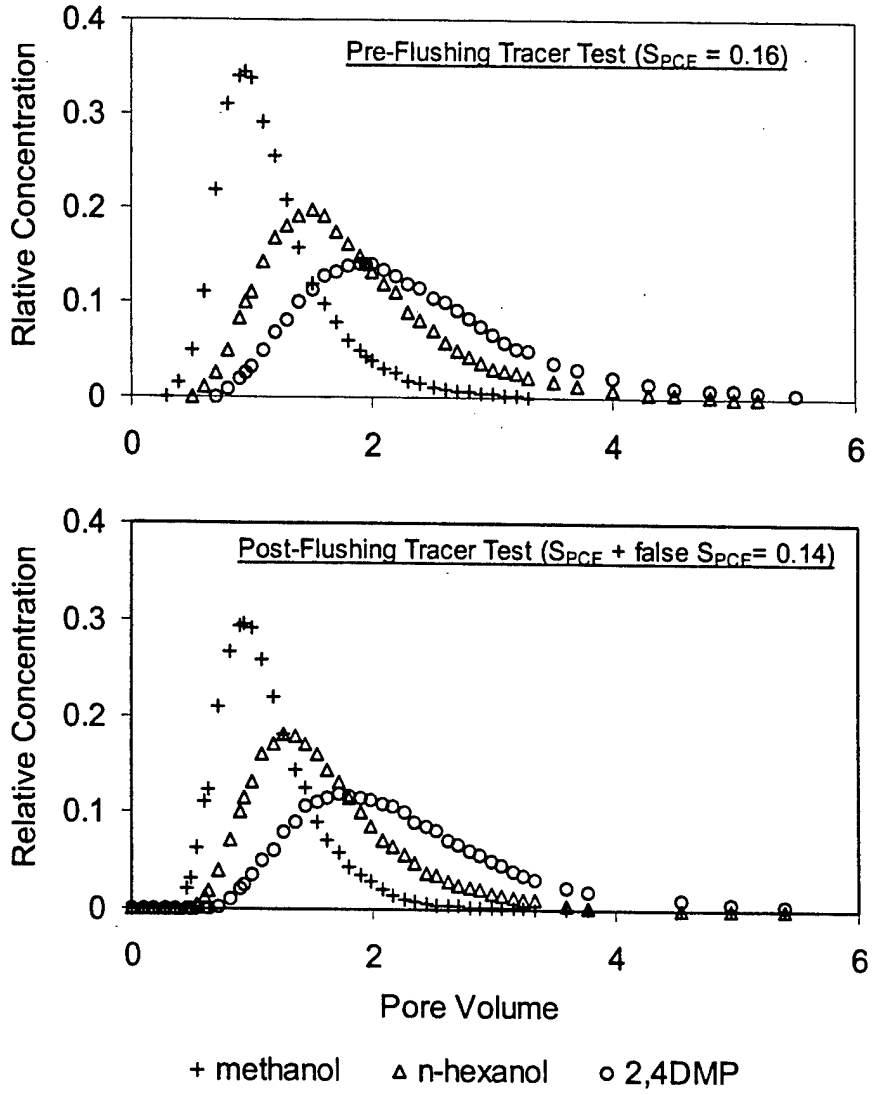
Pre-Flushing Tracer Test (S_{PCE} = 0.16)
Rlative Concentration
0.4
0.3
0.2
0.1
0
0
2
4
6
Post-Flushing Tracer Test (S_{PCE} + false S_{PCE}= 0.14)
Relative Concentration
0.4
0.3
0.2
0.1
0
0
2
4
6
Pore Volume
+ methanol
Δ n-hexanol
o 2,4DMP

Figure 4

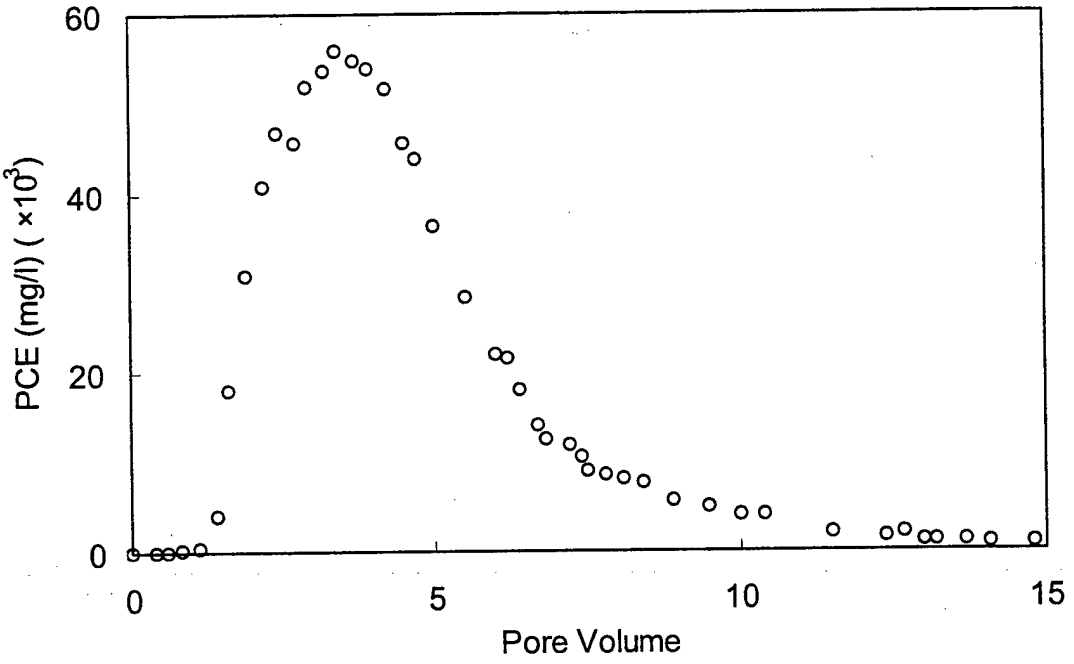

Figure 5

Activated Carbon for the Removal of Tetrachloroethylene (PCE) from Alcohol Solutions

Nancy J. Hayden[1], Michael C. Brooks[2], Michael D. Annable (Associate Member)[3], Hongxun Zhou (Associate Member)[4]

Abstract

Alcohol (cosolvent) flooding is a relatively new, in-situ technique for enhancing the removal of immiscible organic solvents, such as tetrachloroethylene (PCE) and trichloroethylene (TCE), from soil and groundwater aquifers. Recovery of the alcohol solution for reinjection is important for ensuring the cost effectiveness of this technology. The overall goal of this research was to investigate the ability of activated carbon to remove chlorinated compounds such as PCE from alcohol solutions so that the alcohol solution could be reused in the cosolvent-flooding process. Laboratory studies were conducted using PCE or TCE in isopropyl alcohol and PCE in ethanol. Alcohol concentrations in water ranged from 0-80% (v/v), and chlorinated compound concentrations ranged from 10 mg/L – 100,000 mg/L. Recovery and reuse of alcohol was applied to a cosolvent flood at the Dover National Test Site at the Dover Air Force Base, Delaware. The field application consisted of treating a 60-70% (v/v) ethanol solution containing PCE concentrations ranging from 500-2000 mg/L using two carbon drums in series. Laboratory results showed that PCE adsorbed on to activated carbon in the presence of alcohol even at very high alcohol concentrations. However, the Freundlich coefficient (K_f) was reduced by almost two orders of magnitude with increasing alcohol concentrations. Field results showed that activated carbon removed PCE from the ethanol solutions allowing these solutions to be reused in the cosolvent flood. The results demonstrated the technical and economic feasibility of the recovery and reuse of alcohol from cosolvent flooding activities.

[1]Assoc. Prof., Dept. of Civ. And Envir. Engrg., Univ. of Vermont, Burlington, VT 05405. 802-656-1924, 802-656-8446, E-mail: nhayden@emba.uvm.edu

[2]*Post-Doctoral Associate, Dept. of Envir. Engrg. Sci., Univ. of Florida, Gainesville, FL 32611-6450*

[3]*Assoc. Prof., Dept. of Envir. Engrg. Sci., Univ. of Florida, Gainesville, FL 32611-6450*

[4]*Structural Eng., Parsons Brinkerhoff, One Penn Plaza, New York, NY 10119*

Keywords: Activated carbon treatment, alcohol reuse, pilot-scale tests, cosolvent flushing

Introduction

Alcohol (cosolvent) flooding is a relatively new, in-situ technique for enhancing the removal of immiscible organic solvents, such as tetrachloroethylene (PCE) and trichloroethylene (TCE), from soil and groundwater aquifers. One of the main mechanisms of the alcohol flushing process is the enhanced solubility of PCE and TCE in the aqueous/alcohol mixture. Ternary-phase behavior and solubility data for PCE and TCE in alcohol/aqueous mixtures show significant increases in solubility of PCE and TCE in ethanol and isopropyl alcohol, IPA, (propan-2-ol) at increasing alcohol concentrations (Hayden et al. 1999). In the flushing process, alcohol solutions are injected into PCE or TCE contaminated areas, the contaminants dissolve into the alcohol and are then extracted with the flushing solutions. The feasibility of this remediation process has been demonstrated in pilot and field-scale studies (Jawitz et al. 2000; Sillan et al. 1998; Rao et al. 1997).

Recovery and reuse of the alcohol solution in an alcohol flooding remediation scheme is important for reducing the overall cost of remediation and for reducing the volume of hazardous waste generated from the remediation process. However, this aspect of the flushing process has not been studied in either laboratory or field investigations.

Activated carbon has been widely used in the water and wastewater fields to remove nonpolar organic contaminants. Research continues in this area, including investigating the properties of the adsorbate and competing adsorbates on adsorption and modeling the adsorption process (Crittenden et al. 1999, Luehrs et al. 1996, Klecka et al. 1996, Hazourli et al. 1996, Urano et al. 1991, Wujcik et al. 1992, Ying, et al. 1990). However, the adsorption of organic compounds, such as PCE and TCE, from alcohol solutions has not been investigated.

Weber and DiGiano (1996) classify adsorption as solvent-motivated and sorbent-motivated adsorption where solvent-motivated adsorption deals primarily with the repulsion of solute molecules, also called the adsorbate, by the solvent phase. The sorbent-motivated adsorption relies on the attraction of the solute molecules to the adsorbent phase. Activated carbon adsorption is generally affected by both the solute's incompatibility with the solvent and the affinity between the solute and the activated carbon. For example, organic compounds of low aqueous solubility, such as PCE and TCE, are readily adsorbed by activated carbon, however, as the solubility of the organic compounds increases, carbon adsorbability decreases (Weber 1972). Both ethanol and IPA are miscible with water and have low adsorbability to activated carbon.

Increasing the concentration of alcohol in aqueous solutions increases the solubility of PCE and TCE in the solution thereby decreasing the solvent-motivated adsorption. This would likely reduce PCE and TCE adsorbability onto activated carbon. The higher solute concentration due to the increased solubility produces a greater concentration gradient and chemical potential that would likely result in large amounts of PCE adsorbed on the carbon.

Studies on the effect of cosolvents on organic contaminant sorption onto activated carbon were not found in the literature, however, the effect of cosolvents on organic contaminant sorption on soils and soil matrices has been examined and found to greatly influence the sorption process (Nzengung et al. 1996, Wood et al. 1990, Nkedi-Kizza et al. 1987, Fu and Luthy 1986, Rao et al. 1985). For example, sorption coefficients determined from batch isotherms of phenanthrene and naphthalene onto sandy surface soil showed a log-linear decrease as the volume fraction of methanol increased in the solution (Wood et al. 1990). Organic contaminant sorption in soils however is typically defined by a linear sorption coefficient while adsorption of organic contaminants onto activated carbon is nonlinear.

Batch isotherms are typically used to investigate the relationship between the amount of the contaminant on the carbon and the amount in solution at equilibrium and a constant temperature. This relationship is often modeled using a Freundlich isotherm equation (Weber and DiGiano 1996). This empirical model is extremely useful in summarizing batch isotherm data for a variety of applications. The Freundlich equation and its logarithmic form are shown in Equations (1) and (2).

$$q_e = K_F C^N \qquad (1)$$

$$\log q_e = \log K_F + N \log C \qquad (2)$$

Where: q_e (mg/g) is the mass of solute per mass of adsorbent;
K_F (L/g) is a sorption coefficient;
N is the coefficient related to linearity; and
C (mg/L) is the concentration of solute in solution at equilibrium.

While the relationship is empirical, the K_f term is an indicator of adsorption capacity at a specific solution-phase concentration, and is therefore referred to as a specific capacity (Weber

and DiGiano 1996). A higher value of K_F means a higher specific adsorption capacity. The N term indicates the linearity of the isotherm with an N value of 1 indicating a linear isotherm. The Freundlich parameters can be used to compare adsorption capacity for different compounds or the same compound under different conditions. These parameters can also be used for estimating carbon capacity in continuous flow carbon columns (Weber 1972).

Activated carbon columns (carbon beds) are a common way of treating contaminated water and offer some advantages over batch treatment operations. The most significant advantage is that the column is continuously in contact with fresh solution. The carbon column represents a non-equilibrium condition in which the active zone of adsorption (also called the primary adsorption zone or just adsorption zone) continually moves down the column until the carbon is completely spent and equilibrium is achieved. As the adsorption zone moves through the column, more and more solute tends to escape and breakthrough of the contaminant occurs. The shape of the breakthrough curve can be influenced by a variety of factors including flow rate.

The overall goal of this research was to investigate the ability of activated carbon to remove chlorinated compounds such as PCE from alcohol solutions so that the alcohol solution could be reused in the cosolvent-flooding process. The focus of the laboratory experiments was to determine the effect of alcohol concentration on the adsorption of PCE to activated carbon in batch and column studies, while the field test evaluated the technical and economical feasibility of this approach.

Materials and Methods

The activated carbon used in the laboratory studies was Filtrasorb-400 which is a granular

activated carbon manufactured by Calgon Corporation. The granular activated carbon used in the field application was ARTCORP D16, purchased from Advanced Recovery Technologies Corporation. Their supplier was Barneby and Sutcliffe, Corporation. The physical properties, as provided by the suppliers, are listed in Table 1. A smaller particle size was used for the laboratory studies because of the small carbon columns used. This size difference and the fact that laboratory carbon was washed to remove fines were the only major differences between the laboratory and field carbon.

Laboratory Batch Studies

The activated carbon was placed in a # 40 sieve (0.42 mm mesh size) and washed with distilled water to remove fines. It was dried at 110°C for 24 hours and stored in a dessicator until used in the batch isotherm studies. Chemicals included PCE (99.9%), TCE (99.8%), IPA (100%)(Mallinckrodt Baker Inc.), ethanol (dehydrated-200 proof, McCormick Distilling Co.) and methanol (99.8%, EM Industries Inc.) Distilled water was produced by a Corning Mega-Pure™ System.

Solutions of various alcohol/chlorinated solvent/water mixtures were made up 24 hours prior to use to ensure that the PCE was thoroughly dissolved. Batch isotherm experiments with constant initial solution concentrations were conducted using 60 mL crimp-cap bottles. An exact but different amount of activated carbon was placed in each of five bottles, filled with solution, and crimp-capped with a Teflon-coated septum. One duplicate bottle was also run. Two blanks containing solution only were used to correct for losses if any occurred. A sample was taken of the initial solution and the concentration was determined using a gas chromatograph with flame ionization detector (GC/FID), a DB-624 column (J&W Scientific) and a headspace automated

sampler. The eight bottles were placed on a rotary shaker (6 revolutions/min) in the dark for approximately 3 weeks. A preliminary study of the shaking time needed to reach equilibrium showed that this was more than a sufficient time to reach equilibrium. The ambient temperature was (21 ± 1.5)°C. After mixing, the contents were allowed to separate for a minimum of 5 h and samples of the aqueous phase were measured using GC/FID.

A range of alcohol and solute concentrations was used in the isotherm studies to simulate a range of possible scenarios in the field. The variables of interest in the study were alcohol (IPA or ethanol) and chlorinated compound (PCE and TCE) concentrations. The IPA concentrations used were 0, 15, 30 and 60 % (v/v), and ethanol concentrations used were 30, 50 and 80% (v/v). The PCE or TCE concentrations varied depending on the experiment. The maximum concentrations used were slightly less than the solubility in the respective alcohol solution. Solubility information was obtained from Hayden et al. (1999). A summary of the batch isotherm experiments is shown in Table 2. The alcohol concentration, number of isotherms run and the initial solute concentration for each isotherm are shown.

Column studies

Column experiments were performed to evaluate a flow-through system for adsorbing PCE from alcohol solutions. Two different IPA concentrations (30 and 60 %, v/v) and three different PCE concentrations were used. Ten cm glass columns with an internal diameter of 3.1 cm, aluminum end caps, Viton O-rings, and stainless steel Swagelok fittings were used. One cm of the column was left carbon free to reduce end effects. The effective activated bed length in the column was 8 cm which represented a bed to diameter ratio of 2.58. The column parts were tested for PCE

adsorption and the results showed that the column did not adsorb measurable amounts of PCE. Influent solution was stored in a glass reservoir with a floating cap to prevent losses and was supplied by a peristaltic pump to the column. A three-way stainless steel valve was installed at the column inlet for sampling influent concentrations.

The activated carbon as received from the supplier was water-sieved with distilled water to remove fines and soaked for at least 48 hours in order to dispel the air trapped in the internal pores of the carbon. The soaked activated carbon was packed into a glass column under distilled water and then flushed in an upward direction. Column tests were conducted at an ambient temperature of (21 ± 1.5)°C.

The volume of the influent solution needed for a column test was estimated based on the amount of activated carbon packed in the column bed and the adsorption capacity (K_f) of the activated carbon determined in the batch isotherm studies. Effluent and influent samples were taken with a glass syringe, placed in crimp cap headspace vials, and stored in the refrigerator for analysis. The column tests were terminated when the effluent concentration was consistently equal to or greater than 90% the column influent concentration. A summary of the column parameters is shown in Table 3. Superficial velocities were considerably lower than those used in the field because of the small column size, however, the empty bed contact time was kept in a similar range to field values.

Field Study

The use of cosolvent flushing to enhance dissolution of dense nonaqueous phase liquid (DNAPL) contamination was evaluated in an isolated test cell at the Dover National Test Site, located at Dover Air Force Base in Dover, Delaware. The DNAPL source zone, established within the test cell through a controlled release of 92 L of PCE, was flushed with an ethanol solution for approximately 40 days. The alcohol greatly enhanced PCE solubility and thus the removal of the PCE from the subsurface. Details of this study are presented in Brooks (2000).

Alcohol solution extracted from the test cell was treated with activated-carbon and reused in the cosolvent flood. The flood zone within the test cell was separated into upper and lower zones using packers in the injection and extraction wells. Effluent from each zone was stored in separate tanks, and then treated in batches as needed for continual operation of the alcohol flood. The upper-zone fluid was recycled by pumping each batch through two activated carbon drums in series. The batch volumes ranged from 600 L to 1800 L and a summary of treatment parameters is shown in Table 4.

High alcohol concentrations were targeted to the lower zone. A total of 39 batches were treated for lower-zone recycling. Twenty-nine of which were treated by using two or three activated carbon drums in series. The remaining 10 were treated by air stripping and activated carbon (not discussed in this paper). The batch volumes for lower-zone treatment by activated carbon alone ranged from 200 L to 1800 L. The carbon drums contained approximately 79 kg of packed activated carbon. The recycled alcohol solution was augmented with new 95% ethanol solution as needed to maintain the ethanol content in the influent at approximately 70%. A target ethanol content of 70% was used to maintain a large PCE dissolution capacity in the solution while

facilitating cosolvent recycling by minimizing the need to augment treated effluent with the fresh 95% ethanol solution. A summary of the treatment parameters is shown in Table 4.

During treatment, one to three sets of influent and effluent samples were collected from each carbon drum used. Samples were analyzed in the field using a field SRI GC (8610B GC with an auto sampler), to determine real-time information for operational decisions. Influent and effluent PCE concentrations from each drum were monitored, and drums were removed from service once the effluent PCE concentration equaled the influent PCE concentration. Samples were also refrigerated onsite, and later shipped overnight in coolers to the University of Florida for ethanol and PCE analysis. Analytical results from the laboratory are considered more accurate than the field data and therefore are reported here.

Analytical Methods

All samples taken from the laboratory batch and column experiments were measured using a gas chromatograph (GC), with a 30-meter DB-624 glass capillary column (J&W Scientific) and a flame ionization detector (FID) or a 75-meter DB-VRX glass capillary column (J&W Scientific) and a photo ionization detector (PID). An automated headspace sampler was used in conjunction with the GC for all sample analysis. Samples sent to the laboratory from the Dover site were analyzed for ethanol using a GC with a DB-624 capillary column (J&W Scientific) and an FID. Samples were analyzed for PCE by a similar GC/FID method, as well as liquid chromatography using a PAH C18 packed column (Supelco), UV detection, and a methanol (70%) and HPLC grade water (30%) mixture as the mobile phase. Calibration curves from multiple stock solutions were run daily with check standards run after every ten samples. The

maximum holding time for samples in the refrigerator was 2 days for isotherm studies, 3 days for column studies, and 40-70 days for field studies.

Results and Discussion

Batch Studies

Batch isotherm results are shown in Figure 1 for IPA and Figure 2 for ethanol and have been linearized on a log-log scale for ease of comparison. Least square regression lines are also shown on the figure. The Freundlich coefficients (K_f and N), and R^2 values for these lines are summarized in Table 5. The high R^2 values and linear fits shown in Figures 1 and 2 justify the use of the Freundlich isotherm for describing the alcohol/PCE/activated carbon systems. Isotherms conducted using the same solute and alcohol solutions (outlined in Table 2) have been combined in Figure 1. Statistical analysis of isotherm results showed no difference between different initial solute concentrations or carbon dose for the same solute and solvent cases ($p=0.05$). Thus these have been combined on Figure 1 and an overall regression analysis performed. It should be noted that the adsorption capacity (K_f) is the y-intercept on a log-log plot of q_e versus C_e and thus it can easily be seen on Figures 1 and 2 that the specific adsorption capacity decreases with increasing alcohol concentration. This makes sense based on the increasing solubility of the solute with increasing alcohol concentration. The solute has a greater affinity for the solvent and therefore less affinity for the carbon. It is interesting to note that the 0% alcohol isotherm has a K_f value that is approximately an order of magnitude larger than even the 15% IPA case indicating that even a low alcohol concentration can dramatically affect adsorption behavior.

Only one isotherm with TCE and IPA was conducted and the results are shown in Figure 1. The solubility of TCE in water is approximately 7 times that of PCE in water. Hayden et al. (1999) presented ternary diagrams for TCE in IPA and ethanol and these showed larger single-phase regions indicating greater miscibility of TCE in IPA and ethanol than PCE. This is also reflected in the lower K_f value for TCE at 30% IPA than for PCE at the same alcohol concentration indicating the reduced TCE affinity for the carbon. Although only one TCE isotherm was run, it is likely that a similar trend would be exhibited for TCE at higher alcohol concentrations.

Figure 3 shows the relationship between the Freundlich parameters (Table 5) and the alcohol concentration (% v/v). There is a very good correlation between the log K_f and the alcohol concentration. A least square regression analysis has been made and the equations and R^2 values are also shown on the figure. In addition to showing that as the alcohol concentration increases, K_f decreases, these results also show a similar slope between the ethanol and IPA results. The difference is in the y-intercept and this means that IPA has a greater effect for reducing K_f (solute adsorption capacity) than ethanol for the same alcohol concentration. This also follows the solubility results of Hayden et al. (1999) that showed IPA had a greater effect on PCE and TCE solubility than ethanol.

On a log-log plot of q_e versus C_e, N represents the slope. At alcohol concentrations of 30% and greater, the slope of the isotherms was generally constant at around 0.5. This is shown on Figure 3. At 0% alcohol concentrations, an N value of 0.269 was obtained. This is expected based on the high affinity of the solute for the carbon and the solute incompatibility with the water. At 15% IPA concentration, however, there is a large increase in N (N=0.757). The reason for this is

unclear but may suggest more complex cosolvency behavior than at higher alcohol concentrations.

The batch isotherms provide a quick method for comparing adsorption equilibria for different compounds at different alcohol concentrations. These results were used to estimate the parameters for the field study. For example, at an alcohol concentration of 70% ethanol, a log K_f value would be 0.4 and an N value of 0.5 could be used. The carbon capacity for a PCE concentration of 500 mg/L would be 54.8 mg/g or 110 mg/g for a PCE concentration of 2000 mg/L. Thus the batch results can be used to predict the amount of carbon needed for treating solutions in carbon beds.

Column Experiments

Column experiments were conducted using 30% and 60% IPA solutions. These were used to further evaluate the effect of alcohol on the carbon adsorption of PCE in a carbon column bed, and for guidance in the operation of a larger-scale system. The breakthrough curves for these experiments are shown in Figure 4. The normalized concentration is plotted as a function of the logarithm of the cumulative influent volume per gram of carbon in the column. The results for the two 60% IPA columns show a comparison between different flow rates. The breakthrough curve conducted at the lower flow rate has a steeper slope. This is expected because at lower flow rates, the PCE has more time to diffuse into the carbon before it is swept further through the column. This results in a shorter active zone of adsorption and is reflected in steeper breakthrough curve. The results for the 30% IPA columns reflect the much lower PCE concentrations than in the 60% case and the longer time to breakthrough.

The length of the primary adsorption zones was calculated from the breakthrough curves using the method described in Weber (1972) and are shown on Table 6. The primary adsorption zone is affected by the concentration selected for the breakpoint, C_b. Breakpoint is the point where the effluent concentration reaches some designated concentration. For a higher C_b there is a shorter the adsorption zone, and there is a greater alcohol recovery capacity (defined as the volume of alcohol solution treated per carbon mass) for a single bed adsorber.

The results in Table 6 show that the recovery capacity increases and adsorption zone decreases with decreasing flow rate and decreasing PCE concentration. The alcohol recovery capacities for the 60% IPA columns tend to be quite low indicating that at high alcohol and PCE concentrations, activated carbon may not be a very economical means of recovering the alcohol solution. Other methods such as air stripping may be useful. However at lower PCE concentrations, activated carbon provides a high recovery capacity which makes it an easy and economical means of recovering the alcohol solutions, especially when columns are run in series and are allowed to reach exhaustion.

The amount of PCE adsorbed per gram of carbon in the column at the exhaust point is also shown in Table 6 and compared to q_e from the isotherm studies as a percent of saturation. The percent of saturation is the amount of PCE adsorbed in the column divided by q_e times 100. All percent saturations were lower than 100% indicating that the columns were not at complete equilibrium with the influent concentration when the experiments were terminated. The experiments were terminated at effluent concentrations of 90% those of the influent because of the long time necessary to reach complete breakthrough. This resulted in saturation values less

than 100%. However, the column results did compare fairly well to the batch results. The results from these studies suggested that for a field application, carbon beds in series should be used.

Field Studies

The technical feasibility of using activated carbon for treating the cosolvent flooding solutions was shown in the field. Examples of carbon drum performance for two drums are shown in Figures 5 and 6 and are plotted as a function of the cumulative treated volume per carbon mass. Figure 5 shows influent and effluent PCE concentrations for the first carbon drum used in lower-zone treatment. This is the first drum in a series of two to three drums. The cumulative influent and effluent PCE volumes adsorbed by the carbon in the drum is also shown. Approximately 6 L of PCE (or 124 mg PCE/g carbon) were absorbed in the drum before breakthrough occurred. The amount of PCE adsorbed on the carbon in the drum compared extremely well with the carbon capacity calculated from the batch isotherm results presented earlier. For example, for this drum the average ethanol concentration of the influent was 65%. From Figure 2 at this ethanol concentration, N is equal to 0.5, and K_f is 3.29 (solving $\log K_f = -0.026(65)+2.18$). The maximum influent concentration for this drum was approximately 1400 mg/L. Using Equation 1 and the values just given, q_e equals 123 mg/g. The amount loaded based on the actual breakthrough curve was 124 mg/g. These results show the similar PCE adsorption capability of the laboratory and field carbon even though they represented different environmental and operating conditions.

Figure 6 shows another example of a drum used in lower-zone treatment. In this case, there was some variation in the influent concentration shown on the figure between 200 and 250 L/Kg on the x-axis. The influent concentration ranged from 500 mg/L to 1500 mg/L and then went from around 1400 mg/L PCE to near 600 mg/L at the end of the run. The PCE concentration drop in the influent resulted in desorption of PCE from the activated carbon. This resulted in an effluent concentration that exceeded the influent concentration. Again it should be noted that this was the first drum in a series of drums but the column was taken off-line at that point. Desorption of contaminants from carbon filters in not uncommon and can be a problem when there is considerable variation in the influent concentration as there were in the field (Table 5). The variation in influent concentrations was related to some aspects of the cosolvent flooding demonstration and therefore difficult to control. However, influent variations such as these generally affect the end of breakthrough process that represents a small fraction of the total PCE mass adsorbed. If columns are run in series and the effluent from each drum is monitored, this should not affect the overall performance of the carbon treatment.

Field experiments showed a longer time to reach complete breakthrough as compared to laboratory experiments. This was a result of the higher flow rates used in the field. This could result in less efficient treatment of the influent solution if single adsorbers are used since the column would need to be taken off-line at some predetermined breakpoint concentration. When running columns in series it is generally possible to run the first column to complete exhaustion, thus reaching equilibrium, prior to taking it off-line. This was an important reason for running columns in series in the field and resulted in a very good system performance. The concentration of PCE in the recycled ethanol solution typically ranged from 1 to 3 mg/L. However, the field

site was a permitted release facility, and the PCE concentrations in the recycled ethanol solutions were not a regulated parameter.

Cost Analysis

The economic feasibility of reusing the treated alcohol solutions in the flooding process was also demonstrated. Table 7 shows the cost comparison between using fresh alcohol solvent in the flood and reusing the alcohol solution treated with activated carbon. Approximately $9000 or a 13% reduction in cost was achieved by reusing the solvent. This is significant and it is likely that at an actual site (not a research demonstration site) this reduction would be even greater. The main reason would be the reduction in sampling and analysis costs that would occur had this not been a research site. A large number of samples were analyzed to determine the actual breakthrough curves for the carbon drums and this intensity of sampling would not be necessary to ensure good treatment performance at an actual site. A sampling reduction of half would be a realistic number to ensure an understanding of the treatment process and this would decrease the total cost by 22% as opposed to 13%. At high concentrations of PCE, typically observed during the early phase of a cosolvent flood, other technologies such as air stripping or macro-porous molecular polymer may be more cost effective as a pre-treatment to the activated carbon (Jawitz et al. 2000).

Conclusions

Activated carbon was used to remove PCE from various alcohol solutions in both laboratory and field studies. The results showed that activated carbon can be used to recover and reuse alcohol solutions from alcohol flooding remediation schemes. The specific adsorption capacity, K_f, was found to decrease with increasing alcohol concentration. This means that for the same

concentration of PCE, the amount that will be adsorbed onto the carbon will decrease with increasing alcohol concentrations. However, with increasing alcohol concentrations much higher PCE concentrations are possible and therefore the total loading of PCE onto the carbon may increase. The Freundlich model provided a good fit to the isotherm data and the Freundlich K_f correlated well with alcohol concentration for each alcohol. The Freundlich N term was found to be fairly similar at alcohol concentrations of 30% or greater. Predictions of carbon capacity based on the Freundlich model reasonably matched measured carbon capacity at the field site suggesting that these results could be used to estimate PCE adsorption capacity for other field applications. A cost comparison showed that activated carbon treatment of flooding solutions is cost effective. Overall, this study demonstrated the technical and economic feasibility of using activated carbon for removing PCE from alcohol solutions.

Acknowledgments

The authors acknowledge the help of Jaehyun Cho, Clayton Clark, Lane Evans, Kirk Hatfield, Heonki Kim, Irene Poyer, Suresh Rao and William Wise from the University of Florida; Tim McHale, Mark Hogan, and Rob Young from Mantech Environmental Research Services Corporation; Carl Enfield, John Hoggatt, Lynn Wood from the U.S. Environmental Protection Agency; and Major Paul Devane from Armstrong Laboratories, Tyndall AFB. The laboratory portion was funded by the U.S. DOE Federal Energy Technology Center (FETC), Morgantown, WV, contract AR21-96MC33083; the field portion was funded by the Strategic Environmental Research Development Program (SERDP) which is a collaborative effort in the U.S. EPA, U.S. DOE and U.S. DoD. This document has not been subjected to peer review within the funding

agencies, and the conclusions stated here do not necessarily reflect the official views of the agencies nor does this document constitute an official endorsement by the agencies.

References

Brooks, M.C. (2000) *Characterization and Remediation of DNAPL Resulting from a Controlled Release: Field Study and Uncertainty Analysis*, Dept. of Env. Eng. Sci., University of Florida, 147 pgs.

Crittenden, J.C., S. Sanongraj, J.L. Bulloch, D.W. Hand, T.N. Rogers, T.F. Speth, M. Ulmer (1999) Correlation of aqueous-phase adsorption isotherms. *Environ. Sci. Technol.* 33(17): 2926-2933.

Fu, J.K. and R.G. Luthy (1986) Effect of organic solvent on sorption of aromatic solutes onto soils. *J. Environ. Eng.* 112:346-366.

Hayden, N. J., J. Diebold, and G. Noyes (1999) Phase Behavior of Chlorinated Solvent+Water+Alcohol Mixtures with Application to Alcohol Flushing. *J. Chem. Eng. Data* 44(5):1085-1090.

Hazourli, S., G. Bonnecaze, M. Potin-Gauthier (1996) Adsorption and electrosorption of organic compounds on granular activated carbon, Part II – Influence of physicochemical parameters. *Environmental Technology* 17: 1285-1295.

Jawitz, J.W., R.K. Sillan, M. D. Annable, P.S.C. Rao, and K. Warner, (2000) In-situ alcohol flushing of a DNAPL source zone at a dry cleaner site, *Environ. Sci. Technol.*, 34:3722-3729.

Klecka, G.M., S.G. McDaniel, P.S. Wilson, C.L. Carpenter and J.E. Clark (1996) Field evaluation of a granular activated carbon fluid-bed bioreactor for treatment of chlorobenzene in groundwater. *Environmental Progress* 15(2):93-107.

Luehrs, D.C., J.P. Hickey, P.E. Nilsen, K.A. Godbole, and T.N. Rogers (1996) Linear solvation energy relationship of the limiting partition coefficient of organic solutes between water and activated carbon. *Environ. Sci. Technol.* 30(1): 143-152.

Nzengung, V.A., E.A. Voudrias, P. Nkedi-Kizza, J. M. Wampler and C.E. Weaver (1996) Organic cosolvent effects on sorption equilibrium of hydrophobic organic chemicals by organoclays. *Environ. Sci. Technol.* 30:89-96.

Nkedi-Kizza, P., P.S.C. Rao, and A.G. Hornsby (1987) Influence of organic cosolvents on leaching of hydrophobic organic chemicals through soils. *Environ. Sci. Technol.* 21(11): 1107-1111.

Rao, P.S.C., M. D. Annable, R.K. Sillan, D. Dai, K. Hatfield, and W.D. Graham, (1997) Field-scale evaluation of in situ cosolvent flushing for enhanced aquifer remediation, *Water Res. Res.*, 33:2673-2686.

Rao, P.S.C., A.G. Hornsby, D.P. Kilcrease and P. Nkedi-Kizza (1985) Sorption and transport of hydrophobic organic chemicals in aqueous and mixed solvent systems: model development and preliminary evaluation. *J. Environ. Quality* 14(3):376-383.

Sillan, R.K., M.D. Annable, P.S.C. Rao, D. Dai, K. Hatfield, W.D. Graham, A.L. Wood, and C.G. Enfield, (1998) Evaluation of in situ cosolvent flushing dynamics using a network of spatially distributed multilevel samplers, *Water Res. Res.*, 34:2191-2202.

Urano, K., E. Yamamoto, M.Tonegawa and K. Fujie (1991) Adsorption of chlorinated organic compounds on activated carbon from water. *Water Res.* 25(12): 1459-1464.

Weber, W.J. Jr, and DiGiano (1996) *Process Dynamics in Environmental Systems*. John Wiley & Sons, Inc., New York, NY.

Weber W. J. Jr., (1972) *Physicochemical Processes for Water Quality Control*, John Wiley & Sons, Inc., New York, NY.

Wood, A.L., D.C. Bouchard, M.L. Brusseau, and P.S.C. Rao (1990) Cosolvent effects on sorption and mobility of organic contaminants in soils. *Chemosphere* 21:575-587.

Wujcik, W.J., W.L. Lowe, P.J. Marks and W.E. Sisk (1992) Granular activated carbon pilot treatment studies for explosives removal from contaminated groundwater. *Environmental Progress* 11(3):178-189.

Ying, W.C., E.A. Dietz, G.C. Woehr (1990) Adsorptive capacities of activated carbon for organic constituents of wastewaters. *Environmental Progress* 9(1): 1-9.

Table 1. Summary of activated carbon used in laboratory and field studies.

Property	Laboratory	Field
Surface area (m^2/g)	1050-1200	750-950
Pore volume (ml/g)	0.94	N.A.
Particle density (g/ml)	1.82	N.A.
Uniformity coefficient (Max)	1.9	1.9
Effective size (mm)	0.55 to 0.75	0.8-1.0

N.A. not available from supplier

Table 2. Summary of batch isotherm experiments, solute was PCE except where indicated.

Isotherm	Solute and Initial concentrations (mg/L)	Number Isotherms	Carbon Dose Range (mg)	Shaking Times (d)
0% IPA	65, 77,100, 116	4	2.5-20	1.2, 12, 22, 30
15% IPA	115, 158, 172, 240	4	3.2-122	1.2, 19, 22, 30
30% IPA	326, 752, 950	3	19 –765	1.7, 19, 30
60% IPA	120, 1063, 10526, 99000, 10906, 101120	6	19-13669	1.7, 19, 22, 23, 23, 23
30% IPA	TCE (2503)	1	3.5-630	23
30% ethanol	360	1	3.5-540	23
50% ethanol	6626	1	600-13200	21
80% ethanol	44390	1	1260-13200	21
80% ethanol	5383	1	1260-13200	21

Table 3 Summary of the column experimental parameters.

IPA (v/v %)	PCE influent concentration (mg/L)	Flow rate (ml/min)	Superficial velocity (cm/min)	Empty bed contact time (min)
30	330	2.4	0.33	24
30	640	2.4	0.33	24
60	100000	1	0.13	60
60	100000	4	0.51	15

Table 4. Summary of the means and standard deviations (SD) of field experimental parameters.

Extraction zone treated	Flow rate (L/min)	Superficial velocity (cm/min)	Empty bed contact time (min)
Upper	Mean = 8, SD = 4	Mean = 3, SD = 1	Mean = 17, SD = 8.6
Lower	Mean = 9, SD = 6	Mean = 3, SD = 2	Mean = 23, SD = 15

Table 5. Summary of Freundlich model results.

Isotherm	K_f (L/g)	N	R^2
0% alcohol and PCE	168	0.269	0.714
15% IPA and PCE	18.0	0.757	0.964
30% IPA and PCE	7.80	0.629	0.990
60% IPA and PCE	2.23	0.506	0.992
30% Ethanol and PCE	20.8	0.579	0.995
50% Ethanol and PCE	8.76	0.451	0.992
80% Ethanol and PCE	1.39	0.511	0.940
30% IPA and TCE	2.52	0.654	0.967

Table 6. Summary of column results.

Column % IPA	Flow rate (ml/min)	Influent C (mg/L)	Break-point, C_b (mg/L)	Adsorption zone (cm)	Recovery capacity at C_b (L/Kg)	PCE adsorbed (mg/g)	% of saturation
60%	4	100000	1000	14	0.18	608	80
60%	1	100000	1000	4.9	1.1	680	90
30%	2.4	640	10	8	20	370	81
30%	2.4	330	10	4.6	60	258	86

Table 7. Cost comparison between no recycling and recycling based on the field demonstration.

Description	Unit Cost ($)	No. of Units	Subtotal
No Recycling			
Ethanol (95% Solution) (L)	0.59	73,000	$43,100
Flushing solution disposal (L)	0.26	95,000	$24,700
		Total Cost No Recycling	**$67,800**
Carbon Adsorption			
Ethanol (95% Solution) (L)	0.59	42,000	$24,800
Flushing solution disposal (L)	0.26	57,000	$14,800
Carbon Drums (per drum)	580	7	$4,100
Carbon Disposal (per drum)	185	7	$1,300
Pumps, tanks, fittings for batch treatment (LS)	$2,000	1	$2,000
Additional Samples (per sample)	$100	120	$12,000
		Total Cost with Carbon Adsorption	**$59,000**

List of Figures

Figure 1

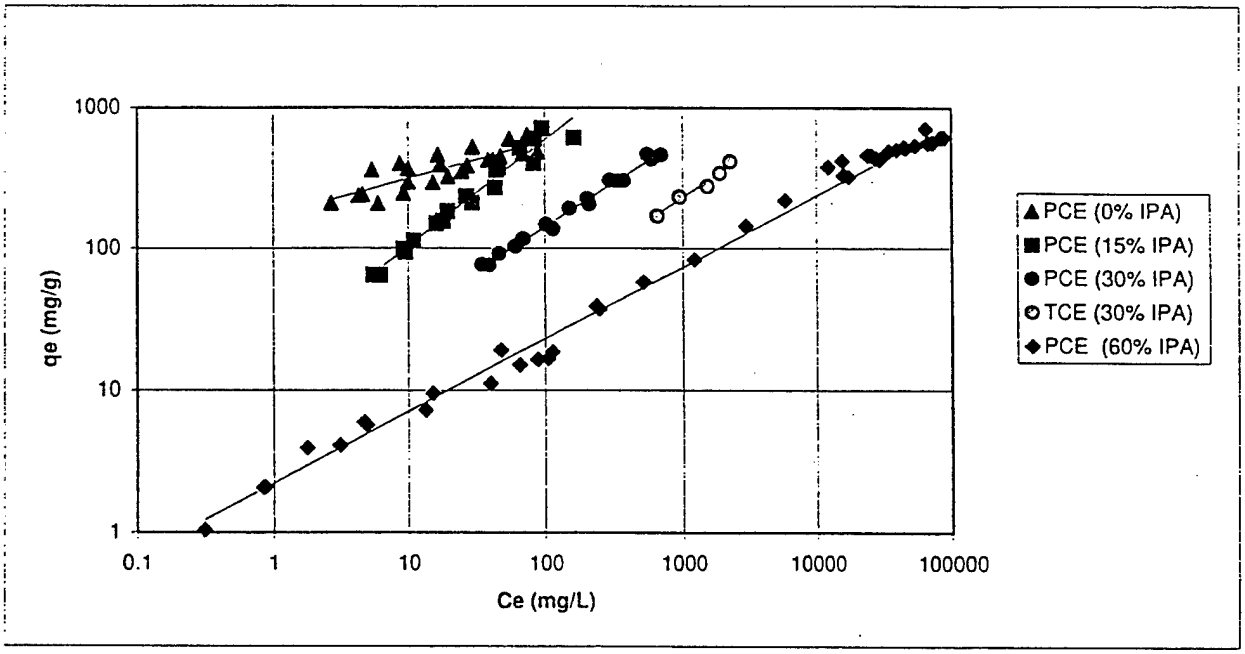

Figure 2

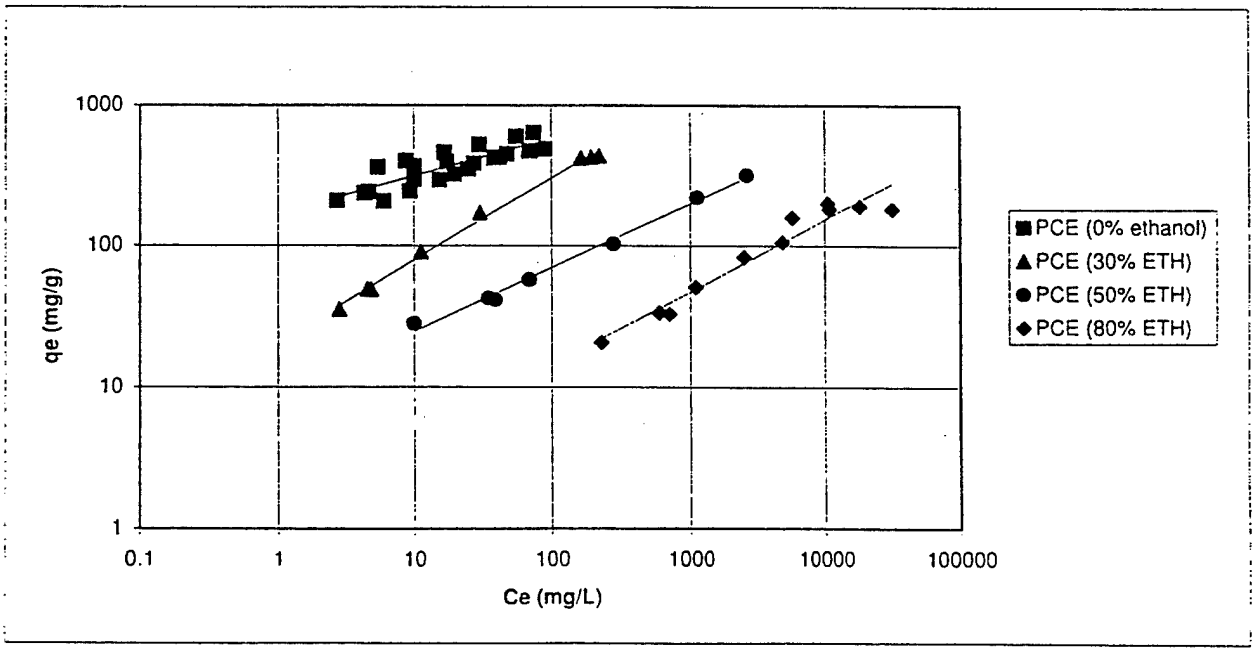

Figure 3

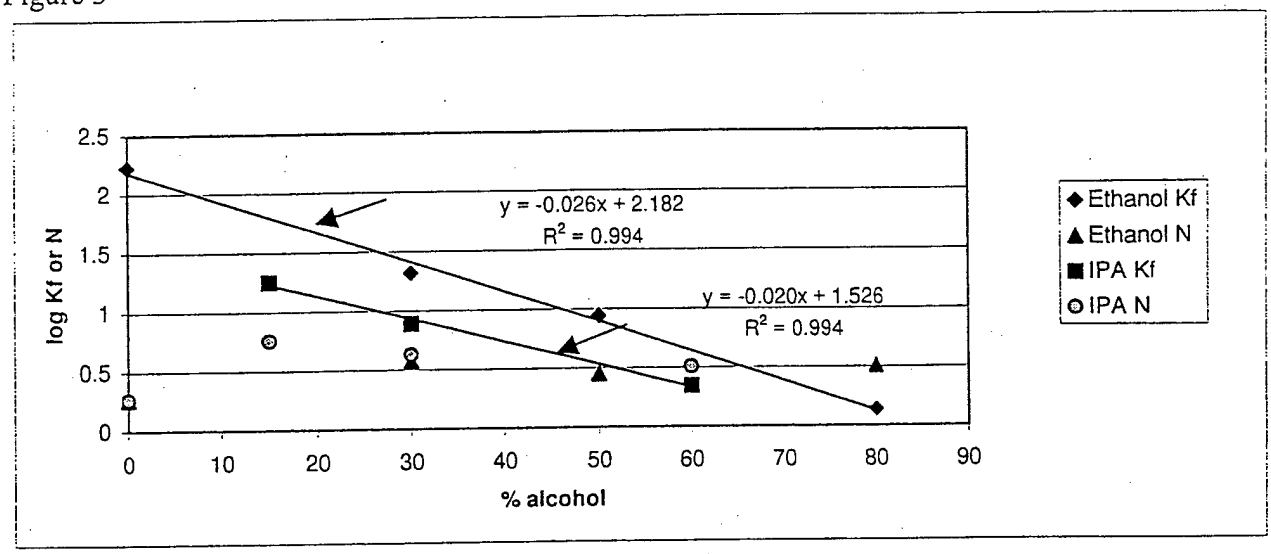

Figure 4

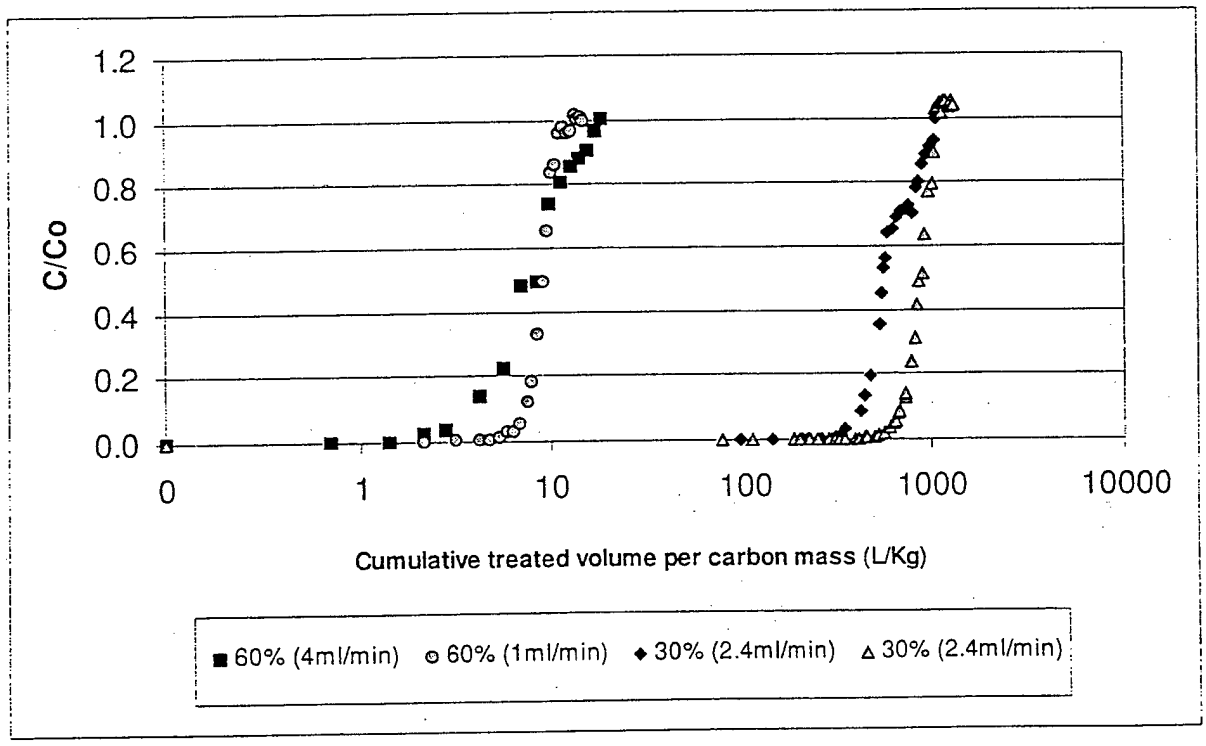

Figure 5

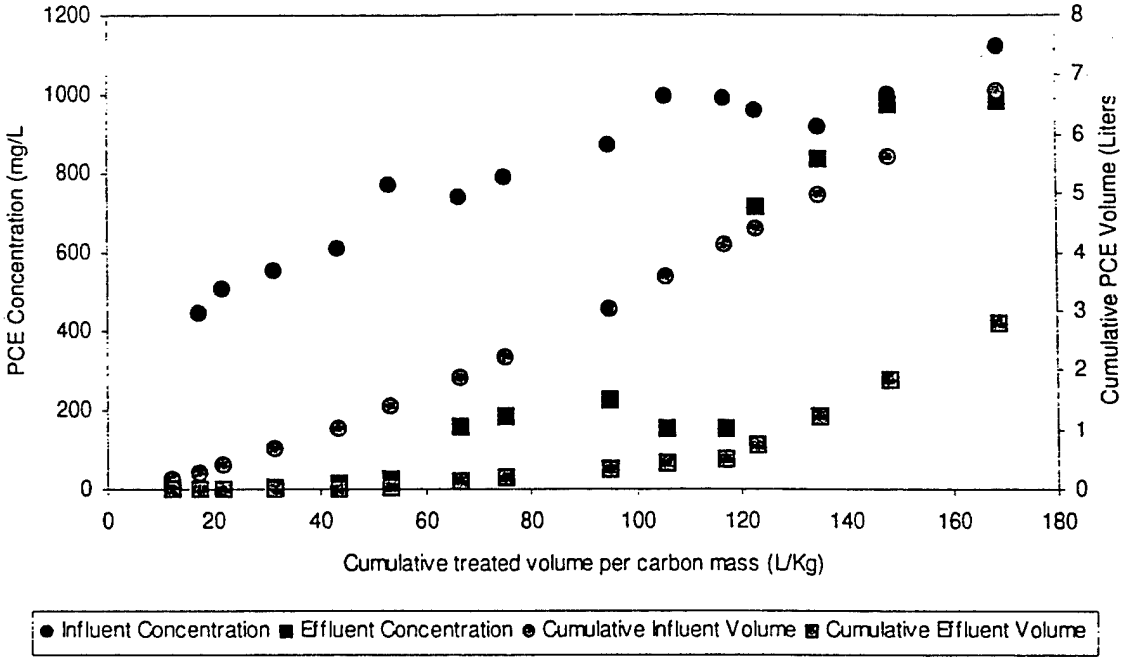

Figure 6

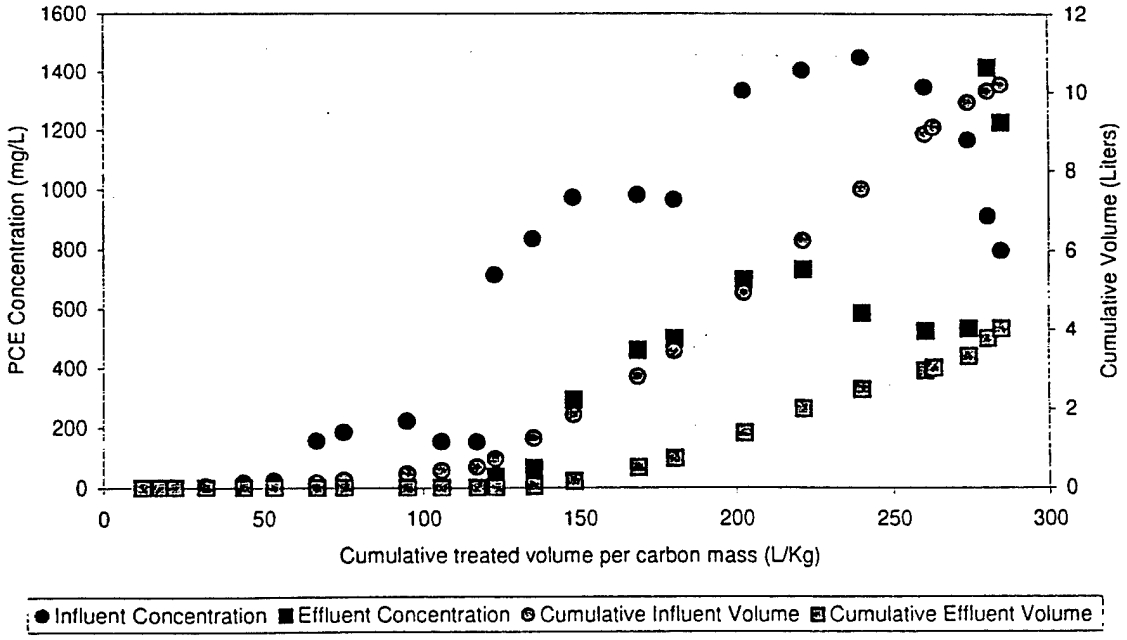

WATER RESOURCES RESEARCH, VOL. 36, NO. 4, PAGES 999–1012, APRIL 2000

Estimation of spatially variable residual nonaqueous phase liquid saturations in nonuniform flow fields using partitioning tracer data

Andrew I. James, Wendy D. Graham, Kirk Hatfield, P. S. C. Rao,[1] and Michael D. Annable

Interdisciplinary Program in Hydrologic Sciences, University of Florida, Gainesville

Abstract. Estimates of spatially variable residual NAPL saturations S_N are obtained in heterogeneous porous media using first temporal moments of breakthrough curves (BTCs) obtained from multilevel samplers during in situ partitioning tracer tests. An approach is adopted in which the distribution of the log NAPL/water volumetric ratio ($Y = \ln [S_N/(1 - S_N)]$) and log hydraulic conductivity ($F = \ln K$) are treated as spatially correlated random fields. A nonlinear Gauss-Newton search technique is used to identify the spatial distribution of Y that minimizes the weighted sum of the deviation of the temporal moment predictions from their measured values and the deviation of the estimate of Y from its prior estimate obtained from the temporal moments of extraction well BTCs. Sensitivities required for the algorithm are obtained using a coupled flow and transport adjoint sensitivity method. In addition to obtaining optimal estimates for the spatial distribution of Y, the method also provides the estimation error covariance. The estimation error covariance can be used to evaluate the information that may be obtained from alternate pumping and monitoring configurations for tracer tests designed to detect NAPL in the subsurface. To this end, we tested the method using two different NAPL distributions (one with a random spatially correlated field and a second that was a block of NAPL) and three different pumping configurations (a double five-spot pattern, an inverted double five-spot pattern, and a line-drive pattern). The results show that measured temporal moments are more sensitive to Y in the double five-spot and inverted double five-spot patterns, and estimates produced in these configurations are slightly superior to those produced in the line-drive pattern.

1. Introduction

Characterization of the volume and spatial distribution of nonaqueous phase liquids (NAPLs) in the subsurface at hazardous waste sites is a problem of tremendous importance. The slow dissolution rates of many NAPLs into groundwater and the highly toxic nature of the contaminants, even at relatively low aqueous concentrations, can lead to serious long-term degradation of groundwater quality. The limited nature of many NAPL spills, where even a few liters of a contaminant can severely impact groundwater quality, requires innovative methods to locate and remediate the source of contamination. To design and implement an appropriate and efficient remediation program requires accurate delineation of the location, extent, and volume of residual NAPL in the subsurface. In the past few years, partitioning tracers have gained acceptance as a means of estimating the volume and/or mass of residual NAPL in the subsurface. A number of authors have shown [*Annable et al.*, 1995, 1998; *Jin et al.*, 1995; *Pope et al.*, 1995] that breakthrough curves (BTCs) of partitioning tracers at extraction wells can be used to obtain an accurate measure of the average saturation and total volume of NAPL present in the volume of aquifer swept by the tracers. Furthermore, BTCs at specific points within the three-dimensional volume of the contaminated aquifer can be obtained by sampling the tracers at specific depths using a network of multilevel samplers (MLSs) [*Sillan et al.*, 1998]. Comparison of the temporal moments of partitioning and nonpartitioning tracer BTCs can be used to deduce areas of high residual NAPL saturation (S_N).

The problem of estimating a spatially distributed parameter such as S_N or saturated hydraulic conductivity (K) in the subsurface based on transport of tracers is the focus of parameter estimation or inverse modeling. There is a large body of work on the problem of inverse modeling in hydrology, most often in the context of estimation of hydraulic conductivity or transmissivity using measurements of piezometric head and/or groundwater fluxes. Additionally, work has been done in estimating the extent of contaminant plumes and groundwater velocities using solute concentration measurements [*Graham and McLaughlin*, 1989a, b, 1991; *Reid and McLaughlin*, 1994].

Our objective here is to develop a method to estimate the spatial distribution of NAPL (saturation or some related quantity) from partitioning tracer BTCs at MLSs. To this end we have extended and refined the technique of *James et al.* [1997], making it more applicable to field experiments. Briefly, *James et al.* [1997] solved directly for temporal moment covariances and cross covariances between temporal moments and retardation, log K, and Darcy flux using a finite difference tech-

[1]Now at School of Civil Engineering, Purdue University, West Lafayette, Indiana.

Copyright 2000 by the American Geophysical Union.

Paper number 2000WR900004.
0043-1397/00/2000WR900004$09.00

nique. These covariances were incorporated into a Bayesian estimation scheme (which is equivalent to a steady state Kalman filtering algorithm or a cokriging algorithm assuming a known unconditional mean field). In this scheme the estimator is a linear function of the measurements [*McLaughlin and Townley*, 1996] resulting in a conditioning algorithm requiring only a single step. Additionally, *James et al.* [1997] assumed that the spatial covariance function of log K was isotropic, that the mean flow field was uniform, and that the Darcy flux covariances could be approximated by infinite-domain results.

We have extended the technique in several areas: First, we use a coupled adjoint sensitivity technique to determine sensitivities of temporal moments to log K and the logarithm of the NAPL/water volumetric ratio (Y). These sensitivities are then used to determine the temporal moment covariances and cross covariances between temporal moments and Y and log K. Use of an adjoint sensitivity technique to determine the covariances significantly reduces the computational overhead [*Sun and Yeh*, 1990, 1992; *Sun*, 1994]. Second, we compute the flow-related sensitivities and covariances numerically [*James and Graham*, 1999], which allows us to examine the effects of nonuniform flow fields. Thus we can now accurately model injection and extraction wells and easily incorporate statistically anisotropic K fields (where the spatial correlation length can depend on the orientation of the separation vector). As a result, we can evaluate the performance of alternative tracer test pumping configurations (e.g., line-drive, double five-spot, or inverted double five-spot configurations) and pick the configuration that results in the lowest overall estimation uncertainty. Furthermore, obtaining an estimate of Y prior to cleanup allows modification of the remediation strategy to target areas with higher S_N. Finally, rather than use a linearized estimator, we use an iterative Gauss-Newton minimization technique [*Tarantola and Valette*, 1982; *Tarantola*, 1987] to obtain the estimates.

2. Mathematical Background

2.1. Parameter Estimation

In general, we are interested in estimating a set of parameters $\mathbf{p}$ (in this case, Y and log K) from a set of experimental data, $\mathbf{d}^*$, here the zeroth and first temporal moments, denoted by $m_0(x)$ and $m_1(x)$, determined from measured tracer BTCs. In general, direct measurements of NAPL saturations (or NAPL/water volumetric ratios) and/or hydraulic conductivity are more difficult to obtain and are not typically taken during partitioning tracer tests. Therefore direct measurements of NAPL saturations and hydraulic conductivity are not included here.

From a modeling viewpoint the relation between the set of true parameters $\mathbf{p}$ and the true values of the data $\mathbf{d}$ can be written in the "forward" form

$$\mathbf{d} = \mathcal{F}(\mathbf{p}), \tag{1}$$

where $\mathcal{F}$ is an operator from the space of model parameters M to the space D of all "conceivable" measurements [*Tarantola*, 1987; *McLaughlin and Townley*, 1996]. Equation (1) describes a perfect relationship between the parameters $\mathbf{p}$ and the data $\mathbf{d}$, meaning that using the parameter set $\mathbf{p}$ in the forward model results in the "true" data $\mathbf{d}$. In reality, both measurement error and model error contribute to noise in the data. Thus we write

$$\mathbf{d}^* = \mathcal{F}(\mathbf{p}) + \mathbf{e}, \tag{2}$$

where the asterisk indicates that the measurements contain an unknown amount of noise, written as a vector $\mathbf{e}$. In what follows, we assume that the parameter vector $\mathbf{p}$ is a finite set discrete values rather than a continuous distribution.

To obtain an estimate of the parameter vector, we use a least squares estimator $E(\mathbf{d}, \mathbf{p})$ that incorporates both the weighted sum of the deviation of the measured data from their predicted values and the deviation of the model parameters from their prior estimates $\bar{\mathbf{p}}$ [*Schweppe*, 1973; *Tarantola*, 1987]

$$E(\mathbf{d}, \mathbf{p}) = [\mathbf{d}^* - \mathcal{F}(\hat{\mathbf{p}})]^T \cdot P_{\mathbf{dd}}^{-1} \cdot [\mathbf{d}^* - \mathcal{F}(\hat{\mathbf{p}})] + (\hat{\mathbf{p}} - \bar{\mathbf{p}})^T \cdot P_{\mathbf{pp}}^{-1} \cdot (\hat{\mathbf{p}} - \bar{\mathbf{p}}), \tag{3}$$

where $P_{\mathbf{pp}}$ is the spatial covariance matrix of the parameters, $P_{\mathbf{dd}}$ is the covariance matrix of measurement errors, and the superscript T indicates a transposed quantity. Our problem is to seek a value of the parameter vector $\hat{\mathbf{p}}$ that minimizes E in (3). In the general case, minimization of E is a problem of nonlinear estimation and corresponds to obtaining the maximum a posteriori estimate of the parameters $\hat{\mathbf{p}}$ [*Tarantola*, 1987; *McLaughlin and Townley*, 1996]. As discussed by *McLaughlin and Townley* [1996], this estimation approach does not require that the forward operator $\mathcal{F}$ be linear nor that the a posteriori density function be Gaussian.

Because the forward problem is not linear, an iterative method is required to find the minimum of E. We use an iterative Gauss-Newton scheme where the estimate at the $k+1$ iteration is given by

$$\hat{\mathbf{p}}_{k+1} = \hat{\mathbf{p}}_k + \varepsilon P_{\mathbf{p}_0\mathbf{p}_0} \cdot G_k^T \cdot (P_{\mathbf{d}_0\mathbf{d}_0} + G_k \cdot P_{\mathbf{p}_0\mathbf{p}_0} \cdot G_k^T)^{-1} \cdot \{[\mathbf{d}^* - \mathcal{F}(\hat{\mathbf{p}}_k)] - G_k \cdot (\hat{\mathbf{p}}_k - \bar{\mathbf{p}})\},$$

where G_k is the matrix of sensitivities after the kth iteration with entries $g_{ij} = \partial d_i / \partial p_j$, ε is a step size parameter, and the zero subscripts on $P_{\mathbf{d}_0\mathbf{d}_0}$ and $P_{\mathbf{p}_0\mathbf{p}_0}$ indicate that the initial values of these covariances are used; that is, they are not updated at each step of the minimization process. This formula is equivalent to (23)–(25) of *Tarantola and Valette* [1982].

Once the minimum is found, the posterior covariance matrix for the parameters $\hat{P}_{\mathbf{pp}}$ can be found using

$$\hat{P}_{\mathbf{pp}} = P_{\mathbf{p}_0\mathbf{p}_0} - P_{\mathbf{p}_0\mathbf{p}_0} \cdot G_\infty^T \cdot (P_{\mathbf{d}_0\mathbf{d}_0} + G_\infty \cdot P_{\mathbf{p}_0\mathbf{p}_0} \cdot G_\infty^T)^{-1} \cdot G_\infty \cdot P_{\mathbf{p}_0\mathbf{p}_0}, \tag{5}$$

where G_∞ is the approximation to the limiting value of the sensitivity matrix [*Tarantola and Valette*, 1982; *Tarantola*, 1987]. We use the value of G obtained from the last iteration of the minimization process.

Thus, given an assumed prior covariance matrix $P_{\mathbf{p}_0\mathbf{p}_0}$ for the parameters, a measurement error covariance matrix $P_{\mathbf{d}_0\mathbf{d}_0}$, a set of data $\mathbf{d}^*$, and a prior estimate of the parameters $\bar{\mathbf{p}}$, we only require the sensitivity matrix at the kth step G_k to obtain an estimate $\hat{\mathbf{p}}_{k+1}$. There are a number of ways to obtain the sensitivity matrix, including direct perturbation of parameters in a forward model, differentiating the governing flow/transport equations with respect to the parameters and solving directly for the sensitivities, or an adjoint sensitivity method. For computational efficiency we use the adjoint sensitivity method.

2.2. Governing Equations

We start with the governing equations for flow and transport equations in a three-dimensional domain Ω. We use the mixed form of the flow equation:

$$\mathbf{q}(x) + K(x) \cdot \nabla h(x) = 0, \tag{6}$$

$$\nabla \cdot \mathbf{q}(x) = Q \qquad x \in \Omega, \tag{7}$$

$$h(x) = h_D \qquad x \in \Gamma_D^{\text{flow}}, \tag{8}$$

$$\mathbf{q}(x) \cdot \mathbf{n} = \mathbf{q}_N \qquad x \in \Gamma_N^{\text{flow}}, \tag{9}$$

where $\mathbf{q}$ is the Darcy flux, h is the piezometric head, K is the hydraulic conductivity (or more precisely, the relative hydraulic conductivity with respect to water saturation, which we assume here to be a scalar quantity), and Q is a source (if >0) or sink term (if <0). We assume that the boundary Γ can be decomposed into Dirichlet (Γ_D) and Neumann (Γ_N) parts such that $\Gamma = \Gamma_D \cup \Gamma_N$. We further assume that the boundary can be decomposed separately for the flow and transport problems; thus Γ_D^{flow} represents a Dirichlet boundary for the flow problem, h_D is the value on the Dirichlet boundaries, $\mathbf{q}_N$ is the flux on the Neumann boundaries, and $\mathbf{n}$ is the outward unit normal on Γ.

For transport we use the advection-dispersion equation for the temporal moments of a tracer BTC [*Harvey and Gorelick*, 1995]:

$$\nabla \cdot [\theta \mathsf{D}(x) \cdot \nabla m_n(x)] - \nabla \cdot [\mathbf{q}(x) m_n(x)] + S_{m_n} = -n\theta R(x) m_{n-1}(x) \qquad x \in \Omega, \tag{10}$$

$$m_n(x) = m_{n_D} \qquad x \in \Gamma_D^{\text{trans}}, \tag{11}$$

$$\frac{\partial m_n(x)}{\partial \mathbf{n}} = 0 \qquad x \in \Gamma_N^{\text{trans}}, \tag{12}$$

where $m_n(x)$ is the nth temporal moment of the solute, $\mathbf{q}$ is the Darcy flux, θ is the volumetric water content, D is the dispersion coefficient, S_{m_n} is a source (or sink) term for the tracer, $R(x)$ is the retardation factor. We use the temporal moment equations rather than the advection-dispersion equation for concentration of a solute $c(x, t)$ since the temporal moment equations are steady state and do not require time stepping to solve numerically. A point sink term can be written as

$$S_{m_n} = m_n(x) Q \delta(x - x_j),$$

where Q is the strength of the sink (from (7)), x_j is the location of the sink, and $\delta(x - x_j)$ is the Dirac delta function at the point x_j. Since there may be several sources and sinks throughout the domain, we adopt the following notation

$$S_{m_n}^{\text{ext}} = \sum_{j=1}^{M} m_{n_j}(x) Q_j \delta(x - x_j)$$

to denote M sinks. The form of a point source term depends on the solute release history. Here we assume that solute at a fixed concentration C_0 is released at a point x_i for a fixed amount of time t_0:

$$c(x_i, t) = \begin{cases} C_0 & 0 < t \le t_0 \\ 0 & t > t_0. \end{cases}$$

For the nth moment this transforms to

$$S_{m_n}^{\text{inj}} = Q \frac{t_0^{n+1} C_0}{n+1} \delta(x - x_i),$$

where Q is the strength of the source. For N sources we have

$$S_{m_n}^{\text{inj}} = \sum_{i=1}^{N} Q_i \frac{t_0^{n+1} C_0}{n+1} \delta(x - x_i).$$

For consistency with the flow equation we introduce a mixed form of (10) by introducing the variable $\mathbf{z}$:

$$\mathbf{z}_n(x) = -\theta \mathsf{D}(x) \cdot \nabla m_n(x). \tag{13}$$

Our system of equations for the temporal moments then becomes

$$\mathbf{z}_n(x) + \theta \mathsf{D}(x) \cdot \nabla m_n(x) = 0, \tag{14}$$

$$\nabla \cdot \mathbf{z}_n(x) + \nabla \cdot [\mathbf{q}(x) m_n(x)] - S_{m_n}^{\text{inj}} - S_{m_n}^{\text{ext}} = n\theta R(x) m_{n-1}(x) \qquad x \in \Omega, \tag{15}$$

$$m_n(x) = m_{n_D} \qquad x \in \Gamma_D^{\text{trans}}, \tag{16}$$

$$\mathbf{z}_n(x) \cdot \mathbf{n} = 0 \qquad x \in \Gamma_N^{\text{trans}}. \tag{17}$$

Note that this system of equations only holds for a pulse input of finite duration, since otherwise the moments would be infinite.

Assuming equilibrium, the retardation factor of a partitioning tracer is a function of S_N and the NAPL-water partitioning coefficient K_N [*Pope et al.*, 1995; *Jin et al.*, 1995]

$$R = 1 + \frac{K_N S_N}{1 - S_N}. \tag{18}$$

As mentioned in section 1, in our procedure we estimate the log NAPL/water volumetric ratio Y, which is defined as

$$Y = \ln\left(\frac{S_N}{1 - S_N}\right).$$

We choose to estimate Y rather than S_N for several reasons. First, we want to avoid generating negative estimates for S_N. Second, we want to avoid generating an estimate of $S_N > 1$. By estimating Y, all values of exp (Y) will fall in the range $0 < e^Y < \infty$, and all values of S_N generated from Y will fall between zero and one. Last, most applications of Gaussian-based estimation algorithms assume that the prior error density is Gaussian [*McLaughlin and Townley*, 1996]. We cannot reasonably assume that the prior errors in S_N are normally distributed since the saturation physically must lie between zero and one, but it is plausible that given our definition for Y, the prior errors in Y are normally distributed.

The retardation R may then be written

$$R = 1 + K_N \exp(Y). \tag{19}$$

Using this relation together with partitioning and nonpartitioning tracer breakthrough curve data at extraction wells, an estimate of the average NAPL saturation (and hence the average value of Y) and total volume of NAPL in the tracer swept volume of the aquifer can be obtained [*Jin et al.*, 1995], provided K_N is known. An estimate of the average value of Y is required by our estimation procedure. This is discussed in more detail in section 3.

2.3. Determination of Sensitivities

To obtain estimates of Y in a variable conductivity field, the sensitivities of the zeroth and first temporal moments at a given point to variations in log K and Y are required by the Gauss-Newton algorithm given in (4). As mentioned in section 2.1, we use an adjoint method to determine the sensitivities.

Applications of adjoint sensitivity theory in groundwater hydrology have been discussed by *Neumann* [1980], *Townley and Wilson* [1985], *Carrera and Neumann* [1986], *Sun and Yeh* [1990, 1992], and *Sun* [1994]. For our problem we follow closely the work of *Sun and Yeh* [1990] and *Sun* [1994] for coupled systems.

To determine these sensitivities, we first require a performance measure of the form

$$\mathcal{G}(\mathbf{p}) = \int_\Omega \mathcal{P}(\mathbf{p}, \mathbf{d}), \tag{20}$$

where $\mathcal{P}$ is a user-chosen function [*Sun and Yeh*, 1990; *Sun*, 1994]. The first-order variation of $\mathcal{G}$ is given by

$$\delta\mathcal{G} = \int_\Omega \left(\frac{\partial \mathcal{P}(\mathbf{p}, \mathbf{d})}{\partial \mathbf{d}} \delta\mathbf{d} + \frac{\partial \mathcal{P}(\mathbf{p}, \mathbf{d})}{\partial \mathbf{p}} \delta\mathbf{p} \right). \tag{21}$$

For our problem, $\mathbf{d}$ is the vector of data given by $[\mathbf{q}\ h\ \mathbf{z}_0\ m_0\ \mathbf{z}_1\ m_1]^T$, while $\mathbf{p}$ is the vector of parameters $[F\ Y]^T$. Substituting these into (21), we have

$$\delta\mathcal{G} = \int_\Omega \left(\frac{\partial \mathcal{P}}{\partial \mathbf{q}} \delta\mathbf{q} + \frac{\partial \mathcal{P}}{\partial h} \delta h + \frac{\partial \mathcal{P}}{\partial \mathbf{z}_0} \delta\mathbf{z}_0 + \frac{\partial \mathcal{P}}{\partial m_0} \delta m_0 + \frac{\partial \mathcal{P}}{\partial \mathbf{z}_1} \delta\mathbf{z}_1 + \frac{\partial \mathcal{P}}{\partial m_1} \delta m_1 \right) + \int_\Omega \left(\frac{\partial \mathcal{P}}{\partial F} \delta F + \frac{\partial \mathcal{P}}{\partial Y} \delta Y \right), \tag{22}$$

where $F = \ln K$.

The first-order variations in the governing system of (6)–(9) and (14)–(17) are [*Sun and Yeh*, 1990; *Sun*, 1994]

$$\delta\mathbf{q}(x) + \frac{\partial K(x)}{\partial F} \delta F \cdot \nabla h(x) + K(x) \cdot \nabla \delta h(x) = 0, \tag{23}$$

$$\nabla \cdot \delta\mathbf{q}(x) = 0 \qquad x \in \Omega, \tag{24}$$

$$\delta\mathbf{z}_0(x) + \theta \mathbf{D}(x) \cdot \nabla \delta m_0(x) = 0, \tag{25}$$

$$\nabla \cdot \delta\mathbf{z}_0(x) + \nabla \cdot [\delta\mathbf{q}(x) m_0(x) + \mathbf{q}(x) \delta m_0(x)] - \delta S^{\text{ext}}_{m_0} = 0 \qquad x \in \Omega, \tag{26}$$

$$\delta\mathbf{z}_1(x) + \theta \mathbf{D}(x) \cdot \nabla \delta m_1(x) = 0, \tag{27}$$

$$\nabla \cdot \delta\mathbf{z}_1(x) + \nabla \cdot [\delta\mathbf{q}(x) m_1(x) + \mathbf{q}(x) \delta m_1(x)] - \delta S^{\text{ext}}_{m_1} - \theta \frac{\partial R(x)}{\partial Y} \delta Y m_0(x) - \theta R(x) \delta m_0(x) = 0 \qquad x \in \Omega \tag{28}$$

and the boundary conditions

$$\delta h(x) = 0 \qquad x \in \Gamma_D^{\text{flow}},\ \delta\mathbf{q}(x) \cdot \mathbf{n} = 0 \qquad x \in \Gamma_N^{\text{flow}}, \tag{29}$$

$$\delta m_0(x) = 0 \qquad x \in \Gamma_D^{\text{trans}},\ \delta\mathbf{z}_0(x) \cdot \mathbf{n} = 0 \qquad x \in \Gamma_N^{\text{trans}}, \tag{30}$$

$$\delta m_1(x) = 0 \qquad x \in \Gamma_D^{\text{trans}},\ \delta\mathbf{z}_1(x) \cdot \mathbf{n} = 0 \qquad x \in \Gamma_N^{\text{trans}}, \tag{31}$$

where

$$\delta S^{\text{ext}}_{m_n} = \sum_{j=1}^{M} \delta m_{n_j}(x) Q_j \delta(x - x_j).$$

Note that the first-order variations of the source terms $S^{\text{inj}}_{m_0}$ and $S^{\text{inj}}_{m_1}$ are zero since t_0 and C_0 are deterministic. The terms $\partial K/\partial F$ and $\partial R/\partial Y$ arise because functions of the parameters rather than the parameters themselves occur in the governing equations, that is, e^Y as opposed to Y. Note that in taking the first-order variations of (23) and (28), we have neglected th deterministic relationship between K and Y by ignoring ter such as $\partial K/\partial Y$. To determine this relationship either deterministically or stochastically requires solution of the multiphase flow equations, which require knowledge of the release history of NAPL as well as knowledge of the functional relationship between NAPL saturation and relative permeability for heterogeneous aquifer materials. Since this information is not usually available, in our estimation procedure we assume no deterministic relationship or cross correlation between NAPL saturation and hydraulic conductivity. Thus when we estimate F, we are estimating the relative hydraulic conductivity in the presence of NAPL. However, we neglect the information that NAPL estimates might give us regarding hydraulic conductivity.

Proceeding with the determination of sensitivities using the adjoint method, each of (23)–(28) is multiplied in turn by the arbitrary functions $\psi_1, \psi_2, \cdots$, and ψ_6, respectively, where ψ_1, ψ_3, and ψ_5 are vector valued functions and ψ_2, ψ_4, and ψ_6 are real valued functions. Furthermore, we require that these functions have the requisite differentiability and satisfy the boundary conditions

$$\psi_1 \cdot \mathbf{n} = 0 \qquad x \in \Gamma_N^{\text{flow}},\ \psi_2 = 0 \qquad x \in \Gamma_D^{\text{flow}},$$

$$\psi_3 \cdot \mathbf{n} = 0 \qquad x \in \Gamma_N^{\text{trans}},\ \psi_4 = 0 \qquad x \in \Gamma_D^{\text{trans}},$$

$$\psi_5 \cdot \mathbf{n} = 0 \qquad x \in \Gamma_N^{\text{trans}},\ \psi_6 = 0 \qquad x \in \Gamma_D^{\text{trans}}.$$

Each equation is integrated over the domain Ω, and Gaus theorem is applied to each of the integrals. Note that the boundary integrals resulting from using Green's theorem vanish upon application of the boundary conditions. Adding the resulting equations to (22) and collecting terms in $\delta\mathbf{q}$, δh, $\cdots$, etc. results in the following equation:

$$\begin{aligned}
\delta\mathcal{G} = &\int_\Omega \left(\frac{\partial \mathcal{P}}{\partial \mathbf{q}} + \psi_1 - \nabla\psi_2 - m_0 \nabla\psi_4 - m_1 \nabla\psi_6 \right) \cdot \delta\mathbf{q} \\
&+ \int_\Omega \left(\frac{\partial \mathcal{P}}{\partial h} - \nabla \cdot [K\psi_1] \right) \delta h + \int_\Omega \left(\frac{\partial \mathcal{P}}{\partial \mathbf{z}_0} + \psi_3 - \nabla\psi_4 \right) \cdot \delta\mathbf{z}_0 \\
&+ \int_\Omega \left(\frac{\partial \mathcal{P}}{\partial m_0} - \nabla \cdot [\theta \mathbf{D} \cdot \psi_3] - \mathbf{q} \cdot \nabla\psi_4 - S^{\text{ext}}_{\psi_4} - \theta R \psi_6 \right) \delta m_0 \\
&+ \int_\Omega \left(\frac{\partial \mathcal{P}}{\partial \mathbf{z}_1} + \psi_5 - \nabla\psi_6 \right) \cdot \delta\mathbf{z}_1 \\
&+ \int_\Omega \left(\frac{\partial \mathcal{P}}{\partial m_1} - \nabla \cdot [\theta \mathbf{D} \cdot \psi_5] - \mathbf{q} \cdot \nabla\psi_6 - S^{\text{ext}}_{\psi_6} \right) \delta m_1 \\
&+ \int_\Omega \left(\frac{\partial \mathcal{P}}{\partial F} + \psi_1 \frac{\partial K}{\partial F} \cdot \nabla h \right) \delta F \\
&+ \int_\Omega \left(\frac{\partial \mathcal{P}}{\partial Y} + \psi_6 \theta m_0 \frac{\partial R}{\partial Y} \right) \delta Y.
\end{aligned} \tag{32}$$

Thus, by solving the system of equations

$$\frac{\partial \mathcal{P}}{\partial \mathbf{q}} + \psi_1 - \nabla\psi_2 - m_0\nabla\psi_4 - m_1\nabla\psi_6 = 0, \quad (33)$$

$$\frac{\partial \mathcal{P}}{\partial h} - \nabla\cdot[K\psi_1] = 0, \quad (34)$$

$$\frac{\partial \mathcal{P}}{\partial \mathbf{z}_0} + \psi_3 - \nabla\psi_4 = 0, \quad (35)$$

$$\frac{\partial \mathcal{P}}{\partial m_0} - \nabla\cdot[\theta\mathbf{D}\cdot\psi_3] - \mathbf{q}\cdot\nabla\psi_4 - S^{\text{ext}}_{\psi_4} - \theta R\psi_6 = 0, \quad (36)$$

$$\frac{\partial \mathcal{P}}{\partial \mathbf{z}_1} + \psi_5 - \nabla\psi_6 = 0, \quad (37)$$

$$\frac{\partial \mathcal{P}}{\partial m_1} - \nabla\cdot[\theta\mathbf{D}\cdot\psi_5] - \mathbf{q}\cdot\nabla\psi_6 - S^{\text{ext}}_{\psi_6} = 0 \quad (38)$$

for the adjoint state variables $\psi_1, \psi_2, \cdots$, and ψ_6, the integrals in (32) containing the terms with the variations $\delta\mathbf{q}$, $\delta h, \cdots$, and δm_1 will vanish. This leaves only the last two integrals in (32),

$$\delta\mathcal{G} = \int_\Omega \left(\frac{\partial \mathcal{P}}{\partial F} + \psi_1 \frac{\partial K}{\partial F}\cdot\nabla h\right)\delta F + \int_\Omega \left(\frac{\partial \mathcal{P}}{\partial Y} + \psi_6\theta m_0 \frac{\partial R}{\partial Y}\right)\delta Y, \quad (39)$$

from which the sensitivities are determined. Note that to solve for the adjoint state variables in the system of (33)–(38), we require $\mathbf{q}(x)$, $m_0(x)$, and $m_1(x)$, which are obtained by solving the primary equations (6)–(9) and (14)–(17). For this investigation we used a mixed finite element method to solve the system of equations for flow, transport, and adjoint state variables [*Allen et al.*, 1985; *Brezzi and Fortin*, 1991; *Chavent and Roberts*, 1991; *Durlofsky*, 1994; *James and Graham*, 1999].

To illustrate the use of the above technique to determine sensitivities, the measurement Jacobian for the sensitivity of the first temporal moment at a point x_i to a variation in the jth value of log conductivity can be found by choosing a performance measure of the type

$$\mathcal{P}(x; \mathbf{d}, \mathbf{b}) = m_1(x)\delta(x - x_i). \quad (40)$$

Then, noting that $\mathcal{G} = m_1(x_i)$, solving (33)–(38) for ψ_1 and using this result in (39) gives

$$\frac{\partial m_1(x_i)}{\partial F_j} = \int_{\Omega_j} \psi_1 K\cdot\nabla h = -\int_{\Omega_j} \psi_1\mathbf{q}, \quad (41)$$

where the integration is performed over the support of the jth discrete value of F. Similarly, the sensitivity of the first temporal moment to the log NAPL/water volumetric ratio is given by

$$\frac{\partial m_1(x_i)}{\partial Y_j} = \int_{\Omega_j} \psi_6\theta m_0 K_N \exp(Y). \quad (42)$$

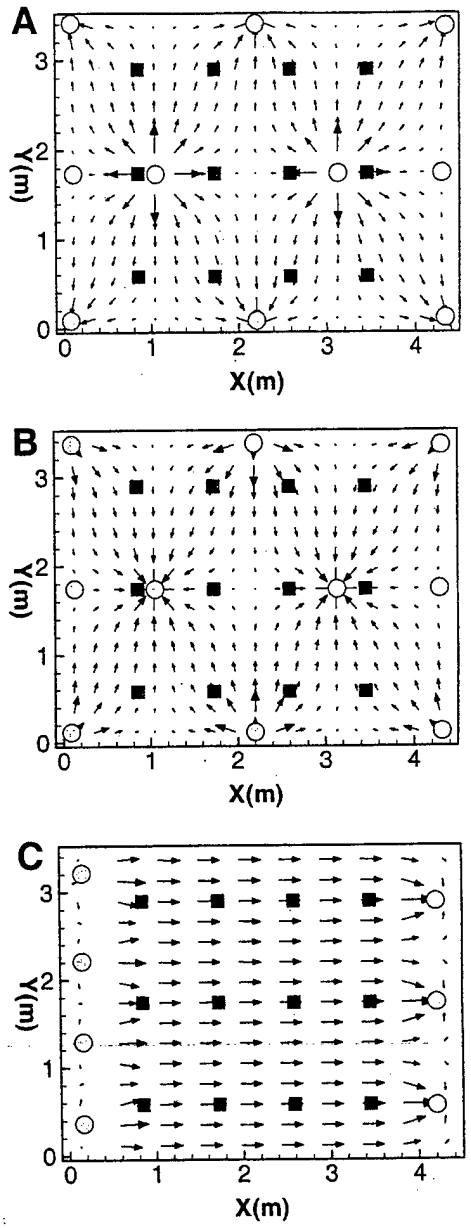

Figure 1. Plan views of the three pumping configurations tested. Squares represent locations of multilevel samplers (MLS), and circles represent locations of wells. Vertical spacing of the MLS locations are approximately 0.38 m. (a) Inverted double five-spot pattern. (b) Double five-spot pattern. (c) Line drive system.

3. Performance Evaluations

To test the performance of our method of estimating Y, we used three different pumping configurations and two types of NAPL distribution. The pumping configurations tested are similar to those used in tracer tests conducted in hydraulically isolated test cells [*Jawitz et al.*, 1999] and include a line-drive system, a double five-spot pattern, and an inverted double five-spot pattern (Figure 1). In these configurations the total injection rates and total extraction rates are equal, since containment is provided by the walls of the test cell. In these contained systems the zeroth moments of the tracers are constant throughout the domain. There are five levels of MLS

Table 1. Parameters Used in Simulation and Estimation of Random NAPL Field

Parameter	Symbol	Value
Mean log hydraulic conductivity	μ_F	2.3
Variance log hydraulic conductivity	σ_F^2	1.0
Mean log NAPL/water volume ratio	μ_Y	−3.65
Variance log NAPL/water volume ratio	σ_Y^2	0.75
Conductivity correlation scale for simulation	λ_{F_x}, λ_{F_y}	1.1 m
	λ_{F_z}	0.38 m
Conductivity correlation scale for estimation	λ_{f_x}, λ_{f_y}	0.78 m
	λ_{f_z}	0.27 m
NAPL correlation scale for simulation	λ_{Y_x}, λ_{Y_y}	1.1 m
	λ_{Y_z}	0.38 m
NAPL correlation scale for estimation	$\lambda_{\hat{Y}_x}$, $\lambda_{\hat{Y}_y}$	1.0 m
	$\lambda_{\hat{Y}_z}$	0.3 m
Measurement error		$0.02\bar{m}_1(x)$
Porosity	θ	0.21
Dispersivity	α_L	0.2 m
	α_T	0.2 m
Injection/extraction rate	Q	11.7 m³/d
Tracer input duration	t_0	0.14 day
NAPL/water partitioning coefficient	K_N	28
Measurement points		60
Convergence tolerance	T	10^{-3}
Simulation grid	Number of blocks	34×27×13
	spacing	0.13 m
Estimation grid	Number of blocks	19×15×8
	spacing	0.23 m

points (the horizontal locations are shown by the squares in Figure 1) with 12 sampling points in each level for a total of 60 sampling points in the domain. The vertical spacing between sample locations is approximately 0.38 m. The staggered MLS pattern provides evenly spaced coverage in the three configurations and has been used in a number of field experiments.

We examine two different types of NAPL distributions. The first is a random, spatially correlated field of Y, while the second is a nonrandom "block" of NAPL. Neither of these scenarios is meant to provide an exhaustive test of the method to determine the "best" pumping configuration; rather, we use these cases to illustrate the veracity of our technique for a random NAPL field, which, in general, adheres to our assumptions regarding statistical structure, as well as a distinctly nonrandom NAPL field which clearly violates our statistical assumptions.

3.1. Example Cases

3.1.1. Case 1. A turning bands algorithm was used to generate a spatially correlated random field for Y with mean μ_Y, variance σ_Y^2, and spatial correlation scales λ_{Y_x}, λ_{Y_y}, and λ_{Y_z}. Recall that for a statistically anisotropic random field, these values will not all be equal. A random, spatially correlated log K field (recall that K is the relative hydraulic conductivity with respect to water saturation) with mean μ_F, variance σ_F^2, and spatial correlation scales λ_{F_x}, λ_{F_y}, and λ_{F_z} was also generated. In both cases the correlation scales were chosen to be an integral multiple of the mesh spacing. The log K field was uncorrelated with the NAPL field. The same random fields were used in all the pumping configurations.

3.1.2. Case 2. This case consisted of two blocks of $S_N = 0.15$: one with dimensions 1.40 m × 1.14 m × 0.25 m and the second with dimensions 1.14 m × 0.89 m × 0.25 m. The NAPL saturation in the remainder of the domain was set to 1.0^{-5}. Three estimates of this distribution were also produced using each of the different pumping configurations. In this case the relative hydraulic conductivity with respect to water was uniform throughout the domain at 10 m/d, except for within each NAPL block where it is 3.0 m/d, and in a 0.25 m thick zone immediately below each block where it is 0.1 m/d.

The parameters used in the forward tracer simulations with the random Y and log K fields to determine the "true" temporal moments, together with those used in the estimation of the random Y field, are given in Table 1. For each of the three pumping configurations and the two NAPL distributions the "true" temporal moments used for the measurements $\mathbf{d}^*$ were determined using a forward simulation of partitioning and nonpartitioning tracers through the synthetic NAPL and conductivity fields. These forward simulations were done on a relatively fine mesh. For computational efficiency the estimation procedure was conducted on a coarser grid than the forward simulation. To increase the stability of the inverse algorithm, we assumed a small amount of error in the true temporal moments of 2% of the measured first moment. In both of the above cases we set the transverse dispersivity equal to the longitudinal dispersivity for numerical convenience, although this can be easily relaxed. The correlation scales used in the estimation procedure were chosen to be close but not exactly equal to those used in the forward simulation. Since these parameters are difficult to estimate from field data, it cannot be expected that these parameters can be determined exactly. The parameters used in the estimation of the NAPL block are the same except that in this case the mean value of $Y = -5.7$. We note here that in the first case, the statistical parameters and structure we used for the parameter estimation procedure are close or match exactly those of the synthetically generated field, while in the second case the parameters ar structure assumptions are clearly not accurate. Also, for t second case the NAPL and conductivity distributions are correlated, although (as discussed above) the estimation procedure assumes that they are uncorrelated. We hope to show that even if the statistical parameters and structure are not perfectly known, some information about NAPL distribution can still be recovered.

In a real-world tracer test the average NAPL saturation, total NAPL volume, and prior (uniform) estimate of Y are obtained from analysis of the tracer breakthrough curves at the extraction wells. For both of our cases the mean values of Y estimated from the synthetic extraction well breakthrough curves are virtually identical to the means of the true fields for the two cases. The estimates of conductivity and porosity require drawdown tests. The values of K and θ used in this study are representative of those determined from field experiments.

3.2. Estimation Procedure

At the beginning of the estimation algorithm the true spatial distributions of the Y and F (log K) fields are unknown. The initial estimates of these fields are assumed to be uniform. The prior first temporal moments are found by simulating tracer transport through the uniform S_N and K fields corresponding to the uniform fields for Y and F, respectively. The prior sensitivities are then found by solving (33)–(38) and using the adjoint variables ψ_1 and ψ_6 in (41) and (42). The covariance matrix $P_{\mathbf{p}_0\mathbf{p}_0}$ is constructed using the variances σ_Y^2 and σ_F^2 and correlation scales $\lambda_{\hat{Y}_x}$, $\lambda_{\hat{Y}_y}$, $\lambda_{\hat{Y}_z}$, $\lambda_{\hat{F}_x}$, $\lambda_{\hat{F}_y}$, and $\lambda_{\hat{F}_z}$ while P is constructed using the assumed measurement error in . mentioned in section 3.1. Updated estimates of Y and F are found using the prior temporal moments and sensitivities in the algorithm given in (4). After a conditioning step k, esti-

mates of $\hat{Y}_k$ and $\hat{F}_k$ for each coarse grid block are produced. The saturation at each coarse grid block in Ω is estimated using

$$\hat{S}_{N_k} = \frac{\exp(\hat{Y}_k)}{1 + \exp(\hat{Y}_k)}, \tag{43}$$

while the updated conductivity is estimated by $\hat{K}_k = \exp(\hat{F}_k)$. The new sensitivities G_k are calculated by resimulating flow and tracer transport through the updated NAPL and conductivity fields to obtain the updated first temporal moments of the partitioning and nonpartitioning tracers $\hat{m}_1^{\mathrm{p}}$ and $\hat{m}_1^{\mathrm{np}}$, respectively, which are then used again in solving the adjoint sensitivity equations. From the updated sensitivities and estimated measurements $\hat{\mathbf{d}}$, new estimates $\hat{Y}_{k+1}$ and $\hat{F}_{k+1}$ are produced. The conditioning steps are repeated until convergence is obtained. The convergence criterion we use here is when the objective function E defined in (3) stops decreasing or decreases only very slowly, that is, if

$$E_k - E_{k+1} < T, \tag{44}$$

where T is some predefined tolerance. For purposes of brevity, in the following discussion we only present and analyze our results for the estimates of Y.

An indication of how the estimation procedure will perform in each of the three pumping configurations can be obtained by examining the sensitivity matrix G_1 of the first temporal moment of the partitioning tracer with respect to the log NAPL/water volumetric ratio produced after the first iteration. This information is independent of the actual NAPL and conductivity distributions and can be used to evaluate alternative pumping configurations prior to obtaining actual MLS data. The ith–jth entry g_{ij} contains information on the sensitivity of the first temporal moment of the partitioning tracer at the ith measurement point to Y in the jth grid block. Figure 2 shows the maximum sensitivity obtained within a grid block with respect to all the sampling points, that is, $\max_i g_{ij}$. Figures 2a–2c each represent one of the three pumping configurations and consist of contour maps of the sensitivities on a series of horizontal slices through the domain. Figure 2 indicates that the first temporal moments have greater sensitivities to the log NAPL/water volumetric ratio in the inverted five-spot and five-spot configurations (Figures 2a and 2b) than in the line-drive system (Figure 2c). Part of the reason for the increased sensitivity in the five-spot and inverted five-spot configurations is due to the wider range of velocities in these configurations. Examination of Figure 1 shows that both of the five-spot patterns have a greater proportion of lower velocities than the line-drive pattern, which has a relatively uniform velocity distribution. Numerical solutions of the adjoint equations (37) and (38) show that the adjoint variable ψ_6 is inversely proportional to the Darcy flux $\mathbf{q}$. Since (42) shows that the sensitivity of m_1 with respect to Y is directly proportional to ψ_6, we can conclude that flow systems with lower mean velocities have larger sensitivities $\partial m_1/\partial Y$.

Owing to the nonlinearity of the estimation problem these increased prior sensitivities for the five-spot patterns do not guarantee that these pumping configurations will be more efficient than line-drive patterns for all NAPL distributions. However, if no additional site-specific information is available, these prior sensitivities indicate that on average five-spot patterns will be more efficient than the line-drive configuration tested here.

3.3. Estimates of Random Field

Shown in Figure 3 are the true and estimated values of the random S_N field using the three different pumping configurations. Again, each view is a series of contour maps of S_N on horizontal slices through the domain. Figure 3a shows the true field, while Figures 3b, 3c, and 3d show the estimates in the inverted five-spot, five-spot, and line-drive configurations, respectively. It is evident that the method yields a reasonable estimate in all three pumping configurations. In particular, the location of the high S_N zones in the upper part of the cell is well resolved in all three pumping configurations. The moderately high values of S_N along the bottom left-hand edge, bottom right-hand edge and, to a lesser extent, in the center of the cell are also resolved in the inverted five-spot and the five-spot configurations. However, the line drive fails to resolve the moderately high saturations in the center and bottom right-hand side of the cell. Note that all the estimates are considerably smoother than the actual NAPL field. This is due to two factors: (1) The estimates are obtained on a coarser grid than the true field, and (2) the regularization term in the objective function penalizes deviations from the smooth prior estimates.

The performance of the various configurations can also be analyzed by examining the reduction in estimation error associated with each configuration. Shown in Figure 4 are maps of the variance of the estimation error as determined by the values on the diagonal of the posterior covariance matrix P'_{YY}. The inverted five-spot pattern (Figure 1a) has the lowest overall variance in the estimation error, particularly in the center of the cell. The line-drive configuration does not show as much reduction in estimation error variance as do the other configurations and, in particular, does not show much in the way of significant lowering of the estimation error along the right-hand edge of the cell. Past the last row of multilevel samplers, no additional spatial information can be gained, and thus the estimate cannot be significantly improved. This effect can be seen in both the estimation error variance maps for the inverted five-spot and five-spot configurations and the maximum sensitivity maps shown in Figure 2. For the five-spot pattern the estimation variance is higher near the extraction wells (in the interior of the cell), compared to the same locations in the inverted five-spot pattern (where the injection wells are located). Again, this demonstrates that spatial information is only available between the source of the tracers (i.e., the injection wells) and the multilevel samplers. "Downstream" of the multilevel samplers, that is, between the last multilevel samplers and the extraction wells, the estimate is not as accurate.

The information contained in the posterior covariance matrix is similar to the information contained in the sensitivity matrix G_1 discussed in section 3.2. This can be deduced from (5) since the sensitivity matrix is used in the update of the covariance matrix. In this context the sensitivity matrix weights the entries in the covariance matrix and reduces the variance in the vicinity of measurement points. Since the sensitivities $\partial m_1/\partial Y$ in (42) are a function of Y, after the first iteration the covariances will be a function of the estimated NAPL distribution, which, in turn, is a function of the measured values of m_1. This results in the lower estimation errors within zones of high estimated NAPL and also accounts for the lack of symmetry in the estimation error variances shown in Figure 4.

Shown in Figure 5 are curves of the actual estimation error $Y^{\mathrm{err}} = Y^{\mathrm{true}} - Y^{\mathrm{est}}$ in the different pumping configurations. The prior curve is the error associated with the initial uniform

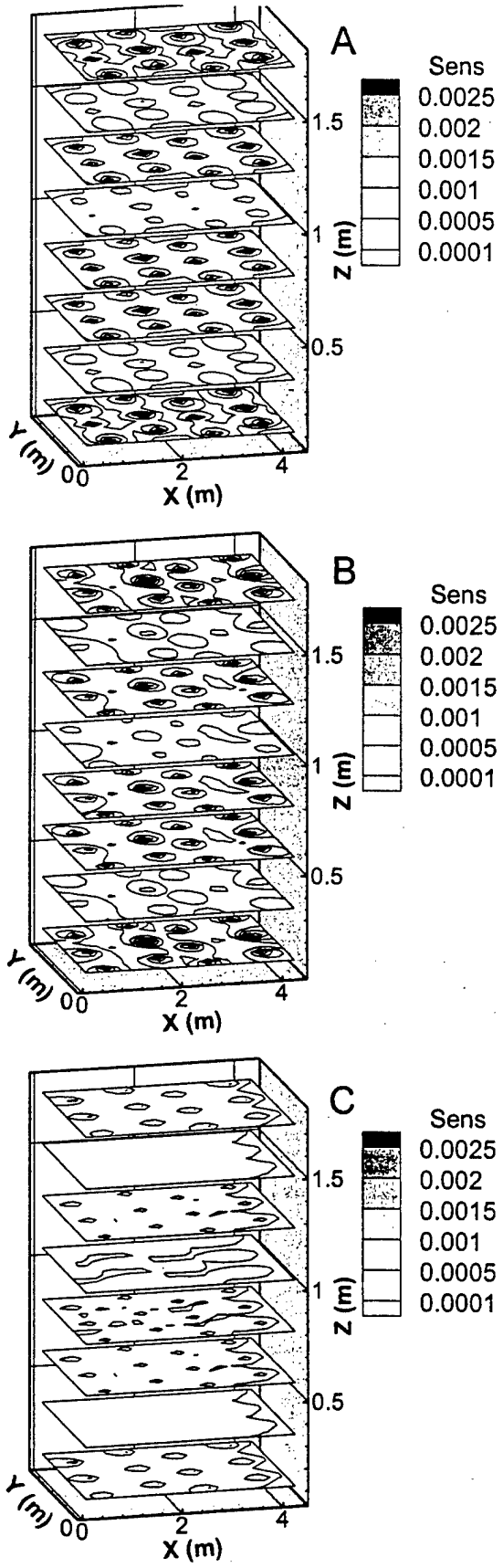

Figure 2. Maximum sensitivities of the first temporal moment to nonaqueous phase liquid (NAPL) in each of the three pumping configurations tested. (a) Inverted double five-spot pattern. (b) Double five-spot pattern. (c) Line drive system.

estimate. The estimates of Y produced in all three pumping configurations show significant improvement over the prior. The estimates produced in both the inverted five-spot and five-spot configurations have nearly identical error distributions, both having variances of 0.35. The estimate produced in the line-drive configuration is also a significant improvement over the prior estimate but is not quite as good as the estimates produced in the two other configurations, having a variance of 0.42. The estimate produced using the line-drive configuration has a slight positive bias. Table 2 shows the quartiles of the error distributions in Figure 5 as well as the interquartile ranges. The last column shows the fraction of estimation errors Y^{err} produced in the three configurations that lie within the interquartile range of the prior error, that is, the fraction of Y^{err} for which $Q_1^{prior} < Y^{err} < Q_3^{prior}$. In all three cases the interquartile ranges of the estimates produced in the three pumping configurations are lower than the prior interquartile range, indicating improvement over the prior estimate. The improvement is greatest for the inverted five-spot pattern, which is also shown by the greater fraction of estimates with errors lying within the prior interquartile range. The next largest improvement is for the five-spot pattern, with the line-drive configuration showing the least improvement.

Also shown in Table 2 are the quartiles and interquartile ranges for errors in estimated S_N. The errors in S_N are not normally distributed, and, in particular, the distribution of the prior estimation errors is significantly skewed, as indicated by the difference in the mean and median (Q_2) values. In each case, however, the interquartile ranges of the estimates are lower than the interquartile range of the uniform prior. The median values of the three estimates are all closer to their means than the prior, indicating that the distributions of the estimation errors are less skewed than the distribution of the prior error. Because the median values of the estimation errors produced in the three pumping configurations are significantly shifted from the median value of the prior, the fraction of estimation errors lying within the prior quartiles does not give a meaningful measure of improvement and is therefore not shown.

Shown in Figure 6 are curves of the moment prediction error in the three different configurations, that is, the difference at the measurement points between the true first temporal moments and the first temporal moments produced using the estimated field, $m_1^{true} - m_1^{est}$. Each graph shows two distributions, one of the prior error (using the initial uniform estimate) and another of the posterior error (after conditioning). The moments predicted using the inverted five-spot (Figure 6a) and five-spot configurations (Figure 6b) show considerable improvement over the initial estimate. Note that the prediction errors in the line-drive configuration (Figure 6c) are distributed similarly to the prediction errors in the two five-spot configurations. In contrast, the initial prediction errors in the line-drive configuration show less spread than the initial prediction errors in the five-spot configurations.

The similarity between the prior and posterior error distributions in the line-drive configuration may be due to several factors. First, as discussed in section 3.2, the five-spot configurations have generally lower flow velocities compared to the line-drive configuration. Since the prediction errors shown in Figure 6 are not normalized, the errors associated with slower flow paths (and thus larger first temporal moments) will be larger in magnitude. A second reason is due to the sensitivity of the temporal moments to the log NAPL/water volumetric

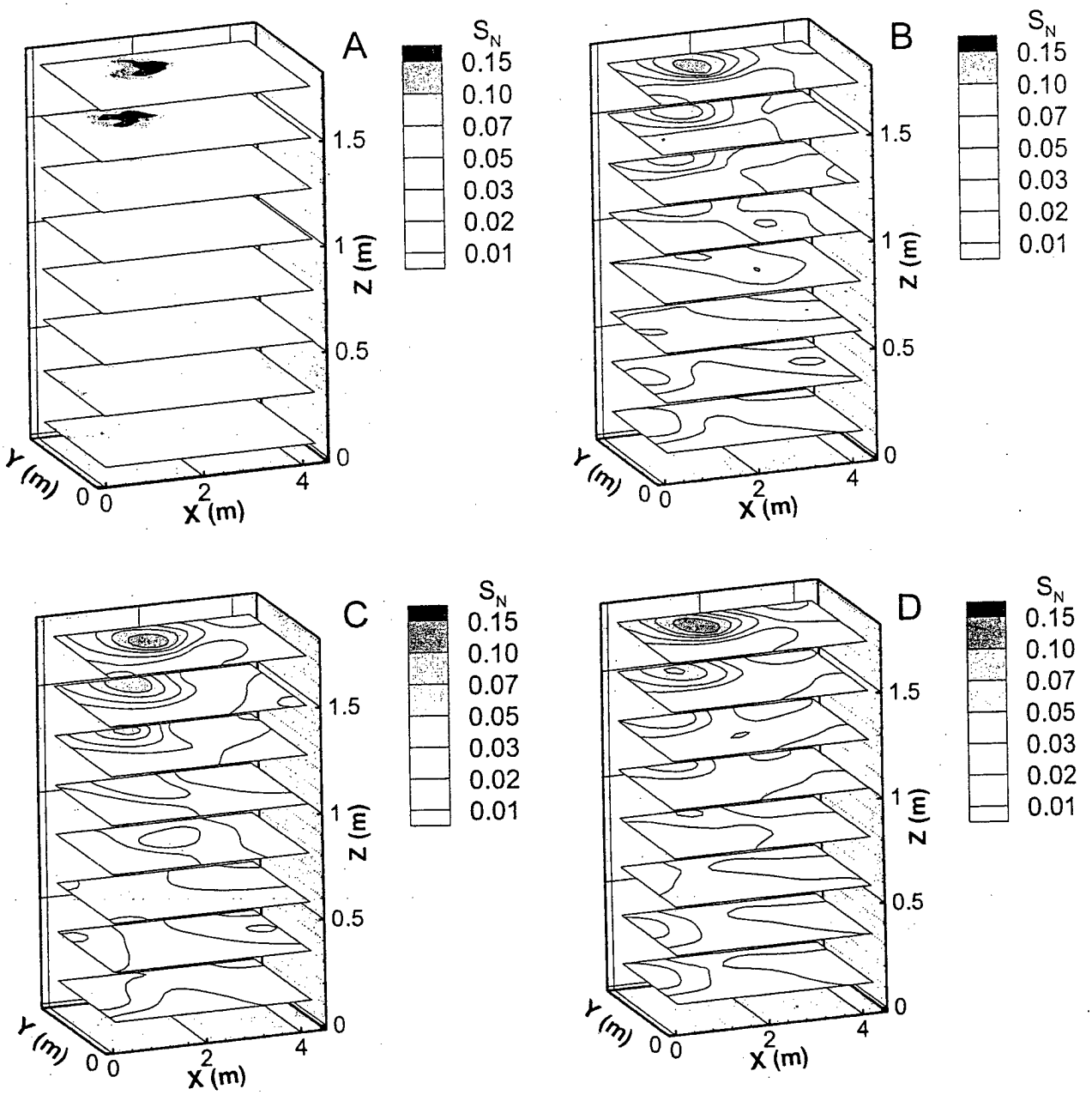

Figure 3. Estimates of random NAPL field. (a) True field. (b) Estimate produced in inverted double five-spot configuration. (c) Estimate produced in double five-spot configuration. (d) Estimate produced in line-drive configuration.

ratio, which, as discussed in section 3.2, is lower in the line-drive system. Rewriting (1) in terms of the log NAPL/water volumetric ratio (the parameter) and the first temporal moments (the data) and expanding in a Taylor series (to first order) about the mean value of Y, we have

$$m_1 = \mathcal{F}(\bar{Y}) + \frac{\mathcal{F}(\bar{Y})}{\partial Y}\,\delta Y,$$

where $\mathcal{F}(\bar{Y})/\partial Y$ are the sensitivities of the system with respect to perturbations in Y. For a given variance of Y a configuration with low sensitivities (such as the line-drive system) will produce output data (m_1) with less spread about the mean value $\bar{m}_1$ than a system with higher sensitivities (such as the inverted five-spot pattern). It follows that a flow configuration with low sensitivities is less effective for estimating accurate distributions of Y.

3.4. Estimates of Block

Shown in Figure 7 are the true and estimated values of S_N for the block of NAPL using the three pumping configurations. Figure 7a shows the true field, while Figures 7b, 7c, and 7d show the estimates in the inverted five-spot, five-spot, and line-drive configurations, respectively. Again, using the method in each of the pumping configurations yields a reasonable estimate of the location of the blocks of NAPL. It appears that the type of pumping configuration has a minor influence on where the estimates of the higher saturations are placed. For example, the block of NAPL at $z = 1.3$ m does not extend

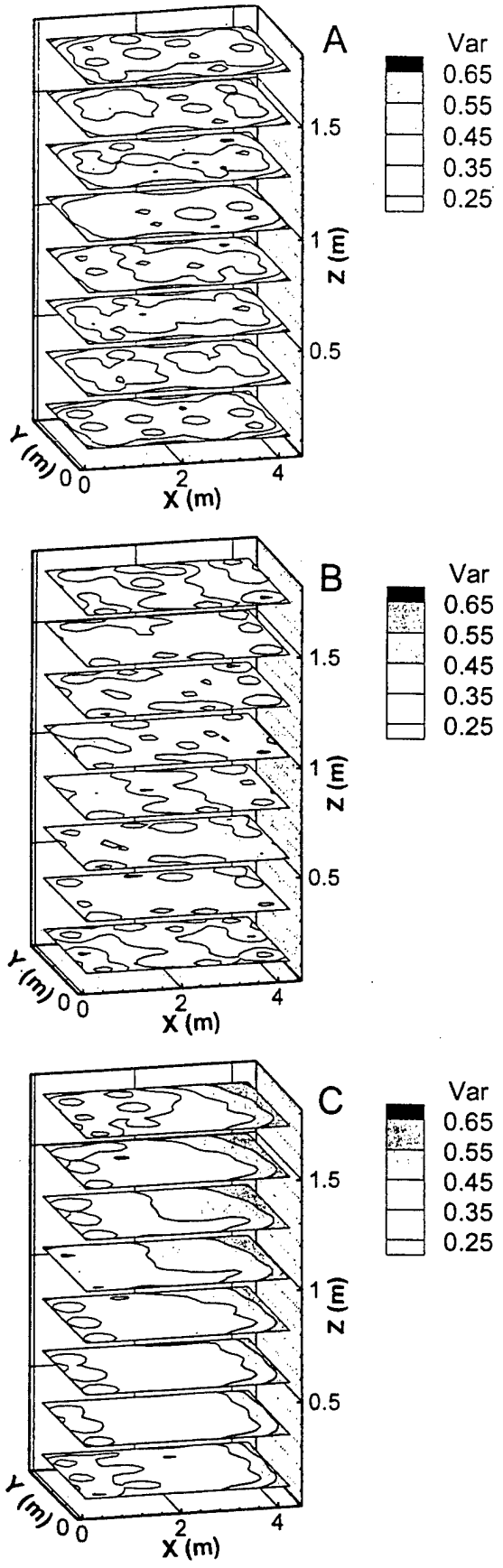

Figure 4. Contour maps of estimation error variance for the random NAPL field. (a) Variance in inverted double five-spot configuration. (b) Variance in double five-spot configuration. (c) Variance in line-drive configuration.

to the edge of the cell, but both the inverted five-spot and five-spot systems produce estimates that have moderately high NAPL saturations along the edge of the cell on the side $y = 0$. The estimate produced in the line-drive configuration shows lower saturations along this edge, more in line with the actual location. This is most likely due to the locations of the multilevel samplers with respect to the NAPL blocks. In each case the highest estimated values of Y are directly upstream of the multilevel sampler location where tracer retardation is seen, even if the highest saturations are not directly upstream. Again, the magnitudes of the estimates are lower than the actual value ($S_N = 0.15$). The highest estimated values are approximately $S_N = 0.07$ for all three pumping configurations.

Shown in Figure 8 are curves of the actual estimation error $Y^{err} = Y^{true} - Y^{est}$ of the different pumping configurations. Again, the prior curve is the error associated with the initial uniform estimate of Y. In this case, since the initial distribution is not random nor normally distributed, the prior curve is strongly multimodal; the main peak is where the true value of Y is very low ($S_N = 1.0^{-5}$, so $Y^{err} \approx -5.8$), with a smaller one where the true value is $Y = -1.73$ ($Y^{err} \approx 4$). There is a third peak at $Y^{err} \approx -3.75$ which results from an averaging effect since the boundaries of the NAPL blocks do not exactly correspond to the grid spacing on the coarse estimation grid. The estimates produced in the three pumping configurations show improvement, but in each case pronounced deviations from the true distribution are evident. Note that the peaks of the distribution obtained in the two five-spot configurations are closer to zero than the distribution obtained using the line-drive configuration. This indicates that the five-spot patterns perform better in locating the blocks of NAPL than the line-drive pattern, as they did in the random case. Because our test distribution does not conform to the statistical parameters and structure (i.e., it violates our assumed spatial correlation scales and lack of cross correlation between NAPL and hydraulic conductivity), it cannot be expected that the method (which gives the best results for Gaussian parameters) will give extremely accurate results. However, it is apparent that the technique is still able to locate the areas of highest NAPL saturation, although the peak values are underestimated because of the smoothing of the estimated fields as discussed in section 3.3.

Shown in Figure 9 are curves of the moment prediction error using the block NAPL field in the three different configurations. In the inverted five-spot configuration (Figure 9a) and

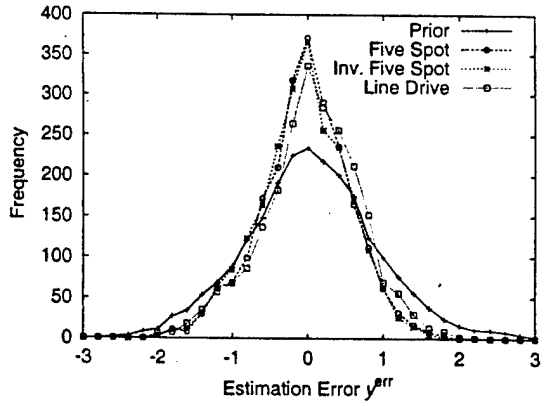

Figure 5. Estimation error Y^{err} of the random NAPL field in the three pumping configurations.

Table 2. Means, Quartiles, and Interquartile Ranges of the Error Distributions of Y and S_N

	Mean	Q_{25}	Q_{50}	Q_{75}	IQR	IQR Relative to Prior Error
Prior Y	0.0	−0.545	−0.015	0.527	1.072	0.500
$\hat{Y}$ inverted five spot	−0.030	−0.393	−0.030	0.341	0.734	0.670
$\hat{Y}$ five spot	−0.093	−0.503	−0.076	0.307	0.810	0.618
$\hat{Y}$ line drive	0.099	−0.435	0.030	0.506	0.941	0.560
Prior S_N	0.0	−0.017	−0.009	0.004	0.021	NA
$\hat{S}_N$ inverted five spot	0.005	−0.006	−0.001	0.0087	0.015	NA
$\hat{S}_N$ five spot	0.005	−0.007	−0.001	0.009	0.015	NA
$\hat{S}_N$ line drive	0.007	−0.005	0.001	0.011	0.016	NA

IQR, interquartile ranges; NA, not applicable.

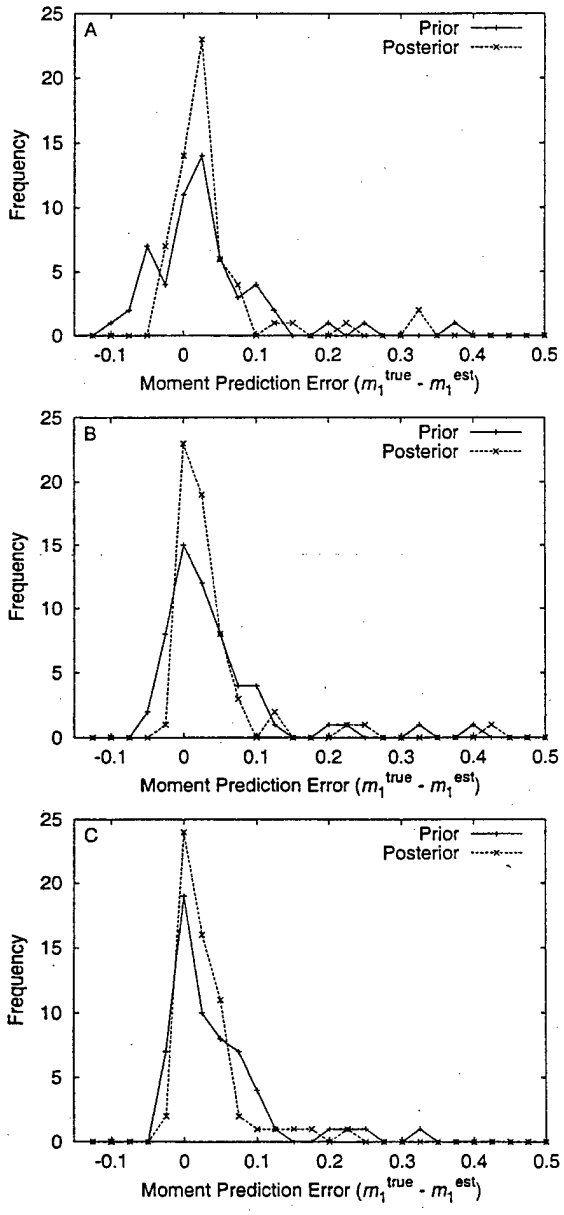

Figure 6. Moment prediction error $m_1^{true} - m_1^{est}$ at the sampling locations in the random NAPL field. (a) Prior and posterior errors in the inverted double five-spot configuration. (b) Prior and posterior errors in the double five-spot configuration. (c) Prior and posterior errors in the line-drive configurations.

five-spot configuration (Figure 9b) the posterior moment prediction errors show a modest improvement over the prior, while in the line-drive configuration (Figure 9c) the posterior and prior prediction errors are nearly identical. Overall, the prediction errors are much lower in magnitude than those associated with the random NAPL field. This is primarily due to the fact that both the NAPL fields and conductivity fields are far more homogeneous than the random case. Additionally, the average value of S_N in the NAPL block case is much less than the random field case. In any case the same trend occurs here: The inverted five-spot and five-spot configurations have prior distributions with higher variances and show subsequently larger improvements. Again, even with a uniform prior, the line-drive case does a better job of matching the actual moments. As in the case with the random NAPL field, we can conclude that the line-drive configuration is less effective than the five-spot patterns in generating an accurate estimate of Y.

4. Summary and Conclusions

We have developed a method to obtain estimates of the spatial distribution of the log NAPL/water volumetric ratio using partitioning tracer concentration data from MLSs in a variety of different flow configurations. We have extended and refined the technique of *James et al.* [1997] to make it more applicable to field experiments by using a coupled adjoint sensitivity technique to determine sensitivities of temporal moments to log K and residual NAPL saturation and computing the flow-related sensitivities and covariances numerically [*James and Graham*, 1999]. The new method allows us to examine the effects of nonuniform flow fields, so we can now accurately model injection and extraction wells and easily incorporate statistically anisotropic K fields. As a result, we can evaluate the performance of alternative tracer test pumping configurations. As a test case, we produced estimates of two different NAPL fields in a hydraulically isolated system using three different pumping configurations: inverted five-spot, five-spot, and line-drive configurations. Our results show that for these cases the inverted five-spot and five-spot configurations have higher sensitivity of the temporal moments to the NAPL/water volumetric ratio and produced more accurate estimates of the NAPL field than did the line-drive system. Owing to the nonlinearity of the estimation problem these increased prior sensitivities for the five-spot patterns do not guarantee that these pumping configurations will be more efficient than line-drive patterns for all NAPL distributions.

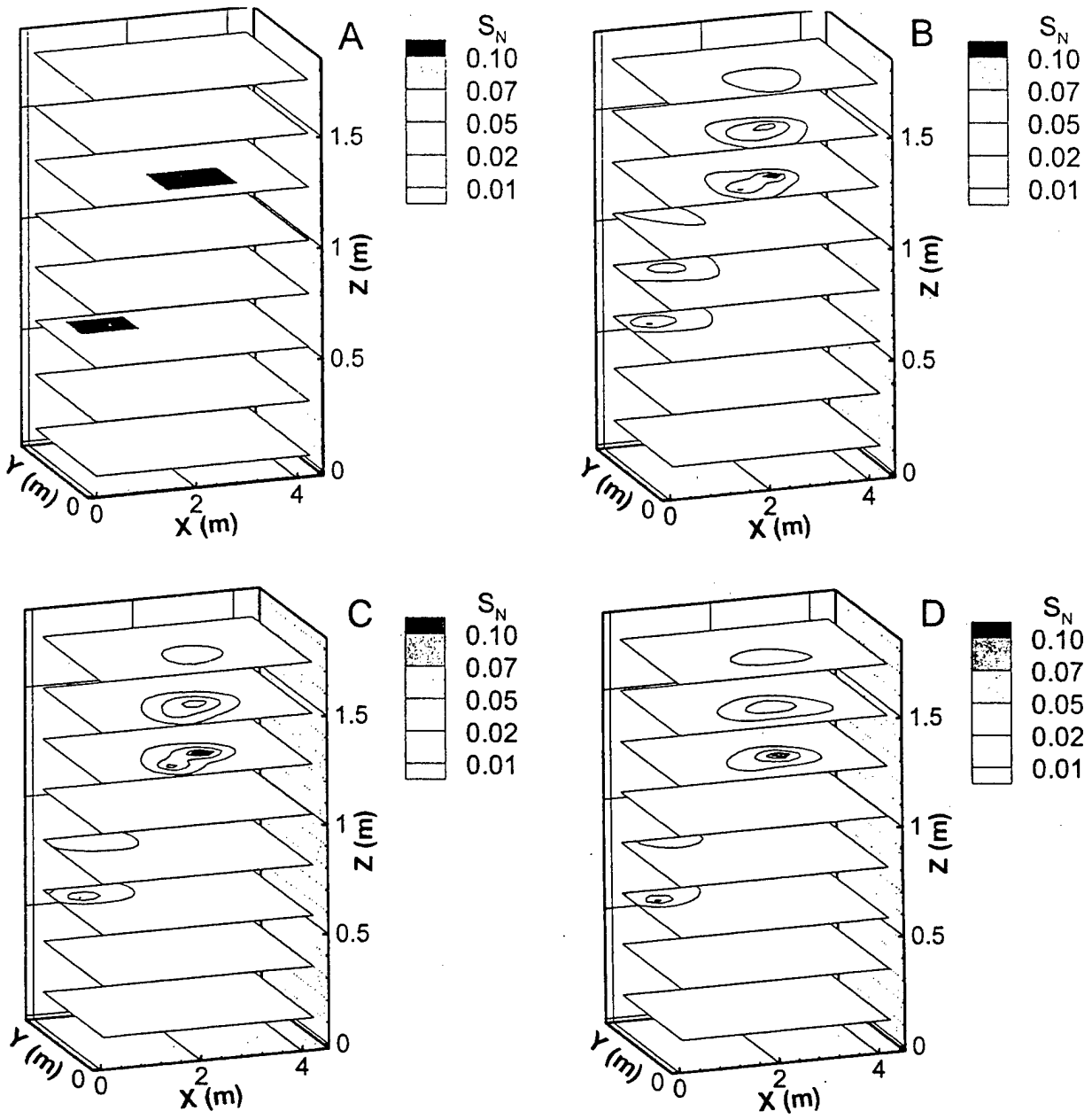

Figure 7. Estimates of NAPL block field. (a) True field. (b) Estimate produced in inverted double five-spot configuration. (c) Estimate produced in double five-spot configuration. (d) Estimate produced in line-drive configuration.

There are several advantages of using the Gauss-Newton technique we adopted for this work. It results in more accurate estimates than a single-pass estimation using a linearized estimator, and it is computationally more efficient than some other widely used parameter estimation techniques, such as simulated annealing. Additionally, there is a large body of work relating to the theoretical underpinnings of the method. Last, it is a straightforward matter to quantify the estimation accuracy by updating the covariance matrix according to (5).

Although a complete set of recommendations for tracer test design is beyond the scope of this work, some guidelines can be suggested. First, it is clear that slower water velocities improve both the sensitivities of the first temporal moments to the log NAPL/water volumetric ratio and the estimation of the spatial distribution of NAPL. While time constraints and other concerns, such as tracer degradation, place a lower limit on injec-

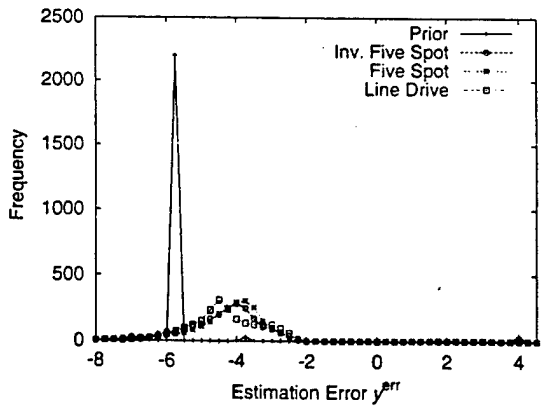

Figure 8. Estimation error Y^{err} of the NAPL block in the three pumping configurations.

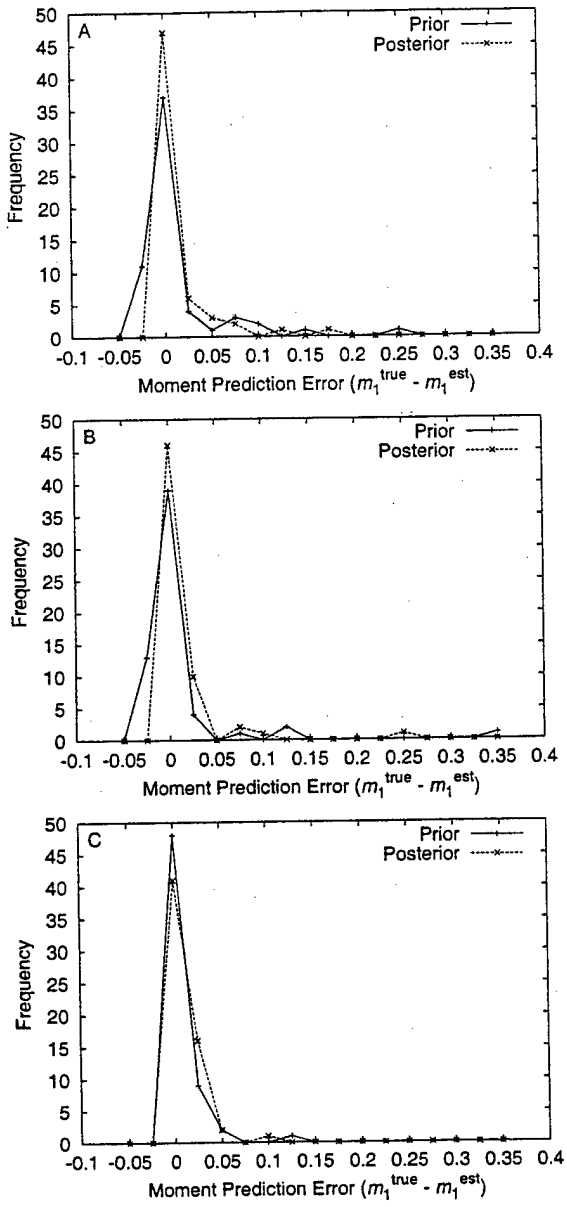

Figure 9. Moment prediction error $m_1^{true} - m_1^{est}$ at the sampling locations for the NAPL block. (a) Prior and posterior errors in the inverted double five-spot configuration. (b) Prior and posterior errors in the double five-spot configuration. (c) Prior and posterior errors in the line-drive configurations.

tion and extraction rates during a tracer test, we have shown that some pumping configurations (e.g., inverted five spots and five spots) result in lower mean velocities than others (line drive) at the same injection/extraction rates. For a specific tracer test a variety of pumping configurations should be examined with respect to determining the distribution of water velocities, the sensitivities of tracer moments to NAPL distribution, and a preliminary estimate of the reduction in NAPL estimation error for each configuration. The configurations tested should take into account any existing knowledge of the release history that would affect the spatial distribution of NAPL. It should be noted that the moment sensitivities provide information similar to the posterior NAPL estimation error without requiring any assumptions regarding the underlying spatial correlation structure of the NAPL and hydraulic conductivity fields. Thus using sensitivities to compare pumping configurations may be preferable when there is little information regarding these spatial correlation structures.

Although only tests in hydraulically isolated cells were investigated for this paper, our technique should perform similarly in nonisolated systems. The primary modification of the technique would be to solve the mean equation for the zeroth moment of the tracers since it would no longer be constant in space in a nonisolated system. Last, it is possible to estimate the NAPL/water volumetric ratio ($S_N/(1 - S_N)$), or even S_N, directly. As discussed in section 2.2, we chose to estimate Y to avoid the possibility of generating negative NAPL saturations. As a result, it is impossible to produce an estimated value of $S_N = 0$. Since a NAPL saturation of zero is not only possible but likely in many situations, this is an undesirable consequence of our choice. Additionally, the variability of Y is considerably greater than the variability of $S_N/(1 - S_N)$ for low values of S_N. It would be a straightforward matter to estimate $S_N/(1 - S_N)$ rather than Y, although negative estimates would have to be modified in an appropriate fashion. Last, taking into account the relationship between K and S_N would improve the estimation algorithm but would require solution of multiphase flow equations and significantly increase the computational effort, as well as requiring knowledge of the release history and the functional relationship between permeability and NAPL saturation.

Acknowledgments. The authors would like to sincerely thank G. Barth, Colin Johnston, and an anonymous reviewer whose comments were very helpful in improving the manuscript. This study was funded in part by the Strategic Environmental Research and Development Program (SERDP), which is a collaborative effort involving the U.S. EPA, U.S. DOE, and U.S. DOD. Although SERDP funds were used in part to support this study, this document has not been subjected to peer review within the agency, and the conclusions stated here do not necessarily reflect the official views of the agency, nor does this document constitute an official endorsement by SERDP. This paper is Florida Agricultural Experiment Station Journal Series number R-07254.

References

Allen, M., R. Ewing, and J. Koebbe, Mixed finite element methods for computing groundwater velocities, *Numer. Methods Partial Differential Equations*, *3*, 195–207, 1985.

Annable, M. D., P. S. C. Rao, W. D. Graham, K. Hatfield, and A. L. Wood, Use of partitioning tracers for measuring residual NAPL distribution in a contaminated aquifer: Preliminary results from a field-scale test, in *2nd Tracers Workshop*, edited by T. Bjornstad and G. A. Pope, pp. 77–85, Inst. for Energy Technol., Kjeller, Norway, 1995.

Annable, M. D., P. S. C. Rao, K. Hatfield, W. D. Graham, A. L. Wood, and C. G. Enfield, Partitioning tracers for measuring residual NAPL: Field-scale test results, *J. Environ. Eng.*, *124*(6), 498–503, 1998.

Brezzi, F., and M. Fortin, *Mixed and Hybrid Finite Element Methods*, Springer-Verlag, New York, 1991.

Carrera, J., and S. P. Neumann, Estimation of aquifer parameters under transient and steady state conditions, 1, Maximum likelihood method incorporating prior information, *Water Resour. Res.*, *22*(2), 199–210, 1986.

Chavent, G., and J. Roberts, A unified physical presentation of mixed, mixed-hybrid finite elements and standard finite difference approximations for the determination of velocities in waterflow problems, *Adv. Water Resour.*, *14*(6), 329–348, 1991.

Durlofsky, L., Accuracy of mixed and control volume finite element approximations to Darcy velocity and related quantities, *Water Resour. Res.*, *30*(4), 965–973, 1994.

Graham, W. D., and D. McLaughlin, Stochastic analysis of nonstationary subsurface solute transport, 1, Unconditional moments, *Water Resour. Res.*, *25*(2), 215–232, 1989a.

Graham, W. D., and D. McLaughlin, Stochastic analysis of nonstationary subsurface solute transport, 2, Conditional moments, *Water Resour. Res.*, *25*(11), 2331–2355, 1989b.

Graham, W. D., and D. McLaughlin, A stochastic model of solute transport in groundwater: Application to the Borden, Ontario, tracer test, *Water Resour. Res.*, *27*(6), 1345–1359, 1991.

Harvey, C. W., and S. M. Gorelick, Temporal moment-generating equations: Modeling transport and mass transfer in heterogeneous aquifers, *Water Resour. Res.*, *31*(8), 1895–1911, 1995.

James, A. I., and W. D. Graham, Numerical approximation of head and flux covariances in three dimensions using mixed finite elements, *Adv. Water Resour.*, *22*(7), 729–740, 1999.

James, A. I., W. D. Graham, K. Hatfield, P. S. C. Rao, and M. D. Annable, Optimal estimation of residual non–aqueous phase liquid saturations using partitioning tracer concentration data, *Water Resour. Res.*, *33*(12), 2621–2636, 1997.

Jawitz, J., M. Annable, R. Sillan, and P. Rao, In situ flushing for remediation of aquifer contaminated source zones: Evaluating performance using a control plane approach, in *Proceedings of the 1999 Contaminated Site Remediation Conference*, edited by C. Johnston, pp. 455–462, Cent. for Groundwater Stud., Fremantle, W. Aust., Australia, 1999.

Jin, M., M. Delshad, V. Dwarakanath, D. C. McKinney, G. A. Pope, K. Sepehrnoori, C. Tilburg, and R. E. Jackson, Partitioning tracer test for detection, estimation, and remediation performance assessment of subsurface nonaqueous phase liquids, *Water Resour. Res.*, *31*(5), 1201–1211, 1995.

McLaughlin, D., and L. R. Townley, A reassessment of the groundwater inverse problem, *Water Resour. Res.*, *32*(5), 1131–1161, 1996.

Neumann, S. P., A statistical approach to the inverse problem of aquifer hydrology, 3, Improved solution method and added perspective, *Water Resour. Res.*, *16*(2), 331–346, 1980.

Pope, G. A., M. Jin, V. Dwarakanath, B. A. Rouse, and K. Sepehrnoori, Partitioning tracer tests to characterize organic contaminants, in *2nd Tracers Workshop*, edited by T. Bjornstad and G. A. Pope, pp. 65–75, Inst. for Energy Technol., Kjeller, Norway, 1995.

Reid, L. B., and D. McLaughlin, *Estimating Continuous Aquifer Properties From Field Mesurements: The Inverse Problem for Groundwater Flow and Transport*, pp. 777–784, Kluwer Acad., Norwell, Mass 1994.

Schweppe, F. C., *Uncertain Dynamic Systems*, Prentice-Hall, Engl wood Cliffs, N. J., 1973.

Sillan, R. K., M. D. Annable, P. S. C. Rao, D. Dai, K. Hatfield, W. D. Graham, A. L. Wood, and C. G. Enfield, Evaluation of in situ cosolvent flushing dynamics using a network of spatially distributed multilevel samplers, *Water Resour. Res.*, *34*(9), 2191–2202, 1998.

Sun, N.-Z., *Inverse Problems in Groundwater Modeling*, Kluwer Acad., Norwell, Mass., 1994.

Sun, N.-Z., and W. W.-G. Yeh, Coupled inverse problem in groundwater modeling, 1, Sensitivity analysis and parameter identification, *Water Resour. Res.*, *26*(10), 2507–2525, 1990.

Sun, N.-Z., and W. W.-G. Yeh, A stochastic inverse solution for transient groundwater flow: Parameter identification and reliability analysis, *Water Resour. Res.*, *28*(12), 3269–3280, 1992.

Tarantola, A., *Inverse Problem Theory: Methods for Data Fitting and Model Parameter Estimation*, Elsevier Sci., New York, 1987.

Tarantola, A., and B. Valette, Generalized nonlinear inverse problems solved using the least squares criterion, *Rev. Geophys.*, *20*(2), 219–232, 1982.

Townley, L., and J. Wilson, Computationally efficient algorithms for parameter estimation and uncertainty propagation in numerical models of groundwater flow, *Water Resour. Res.*, *21*(12), 1851–1860, 1985.

M. D. Annable, W. D. Graham, K. Hatfield, and A. I. James, Agricultural and Biological Engineering, University of Florida, P. O. Box 110570, Gainesville, FL 32611-0570. (graham@agen.ufl.edu; khat@ce.ufl.edu; ajames@agen.ufl.edu)

P. S. C. Rao, School of Civil Engineering, Purdue University, West Lafayette, IN 47907-1284. (pscr@ecn.purdue.edu)

(Received June 16, 1999; revised December 14, 1999; accepted January 4, 2000.)

Groundwater Quality: Remediation and Protection (Proceedings of the GQ'98 Conference held at Tübingen, Germany, September 1998). IAHS Publ. no. 250, 1998

Characterizing the spatial distribution of non-aqueous phase contaminants using partitioning tracers and the method of moments

JAMES W. JAWITZ, MICHAEL D. ANNABLE & P. SURESH C. RAO

Interdisciplinary Program in Hydrologic Sciences, University of Florida, Gainesville, Florida 32611, USA

Abstract The design of effective subsurface remediation strategies requires knowledge of both the amount and spatial distribution of the contaminants present. Inter-well partitioning tracers have been shown to be effective at determining the mass of non-aqueous phase liquid (NAPL) contaminants present in porous media. However, to date the determination of the spatial distribution of the NAPL mass within the flow domain has required partitioning tracer characterization at multiple sampling locations. This paper describes the use of partitioning tracers and the method of moments to characterize the spatial distribution of NAPL in porous media using only one sampling location. An analytical technique utilizing partitioning tracer second temporal moments is described that accurately estimates the fraction of the flow domain that contains NAPL.

INTRODUCTION

Inter-well partitioning tracers have been used at both the laboratory and field scales to detect and quantify residual NAPL contaminants in the subsurface. Average residual NAPL saturations are calculated from measured tracer breakthrough curves (BTCs) using the ratio of the nonpartitioning and partitioning tracer mean arrival times (i.e. first temporal moments) as described by Jin *et al.* (1995). In this paper, a methodology is presented for ascertaining information about the spatial distribution of NAPL contaminants using second temporal moments. Laboratory experiments and numerical simulations were conducted; however, in this limited presentation we describe only the method and present some simple simulation results.

METHOD

One-dimensional solute transport through porous media can be described by the advection-dispersion equation (ADE). Valocchi (1985) described how the ADE parameters can be determined from BTCs using the method of moments, where the nth moment, m_n, is defined:

$$m_n = \int_0^\infty t^n C(x,t)\,dt \qquad (1)$$

For the ADE, Valocchi (1985) showed that the first two pulse-corrected, normalized temporal moments, μ_1' and μ_2', of tracer BTCs measured at position L are defined:

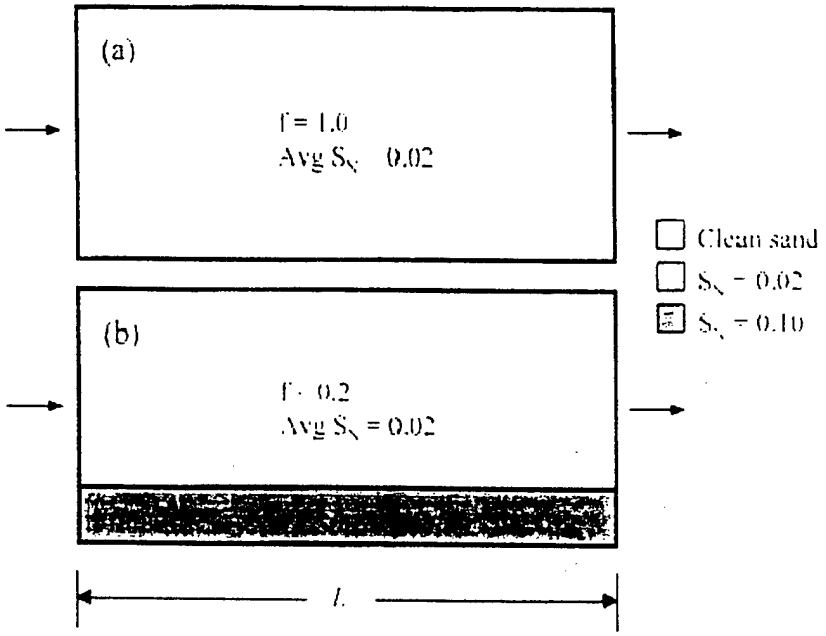

Fig. 1 Schematic representation of two-dimensional domain with (a) uniformly distributed NAPL, and (b) the same volume of NAPL distributed over only 20% of the domain.

$$\mu_1' = \frac{m_1}{m_0} = \frac{LR}{v} + \frac{t_w}{2}$$
$$\mu_2' = \frac{m_2}{m_0} = \frac{2DLR}{v^2} + \left(\frac{LR}{v} + \frac{t_w}{2}\right)^2 + \frac{t_w^2}{12} \tag{2}$$

where R is the retardation factor, v is the pore-water velocity, and D is the hydrodynamic dispersion coefficient.

Here we describe a two-dimensional domain, wherein a fraction of the domain, f, is contaminated with NAPL at saturation S_N (Fig. 1). It is assumed that flow is one-dimensional and that the effect of the NAPL on media permeability is negligible. The normalized moments, μ_n', of BTCs measured through the contaminated fraction, f, and the uncontaminated fraction, $1-f$, of the domain can be added to obtain the moments of a BTC measured through the entire domain. For a BTC measured through the entire domain, the first two normalized temporal moments, μ_1' and μ_2', can then be expressed:

$$\mu_1' = f\left[\frac{LR(1-S_N)}{v}\right] + (1-f)\left(\frac{L}{v}\right) - \frac{t_w}{2} \tag{3}$$

$$\mu_2' = f\left[\frac{2DLR^2}{\left(\frac{v}{1-S_N}\right)^2} + \left\{\frac{LR(1-S_N)}{v} + \frac{t_w}{2}\right\}^2\right] + (1-f)\left[\frac{2DL}{v^2} + \left\{\frac{L}{v} - \frac{t_w}{2}\right\}^2\right] + \frac{t_w^2}{12} \tag{4}$$

where $R = 1 + K_N S_N/(1 - S_N)$ and K_N is the tracer NAPL–water partitioning coefficient. Measuring the first two moments of BTCs from both a nonpartitioning

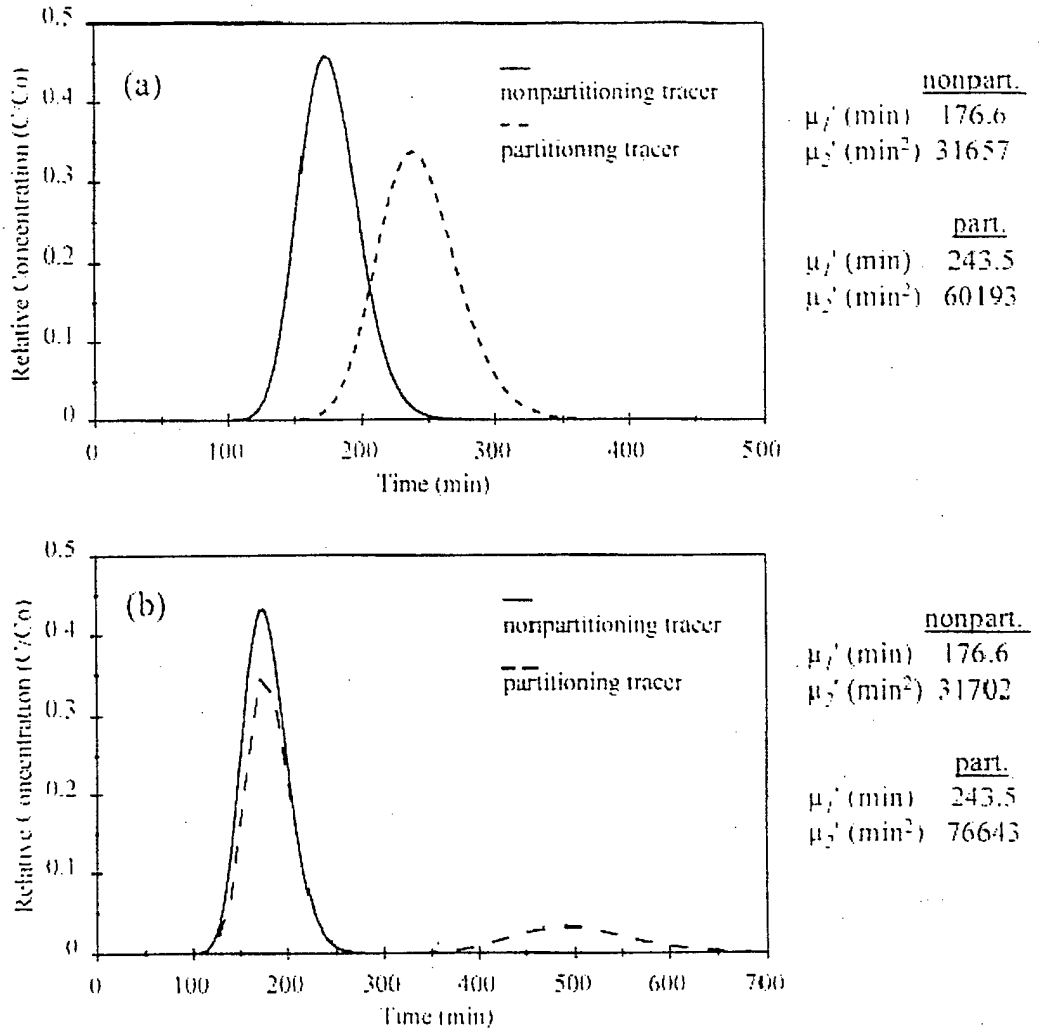

Fig. 2 Simulated BTCs for nonpartitioning and partitioning tracers through the domains described in Fig. 1.

and a partitioning tracer will result in four equations, which can then be solved for the four unknowns, v, D, f and S_N.

RESULTS

The BTCs presented in Fig. 2 were generated using the solution to the ADE presented by Brenner (1962). The parameters used were selected to approximate laboratory experiments conducted in a two-dimensional flow chamber that was packed with various combinations of clean Ottawa sand and sand residually-saturated with decane (pulse duration t_o = 25 min, K_N = 20, L = 62 cm, v = 0.37 cm min^{-1}, D = 0.19 cm^2 min^{-1}). The BTCs of Fig. 2(a) and (b) were generated based on the scenarios described in Fig. 1(a) and (b), respectively. Using the four temporal moments shown in Fig. 2(b), the values for the input parameters v, D, f and S_N were reproduced by solving the system of four equations described by expanding equations (3) and (4) for both the nonpartitioning and partitioning tracers.

Forthcoming publications will present results from the application of this approach to laboratory experimental data and to scenarios with more complex NAPL distributions.

REFERENCES

Brenner, H. (1962) The diffusion model of longitudinal mixing in beds of finite length: numerical values. *Chem. Engng Sci.* **17**, 229–243.

Jin, M., Delshad, M., Dwarakanath, V., McKinney, D. C., Pope, G. A., Sepehrnoori, K., Tilburg, C. E. & Jackson, R. E. (1995) Partitioning tracer tests for detection, estimation, and remediation performance assessment of subsurface nonaqueous phase liquids. *Wat. Resour. Res.* **31**, 1201–1211.

Valocchi, A. J. (1985) Validity of the local equilibrium assumption for modeling sorbing solute transport through homogeneous soils. *Wat. Resour. Res.* **21**, 808–820.

MOBILIZATION AND ENTRY OF DNAPL POOLS INTO FINER SAND MEDIA BY COSOLVENTS: TWO-DIMENSIONAL CHAMBER STUDIES

Michael E. Van Valkenburg[1*] and Michael D. Annable[2]

Submitted to:
Journal of Contaminant Hydrology

July, 2000

* Corresponding Author; Department of Chemistry, 2355 Fairchild Dr, Suite 2N225, USAF Academy, CO 80840-6230 (Phone (719) 333-4205, Fax (719) 333-2947, e-mail mike.vanvalkenburg@usafa.af.mil)

1 Department of Chemistry, United States Air Force Academy, Colorado Springs, CO 80840

2 Department of Environmental Engineering Sciences, University of Florida, Gainesville, FL 32611

MOBILIZATION AND ENTRY OF DNAPL POOLS INTO FINER SAND MEDIA BY COSOLVENTS: TWO-DIMENSIONAL CHAMBER STUDIES

Abstract

Two-dimensional chamber studies were conducted to determine qualitative and quantitative performance of cosolvents targeted at pooled DNAPL (perchlorethylene, PCE) residing above a finer capillary barrier. Downward mobilization of DNAPL, up gradient along an overriding cosolvent front, was observed. This produced significant pooling above a finer layer that in some cases lead to entry into the finer capillary barrier beneath. Entry pressure calculations using physical and hydrogeological parameters provided an excellent prediction of breakthrough of DNAPL into the capillary barrier. Calculations predict approximately 0.5 meters of DNAPL would be necessary to enter a Beit Netofa clay, under extreme cosolvent flooding conditions. Gradient injection of cosolvent did not appear to provide any benefit because of the rapid rate if interfacial tension decrease compared to the rate of DNAPL solubilization. Use of a partitioning alcohol (tertiary butyl alcohol) resulted in DNAPL swelling and reduced entry into the capillary barrier. However, the trapping of PCE-containing flushing phase could potentially lead to longer remediation times.

Introduction

In-situ flushing remediation is currently a developing method for removing source-zone contamination. Whether applying surfactants, alcohols, or oxidants as injection fluids to accelerate the displacement, dissolution, or chemical transformation of contaminants, control of contaminant movement is critical. Evaluation of contaminant control is vital during the project planning and proposal stages. Proposals to site managers are more likely to gain approval after sound recommendations and strategies for contaminant control have been outlined. The basis for these *a priori* strategies often include theoretical chemical and hydrologic calculations or modeling, but the most

valuable input arises from field experience. Test cells constructed to study flushing technologies, including one at Hill Air Force Base (AFB), Utah (Annable et al. 1996) and one currently being studied at Dover AFB, Delaware provide excellent opportunities from which to draw conclusions and apply them to the "open-field" real remediation situation. However, an important experimental method that lies between these two study options in scale is the use of a 2-dimensional (2-D) chamber or aquifer model to study the movement and remediation processes of these flushing chemicals. A review of 2-D laboratory experiments can be found in Chevalier and Peterson (1999). 2-D chambers provide not only the horizontal dimension to simulate the hydrologic flushing process involving injection and extraction wells, but the added vertical dimension. This vertical dimension becomes important when studying non-aqueous phase liquids (NAPLs) that are much lighter or heavier than water or the flushing agent. In the case of dense non-aqueous phase liquids (DNAPLs), movement downward and out of the hydrologic control of the remediation flow paths is undesired.

NAPL migration in subsurface environments is affected by the: (1) volume of the NAPL released; (2) area of infiltration; (3) time duration of the release; (4) properties of the NAPL; (5) properties of the media; and subsurface flow conditions (Feenstra and Cherry 1988). A cross-sectional schematic of the distribution of organic chemicals resulting from a release of a DNAPL is depicted in Figure 1. DNAPLs percolate through the unsaturated (vadose) zone due to gravity effects leaving behind trapped DNAPL globules and volatilized constituents in the gaseous phase. Some lateral spreading occurs due to the effect of capillary forces (Schwille 1988) and due to slight media heterogeneity in the vertical dimension (layering). If enough DNAPL is introduced to the

medium it can move through the saturated zone leaving behind trapped globules (residual saturation). This entrapment process is due to interfacial tension (IFT) effects and thus capillary forces. The residual DNAPL can solubilize into water moving through the saturated zone forming a contaminant plume down gradient. Due to their low water solubility, DNAPLs can serve as a long-term source of groundwater contamination. Eventually, large DNAPL volumes can migrate downward to a region that has lower permeability than the zone in which it resides. At this point, it spreads horizontally on top of this finer medium until mechanical equilibrium conditions are achieved. This resulting zone of contamination consists of high saturations of DNAPL (approximately 50% of the pore volume), and is considered "pooled" on top of the finer, NAPL capillary barrier.

The process leading to DNAPL pools has been described by McWhorter and Kueper (1996). In a pool, the maximum capillary pressure occurs at the base of a DNAPL pool. This pressure is directly proportional to both the pool thickness and the density difference between the DNAPL and aqueous phases. The DNAPL accumulates above the capillary barrier since the capillary pressure due to the pool does not exceed the displacement pressure of the capillary barrier. The requirements for entry of the DNAPL into the less permeable capillary barrier is given by (McWhorter and Kueper 1996),

$$\Delta\rho g T = p_d \tag{1}$$

where $\Delta\rho$ [ML^{-3}] is the density difference between the DNAPL and the fluid resident in the smaller pores below, T is the pool thickness [L], g is acceleration of gravity [LT^{-2}],

and p_d is the displacement pressure of the capillary barrier [$ML^{-1}T^{-2}$]. Converting pressures to head leads to the following equation,

$$\frac{\Delta\rho T}{\rho_{dnapl}} = h_d^{rs/dnapl} \tag{2}$$

where ρ_{dnapl} is the density of the DNAPL upon entering the capillary barrier and $h_d^{rs/dnapl}$ is the displacement head of the capillary barrier when DNAPL is displacing resident solution fluid filled pores. During cosolvent flushing, the resident solution (*rs*) may become cosolvent. This value, $h_d^{rs/dnapl}$, can be determined following methods in McWhorter and Kueper 1996,

$$h_d^{a/w}\frac{\gamma_{rs/dnapl}\cos\theta_{rs/dnapl}}{\gamma_{a/w}\cos\theta_{a/w}} = h_d^{rs/dnapl} \tag{3}$$

where $h_d^{a/w}$ is the air-water displacement head and θ is the contact angle of the fluid pair. Note that the ratio of contact angles is approximately unity (McWhorter and Kueper 1996). This is thought to not contribute significantly to these estimations and is therefore excluded from further analysis. However, as complexity is introduced by in-situ flooding chemicals and their associated chemical and physical properties, the movement of contaminant becomes more difficult to predict and these factors may need to be considered.

Prediction of DNAPL mobilization into and through an underlying finer medium is necessary before a specific flushing strategy is employed, or even proposed at a remediation site. Cosolvents, such as ethanol (C_2H_5OH), are used to increase the rate of dissolution of the contaminant pool and associated residual zones into the flushing alcohol mixture (Augustijn et al., 1994). However, concurrent interfacial tension

reduction can become severe, especially at high alcohol volume fractions, allowing DNAPL to mobilize out of pores it was previously entrapped in and enter smaller pores. If the IFT and gravitational forces are severe enough, this may allow the DNAPL to enter the smaller pores of the underlying layer (capillary barrier) upon which it originally was pooled. Predictions of the maximum pool height required to prevent entry into a capillary barrier, under specific flushing regimes would be beneficial. Thus, a systematic approach of determining DNAPL entry into an underlying capillary barrier, using a 2-D chamber setup with known media sizes, is warranted. Basic force balance calculations exist to quantitatively predict whether entry into smaller pores is possible. Visualization and thus verification of this is not possible in the field, so use of a 2-D chamber is justified.

Numerous studies exist that use 2-D chambers and focus on flow instabilities resulting from density and viscosity differences, especially in petroleum recovery journals (e.g., Morrow and Songkran 1981). Other studies on effects of heterogeneities and flow instabilities are Kueper and Frind (1988), Held and Illangasekare (1995), and Illangasekare et al. (1995). Studies on dissolution of pooled DNAPLs was investigated by Johnson and Pankow (1992). Grubb et al. (1996) investigated the removal of a light NAPL (LNAPL), toluene, using a combined pure and 50/50 (vol. %) ethanol-water flooding strategy. Downward mobilization of the LNAPL below the lighter overriding flushing phase eventually resulted in trapped LNAPL. The use of the heavier 50/50 mixture subsequently removed this zone via solubilization and physical displacement. Pennell et al. (1996a) qualitatively studied the dissolution of PCE and the downward movement of a DNAPL pool in sand and aquifer material while flushing with surfactant

solutions. They concluded that mobilization of DNAPLs via surfactant flooding should be avoided and dissolution of DNAPLs should be the primary removal mechanism.

In summary, little research has been published on experiments to predict and verify mathematical relationships describing DNAPL entry into finer media under cosolvent flooding regimes. This was therefore the focus and objective of this study. In addition, the effects of enhancements using gradient injection and swelling alcohols were assessed.

Materials and Methods

A 2-dimensional (2-D) chamber, previously constructed by Jawitz et al. (1998a), was used for this study. The overall dimensions of this box are 61 cm in width, 39.4 cm tall and 1.4 cm thick. The inlet and outlet wells were square aluminum tubes, with 0.05 mm slots spaced at 5 mm intervals. The bottom of the box was the same aluminum tubing, without any perforations. Together, this aluminum square tubing made up both sides and the bottom of the 2-D chamber. Clear glass, 0.5 cm thick, was used for the sides of the chamber. The 1.4 cm thickness of the 2-D chamber was over 16 times the largest grain size used in these studies. This thickness was chosen by Jawitz et al. to minimize wall effects (1998a).

General 2-D Chamber Packing Procedure

Nanopure water, adjusted to pH 8, was added to the box and the box leak checked. The pH adjustment was necessary to minimize adsorption of the Brilliant Blue FCF dye (Erioglaucine A, CAS 94082765, Fluka Chemical, Ronkonkoma, New York) to sand used in these studies (Jawitz et al. 1998a). Flury and Fluhler (1995) found that as pH increases Brilliant Blue FCF dissociates to a mono- and eventually to a bivalent anion

(pK_{a1} = 5.83 and pK_{a2} = 6.58). This pH adjustment ensured that the dye would be in the bivalent anionic form, which minimized adsorption to the sand used. Brilliant Blue FCF has low adsorption (K_d of 0.19 dm^3/kg) in soil with low organic carbon content (0.43%) and a soil pH of 5.8 (Flury and Fluhler 1995). Similar to the Jawitz et al. (1998a) study and the study of Schincariol and Schwartz (1990), dye traveling only in the first few grain diameters against the glass would appear lighter in dye color than the bulk front. Thus, movement of the dye through the 2-D chamber can be assumed to be entirely due to bulk flow.

Number 20-30 Ottawa Sand (U.S. Silica) was used as the background media into which a single, 1-cm thick, layer of other sand was introduced. This media was sieved and used with no further treatment. The coefficient of uniformity is estimated to be 1.2 and the manufacturer reported the roundness and sphericity coefficients of 0.8-0.9 for this sand (Grubb et al. 1996). The sand can therefore be classified as rounded-subrounded. This sand was added to the box underwater in a layered fashion (each layer approximately 2 cm thick), with vibration applied at the end of each layer addition. The subsequent layer was then added and mixed with the upper portions of the previous layer using a rod to minimize layered effects. This was continued to a depth of 3.3 cm from the bottom of the box. Then a 1 cm thick lens of finer media (this media size varied) was added. Application of this finer media within 5 cm of either well screen was avoided due to possible grain loss through the well screen, especially for the finer media. Upon vibration, this settled and spread to a distance of approximately 3 cm from either well. Again, the background 20-30 medium was added in layers, vibrated, and mixed up to a total depth of 11 cm. This packing procedure was repeated for each scenario to provide

as much hydraulic and media consistency possible. This packing method resulted in a pore volume of 325-330 ml, and a porosity of 0.35. These figures were constant over all packing combinations as the capillary barrier contributes little to the total 2-D chamber parameters.

The sand sizes used for the 1-cm thick sand lenses (Sieve nos. 100-140; 60-70; 40-50; and 30-40) were further characterized to determine fluid displacement pressures needed to predict DNAPL mobilization through capillary barriers. Air-water displacement pressures for the sand media were determined using Tempe Cell (Soil Moisture Equipment Corp., Santa Barbara, California) desaturation profiles. The desaturation data were fitted with both Brooks and Corey (1964) and van Genuchten (1980) parameters. Curve fitting was accomplished by minimization of the sum of squares of the differences between the data and the fitted prediction. Spreadsheet solver macros were use to iterate and arrive at a minimized error. The parameters resulting from these curve fits are presented in Table 1 along with media particle size ranges.

Dye Tracer Displacement

To determine the hydrodynamic characteristics of the 2-D flow system, and to qualitatively visualize the baseline flow patterns, 30-50 ml of the Brilliant Blue FCF dyed water (approximately 50 mg/L) was injected into a colorless, water-resident medium at a flow rate of 3.5 ml/min (5.0 ml/min for Runs I and II). This was subsequently flushed through the box with colorless water under controlled hydraulic conditions, similar to those used during actual flushing runs. This concentration of dye results in a density increase of 0.005% (Jawitz et al. 1998a). A flow rate of 3.5 ml/min equates to a horizontal flow velocity of 9.7 m/day (13.9 m/day for Runs I and II). For all

experiments, the profile of the dye front was traced at approximately 5 minute intervals, as the front moved across the flow chamber. As in Jawitz et al. (1998a), the mixing zone at the interface between the colorless resident fluid and the dyed displacing fluid was generally less than 1 cm wide. In situations when the mixing zone had a width of more than 1 cm, the location of the front was concluded to be at the center of the visible mixing zone. This tracer displacement process was accomplished to determine background flow profiles to qualitatively compare them to profiles with DNAPL pools present.

DNAPL Introduction

HPLC grade PCE (CAS 127-18-4), colored red with Oil-red-O dye ($\leq 1\times10^{-4}$ M, CAS 1320-06-5) was injected into the sand media approximately 1 cm above the fine layer, using a 16 gauge long stainless steel needle, attached to a 20 ml glass syringe. Effects of the dye on important physical characteristics of DNAPLs are not significant at this level of concentration (Pennell et al., 1996b). The rate of injection varied due to difficulties with PCE traveling back up the needle to the sand surface. This was minimized by vibration of the media around the needle after insertion. However, DNAPL zone shapes and saturations were reproduced in a visually consistent manner via this method. Generally, 2.7 to 3.5 ml of PCE were injected and remained in the media. A typical box configuration prior to flooding is shown in Figure 2.

Hydraulic Controls During 2-D chamber Experiments

The influent was maintained at constant head with a Marriott bottle, with the head adjusted to maintain the water table right at the top surface of the sand media. The effluent flow was maintained by a Master Flex pump at 3.5-5.0 ml/min. The flow rate

was chosen to avoid air intake in the extraction tube and a minimum of 5 cm of water in the well. The influent line was split by a nylon T-valve to allow for easy switching of injection fluids.

At least one pore volume of background water was passed through the media to achieve steady flow. 30 to 50 ml of dyed flushing phase was then injected with a Harvard 22 syringe pump at a flow rate equal to the effluent rate. This was done to provide visual detection of flushing front and override characteristics. Flow was then switched over to non-dyed flushing fluid. The alcohol used as the cosolvent in all flooding studies was reagent grade alcohol (Fisher Scientific; 90.4 vol. % ethanol, 4.6% methanol, 5.0% isopropanol). The reagent grade alcohol was assumed to have the same properties as pure ethanol (Grubb et al. 1996). Isopropanol and methanol should have minor and compensating effects on mixture equilibria (Sorenson and Arlt 1980). Tertiary butyl alcohol (TBA) was obtained from Fisher Scientific (chromatography grade, 99%). An initial solution of 95/5 vol % TBA/water was made to avoid freezing of the stock solution at fluctuating storage temperatures. Subsequent solutions used in the study were made by appropriate volumetric mixing with Nanopure water.

Results and Discussion

Three types of studies were conducted. Step inputs of reagent alcohol (causes essentially no swelling of the PCE), gradient input of reagent alcohol, and step inputs of tertiary butyl alcohol (TBA), a PCE swelling alcohol. All experiments were conducted at a room temperature of 23 ± 1°C. Between each run that used the same 2-D chamber packing, at least five pore volumes of water were flushed to remove all quantities of

alcohol from the sand media. Run summaries are presented in Table 2 and discussed sequentially below.

Reagent Alcohol Experimental Results

100-140 Fine Layer

Step input of 100% alcohol. Flushing with 100% reagent alcohol was conducted to provide a worst-case mobilization scenario in terms of this media combination. The DNAPL volume injected was 2.7 ml (similar distribution as shown in Figure 2). At roughly one-third of a pore volume, downward migration of the up gradient portions of the DNAPL zone was noticeable, as IFT's were reduced and mobilization of high saturations was possible. Solubilization diminished the size of the DNAPL zone and light red 'streams' developed down gradient. This reddish color was due to slight partitioning of the Oil-red-O dye into the flushing phase. Partitioning of the dye was enhanced likely due to the high amount of PCE solubilized into the alcohol (>200,000 mg/l). This "banding of dye" has also been seen in one-dimensional sand columns using both alcohols and surfactants (Van Valkenburg, 1999, Pennell et al., 1996b) and generally occurs when 80 to 85% alcohol is used as the flushing phase. Due to dispersion, these percentages can occur ahead of the 100% alcohol front.

By 0.62 PV into the flush, further migration of DNAPL formed a distinct pool on top of the finer 100-140 layer ranging from 0.4 to 0.5 cm in thickness (Fig. 3, schematic of DNAPL collapse into a pool)). This thin pool was most prevalent ahead of the original DNAPL area and then spread down gradient as a function of time. As the PCE-

alcohol IFT was decreasing, DNAPL from up gradient portions of the initial pool (above residual saturations) mobilized quickly in the coarse medium, in a direction along the sloping alcohol front and eventually into the capillary barrier. This was noticed as early as 0.5 PV into the run. The sloped nature of the cosolvent front was a result of the alcohol/water density difference and the reduction in relative permeability that occurs when the DNAPL accumulates at higher saturations along lower portions of the sloping front. The mobilization occurred in a very thin stream, most likely due to the very sharp interface between the displacing alcohol and the resident water, which is on the order of tenths of centimeters (Grubb et al. 1996). Similar observations have been made by others (Grubb et al. 1996; Pennell et al. 1996b) where DNAPL flows downward due to the higher density, preferentially through regions with reduced IFT and thus can flow back against hydraulic gradients. Further breakthrough of PCE into the capillary barrier occurred 36-38 cm from the injection well at 0.77 PV. This occurred when the alcohol front had sufficiently moved into the capillary barrier underneath the PCE, allowing entry into the finer pores, and ultimately through the finer layer.

Step input of 80% alcohol. To decrease the solubilization capacity of the flushing phase and still have low IFTs that could potentially cause mobilization, 80% reagent alcohol was used for the Nos. 100-140 capillary barrier. Here, 3.2 ml of PCE was injected as described in procedures above. No entry of DNAPL into the capillary barrier was observed during this entire run. Very clear progression of pool collapse occurred eventually resulting in an extended pool thickness of 0.2 to 0.4 mm. The spreading of the pool occurred only down gradient of the injection zone. No up gradient spreading of the DNAPL was observed.

60-70 Fine Layer

Step input of 80% alcohol. Based on the lack of entry into the 100-140 layer using an 80% alcohol step input, the next scenario chosen was to flood using the same flushing fluid, but decrease the contrast between the bulk and capillary barriers from Nos. 20-30 vs. 100-140 to Nos. 20-30 vs. 60-70 mixture. 4.5 ml of PCE was injected for this run. Collapse of the pool occurred with up gradient mobilization on top of the finer 60-70 layer (Fig. 4). The pool spread approximately 6 cm toward the injection well and 25 cm down gradient from the injection zone, eventually draining off the edge and flowing vertically downward due to density differences. This occurred only in this scenario; most likely due to the increased amount of PCE injected (4.5 ml). However, no entry of free phase DNAPL was observed into the capillary barrier (Fig.4).

40-50 Fine Layer

Background dye displacement after DNAPL injection. Due to the lower contrast between the background and capillary barrier media (now 20-30 vs. 40-50), a dye displacement was conducted to understand the flow characteristics of the 2-D chamber. A total of 3.3 ml of PCE was injected for this run. Significant flow of the displacing dye was observed underneath the DNAPL pool, within the capillary barrier, which was not observed in previous runs. The permeability of the aqueous phase in the 40-50 layer was likely greater than the aqueous phase permeability of the DNAPL saturated zone. This caused significant flow of dye through the capillary barrier, underneath the DNAPL pool, instead of solely override as observed in previous scenarios, with finer, less permeable media. Fronts in the capillary barrier lagged the front in the 20-30 media only by 0.1 PV.

Step input of 80% alcohol. The DNAPL pool was then removed using a step-input of 80% reagent alcohol. Collapsing of the DNAPL pool occurred causing the PCE pool to move approximately 4.2 cm up gradient. The pool also migrated a total of 17.5 cm down gradient. No entry of a separate phase occurred into the capillary barrier, although, based on the presence of dye, solubilized PCE did breakthrough into the capillary barrier and into the coarse layer below. However, no free phase PCE was generated below the capillary barrier.

30-40 Fine Layer

Step input of 80% alcohol. Entry of PCE into the 30-40 fine layer occurred in three different locations. Two up gradient (1.8 cm and 6.5 cm) from the injection zone and one down gradient (6.4 cm) (see schematic in Fig. 5 and photo in Fig. 6). This movement through the capillary barrier, based on visual observations, was completely different from the solubilized movement discussed in the previous runs. This true mobilization of DNAPL as a separate phase occurred at one or two pores locations and migrated downward due to density differences.

Step input of 70% alcohol. Similar to the 80% alcohol run, PCE entry occurred in three different locations. However, only one was up gradient (3.3 cm) from the injection zone and two down gradient (7.4 cm and 10.9 cm). DNAPL mobilization was very similar to that of Run 7. One area of breakthrough into the capillary barrier matched exactly with one from the previous run, indicating the possibility of one preferential channel at that location for this packing.

"Multi-Step input" of 50% to 60% alcohol. As the injection alcohol concentration decreases, the solubilizing capacity decreases, and longer times are

required to remove the DNAPL. However, initial up gradient mobilization of DNAPL in the coarser layer, from the up gradient side of the injected pool, occurred approximately at the same run times, during both the 80% or 50% alcohol step input. This indicates that the impact of IFT reduction is manifested earlier than the reduction in saturation due to solubilization. However, once immobilized on top of the capillary barrier, the IFT reduction is not severe enough within the smaller pores, and thus the capillary pressure within these pores is too great for the DNAPL to enter. Similar to previous runs, the lateral spreading of the PCE resulted in a DNAPL layer of 0.4 to 0.5 cm in thickness. No entry into the 30-40 fine layer occurred during this run. After 1 PV of 50% alcohol the flushing concentration was step increased to 60% and flushed for another pore volume. This was done to determine if this slowly solubilizing DNAPL pool could enter the capillary barrier. This flushing was continued until this injected fluid saturated the capillary barrier and thus a similar prediction of DNAPL entry could be estimated. Entry did not occur for this mixture. This additional pore volume of 60% alcohol reduced DNAPL saturation further due to slow solubilization. A final step increase to 80% alcohol was made to determine if the reduced saturation and thickness of DNAPL on top of the capillary barrier could be mobilized with the new 80% alcohol flushing mixture. No mobilization was seen during this step increase as well. However, due to a log-linear increase in solubilization of the leading edge of the collapsed DNAPL pool, it is likley that physical parameters of the fluids at the capillary barrier interface never approached those which might have caused mobilization.

Gradient Injection (10-90%) of Alcohol

In an effort to assess the potential to reduce mobilization and entry into the capillary barrier, a gradient alcohol injection test was conducted. In this experiment, a DNAPL volume of 3.1 ml was injected into the background 20-30 medium, resting on a 60-70 medium. A gradient injection from 10% -90% (v/v) alcohol was applied over 1 PV into the 2-D chamber, using a Shimadzu HPLC pump with a solvent mixer. During the gradient injection, a Brilliant Blue dyed solution was added at 58% alcohol and discontinued at 75% alcohol in order to observed the front progressions. Thus, a blue band of alcohol phase represented a concentration range from 58 to 75% alcohol. Typical collapsing of the DNAPL zone was observed, with the most significant movement occurring under an alcohol concentration of approximately 50% by volume. Again, horizontal spreading was observed up gradient, as well as down gradient, from the injection zone as shown in Figure 7. Light red bands of PCE-containing alcohol entered into the finer media, moved through the layer and then exited into the coarser medium below where, due to density induced override, lower alcohol concentrations were present. This resulted in PCE coming out of the flushing phase and reestablishment of a separate DNAPL phase (see Fig. 7). This suggests that remedial designs which completely flood underneath the contaminant zone and supporting capillary barrier with 100% alcohol may be beneficial. Pre- established presence of pure alcohol would severely minimize this regeneration of a new DNAPL phase. This may be accomplished in the field using vertical circulation wells for alcohol delivery.

An observation from the gradient flood was that interfacial tension quickly decreased during gradient injection, yet the ability of the cosolvent to solubilize PCE was

not keeping pace with the decreasing IFT. In the case of a step input, although IFTs are very rapidly reduced, the capacity of the pure alcohol solution to solubilize PCE overwhelms the IFT reduction. Essentially, the DNAPL saturation reduction is faster due to solubilization and quick enough to prevent mobilization.

Two-Dimensional Studies with Tertiary Butyl Alcohol

TBA was chosen to evaluate its effects on DNAPL solubilization, mobilization, and breakthrough behavior in the 2-D environment used earlier. TBA partitions significantly into the PCE causing the DNAPL to swell, thereby reducing its density. This process can influence potential mobilization and entry into the capillary barrier. The experimental setup, flow rates and head gradients were kept similar to those described above for the reagent alcohol studies.

Step input of 30% TBA: 30-40 capillary barrier. Dyed PCE (3.3 ml) was injected on top of the finer 30-40 layer. A step input of 30% v/v of TBA (equilibrated IFT with PCE of approximately 5.2 dynes/cm, compared to 4.5 dynes/cm for 60% v/v ethanol) was applied to the chamber, removed at a flow rate of 3.5 ml/min, with the influent head maintained at the top surface of the sand medium. Entry of DNAPL into the capillary barrier occurred at 0.47 PV as three fingers slowly progressed into the capillary barrier. Progression of DNAPL through the capillary barrier was noticeably different than that observed in the ethanol experiments. Movement of the DNAPL fingers was slower in the downward direction and more lateral spreading occurred, most likely due to the lower density of the DNAPL (approximate equilibrated density of 1.53 g/ml) caused by the partitioning of the TBA cosolvent into the PCE phase. Similar

lateral spreading of free phase DNAPL was observed in the background 20-30 layer, both behind (up gradient) and in front (down gradient) of the original PCE pool.

The volume of the PCE in the DNAPL pool after contact with the TBA solution occupied a larger volume than in previous reagent alcohol runs. Even at larger runs times when significant solubilization had occurred, the pool volume remained larger than expected or observed in the reagent alcohol experiments. This was again due to the swelling of the PCE from the partitioning of the TBA (approximately 15% swelling based on equilibrium studies: see Van Valkenburg, 1999).

Step input of 40% TBA: 100-140 capillary barrier. The 2-D chamber was repacked with Nos. 100-140 sand. This was chosen as the capillary barrier to avoid entry into this finer layer. An increase in volume fraction of TBA was applied to determine swelling effects of a higher percentage of TBA while maintaining all of the DNAPL above the capillary barrier. This scenario would more closely represent those experienced in horizontal flooding field situations, where even a more impermeable clay layer is supporting a pooled DNAPL.

A volume of 3.2 ml of dyed PCE was injected onto the 100-140 capillary barrier. The step input of 40% TBA was applied as previously described. Significant differences were observed in pool properties, compared to the 30% TBA run. No entry of DNAPL into the capillary barrier was observed during this run. All DNAPL remained above the capillary barrier as desired. Down-gradient movement of DNAPL was observed that was different from the reagent alcohol runs. This movement of DNAPL had more of a horizontal characteristic, due to a lower density contrast, compared to the reagent alcohol studies. The pool appeared to mobilize with a large horizontal component until the

density contrast was great enough to begin downward movement. This was apparently due to the transition from water-diluted pores below the DNAPL to alcohol saturated pores that increase the density contrast and promote downward mobilization. In the process of this "two-step" mobilization of DNAPL, quantities of injected cosolvent became trapped and isolated on top of the capillary barrier (see Figure 8). These pores required a significant amount of time to flush due to the low relative permeability to the wetting phase around these areas. This can possibly lead to long tailing of PCE concentrations during the removal process.

The swelling of the DNAPL pool was definitely observable compared to reagent alcohol experiments (Fig. 10 vs. Fig 3). Batch studies with 10 ml of 40% TBA/H_20 and 10 ml of PCE resulted in an equilibrated DNAPL volume of 13.5 ml, indicating a swelling of approximately 35% (Van Valkenburg, 1999). Thus, the 3.2 ml originally injected could potentially swell to a volume of 4.3 ml. The volume shown in Figure 10 is difficult to estimate due to the variability of DNAPL saturation. However, a rough estimation of the entire bulk volume of the pool is 24 cm^3, which using a porosity of 0.35, leads to a pore volume of 8.4 cm^3. Assuming 50% DNAPL saturation would result in a final estimated DNAPL volume of 4.2 ml.

Prediction of Mobilization into Capillary barriers

To evaluate results and determine if the qualitative nature observed in this set of experiments matched what could be estimated based on porous media and fluid properties used in each scenario, calculations based on air-water displacement pressures for each media used were made. DNAPL entry values were calculated for each scenario

based on the ratio of IFT of the fluids and the IFT between air and water measured with a du Nuoy ring tensiometer (72.1 dynes/cm). This then incorporates pore size into the calculation based on this entry value. Entry of DNAPL into the finer media can only occur if the pressure head caused by the height of the DNAPL pool can overcome the capillary head of the pore below it in the capillary barrier. This calculation assumes that fluids have reached equilibrated values in the 2-D chamber at the time of possible entry and ignores pressures caused by fluid flow. Although these parameters may approximate *in situ* 2-D chamber values, differences would be slight and not significant to these predictions. For comparative purposes, the results of these calculations are shown in Table 3.

Except for runs V and X, all calculations accurately predict whether mobilization into the capillary barrier occurred. However, runs V and X cosolvent/DNAPL entry pressures into the finer medium ($h_d^{cs/dnapl}$ = 0.38 cm and $h_d^{cs/dnapl}$ = 0.91cm) are well within reasonable errors associated with estimating DNAPL depth (h^{dnapl}) alone. DNAPL pool depths were estimated visually and were clear in the 20-30 sand but may be very difficult to observe in more complex soils. These results indicate that breakthrough of PCE/DNAPL is a function of the medium displacement pressure and the solution that resides in the pores into which the DNAPL can enter, confirming the relationship presented in McWhorter and Kueper (1996). Thus, it is critical to determine the displacement pressure of the medium and the height of DNAPL expected to pool. From the results presented, a guideline to avoid entry of a PCE-ethanol equilibrated DNAPL into finer layers is a predicted $h_d^{cs/dnapl}$ exceeding a value of 0.4 to 0.5 cm. For reference, data taken from van Genuchten (1980) for a Beit Netofa clay is used to calculate a

corresponding entry pressure under typical cosolvent flushing conditions to remove a DNAPL like PCE. Assuming conditions comparable to experiment number one with 100% reagent grade alcohol (Table 2), approximately 0.5 meters of DNAPL would be required to enter the Beit Netofa clay. While this calculation greatly simplifies the process, it provides a measure of conditions expected for clays.

Conclusions

Removal of pooled DNAPL (PCE) on top of finer, less permeable layers during 2-dimensional chamber cosolvent floods, presents interesting qualitative conclusions. These can be supported semi-quantitatively with pore force-balance calculations.

Pooled DNAPL will spread laterally along a capillary barrier under reduced IFT conditions, and if local saturations are high enough, can mobilize downward and up gradient along overriding cosolvent fronts. This can cause significant build up of DNAPL on the lower confining layer, up gradient from a pooled DNAPL system. This allows increased exposure to lower IFT cosolvent solutions that may permeate into the capillary barrier. Entry into capillary barriers can occur. In general, the most significant production of DNAPL through any fine layer in these studies was actually up gradient from the source zone. In this region, cosolvent had displaced water in the capillary barrier reducing the IFT promoting mobilization.

Gradient injection to remove DNAPLs does not appear to provide significant benefit over step inputs. Override characteristics are not improved significantly. Furthermore, in these experiments, interfacial tension between injected fluid and DNAPL decreases almost instantaneously compared to removal of DNAPL due to solubilization. Movement of DNAPL down onto the capillary barrier occurs well before significant

reduction of saturations due to solubilization. Here, solubilization of DNAPL becomes even less efficient due to significantly reduced contact area.

Use of the partitioning alcohol (TBA) in the 2-D setup presented interesting qualitative observations. Significant swelling of the PCE resulted, especially for the 40%v/v TBA cosolvent step-input. This swelling of the DNAPL is caused by TBA partitioning and subsequently delays any downward mobilization due to resulting density decreases. This helps to avoid breakthrough of DNAPL into finer zones, but can also lead to the PCE enriched cosolvent becoming trapped on top of capillary barriers. This effect is due to the decreasing density of the flushing fluid after the initial front. At that time, the DNAPL phase becomes denser and quick movement downward occurs, trapping PCE enriched cosolvent behind it. Due to reduced permeability and therefore flushing efficiency, this volume of cosolvent can lead to increased tailing of contaminant removal and increase remediation times. Further study into its avoidance is warranted.

Entry pressure calculations using the physical and hydrogeologic parameters of the chemical phases and media, respectively, predicted breakthrough of PCE into the finer media in excellent fashion. Breakthrough of PCE under typical ethanol flooding conditions (80% v/v) can generally be assumed to occur in homogeneous sand media when $h_d^{cs/dnapl} < 0.5$ cm. Basic calculations for a Beit Netofa clay estimated that approximately a half a meter worth of equilibrated PCE-type DNAPL would have to accumulate before entry into the clay pores under extreme cosolvent flooding conditions.

Acknowledgements

We would like to than the USAF, Air Force Institute of Technology (AFIT) and the USAF Academy for sponsorship of Mike Van Valkenburg's Ph.D. program. We are grateful to committee members Dr. Joe Delfino, Dr. Kirk Hatfield, Dr. Robert Kennedy, and Dr. Bill Wise. Also a large thank you to now Dr. Jim Jawitz (University of Illinois-Chicago) for the use of his "2-D box" and great help in discussions.

Table 1 – Summary of desaturation profile curve fitting parameters. Beit Netofa Clay values (α, n, and m) are from van Genuchten (1980). Pore radius for the clay is taken from Wise (1992).

Maximum particle diameter (mm)	Minimum particle diameter (mm)	Sand Mixture (Sieve No.)	Brooks-Corey parameters			van Genuchten parameters			
			λ	Air entry head, (cm H_20)	Average pore radius (mm)	α (cm^{-1})	n	m	Average pore radius (mm)
0.841	0.595	20-30	4.67	7.02	0.174	0.11	11.0	0.91	0.166
0.595	0.420	30-40	3.22	10.6	0.108	0.075	10.2	0.90	0.115
0.420	0.297	40-50	4.33	18.7	0.0635	0.045	14.0	0.93	0.0659
0.250	0.210	60-70	9.33	26.9	0.0499	0.034	25.3	0.96	0.0504
0.149	0.105	100-140	9.99	50.7	0.0270	0.019	16.4	0.94	0.0277
		Beit Netofa Clay				0.00152	1.17	0.15	0.00019

Table 2. Summary of Experimental Runs in 2-Dimensional Box Studies

Run Number	Capillary barrier Sieve Size (No.)	Volume PCE Injected (ml)	Flushing Mode	Alcohol Concentration (%v/v)	Entry into capillary barrier?	Remarks
I	100-140	2.7	Step	100	Yes[(1)]	(1) along front only
II	100-140	3.2	Step	80	No	
III	60-70	4.8	Step	80	No	
IV	60-70	3.1	Gradient	10 - 90 (1 PV)	No[(2)]	(2) PCE did appear below capillary barrier
V	40-50	3.3	Step	80	No	
VI	30-40	3.9	Step	80	Yes	
VII	30-40	3.0	Step	70	Yes	
VIII	30-40	3.2	Multi - Step	50; 60; 80 (1 PV ea)	No; No; No[(3)]	(3) Reduced DNAPL Saturation
IX	30-40	3.3	Step	30 TBA	Yes	Movement of PCE more lateral due to lower density
X	100-140	3.2	Step	40 TBA	No	Significant swelling

Table 3 – Results of globule force balance calculations. Mobilization of globule is predicted if $h_{dnapl} > h_d^{cs/dnapl}$. Permeability of 20-30 medium measured to be 6.35E-7 cm^2. Fluid property values are measured post equilibrium (Van Valkenburg, 1999). These initial volume fractions are used to help the reader associate performance, based on potential initial field conditions.

Run Number	Fine Layer (Sieve #)	Flushing Mode	%v/v Alcohol [a]	$\gamma_{cs/dnapl}$ (dynes/cm)[b]	Solubility (g/L)	ρ_{dnapl} (g/ml) [b]	ρ_{cs} (g/ml)[b]	$\Delta\rho$ (g/ml)	$h_d^{a/w}$, (cm)	$h_d^{cs/dnapl}$, (cm) required	Exp. h_{dnapl} (cm)	Did Entry Occur?
I	100-140	Step	100	~0.5	Misc.	1.55	1.01	0.54	34	0.13	0.4	Y
II	100-140	Step	80	2.1	202	1.55	1.01	0.54	34	0.53	0.4	N
III	60-70	Step	80	2.1	202	1.58	0.93	0.65	26.8	0.54	0.4	N
IV	60-70	Gradient	10-90	variable [c]	-	1.58	0.93	-	26.8	-	0.4	N
V	40-50	Step	80	2.1	202	1.58	0.93	0.65	18.6	0.38	0.4	N
VI	30-40	Step	80	2.1	202	1.58	0.93	0.65	10.6	0.21	0.4	Y
VII	30-40	Step	70	3.2	78.4	1.59	0.91	0.68	10.6	0.35	0.4	Y
VIIIb	30-40	Step	60	4.5	30.9	1.6	0.92	0.68	10.6	0.49	0.4	N
VIIIa	30-40	Step	50	6.3	11.3	1.61	0.93	0.68	10.6	0.67	0.4	N
IX	30-40	Step	30 TBA	5.2	-	1.53	0.99	0.54	10.6	0.41	0.4-0.8	Y
X	100-140	Step	40 TBA	3.9	-	1.46	0.98	0.48	34	0.91	0.5-1.0	N

[a] Alcohol % values are prior to equilibration with PCE.

[b] Densities and IFTs used in these calculations were determined by batch experiments reported in Van Valkenburg, 1999.

[c] IFT's at 20% Alcohol = 18 dynes/cm, at 40% alcohol = 8.5 dynes/cm.

List of Figures

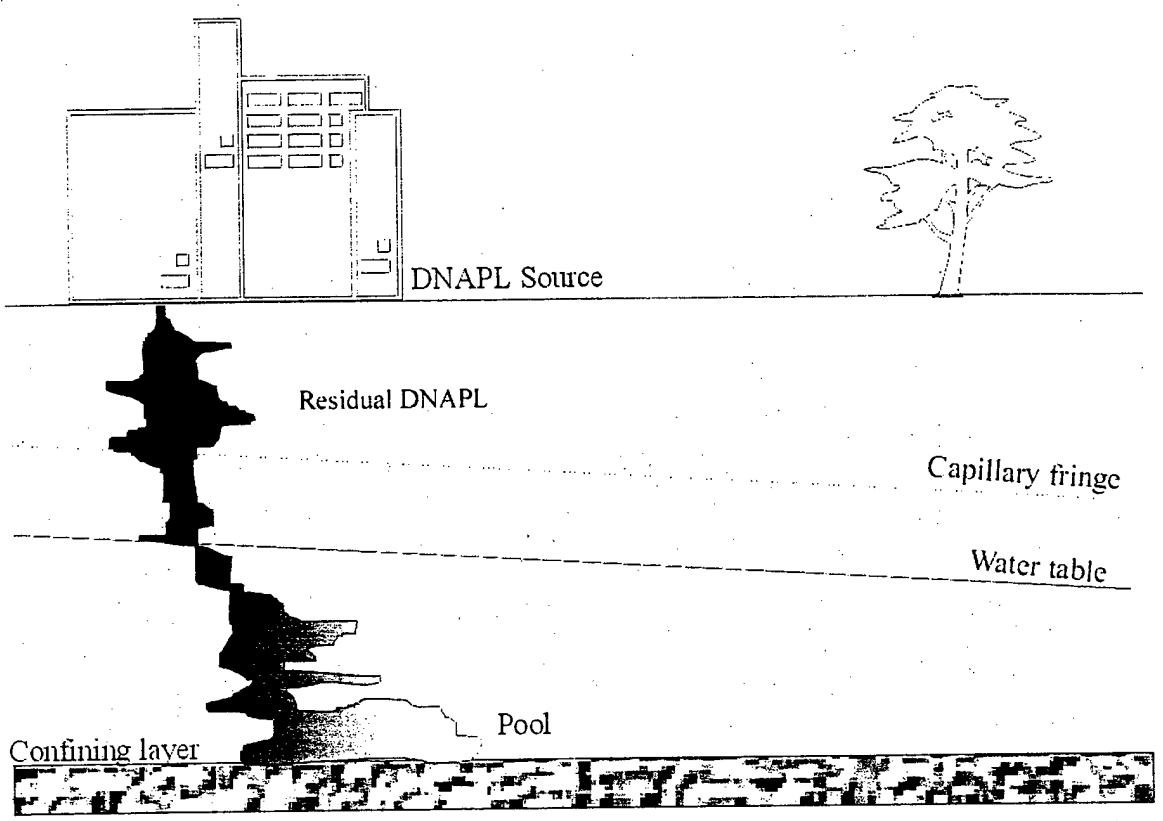

Figure 1. General diagram of the subsurface contamination due to a DNAPL from an industrial source.

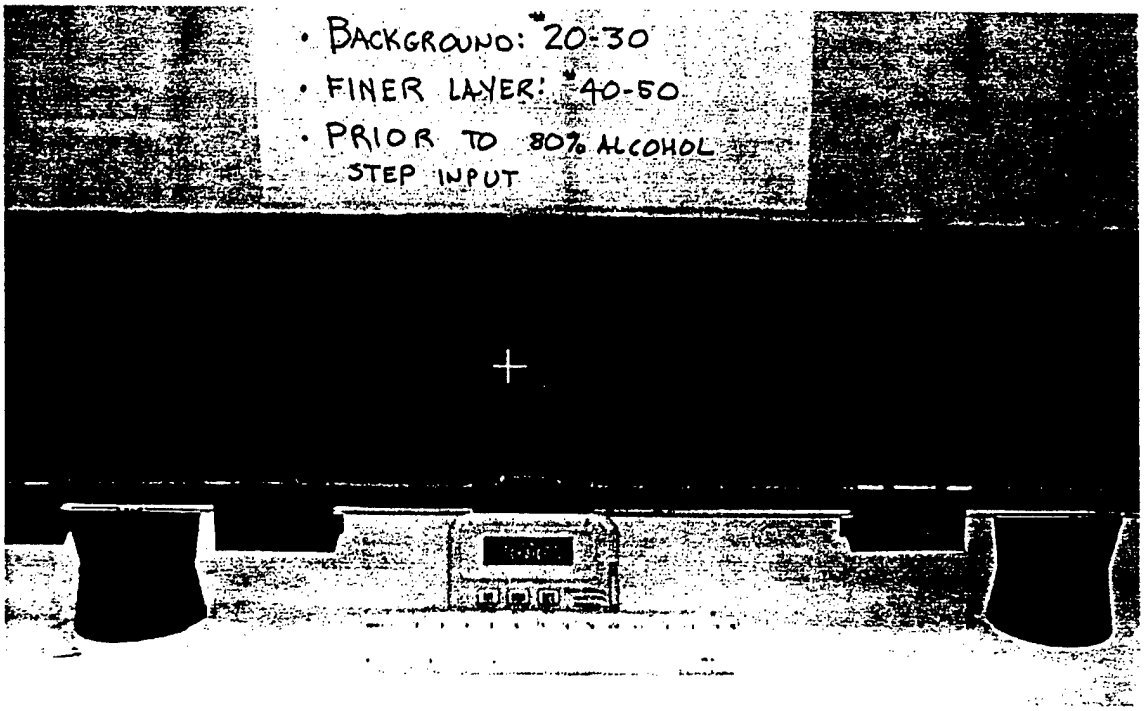

Figure 2. Typical 2-D chamber setup after injection of PCE, prior to any flushing. The white "+" indicates the point of PCE injection.

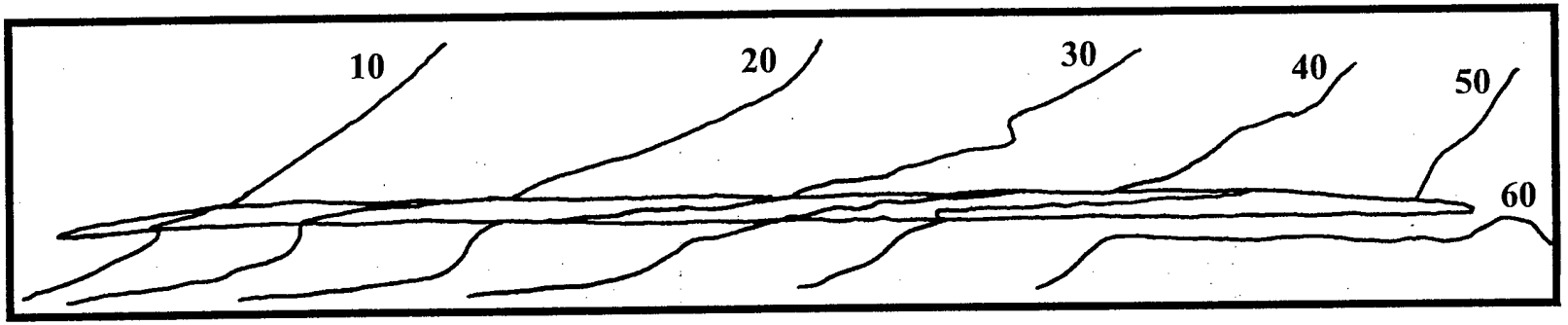

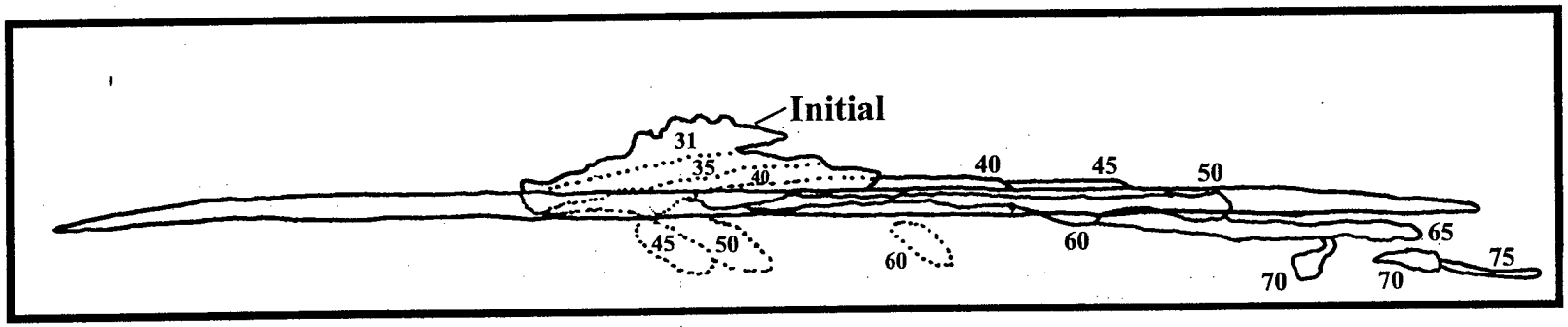

Figure 3

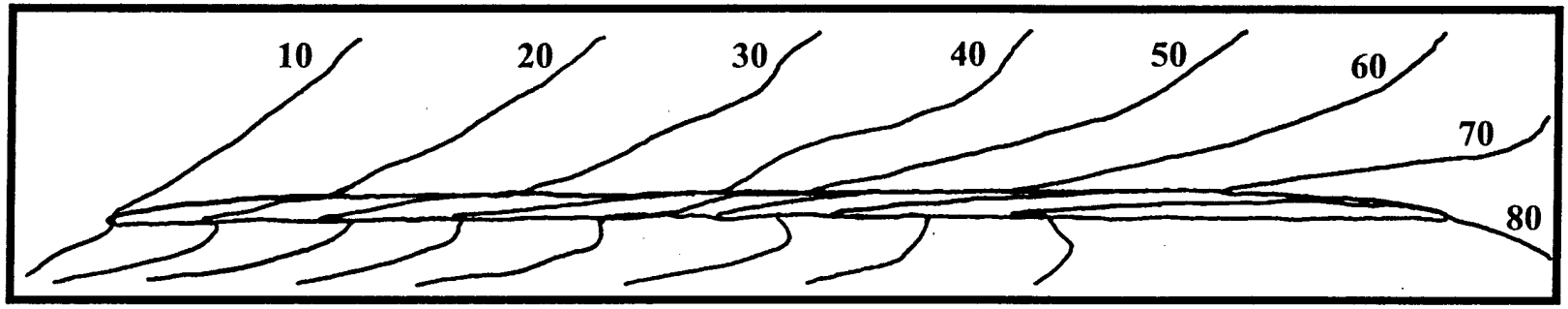

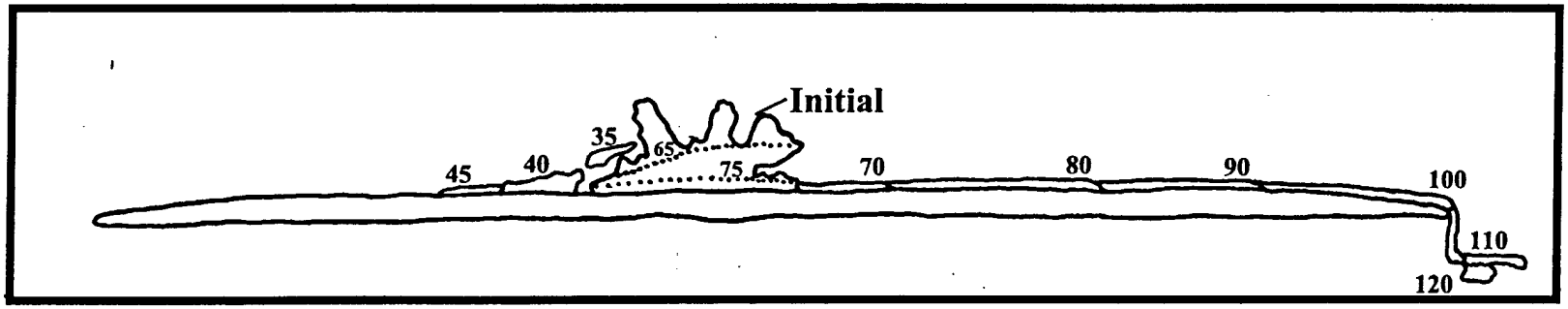

Figure 4

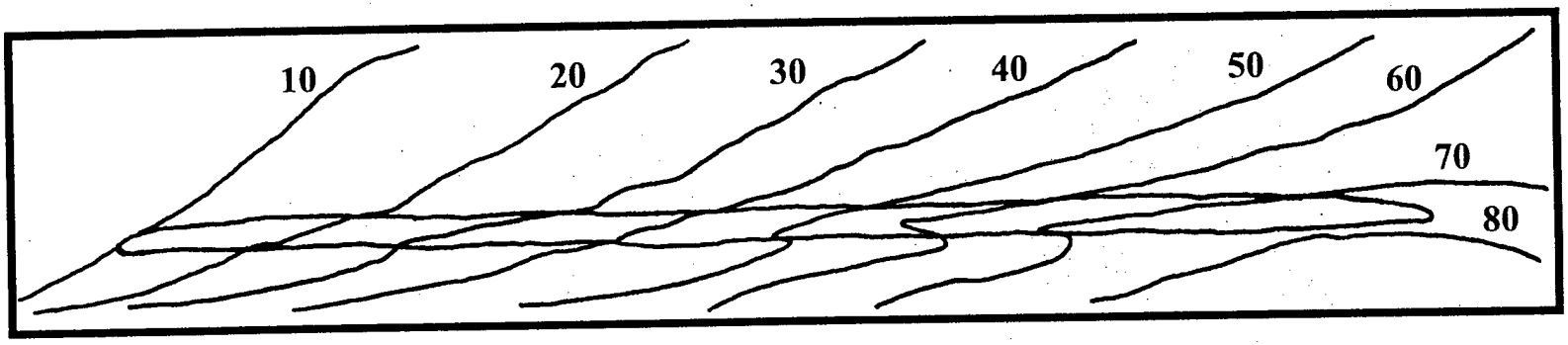
10
20
30
40
50
60
70
80

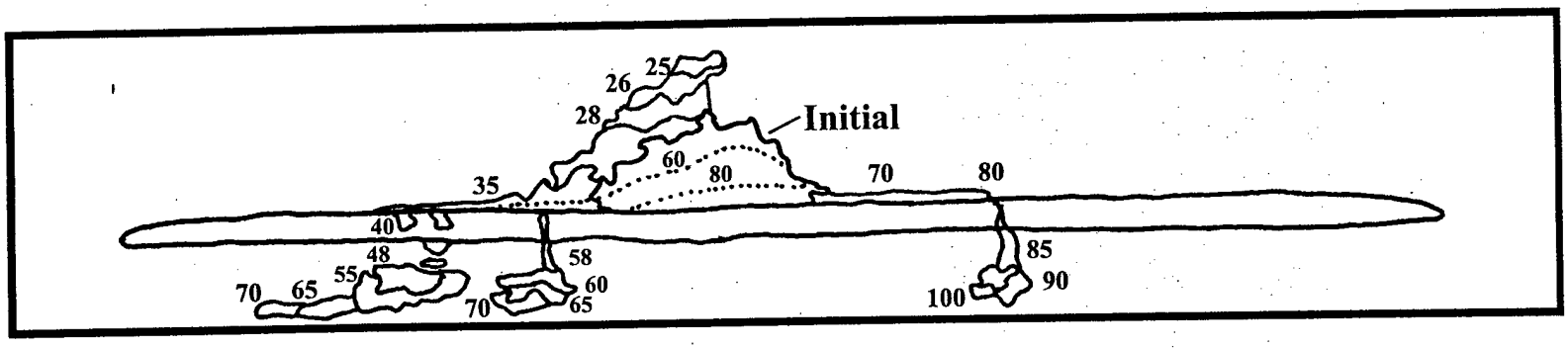
25
26
28
Initial
60
80
70
80
35
40
48
55
70
65
58
60
70
65
85
90
100

Figure 5

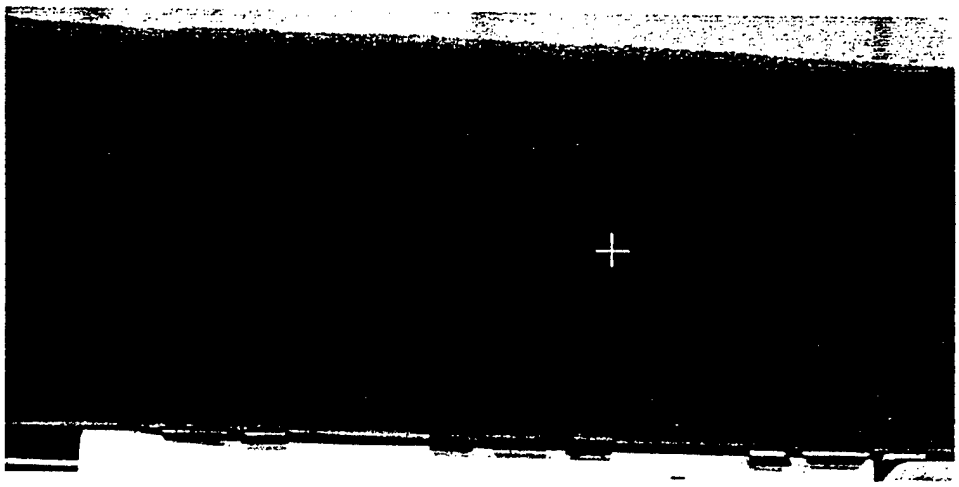

Figure 6. Entry of DNAPL into the capillary barrier due to a step input of 80% alcohol - Nos. 30-40 finer layer. The white "+" indicates the point of original injection. At a later time, another entry occurred slightly down gradient from this location.

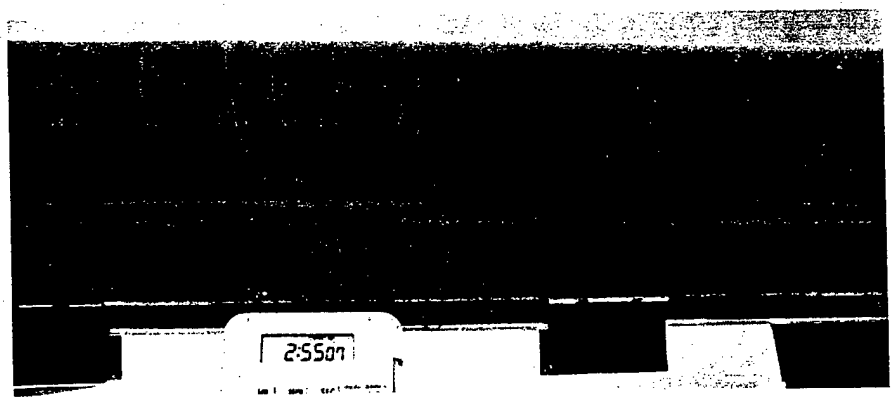

Figure 7. Gradient run with Nos. 60-70 media as the capillary barrier. Entry of highly concentrated PCE containing cosolvent phase into the barrier is shown, with reemergence into the coarser layer below, and reestablishment of separate DNAPL phase due to lowering of alcohol concentrations from dilution.

Figure 8. Down gradient mobilization of the PCE pool by a 40% v/v TBA cosolvent mixture (1 PV). Zones of trapped flushing phase developed on top of the capillary barrier (Nos. 100-140), resulting in less efficient sweeping of the DNAPL and longer removal times.

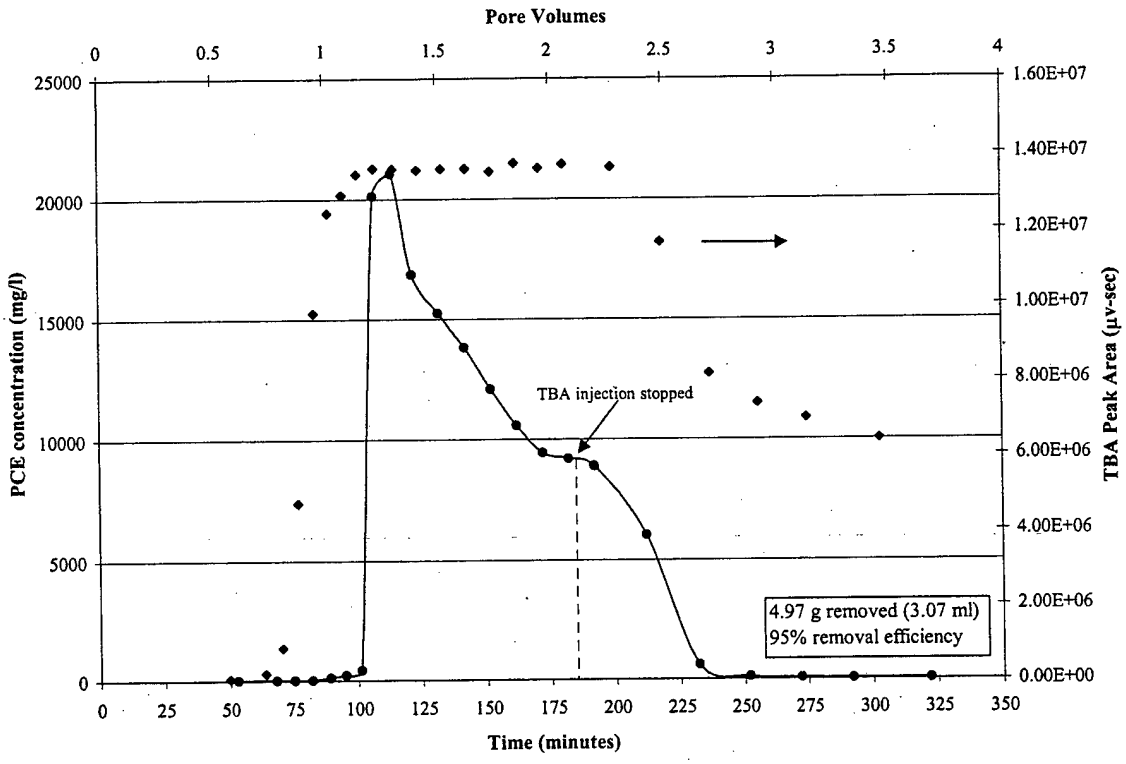

Figure 9. PCE and TBA elution profiles from 2D chamber after a step input of 40% v/v TBA/H_2O. TBA profile data are shown as GC peak areas for reference.

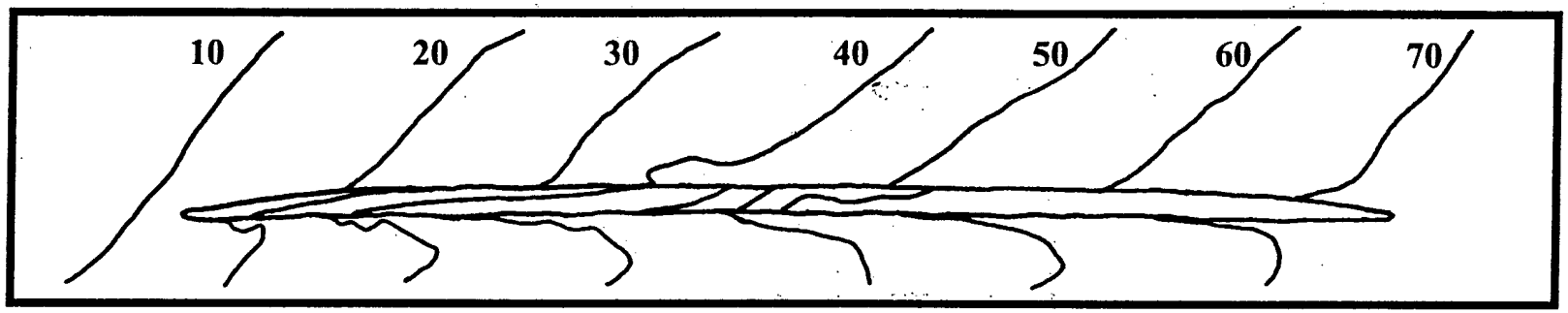
10
20
30
40
50
60
70

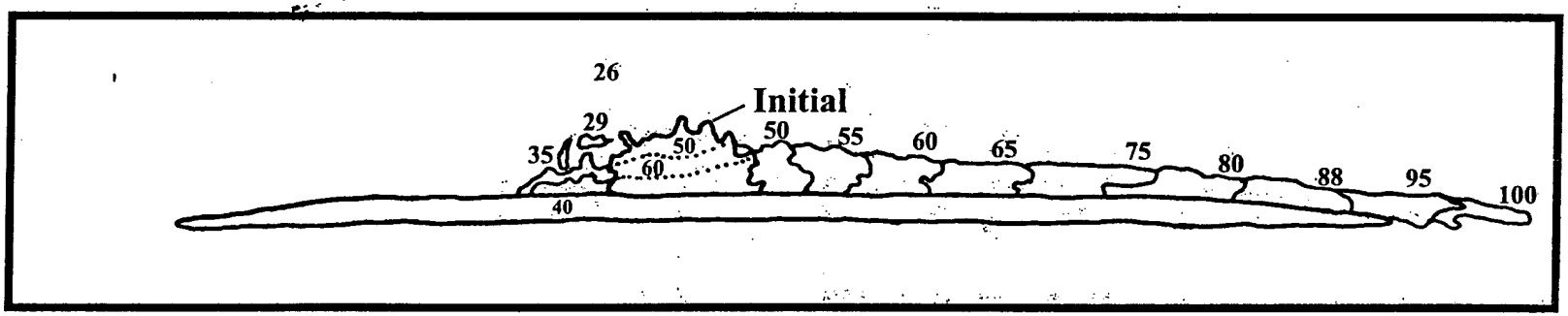
26
Initial
29
35
50
60
50
55
60
65
75
80
88
95
100
40

Figure 10